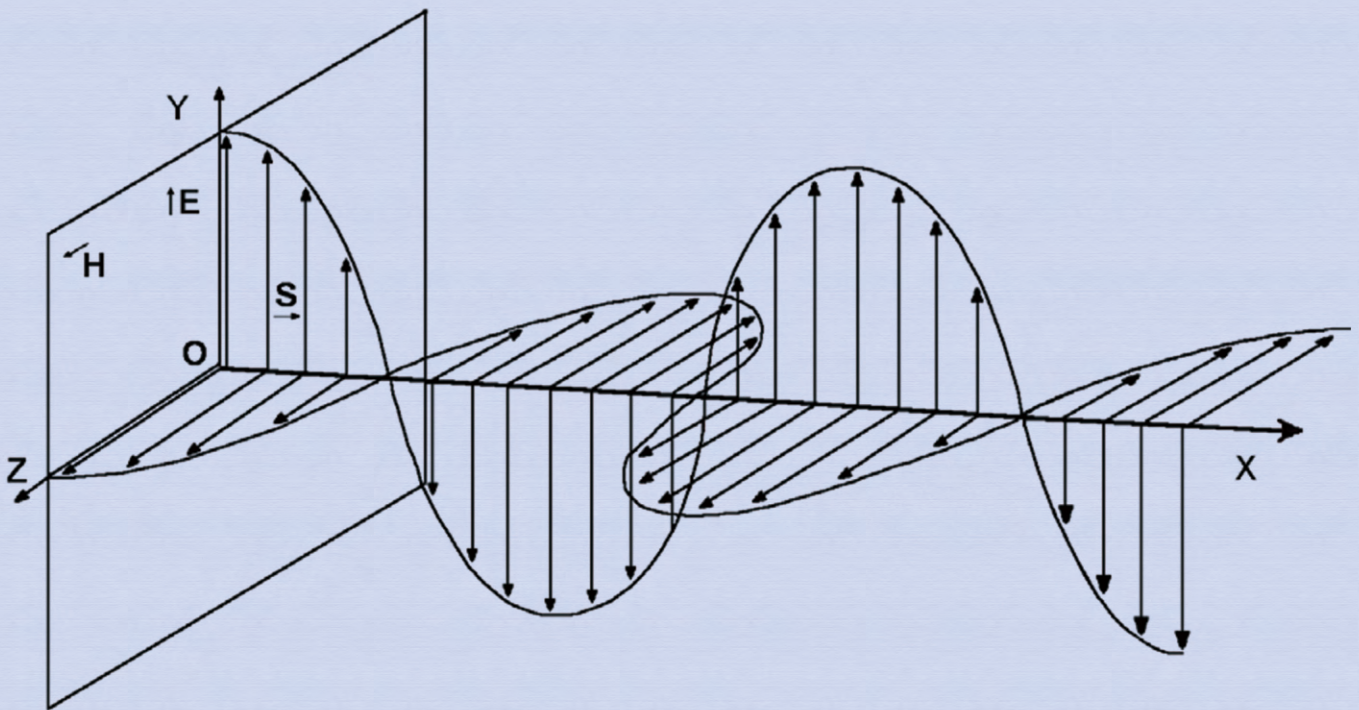


Journal of Modern Physics



ISSN: 2153-1196



<https://www.scirp.org/journal/jmp>

Journal Editorial Board

ISSN: 2153-1196 (Print) ISSN: 2153-120X (Online)

<https://www.scirp.org/journal/jmp>

Editor-in-Chief

Prof. Yang-Hui He

City University, UK

Editorial Board

Prof. Nikolai A. Sobolev

Universidade de Aveiro, Portugal

Dr. Mohamed Abu-Shady

Menoufia University, Egypt

Dr. Hamid Alemohammad

Advanced Test and Automation Inc., Canada

Prof. Emad K. Al-Shakarchi

Al-Nahrain University, Iraq

Prof. Tsao Chang

Fudan University, China

Prof. Stephen Robert Cotanch

NC State University, USA

Prof. Peter Chin Wan Fung

University of Hong Kong, China

Prof. Ju Gao

The University of Hong Kong, China

Prof. Sachin Goyal

University of California, USA

Dr. Wei Guo

Florida State University, USA

Prof. Cosmin Ilie

Los Alamos National Laboratory, USA

Prof. Haikel Jelassi

National Center for Nuclear Science and Technology, Tunisia

Prof. Santosh Kumar Karn

Dr. APJ Abdul Kalam Technical University, India

Prof. Christophe J. Muller

University of Provence, France

Prof. Ambarish Nag

National Renewable Energy Laboratory, USA

Dr. Rada Novakovic

National Research Council, Italy

Prof. Tongfei Qi

University of Kentucky, USA

Prof. Mohammad Mehdi Rashidi

University of Birmingham, UK

Dr. A. L. Roy Vellaisamy

City University of Hong Kong, China

Prof. Yuan Wang

University of California, Berkeley, USA

Prof. Fan Yang

Fermi National Accelerator Laboratory, USA

Prof. Peter H. Yoon

University of Maryland, USA

Prof. Meishan Zhao

University of Chicago, USA

Prof. Pavel Zhuravlev

University of Maryland at College Park, USA

Table of Contents

Volume 11 Number 1

January 2020

Determining the Cosmological Constant Using Gravitational Wave Observations

T. L. Wilson.....1

Calculation of the Spinning Speed of a Free Electron

M. Saglam, B. Bayram, Z. Saglam, H. Gur.....9

Electromagnetism According to Maxwell’s Initial Interpretation

A. Michaud.....16

Expression of Some Special Functions through q -Exponentials of the Nonadditive Statistical Mechanics

L. S. Lima.....81

Effect of Reactor Neutrinos on Beta-Decay

B. V. Vasiliev.....91

Erratum to “Hypothesis of Primary Particles and the Creation of the Big Bang and Other Universes” [Journal of Modern Physics Volume 10 (2019) 1532-1547]

S. Spremo.....97

Reciprocity as an Ever-Present Dual Property of Everything

H. H. Otto.....98

An Introduction to Information Sets with an Application to Iris Based Authentication

M. Hanmandlu, M. Bansal, S. Vasikarla.....122

Relativistic Paradox of a Uniformly Charged Sphere Moving with Constant Velocity

V. A. Leus.....145

Journal of Modern Physics (JMP)

Journal Information

SUBSCRIPTIONS

The *Journal of Modern Physics* (Online at Scientific Research Publishing, <https://www.scirp.org/>) is published monthly by Scientific Research Publishing, Inc., USA.

Subscription rates:

Print: \$89 per issue.

To subscribe, please contact Journals Subscriptions Department, E-mail: sub@scirp.org

SERVICES

Advertisements

Advertisement Sales Department, E-mail: service@scirp.org

Reprints (minimum quantity 100 copies)

Reprints Co-ordinator, Scientific Research Publishing, Inc., USA.

E-mail: sub@scirp.org

COPYRIGHT

Copyright and reuse rights for the front matter of the journal:

Copyright © 2020 by Scientific Research Publishing Inc.

This work is licensed under the Creative Commons Attribution International License (CC BY).

<http://creativecommons.org/licenses/by/4.0/>

Copyright for individual papers of the journal:

Copyright © 2020 by author(s) and Scientific Research Publishing Inc.

Reuse rights for individual papers:

Note: At SCIRP authors can choose between CC BY and CC BY-NC. Please consult each paper for its reuse rights.

Disclaimer of liability

Statements and opinions expressed in the articles and communications are those of the individual contributors and not the statements and opinion of Scientific Research Publishing, Inc. We assume no responsibility or liability for any damage or injury to persons or property arising out of the use of any materials, instructions, methods or ideas contained herein. We expressly disclaim any implied warranties of merchantability or fitness for a particular purpose. If expert assistance is required, the services of a competent professional person should be sought.

PRODUCTION INFORMATION

For manuscripts that have been accepted for publication, please contact:

E-mail: jmp@scirp.org

Determining the Cosmological Constant Using Gravitational Wave Observations

Thomas L. Wilson

Johnson Space Center, NASA, Houston, TX, USA

Email: Thomas.Wilson@cern.ch

How to cite this paper: Wilson, T.L. (2020) Determining the Cosmological Constant Using Gravitational Wave Observations. *Journal of Modern Physics*, 11, 1-8. <https://doi.org/10.4236/jmp.2020.111001>

Received: December 10, 2019

Accepted: December 30, 2019

Published: January 2, 2020

Copyright © 2020 by author(s) and Scientific Research Publishing Inc. This work is licensed under the Creative Commons Attribution International License (CC BY 4.0). <http://creativecommons.org/licenses/by/4.0/>



Open Access

Abstract

It is shown in Einstein gravity that the cosmological constant Λ introduces a graviton mass m_g into the theory, a result that will be derived from the Regge-Wheeler-Zerilli problem for a particle falling onto a Kottler-Schwarzschild mass with $\Lambda \neq 0$. The value of m_g is precisely the Spin-2 gauge line appearing on the Λ - m_g^2 phase diagram for Spin-2, the partially massless gauge lines introduced by Deser & Waldron in the (m_g^2, Λ) phase plane and described as the Higuchi bound $m_g^2 = 2\Lambda/3$. Note that this graviton is unitary with only four polarization degrees of freedom (helicities $\pm 2, \pm 1$, but not 0 because a scalar gauge symmetry removes it). The conclusion is drawn that Einstein gravity (EG, $\Lambda \neq 0$) is a partially massless gravitation theory which has lost its helicity 0 due to a scalar gauge symmetry. That poses a challenge for gravitational wave antennas as to whether they can measure the loss of this gauge symmetry. Also, given the recent results measuring the Hubble constant H_o from LIGO-Virgo data, it is then shown that Λ can be determined from the LIGO results for the graviton mass m_g and H_o . This is yet another multi-messenger source for determining the three parameters Λ , m_g and H_o in astrophysics and cosmology, at a time when there is much disparity in measurements of H_o .

Keywords

Gravitation, General Relativity

1. Introduction

In order to determine the graviton mass of Einstein gravity (EG), we proceed as follows. A curved Kottler-Schwarzschild (KS) metric with $\Lambda \neq 0$ will be applied to the Regge-Wheeler-Zerilli (RWZ) problem [1] [2] [3] [4] [5] representing gravitational radiation perturbations produced by a particle falling onto a large

mass M . The RWZ result ($\Lambda = 0$) will be extended to the general EG problem with $\Lambda \neq 0$ (EG Λ), in the fashion that Kottler extended the Schwarzschild metric to de Sitter space (Sds).

One begins with a small perturbative expansion of the Einstein field equations

$$R_{\mu\nu} - \frac{1}{2}g_{\mu\nu}R + \Lambda g_{\mu\nu} = -\kappa T_{\mu\nu} \tag{1}$$

about the known exact solution $\eta_{\mu\nu}$ where the metric tensor is $g_{\mu\nu} = \eta_{\mu\nu} + h_{\mu\nu}$, with $h_{\mu\nu}$ the dynamic perturbation of the background raising and lowering operator $\eta_{\mu\nu}$. The most general spherically symmetric solution is well-known to be a Kottler-Schwarzschild (KS) metric

$$ds^2 = -e^v dt^2 + e^\zeta dr^2 + r^2 d\Omega^2 \tag{2}$$

where

$$e^v = 1 - \frac{2M}{r} - \frac{\Lambda}{3}r^2 = e^{-\zeta} \tag{3}$$

with $M = GM^*/c^2$, $d\Omega^2 = (d\Theta + \sin^2 \Theta d\phi^2)$, and $\eta_{\mu\nu} = \text{diag}(e^v, e^{-v}, r^2, r^2 \sin^2 \Theta)$ in spherically symmetric coordinates. Its contravariant inverse $\eta^{\mu\nu}$ is defined such that $\eta_{\mu\nu}\eta^{\mu\nu} = \delta_\mu^\nu$.

The wave equation for gravitational radiation $h_{\mu\nu}$ on the non-flat background containing Λ in (1) will follow as (9) below, derived now from the procedure developed in the RWZ formalism. Perturbation analysis of (1) for a stable background $\eta^{\mu\nu} = g^{(0)}_{\mu\nu}$ produces the following

$$\begin{aligned} & [h_{\mu\nu;\alpha}{}^{;\alpha} - h_{\mu\alpha;\nu}{}^{;\alpha} - h_{\nu\alpha;\mu}{}^{;\alpha} + h_{\alpha}{}^{\alpha}{}_{;\mu\nu}] + \eta_{\mu\nu} [h_{\alpha\gamma}{}^{;\alpha;\gamma} - h_{\alpha}{}^{\alpha}{}_{;\gamma}{}^{;\gamma}] \\ & + h_{\mu\nu} (R - 2\Lambda) - \eta_{\mu\nu} h_{\alpha\beta} R^{\alpha\beta} = -2\kappa\delta T_{\mu\nu} \end{aligned} \tag{4}$$

Stability must be assumed in order that $\delta T_{\mu\nu}$ is small. This equation can be simplified by defining the function (introduced by Einstein himself)

$$\bar{h}_{\mu\nu} \equiv h_{\mu\nu} - \frac{1}{2}\eta_{\mu\nu}h \tag{5}$$

and its divergence

$$f_\mu \equiv \bar{h}_{\mu\nu}{}^{;\nu} \tag{6}$$

Substituting (5) and (6) into (4) and re-grouping terms gives

$$\begin{aligned} & \bar{h}_{\mu\nu;\alpha}{}^{;\alpha} - (f_{\mu;\nu} + f_{\nu;\mu}) + \eta_{\mu\nu} f_\alpha{}^{;\alpha} - 2\bar{h}_{\alpha\beta} R^\alpha{}_{\mu\nu}{}^\beta - \bar{h}_{\mu\alpha} R^\alpha{}_{\nu}{}^\beta - \bar{h}_{\nu\alpha} R^\alpha{}_{\mu}{}^\beta \\ & + h_{\mu\nu} (R - 2\Lambda) - \eta_{\mu\nu} h_{\alpha\beta} R^{\alpha\beta} = -2\kappa\delta T_{\mu\nu} \end{aligned} \tag{7}$$

Now impose the Hilbert-Einstein-de-Donder gauge which sets (6) to zero ($f_\mu = 0$), and suppresses any vector gravitons. Wave Equation (7) reduces to

$$\begin{aligned} & \bar{h}_{\mu\nu;\alpha}{}^{;\alpha} - 2\bar{h}_{\alpha\beta} R^\alpha{}_{\mu\nu}{}^\beta - \bar{h}_{\mu\alpha} R^\alpha{}_{\nu}{}^\beta - \bar{h}_{\nu\alpha} R^\alpha{}_{\mu}{}^\beta - \eta_{\mu\nu} h_{\alpha\beta} R^{\alpha\beta} + h_{\mu\nu} (R - 2\Lambda) \\ & = -2\kappa\delta T_{\mu\nu} \end{aligned} \tag{8}$$

In an empty ($T_{\mu\nu} = 0$), Ricci-flat ($R_{\mu\nu} = 0$) space without Λ ($R = 4\Lambda = 0$), (8) further reduces to

$$\bar{h}_{\mu\nu;\alpha}{}^{;\alpha} - 2R^\alpha{}_{\mu\nu}{}^\beta \bar{h}_{\alpha\beta} = -2\kappa\delta T_{\mu\nu} \tag{9}$$

which is the starting point for the RWZ formalism.

Weak-Field Limit, de Sitter Metric. The Schwarzschild character of the RWZ problem above will now be relaxed, with $\eta_{\mu\nu}$ again diagonal, but $M=0$ and $\Lambda \neq 0$ in (2) and (3). The wave equation of paramount importance will follow as (17).

We know that the trace of the field Equations (1) gives $4\Lambda - R = -\kappa T$, whereby they become

$$R_{\mu\nu} - \Lambda g_{\mu\nu} = -\kappa \left[T_{\mu\nu} - \frac{1}{2} g_{\mu\nu} T \right] \tag{10}$$

For an empty space ($T_{\mu\nu} = 0$ and $T = 0$), (10) reduces to de Sitter space

$$R_{\mu\nu} = \Lambda g_{\mu\nu} \tag{11}$$

and the trace to $R = 4\Lambda$.

Substitution of R and $R_{\mu\nu}$ from (11) into (8) using (5) shows that the contributions due to $\Lambda \neq 0$ are of second order in $h_{\mu\nu}$. Neglecting these terms (particularly if Λ is very, very small) simplifies (8) to

$$\bar{h}_{\mu\nu;\alpha}{}^{;\alpha} - 2R^{\alpha}{}_{\mu\nu}{}^{\beta} \bar{h}_{\alpha\beta} = -2\kappa\delta T_{\mu\nu} \tag{12}$$

One can arrive at (12) to first order in $h_{\mu\nu}$ by using $g_{\mu\nu}$ as a raising and lowering operator rather than the background $\eta_{\mu\nu}$ —a result which incorrectly leads some to the conclusion that Λ terms cancel in the gravitational wave equation.

Note with caution that (12) and the RWZ Equation (9) are not the same wave equation. Overtly, the cosmological terms have vanished from (12), just like (9) where Λ was assumed in the RWZ problem to be nonexistent in the first place. However, the character of the Riemann tensor $R^{\alpha}{}_{\mu\nu}{}^{\beta}$ is significantly different in these two relations where $\Lambda = 0$ in one but not the other.

Simplifying the SdS metric by setting the central mass M in $\eta_{\mu\nu}$ to zero, produces the de Sitter space (11) of constant curvature $K = 1/R^2$, where we can focus on the effect of Λ . The Riemann tensor is now

$$R_{\gamma\mu\nu\delta} = +K (g_{\gamma\nu} g_{\mu\delta} - g_{\gamma\delta} g_{\mu\nu}) \tag{13}$$

and reverts to

$$R^{\alpha}{}_{\mu\nu}{}^{\beta} = +K (g^{\alpha}{}_{\nu} g_{\mu}{}^{\beta} - g^{\alpha\beta} g_{\mu\nu}) \tag{14}$$

for use in (12). This substitution (raising and lowering with $\eta_{\mu\nu}$) into (12) next gives K and Λ term contributions

$$\begin{aligned} & -2K \left[(\bar{h}_{\mu\nu} - \eta_{\mu\nu} \bar{h}) + (\bar{h}_{\alpha\mu} h^{\alpha}{}_{\nu} + \bar{h}_{\nu\beta} h^{\beta}{}_{\mu} - \bar{h} h_{\mu\nu} - \eta_{\mu\nu} h^{\alpha\beta} \bar{h}_{\alpha\beta}) \right] \\ & + [2h_{\mu\alpha} \bar{h}_\nu{}^\alpha + \eta_{\mu\nu} h_{\alpha\beta}^2] \end{aligned} \tag{15}$$

to second order in $h_{\mu\nu}$. Recalling that curvature K is related to Λ by $K = \Lambda/3$, substitution of (15) back into (12) gives to first order

$$\bar{h}_{\mu\nu;\alpha}{}^{;\alpha} - \frac{2}{3} M \bar{h}_{\mu\nu} + \frac{2}{3} \Lambda \eta_{\mu\nu} \bar{h} = -2\kappa\delta T_{\mu\nu} \tag{16}$$

There is no cancellation of the Λ contributions to first order. Noting from (5) that $\bar{h} = h(1 - 1/2\eta)$, then a traceless gauge $\bar{h} = 0$ means either that $h = 0$ or η

= 2. Since $\eta = 4$, (16) reduces to

$$\bar{h}_{\mu\nu;\alpha}{}^{;\alpha} - \frac{2}{3}\Lambda\bar{h}_{\mu\nu} = -2\kappa\delta T_{\mu\nu} \tag{17}$$

in a traceless Hilbert-Einstein-de Donder gauge where $\bar{h}_{\mu\nu}{}^{;\nu} = 0$ and $\bar{h}_{\mu}{}^{\mu} = 0$. (17) is a wave equation involving the Laplace-Beltrami operator term $\bar{h}_{\mu\nu;\alpha}{}^{;\alpha}$ for the Spin-2 gravitational perturbation $\bar{h}_{\mu\nu}$ bearing a mass

$$m_g = \sqrt{2\Lambda/3} \tag{18}$$

similar to the Klein-Gordon Equation $(\square - m^2)\varphi = 0$ for a Spin-0 scalar field φ in flat Minkowski space. The *Locally Flat Limit* section which follows demonstrates that $\bar{h}_{\mu\nu;\alpha}{}^{;\alpha} \rightarrow \square\bar{h}_{\mu\nu}$ in (17) for the limit $r \rightarrow 0$. From (17) and (18) then

$$(\square - m_g^2)\bar{h}_{\mu\nu} = -2\kappa\delta T_{\mu\nu} \tag{19}$$

in the locally flat-space limit $r \ll 1$.

Note that Penrose [6] has pointed out that due to conformal invariance arguments, the massless Klein-Gordon equation becomes $(\square - R/6)\varphi = 0$ on a curved background. This necessarily gives (18) since $R = 4\Lambda$ in de Sitter space. Also in passing, by rescaling \bar{h} as $h_2 \rightarrow 1/2\bar{h}_1$ in (12) and (17), then (18) becomes

$$m_g = \sqrt{\Lambda/3} \tag{20}$$

which is the surface gravity $\kappa_C = m_g$ of the cosmological event horizon identified by Gibbons & Hawking [7]. It is also found in Weinberg [8].

Locally Flat Limit of Wave Equation (17): It is necessary to demonstrate that hidden Λ -terms arising from $\bar{h}_{\mu\nu;\alpha}{}^{;\alpha}$ in (17) do not cancel the mass term in (18)-(20) when $r \rightarrow 0$ and $\bar{h}_{\mu\nu;\alpha}{}^{;\alpha} \rightarrow \bar{h}_{\mu\nu;\alpha}{}^{;\alpha} = \square\bar{h}_{\mu\nu}$, the d'Alembertian in a locally flat region of dS studied above. Λ -terms appear but cancel out as shown below.

To simplify calculations, now note that $r^2 d\Omega^2$ in (2) is of second-order in r and is negligible as $r \rightarrow 0$. Thus the focus is on e^ν (with $M = 0$) in (3) appearing in the diagonal of $\eta_{\mu\nu}$ and its inverse $\eta^{\mu\nu}$. Hence, $\eta_{00} = -c$ and $\eta^{00} = -c^{-1}$, while $\eta_{11} = c^{-1}$ and $\eta^{11} = c$. Also, note that $c(r) \rightarrow 1$ and $c(r)^{-1} \rightarrow 1$ as $r \rightarrow 0$.

Introducing the Christoffel symbol $\Gamma_{\alpha\beta}^\gamma$, we can write

$$\bar{h}_{\mu\nu;\alpha}{}^{;\alpha} = g^{\alpha\beta}\bar{h}_{\mu\nu;\alpha;\beta} = g^{\alpha\beta}\left[\bar{h}_{\mu\nu;\alpha;\beta} - (\Gamma_{\alpha\mu}^\epsilon\bar{h}_{\epsilon\nu})_{;\beta} - (\Gamma_{\alpha\nu}^\epsilon\bar{h}_{\mu\epsilon})_{;\beta}\right] \tag{21}$$

Define

$$\bar{h}_{\mu\nu;\alpha}{}^{;\alpha} = \square\bar{h}_{\mu\nu} + A_{\mu\nu} + B_{\mu\nu} + C_{\mu\nu} \tag{22}$$

where

$$\square\bar{h}_{\mu\nu} = \bar{h}_{\mu\nu;\alpha}{}^{;\alpha} \tag{23}$$

$$A_{\mu\nu} = -\Gamma_{\beta\mu}^\epsilon\bar{h}_{\epsilon\nu}{}^{;\beta} - \Gamma_{\beta\nu}^\epsilon\bar{h}_{\mu\epsilon}{}^{;\beta} - \Gamma_{\beta\alpha}^\epsilon\bar{h}_{\mu\nu;\epsilon}\eta^{\alpha\beta} - \Gamma_{\alpha\mu}^\epsilon\bar{h}_{\epsilon\nu}{}^{;\alpha} - \Gamma_{\alpha\nu}^\epsilon\bar{h}_{\mu\epsilon}{}^{;\alpha} \tag{24}$$

$$B_{\mu\nu} = -(\Gamma_{\alpha\mu}^\epsilon)^{\alpha}\bar{h}_{\epsilon\nu} - (\Gamma_{\alpha\nu}^\epsilon)^{\alpha}\bar{h}_{\mu\epsilon} \tag{25}$$

$$C_{\mu\nu} = -\eta^{\alpha\beta} \left[\left(\Gamma_{\beta\delta}^\epsilon \Gamma_{\alpha\mu}^\delta - \Gamma_{\beta\alpha}^\delta \Gamma_{\delta\mu}^\epsilon - \Gamma_{\beta\mu}^\delta \Gamma_{\alpha\delta}^\epsilon \right) \bar{h}_{\epsilon\nu} - \Gamma_{\beta\epsilon}^\delta \Gamma_{\alpha\mu}^\epsilon \bar{h}_{\delta\nu} - \Gamma_{\beta\nu}^\delta \Gamma_{\alpha\mu}^\epsilon \bar{h}_{\epsilon\delta} \right. \\ \left. + \left(\Gamma_{\beta\delta}^\epsilon \Gamma_{\alpha\nu}^\delta - \Gamma_{\beta\alpha}^\delta \Gamma_{\delta\nu}^\epsilon - \Gamma_{\beta\nu}^\delta \Gamma_{\alpha\delta}^\epsilon \right) \bar{h}_{\mu\epsilon} - \Gamma_{\beta\mu}^\delta \Gamma_{\alpha\nu}^\epsilon \bar{h}_{\delta\epsilon} - \Gamma_{\beta\epsilon}^\delta \Gamma_{\alpha\nu}^\epsilon \bar{h}_{\mu\delta} \right]. \quad (26)$$

$B_{\mu\nu}$ is the term of interest. $A_{\mu\nu}$ and $C_{\mu\nu}$ contain factors of second order, or terms that vanish in locally flat space ($r \ll 1$). Furthermore, only the first-order second derivatives in $B_{\mu\nu}$ remain as $r \rightarrow 0$. These terms are

$$B_{\alpha\mu\nu}^*{}^\alpha = -\frac{1}{2} \eta^{\epsilon\gamma} \left[\left(\eta_{\alpha\gamma,\mu}{}^{,\alpha} + \eta_{\mu\gamma,\alpha}{}^{,\alpha} - \eta_{\alpha\mu,\gamma}{}^{,\alpha} \right) \bar{h}_{\epsilon\nu} \right. \\ \left. + \left(\eta_{\alpha\gamma,\nu}{}^{,\alpha} + \eta_{\nu\gamma,\alpha}{}^{,\alpha} - \eta_{\alpha\nu,\gamma}{}^{,\alpha} \right) \bar{h}_{\mu\epsilon} \right] \quad (27)$$

which can be defined as

$$B_{\alpha\mu\nu}^*{}^\alpha = F_{\mu\nu} + G_{\mu\nu} + H_{\mu\nu} \quad (28)$$

where

$$F_{\mu\nu} = -\frac{1}{2} \eta^{\epsilon\gamma} \left[(\square \eta_{\mu\gamma}) \bar{h}_{\epsilon\nu} + (\square \eta_{\nu\gamma}) \bar{h}_{\mu\epsilon} \right] \quad (29)$$

$$G_{\mu\nu} = -\frac{1}{2} \eta^{\epsilon\gamma} \left[\eta_{\alpha\gamma,\mu}{}^{,\alpha} \bar{h}_{\epsilon\nu} + \eta_{\alpha\gamma,\nu}{}^{,\alpha} \bar{h}_{\mu\epsilon} \right] \quad (30)$$

$$H_{\mu\nu} = +\frac{1}{2} \eta^{\epsilon\gamma} \left[\eta_{\alpha\mu,\gamma}{}^{,\alpha} \bar{h}_{\epsilon\nu} + \eta_{\alpha\nu,\gamma}{}^{,\alpha} \bar{h}_{\mu\epsilon} \right] \quad (31)$$

In this approximation, $\square = -\partial_t^2 + \nabla^2 \rightarrow \nabla^2$. Also $\square \eta_{00} \rightarrow \nabla^2 \eta_{00} = +2/3 \lambda$ and $\square \eta_{11} \rightarrow \nabla^2 \eta_{11} = +2/3 \lambda$.

We find that

$$F_{\mu\nu} = -\frac{1}{2} \eta^{00} \left[(\square \eta_{\mu 0}) \bar{h}_{0\nu} + (\square \eta_{\nu 0}) \bar{h}_{\mu 0} \right] - \frac{1}{2} \eta^{11} \left[(\square \eta_{\mu 1}) \bar{h}_{1\nu} + (\square \eta_{\nu 1}) \bar{h}_{\mu 1} \right] \quad (32)$$

whereby (all other terms do not contribute)

$$F_{00} = -\eta^{00} \left[(\square \eta_{00}) \bar{h}_{00} \right] = +\frac{2}{3} \lambda \bar{h}_{00} \quad (33)$$

$$F_{11} = -\eta^{11} \left[(\square \eta_{11}) \bar{h}_{11} \right] = -\frac{2}{3} \lambda \bar{h}_{11} \quad (34)$$

Next

$$G_{\mu\nu} = -\frac{1}{2} \eta^{11} \left[\eta_{11,\mu}{}^{,1} \bar{h}_{1\nu} + \eta_{11,\nu}{}^{,1} \bar{h}_{\mu 1} \right] \quad (35)$$

whereby (all other terms do not contribute)

$$G_{01} = -\frac{1}{3} \lambda \bar{h}_{01}; \quad G_{10} = -\frac{1}{3} \lambda \bar{h}_{10}; \quad G_{11} = -\frac{2}{3} \lambda \bar{h}_{11}. \quad (36)$$

And lastly,

$$H_{\mu\nu} = \frac{1}{2} \eta^{11} \left[\eta_{\alpha\mu,1}{}^{,\alpha} \bar{h}_{1\nu} + \eta_{\alpha\nu,1}{}^{,\alpha} \bar{h}_{\mu 1} \right] \quad (37)$$

whereby

$$H_{00} = 0; \quad H_{11} = \frac{2}{3} \lambda \bar{h}_{11}; \quad H_{01} = \frac{1}{3} \lambda \bar{h}_{01}; \quad H_{10} = \frac{1}{3} \lambda \bar{h}_{10} \quad (38)$$

Summarizing, the two contributing terms to $F_{\mu\nu}$ in (33) and (34) are equal and opposite thereby cancelling in (32). Thus, $F_{\mu\nu} = 0$. Similarly, the collective $G_{\mu\nu}$ and $H_{\mu\nu}$ terms in (36) and (38) cancel one another, giving $G_{\mu\nu} + H_{\mu\nu} = 0$. Hence $B_{\alpha\mu\nu}^*{}^\alpha = B_{\mu\nu} \equiv 0$ in (28) and (25). Therefore we get $\bar{h}_{\mu\nu;\alpha}{}^{;\alpha} \rightarrow \bar{h}_{\mu\nu;\alpha}{}^{;\alpha} = \square \bar{h}_{\mu\nu}$ in the locally flat limit of (17).

The graviton mass (18) for EGA thus follows from this analysis, a result first determined many years ago [9].

Identifying Einstein Gravity as a Partially Massless Theory. The cosmological phase diagrams for partially massless fields of arbitrary spin in de Sitter space ($\Lambda \neq 0$) are well understood thanks to the seminal work of Deser & Nepomechie [10] and Deser & Waldron [11]-[17], in conjunction with that of Higuchi [18] [19] [20] [21].

(18) removes the scalar helicity-0 mode along the Higuchi partially-massless gauge line for Spin-2, leaving only 4 instead of 5 propagating degrees of freedom [15]—hence the term partially massless gravity. With respect to gravitational wave polarization analysis, this partially massless feature of EGA went unnoticed earlier on in initial polarization studies of gravitational waves which focused on Pauli-Fierz massive gravity effects [21] [22] [23] [24]. The latter do not address partial masslessness in gravitational radiation behavior.

Derived directly from EGA in (1)-(3), (18) proves that EGA is a partially massless theory because that is specifically the Higuchi bound established by Deser and Nepomechie [10], Deser and Waldron [11]-[17], and articulated by Higuchi [18] [19] [20] [21]. Massive gravity thus finds its roots when Einstein first introduced Λ into GR, rather than later when Pauli & Fierz (P-F) [25] pursued the study of massive gravity by adding appropriate terms to the Einstein-Hilbert Lagrangian.

Determining Λ from Gravitational Wave Observations. (18) is hence a direct prediction of EGA in (1). Recalling that gravitational wave observations can be used to determine the Hubble constant H_o [26] [27], we know that $H_o^2 = \Lambda/3$ in de Sitter space ([8], Equation 2.6) from which Λ can be determined. Given the currently known disparity in H_o determinations [28] [29], Λ , m_g and H_o must eventually be brought into reconciliation. The question now becomes how to measure these effects using LIGO, VIRGO, and future LISA antenna configurations to determine whether polarization measurements can establish the loss of the helicity 0 excitation due to a scalar gauge symmetry but not the loss of helicity ± 1 , as predicted by the partially massless theory [12] [30].

2. Conclusions

In Conclusion: These results come directly from the RWZ Equation (9). The consequence is yet another way to determine the cosmological constant Λ , but from gravitational wave observations. It constitutes an entirely new prediction from Einstein's theory, that Λ , c , H_o , and m_g (having only 4 Spin-2 DOFs with helicities $\pm 2, \pm 1$), and conventional Λ -lore such as dark matter in Λ CDM models, are

interrelated. For that reason alone, (18) needs to be verified experimentally. In addition, all of these parameters must collectively produce self-consistent values. The answer may also contribute to our understanding of galactic-rotation-curve behavior. Such predictions by EGA need to be investigated further.

The fundamental question for partially massive gravity is whether existing gravitational wave antenna configurations can be used to measure or determine the loss of the helicity 0 polarization caused by loss of a scalar gauge symmetry. It will probably require additional antenna configurations and possibly more antennas.

Conflicts of Interest

The author declares no conflicts of interest regarding the publication of this paper.

References

- [1] Regge, T. and Wheeler, J.A. (1957) *Physical Review*, **108**, 1063.
<https://doi.org/10.1103/PhysRev.108.1063>
- [2] Peters, P.C. (1966) *Physical Review*, **146**, 938.
<https://doi.org/10.1103/PhysRev.146.938>
- [3] Isaacson, R.A. (1968) *Physical Review*, **166**, 1263.
<https://doi.org/10.1103/PhysRev.166.1272>
- [4] Zerilli, F.J. (1970) *Physical Review D*, **2**, 2141.
<https://doi.org/10.1103/PhysRevD.2.2141>
- [5] Zerilli, F.J. (1970) *Physical Review Letters*, **24**, 737.
<https://doi.org/10.1103/PhysRevLett.24.737>
- [6] Penrose, R. (1964) Conformal Treatment of Infinity. In: DeWitt, C.B., Ed., *Relativity, Groups, & Topology*, Gordon & Breach, London, 565-584.
- [7] Gibbons, G.W. and Hawking, S. (1977) *Physical Review D*, **15**, 2738.
<https://doi.org/10.1103/PhysRevD.15.2738>
- [8] Weinberg, S. (1989) *Reviews of Modern Physics*, **61**, 1.
<https://doi.org/10.1103/RevModPhys.61.1>
- [9] Wilson, T.L. (1973) Gravitational Radiation Theory. Master's Thesis, Rice University, Houston. Available Online as NASA TMX-58132.
- [10] Deser, S. and Nepomechie, R.I. (1983) *Physics Letters B*, **132**, 321-324.
[https://doi.org/10.1016/0370-2693\(83\)90317-9](https://doi.org/10.1016/0370-2693(83)90317-9)
Deser, S. and Nepomechie, R.I. (1984) *Annals of Physics*, **154**, 396-420.
[https://doi.org/10.1016/0003-4916\(84\)90156-8](https://doi.org/10.1016/0003-4916(84)90156-8)
- [11] Deser, S. and Waldron, A. (2001) *Physical Review Letters*, **87**, Article ID: 031601.
<https://doi.org/10.1103/PhysRevLett.87.031601>
- [12] Deser, S. and Waldron, A. (2001) *Physics Letters B*, **508**, 347-353.
[https://doi.org/10.1016/S0370-2693\(01\)00523-8](https://doi.org/10.1016/S0370-2693(01)00523-8)
- [13] Deser, S. and Waldron, A. (2001) *Physics Letters B*, **513**, 137-141.
[https://doi.org/10.1016/S0370-2693\(01\)00756-0](https://doi.org/10.1016/S0370-2693(01)00756-0)
- [14] Deser, S. and Waldron, A. (2001) *Nuclear Physics B*, **607**, 577-604.
[https://doi.org/10.1016/S0550-3213\(01\)00212-7](https://doi.org/10.1016/S0550-3213(01)00212-7)

- [15] Deser, S. and Waldron, A. (2002) *Nuclear Physics B*, **631**, 369-387.
[https://doi.org/10.1016/S0550-3213\(02\)00199-2](https://doi.org/10.1016/S0550-3213(02)00199-2)
- [16] Deser, S. and Waldron, A. (2003) *Nuclear Physics B*, **662**, 379-392.
[https://doi.org/10.1016/S0550-3213\(03\)00348-1](https://doi.org/10.1016/S0550-3213(03)00348-1)
- [17] Deser, S. and Waldron, A. (2004) *Physics Letters B*, **603**, 30-34.
<https://doi.org/10.1016/j.physletb.2004.10.007>
- [18] Higuchi, A. (1987) *Nuclear Physics B*, **282**, 397-436.
[https://doi.org/10.1016/0550-3213\(87\)90691-2](https://doi.org/10.1016/0550-3213(87)90691-2)
- [19] Higuchi, A. (1989) *Nuclear Physics B*, **325**, 745-765.
[https://doi.org/10.1016/0550-3213\(89\)90507-5](https://doi.org/10.1016/0550-3213(89)90507-5)
- [20] Higuchi, A. (1987) *Journal of Mathematical Physics*, **28**, 1553.
<https://doi.org/10.1063/1.527513>
- [21] Eardley, D.M., *et al.* (1973) *Physical Review Letters*, **30**, 884.
<https://doi.org/10.1103/PhysRevLett.30.884>
- [22] Will, C.M. (2014) *Living Reviews in Relativity*, **17**, 4.
- [23] Will, C.M. (2006) *Living Reviews in Relativity*, **9**, 3.
- [24] Abbott, B.P., *et al.* (2018) *Physical Review Letters*, **120**, Article ID: 201102.
- [25] Fierz, M. and Pauli, W. (1939) *Proceedings of the Royal Society of London. Series A*, **173**, 211. <https://doi.org/10.1098/rspa.1939.0140>
- [26] Schutz, B.F. (1986) *Nature*, **323**, 310-311. <https://doi.org/10.1038/323310a0>
- [27] LIGO-VIRGO Collaborations (2017) *Nature*, **551**, 85.
- [28] Poulin, V., *et al.* (2019) *Physical Review Letters*, **122**, Article ID: 221301.
<https://doi.org/10.1103/PhysRevLett.122.221301>
- [29] Riess, A.G., *et al.* (2019) *The Astrophysical Journal*, **876**, 85.
<https://doi.org/10.3847/1538-4357/ab1422>
- [30] Deser, S. (2002) *International Journal of Modern Physics A*, **17**, 32-46.
<https://doi.org/10.1142/S0217751X02012995>

Calculation of the Spinning Speed of a Free Electron

Mesude Saglam¹, Burcin Bayram², Ziya Saglam³, Hanasli Gur⁴

¹Department of Physics, Faculty of Science, University of Ankara, Ankara, Turkey

²Department of Physics, Miami University, Oxford, OH, USA

³Department of Physics, Faculty of Science, University of Aksaray, Aksaray, Turkey

⁴Department of Engineering in Physics, Ankara University, Ankara, Turkey

Email: saglam@science.ankara.edu.tr

How to cite this paper: Saglam, M., Bayram, B., Saglam, Z. and Gur, H. (2020) Calculation of the Spinning Speed of a Free Electron. *Journal of Modern Physics*, 11, 9-15.

<https://doi.org/10.4236/jmp.2020.111002>

Received: November 2, 2019

Accepted: January 5, 2020

Published: January 8, 2020

Copyright © 2020 by author(s) and Scientific Research Publishing Inc.

This work is licensed under the Creative Commons Attribution International License (CC BY 4.0).

<http://creativecommons.org/licenses/by/4.0/>



Open Access

Abstract

In a recent work, we calculated the magnetic field inside a free electron due to its spin, and found it to be about $B = 8.3 \times 10^{13}$ T. In the present study we calculate the spinning speed of a free electron in the current loop model. We show that spinning speed is equal to the speed of light. Therefore it is shown that if electron was not spinning the mass of electron would be zero. But since spinning is an unseparable part of an electron, we say that mass of electron is non-zero and is equal to ($m = 9.11 \times 10^{-28}$ g).

Keywords

Spinning Speed, Intrinsic Current, Intrinsic Magnetic Field, The Intrinsic Flux of Electron, Current Loop Model

1. Introduction

Recently we have calculated the magnetic field inside a free electron due to spinning motion [1] and showed that it is about 8.3×10^{13} T. This field is about 8.3×10^{11} times bigger than the highest magnetic field obtained in today's laboratories [2] [3] and 10^3 times bigger than that in neutron stars (magnetars) [4] [5]. In that calculations [1], which are based on the current loop model, the intrinsic magnetic flux associated with its spinning motion of the electron which is calculated either by a semiclassical method or by a full quantum mechanical solution of Dirac equation [6] [7] [8] gives the same result: $\Phi_e^{(s)} = \pm hc/2e$. The current loop model is mainly based on the magnetic top model which was first introduced by Barut *et al.* [9] and used by N. Rosen [10] and L. Schulman [11]. But the magnetic top model was rather primitive as the spin vector was only attached

to that spherical charge distribution. To overcome this difficulty we introduced current loop model [6]. In this study using the current loop model we have found that: electron's spinning angular frequency, $\omega_s = 7.77 \times 10^{22}$ rad/sec. Most importantly through this model we had calculated magnetic flux associated with its spinning motion and we have found the above mentioned result: $\Phi_e^{(s)} = \pm hc/2e = \pm \Phi_0/2$ where (+) sign stands for spin-down electron and (-) sign for spin-up electron. Therefore the current loop model is the best one to describe the magnetic properties of the electron. Further we have found that the spinning speed of an electron is exactly equal to speed of light. Furthermore, if $v = c$, according to the relativity theory [12], the relativistic mass, m of a speedy particle will have a non-zero limit if and only if m_0 is zero:

$$m = \frac{m_0}{\sqrt{1 - \frac{v^2}{c^2}}} \quad (1)$$

where m_0 is the mass with zero speed. Therefore the Equation (1) can only be non-zero if and only if m_0 is zero. Since spinning is an unseperable part of electron we may say that mass of electron is non-zero and is equal to 9.11×10^{-28} g.

2. Formalism

As we said earlier the current loop model [6] is an idealistic model for a spinning electron. In this model the spinning electron is made equivalent to a circular current loop with the radius R in x - y plane and the electron motion is considered in two parts namely an "external" motion which can be interpreted as the motion of the center of mass (and hence the central of charge) and an "internal" one whose average disappears in the calssical limit. The latter is caused by the spin of the electron.

To calculate the quantum flux for any quantum orbit [6] we calculate the magnetic flux for one turn, then multiply it by the number of turns, during the cyclotron period T_c :

$$\Phi = \int \mathbf{B} \cdot d\mathbf{a} = \int_0^{T_c} \frac{\mathbf{B}}{2} \cdot \left(\mathbf{r} \times \frac{d\mathbf{r}}{dt} \right) dt = \frac{\omega_s}{\omega_c} \int_0^{T_c} \frac{\mathbf{B}}{2} \cdot \left(\mathbf{r} \times \frac{d\mathbf{r}}{dt} \right) dt = \frac{\omega_s}{\omega_c} \pi R^2 B \quad (2)$$

Here we distinguish spin angular frequency ω_s from the cyclotron frequency $\omega_c = eB/mc$. When an electron is placed in an external magnetic field B , during the cyclotron period T_c it completes one turn around the cyclotron orbit, but it spins (ω_s) times about itself (Figure 1) [13]. We will see that ($\omega_s \gg \omega_c$).

Now we want to look at the Equation (2) in detail: To consider the spin dependence in the flux expression [6], we assume that the spin angular momentum of electron is produced by the fictitious point charge ($-e$) rotating in a circular orbit with a radius R in x - y plane and an angular frequency, ω_s ; that is what we call the current loop model. In the presence of a magnetic field, $\mathbf{B} = B\hat{z}$ ($B > 0$), the vector going to this fictitious point charge can be written as:

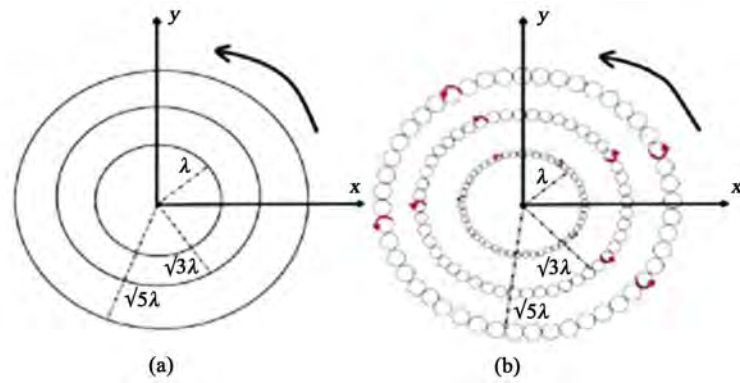


Figure 1. Landau orbits for electrons: (a) without spin; (b) in real space for spin-up electrons.

$$\dot{\mathbf{r}} = \mathbf{r} + \mathbf{R} \quad (3)$$

where \mathbf{r} is the vector going from origin to the centre of mass of the electron and \mathbf{R} is the vector going from centre of mass to this fictitious point charge ($R \ll r$). So the vector \mathbf{r} in Equation (3) reads:

$$\mathbf{r} = r \cos(\omega_c t + \mathcal{G}_c) \hat{x} + r \sin(\omega_c t + \mathcal{G}_c) \hat{y} \quad (4)$$

here \mathcal{G}_c is the angle at $t = 0$.

Depending on the spin orientation, the vectors $\mathbf{R}(\uparrow)$ and $\mathbf{R}(\downarrow)$ namely for spin up and spin down electrons read:

$$\mathbf{R}(\uparrow) = R \cos(\omega_s t + \mathcal{G}_s) \hat{x} - R \sin(\omega_s t + \mathcal{G}_s) \hat{y} \quad (5)$$

$$\mathbf{R}(\downarrow) = R \cos(\omega_s t + \mathcal{G}_s) \hat{x} + R \sin(\omega_s t + \mathcal{G}_s) \hat{y} \quad (6)$$

where \mathcal{G}_s is the angle at $t = 0$.

Here we distinguish the spin angular frequency ω_s from the cyclotron angular frequency $\omega_c = eB/mc$. During the cyclotron period, T_c electron completes one turn around the cyclotron orbit, but it spins ω_s/ω_c times about itself and hence the fictitious point charge completes ω_s/ω_c loops with the area πR^2 . It can be shown that the number of turns, $N = \omega_s/\omega_c$ is very large. We will see that $\omega_s = 7.77 \times 10^{22}$ rad/sec and $\omega_c = eB/mc$ can be made as small as possible. But if we take a huge magnetic field let us say for $B = 10$, $T = 10^5$ G then the value of ω_c becomes: $\omega_c \cong 1.76 \times 10^{12}$ rad/sec. Therefore we can say $\omega_s \gg \omega_c$.

If we take the time derivative of (3), we find the corresponding velocities:

$$\dot{\mathbf{v}} = \mathbf{v} + \mathbf{V} \quad (7)$$

Here \mathbf{v} and $\dot{\mathbf{v}}$ are the velocities of the electron itself and fictitious point charge ($-e$) with respect to the origin and \mathbf{V} is the velocity of the fictitious point charge with respect to the centre of mass of the electron.

Next, following Saglam and Boyacioglu [6], we can calculate the total magnetic flux $\Phi'(\uparrow)$ contained within the spinning orbit of the fictitious charge during

the time interval T_c :

$$\begin{aligned} \Phi'(\uparrow) &= \oint \mathbf{B} \cdot \frac{\mathbf{r} \times d\mathbf{r}}{2} = \oint_0^{T_c} \frac{\mathbf{B}}{2} \cdot (\mathbf{r}' \times \mathbf{v}') dt \\ &= \oint_0^{T_c} B [\omega_c r^2 - \omega_s R^2 + \text{cross terms}] dt \end{aligned} \tag{8}$$

where the cross terms contains the product of different angular frequencies like $\cos \omega_c t \cos \omega_s t \dots$ and so on. When we take the integral of cross terms, they vanish and the Equation (8) reduces to

$$\Phi'(\uparrow) = \frac{B}{2} [\omega_c r^2 - \omega_s R^2] \frac{2\pi}{\omega_c} = \pi r^2 B - \frac{\omega_s}{\omega_c} \pi R^2 B \tag{9}$$

As it is shown in [6] that the first term can be written as:

$$\pi r^2 B = \left(n + \frac{1}{2}\right) \Phi_0 = \left(n + \frac{1}{2}\right) \frac{hc}{e} \tag{10}$$

which is the quantum flux without considering electron spin. But the second term in Equation (9) is the contribution of spin to the total flux for spin-up electron. To calculate it we use Equation (20) of the following section:

$$\omega_s = \frac{\hbar}{mR^2} \equiv \frac{h}{2\pi mR^2} \tag{11}$$

Substituting Equation (10) and Equation (11) in Equation (9) and using the relation $\omega_c = eB/mc$ we find:

$$\Phi'(\uparrow) = \left(n + \frac{1}{2}\right) \frac{hc}{e} - \frac{hc}{2e} = \frac{nhc}{e} = n\Phi_0 \quad (n = 0, 1, 2, 3, \dots) \tag{12}$$

If we follow a similar procedure for spin-down electron the total flux for spin-down electron takes the form:

$$\Phi'(\downarrow) = \pi r^2 B + \frac{\omega_s}{\omega_c} \pi R^2 B \tag{13}$$

With a similar procedure we find:

$$\Phi'(\downarrow) = \left(n + \frac{1}{2}\right) \frac{hc}{e} + \frac{hc}{2e} = (n+1) \frac{hc}{e} = (n+1)\Phi_0 \quad (n = 0, 1, 2, 3, \dots) \tag{14}$$

From Equations (12) and (14) it is seen that the spin contribution to the total flux is $-\Phi_0/2$ for spin-up electron and $\Phi_0/2$ for spin-down electron:

$$\Phi(\uparrow) = -\frac{hc}{2e} = -\frac{\Phi_0}{2} \tag{15a}$$

$$\Phi(\downarrow) = \frac{hc}{2e} = \frac{\Phi_0}{2} \tag{15b}$$

Here the obtained net results show that the current loop model for electron spin is really a satisfactory model.

To proceed further we write the spin magnetic moment μ for a free electron [14]:

$$\mu = -g\mu_B \mathbf{S} \tag{16}$$

Here $\hbar\mathbf{S}$ the spin angular momentum of the electron.

When we introduce the magnetic field $\mathbf{B} = B_z \hat{z}$, the z -component of the magnetic moment for a spin-down electron [6] becomes ($g = 2$ for a free electron);

$$\mu_z = \frac{e\hbar}{2mc} \quad (17)$$

In the current loop model z -component of the magnetic moment for a spin-down electron is:

$$(\mu_e)_z = \frac{IA}{c} = \frac{eR^2\omega_s}{2c} \quad (18)$$

where $A = \pi R^2$ and R is the radius of the current loop. From Equation (17) and (18) we obtain:

$$R = \left(\frac{\hbar}{m\omega_s} \right)^{1/2} \quad (19)$$

If we solve ω_s , from Equation (19) we find the spinning angular velocity of electron in terms of the radius of the current loop, R :

$$\omega_s = \frac{\hbar}{mR^2} \quad (20)$$

Now with a rough approach we want to calculate spinning speed of electron in the current loop model. If we take the radius of this current loop equal to the electron radius, $R(el) = 2.82 \times 10^{-13}$ cm and the mass of electron, $m = 9.11 \times 10^{-28}$ g [15], from Equation (20) we find:

$$\omega'_s = 9.11 \times 10^{25} \text{ rad/sec} \quad (21)$$

and writing $v(el) = R(el)\omega'_s$ we find electron velocity as:

$$v(el) = 410 \times 10^{10} \text{ cm/sec} \quad (22)$$

which is larger than the speed of light, c . This is impossible! The reason for this is that the radius of the mentioned current loop is not equal to the electron radius. Therefore the right value of the radius of this current loop must be taken into account. We know that (please see the discussion section of [6]) the radius of the current loop is a dummy variable. As far as the flux calculations are concerned the radius R of the current loop is a phenomenal concept whose detailed calculation is not important. Therefore we chose the radius of this current loop such that the above speed should not exceed the speed of light, c .

$$v = R\omega_s = c \quad (23)$$

When we solve Equations (20) and (23) together we find:

$$R = 3.86 \times 10^{-11} \text{ cm} \quad (24)$$

and

$$\omega_s = 7.77 \times 10^{22} \text{ rad/sec} \quad (25)$$

So we can say that in the current loop model electron is spinning in a circular ring of radius $R = 3.86 \times 10^{-11}$ cm with the speed of light, c and with an angular

velocity $\omega_s = 7.77 \times 10^{22}$ rad/sec. Furthermore, since $v = c$, according to the relativity theory [12], the relativistic mass, m of a speedy particle will have a non-zero limit if and only if m_0 is zero:

$$m = \frac{m_0}{\sqrt{1 - \frac{v^2}{c^2}}} \quad (26)$$

That is to say; If the spinning speed is equal to the speed of light, c , the Equation (26) can only be non-zero if and only if m_0 is zero. Since spinning is an unseparable part of electron we may say that mass of electron is non-zero and is equal to the mass, $m = 9.11 \times 10^{-28}$ g.

3. Conclusions

We have calculated the spinning speed of a free electron in the current loop model which is a correct one as it produced the magnetic flux due to spin of electron as $\Phi_e^{(s)} = \frac{hc}{2e} = \Phi_0/2$.

By using the Equation (20) and $R\omega_s = c$, we were able to calculate the radius of this current loop R and cyclotron frequency, ω_s of electron on this current loop. These values are: $R = 3.86 \times 10^{-11}$ cm and $\omega_s = 7.77 \times 10^{22}$ rad/sec.

More importantly it is shown that if electron was not spinning the mass of electron would be zero. But since spinning is unseparable part of electron we say that mass of electron is non-zero and is equal to $m = 9.11 \times 10^{-28}$ g.

Conflicts of Interest

The authors declare no conflicts of interest regarding the publication of this paper.

References

- [1] Saglam, M., Sahin, G. and Gur, H. (2018) *Results in Physics*, **10**, 973. <https://doi.org/10.1016/j.rinp.2018.08.014>
- [2] <http://phys.org/news/2016-11-national-maglab-racks-world-hybrid.html>
- [3] <https://www.ru.nl/hfml/facility/experimental/magnets>
- [4] Potekhin, A.Y., Yakovlev, D.G., Chabrier, G. and Gnedin, O.Y. (2003) *The Astrophysical Journal*, **594**, 404-418. <https://doi.org/10.1086/376900>
- [5] Alaa, I.I., Swank, J.H. and William, P. (2003) *The Astrophysical Journal*, **584**, L17-L21. <https://doi.org/10.1086/345774>
- [6] Saglam, M. and Boyacioglu, B. (2002) *International Journal of Modern Physics B*, **16**, 607. <https://doi.org/10.1142/S0217979202010038>
- [7] Wan, K. and Saglam, M. (2006) *International Journal of Theoretical Physics*, **45**, 1132. <https://doi.org/10.1007/s10773-006-9118-z>
- [8] Yilmaz, O., Saglam, M. and Aydin, Z.Z. (2007) *Old and New Concepts of Physics*, **4**, 141. <https://doi.org/10.2478/v10005-007-0007-x>
- [9] Barut, A.O., Bozic, M. and Maric, Z. (1992) *Annals of Physics*, **214**, 53. [https://doi.org/10.1016/0003-4916\(92\)90061-P](https://doi.org/10.1016/0003-4916(92)90061-P)

- [10] Rosen, N. (1951) *Physical Review*, **82**, 621. <https://doi.org/10.1103/PhysRev.82.621>
- [11] Schulman, L. (1968) *Physical Review*, **176**, 1558. <https://doi.org/10.1103/PhysRev.176.1558>
- [12] Griffiths, D.J. (1999) *Introduction to Electrodynamics*. 3rd Edition, Prentice-Hall, London.
- [13] Saglam, Z. and Boyacioglu, B. (2018) *Acta Physica Polonica A*, **133**, 1129-1132. <https://doi.org/10.12693/APhysPolA.133.1129>
- [14] Sakurai, J.J. and Napolitano, J. (2010) *Modern Quantum Mechanics*. 2nd Edition, Pearson Education Inc., London.
- [15] Feynman, R.P. and Leighton, R.B. (1964) *Matthew Sands*. 4th Edition, Addison Wesley Publishing Company, Boston.

Electromagnetism According to Maxwell's Initial Interpretation

André Michaud

Service de Recherche Pédagogique, Québec, Canada

Email: srp2@srpinc.org

How to cite this paper: Michaud, A. (2020) Electromagnetism According to Maxwell's Initial Interpretation. *Journal of Modern Physics*, 11, 16-80.

<https://doi.org/10.4236/jmp.2020.111003>

Received: December 6, 2019

Accepted: January 7, 2020

Published: January 10, 2020

Copyright © 2020 by author(s) and Scientific Research Publishing Inc. This work is licensed under the Creative Commons Attribution International License (CC BY 4.0).

<http://creativecommons.org/licenses/by/4.0/>



Open Access

Abstract

It is well established that classical electrodynamics, quantum electrodynamics (QED) as well as Quantum Field Theory (QFT) are grounded on Maxwell's wave theory and on his equations, but it is much less well understood that they are not grounded on his initial interpretation of the relation between the \mathbf{E} and \mathbf{B} fields, but are rather grounded on Ludvig Lorenz's interpretation of this relation, with which Maxwell disagreed. Maxwell considered that both fields had to mutually induce each other cyclically for the velocity of light to be maintained while Lorenz considered that both fields had to synchronously peak at maximum at the same time for this velocity to be maintained, both interpretations being equally consistent with the equations. Two recent breakthroughs however now allow confirming that Maxwell's interpretation was correct because, contrary to the Lorenz interpretation, it allows to seamlessly reconcile Maxwell's electromagnetic wave theory, so successfully applied at our macroscopic level, with the electromagnetic characteristics that apply at the subatomic level to localized electromagnetic photons and to all localized charged and massive elementary electromagnetic particles of which all atoms are made, and finally allows establishing a clear mechanics of electromagnetic photon emission and absorption by electrons during their interaction at the atomic level.

Keywords

Magnetic Mass, Magnetic Field, Electric Field, Electron, Photon Emission, Photon Absorption

1. Introduction

In 1845, Michael Faraday observed that by placing a glass plate between the poles of an electromagnet, the magnetic field caused the polarization plane of the

light passing through the plate to rotate. He immediately informed his friend James Clerk Maxwell of this major discovery that demonstrated for the first time the direct relation between the magnetic field and light [1].

It is therefore this specific experiment by Faraday which is at the origin of the integrated electromagnetic theory then developed by Maxwell, because, having already observed that second derivatives of the previously established equations for the electric field and the magnetic field revealed that electric energy and magnetic energy were separately associated with the speed of light [2], Maxwell concluded that light had to be electromagnetic in nature and then made the fundamental discovery that electromagnetic energy implied a three-way orthogonal relationship between its three fundamental aspects; that is, its electric and magnetic aspects, perceived as being perpendicular to each other and simultaneously inducing each other in a cyclic transverse stationary oscillating motion, with respect to the direction of motion of this energy in space (see **Figure 1**); that is, a three-way orthogonal relationship corresponding to the familiar vector cross product of the \mathbf{E} and \mathbf{B} fields, resulting in a third motion vector structurally perpendicular to the first two [3] [4].

The following fact may come as a surprise to many, but this solution discovered by Maxwell, who is also well known for having derived the speed of light from the relation that he established between the two fundamental constants of vacuum ϵ_0 and μ_0 [2], is not the only working solution that was discovered to relate both \mathbf{E} and \mathbf{B} fields to the speed of light.

Briefly summarized, mathematician Ludvig Lorenz established independently from Maxwell that if both \mathbf{E} and \mathbf{B} fields representations of free moving electromagnetic energy are mathematically made to peak to maximum synchronously at the same time, this also allows explaining the speed of light in vacuum of electromagnetic waves as well as if both fields are 180 degrees out of phase as in Maxwell's solution.

But the “Lorenz gauge” is a generalizing concept, that regroups both \mathbf{E} and \mathbf{B} aspects of fundamental energy into a “single” electromagnetic field that distracts from immediate attention the different vectorial orientations of both aspects, particularly the fact that the energy dipole represented by \mathbf{E} becomes spacewise oriented and distributed while the energy dipole represented by \mathbf{B} becomes

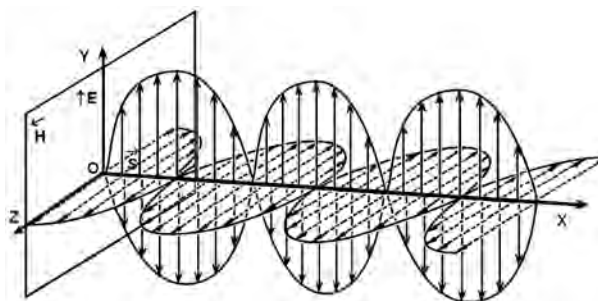


Figure 1. Mutually inducing 180° out of phase bipolar representation of \mathbf{E} and \mathbf{B} fields of Maxwell's interpretation.

timewise oriented and distributed as they cyclically mutually induce each other transversely to the vectorial direction of motion of the oscillating energy in vacuum.

The representation of **Figure 2**, which is found in all textbooks on electromagnetism, while agreeing with Maxwell's wave theory describing electromagnetic energy as a pulse propagating in an underlying aether, and which is also in agreement with his equations, is however generally and incorrectly assumed as also being Maxwell's conclusion.

Indeed, Maxwell disagreed with this approach, because the concept of "gauge" developed by Lorenz had the consequence of treating both fields \mathbf{E} and \mathbf{B} as a *single electromagnetic field* at the general level, without any apparent internal structure at first glance, which easily obscures the fact that both fields are of equal and separate importance in Maxwell's theory, with different and irreconcilable characteristics, in addition to mutually inducing each other, contrary to the Lorenz solution, as put in perspective in reference [3].

The fact that this second solution was developed by Lorenz, however, is not well known in the scientific community because it is specifically associated only to the so-called *Lorenz gauge* defined by him, and this, only in high level specialized reference works on electromagnetism [5], because it lends itself more easily than Maxwell's representation to various mathematical generalization processes, but the true origin of the solution represented by **Figure 2** is not clearly explained in introductory textbooks and general reference works on physics [6] [7].

Consequently, unless they specialize in electromagnetism, most physicists are not directly informed that it was not Maxwell who developed this second approach, and that classical electrodynamics and quantum field theory (QFT), from which quantum electrodynamics (QED) emerged [8] [9] are in reality grounded on Lorenz's interpretation, because this fact is nowhere clearly highlighted in reference works on electrodynamics and QFT, which were of course developed by specialists in electromagnetism for whom this fact was obvious. So contrary to established facts, the outcome is a general impression in the community that Maxwell is also the author of this second solution and that electrodynamics and QFT are grounded strictly on Maxwell's theory.

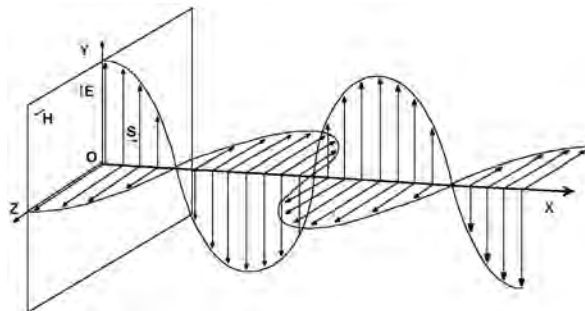


Figure 2. Standard simultaneously in phase peaking \mathbf{E} and \mathbf{B} fields monopolar representation of Lorenz's interpretation.

The distinction to be made is important however, because de Broglie's hypothesis about the localized double-particle photon that emerges directly from Maxwell's solution is consequently at odds with classical electrodynamics and QED, because the Lorenz approach obscures the fact that both \mathbf{E} and \mathbf{B} fields are of equal and separate importance. For example, the predominant role given to the electric charges in QED seems to leave no precise function to the magnetic aspect of electromagnetic energy in a possible mutual induction mechanics that would involve the two separate fields, contrary to Maxwell's interpretation. Even the fact that as formulated, QED cannot explain the mutual induction of both fields in LRC systems doesn't seem to attract attention to this issue.

2. Setting up the Perspective According to Relative Magnitude Levels

To put in correct perspective the possibility of describing the energy which is the very substance of which all localized elementary particles such as electromagnetic photons, electrons and positrons are made at the subatomic level, in a manner that would not conflict with the well established Maxwell continuous wave electromagnetic theory, which is so successfully applied at our macroscopic level, it must first be realized that all objects and processes that we can detect and measure in objective reality can be categorized as belonging to one of the following four orders of magnitude. In decreasing order of amplitude, these orders of magnitude can be defined very generally as follows:

- 1) *Astronomical level*: Order of magnitude exceeding the dimensions of planet Earth.
- 2) *Macroscopic level*: Order of magnitude in which any object or process can be directly measured at the Earth's surface and its environment.
- 3) *Sub-microscopic or atomic level*: Order of magnitude of molecules and atoms.
- 4) *Subatomic level*: Order of magnitude of the elementary particles of which the atoms are made, as well as the electromagnetic energy of which their substance is made, that supports their motion, determines their inertia, and that can also circulate freely in quantized form at the speed of light when not directly associated with one of these elementary particles.

The first 3 levels are generally familiar to all, but the subatomic level is not. We can directly perceive and measure objects and processes in our environment at the macroscopic level, and we indirectly perceive and measure objects and processes of other orders of magnitude with increasing precision as our instruments improve.

It may seem paradoxical to so firmly assert that electromagnetic energy can be directly defined as being quantized as localized electromagnetic photons at the subatomic level in full accordance with Maxwell's equations while remaining in complete harmony with his continuous electromagnetic waves theory which has been so successfully applied at our macroscopic level, which is an issue that has been the object of a continuous debated for the past hundred years.

It must be put in perspective here that we perceive however no paradox whatsoever with the fact that “*we directly observe*” that the image on a TV screen appears smoothly continuous as seen from a few meters, while being well aware that if we get close enough, “*we also directly observe*”, directly at our macroscopic level, that in physical reality, the image is physically generated by thousands of clearly separated rows of clearly separated very small pixels.

Interestingly, we find no paradox either in treating water as a fluid without any internal structure at our macroscopic level, while being well aware that at the submicroscopic level, it is made only of localized molecules, themselves made of localized atoms, themselves made at the subatomic level of localized elementary electrically charged electrons plus nucleons, themselves made of localized electrically charged elementary particles, that all are individually massive and quantized, even if we cannot directly see these molecules at our macroscopic level as in the case of the TV screen.

The reason why we see no problem in perceiving and treating water as a fluid at the macroscopic level, even mathematically, even if we cannot directly observe the localized molecules of which its substance is made, as we can directly do with the individual pixels of the TV screen, is that we understand that what we perceive as the “*fluidity*” of water at our macroscopic level is in reality a “*crowd effect*” due to countless localized water molecules smoothly sliding against each other at the submicroscopic level. Moreover, our powerful modern instruments of electronic microscopy allow us to indirectly detect these individual molecules and the atoms of which they are made at the submicroscopic level.

In the case of electromagnetic energy, however, its granular nature at the subatomic level is far from being as obvious to perceive as in the case of the television screen, in which to approach the image by only a few meters, is sufficient, to go from the order of magnitude that lets us perceive it as an apparently uniformly fluid image to the slightly lower order of magnitude still at the macroscopic level that makes it possible to perceive the reality of its granular structure when directly observed at greater proximity; or in the case of water, whose granularity at the atomic level can be indirectly observed with our electron microscopes.

The case of water obviously requires an even greater jump in orders of magnitude towards the infinitely small scale between the perception of its fluidity at the macroscopic level and the perception of its submicroscopic granularity. To really become aware of the difference between these two orders of magnitude, it suffices to think that the atoms making up water molecules are as far away towards the extremely small submicroscopic level that the galaxies are far towards the infinitely large astronomical level with respect to our own terrestrial macroscopic level. But to perceive the subatomic granularity of electromagnetic energy, the jump from our macroscopic order of magnitude is larger yet; as far in fact, further down towards the infinitely small from the already far order of magnitude of the atomic scale than this atomic scale is far from our own macroscopic level.

To really conceptualize how far down from the atomic scale the granularity of electromagnetic energy actually is, let's consider that if the proton of a hydrogen atom, two of which are part of a water molecule, was enlarged to become as big as the sun, the electron which is stabilized in its least action orbital distance from the proton would then be as far away from this enlarged proton as the orbit of Neptune is from the Sun in the Solar system, meaning that the hydrogen atom would become as large as the entire Solar System, and that the electromagnetic photons that constitute the "granular level" of electromagnetic energy is of the same order of magnitude as the energy making up the rest mass of the electron and of the other massive elementary electrically charged electromagnetic particles that exist inside the structure of the proton and of the neutron.

The main problem that we are confronted with regarding this subatomic level of granularity of electromagnetic energy and of the energy constituting the rest masses of elementary particles of which atoms are made, is that there exists no instrument powerful enough that would allow observing even indirectly this subatomic level, unlike the deepest level at which it remains physically possible, which is the atomic order of magnitude, that allows indirectly verifying the granularity of water and of all the other material substances of our environment; in short, an indirectly verifiable granularity of all atoms of the periodic table, which is unavailable for the subatomic granularity level of electromagnetic energy.

The only physically verifiable telltales that we have of the permanent localization of elementary charged particles such as the electron and of electromagnetic energy quanta are the following:

1) We have easily reproducible experimental proof that electrons and electromagnetic photons systematically behave almost point-like during all scattering experiments (see Section 23 further on and reference [10]).

2) We have easily reproducible proof that photons have longitudinal inertia as demonstrated by Einstein photoelectric experiment, and that they have transverse inertia amounting to half their longitudinal inertia, as demonstrated by the deflexion angle of light by the Sun during numerous experiments carried out during solar eclipses [3] [11].

3) We also have experimental proof since 1933 that electromagnetic photons of 1.022 MeV or more convert into electron-positron pairs when they graze massive particles [12] and that such pairs reconvert to electromagnetic photons when meeting again; which means that we have the experimental proof that the invariant mass of electrons and positrons is made up of the same "*electromagnetic energy substance*" as electromagnetic photons. We also have experimental proof since 1997 that electromagnetic photons that exceed the 1.022 MeV energy threshold level can be destabilized into converting to electron-positron pairs by other electromagnetic photons, without any massive nuclei being close by [13].

4) We have easily reproducible experimental proof that free moving electrons have an invariant rest mass of $9.10938188E-31$ kg and an invariant electric charge of $1.602176462E-19$ C.

5) We have conclusive experimental evidence that electrons are elementary

particles and that the protons and neutrons that constitute the nuclei of all atoms are not elementary particles, but rather are systems of elementary particles (see **Figure 5-7**, and reference [10]).

Since the subatomic level cannot be directly nor indirectly observed, we are therefore necessarily reduced in our exploration of this level to proceed by reverse engineering [4], meaning that we must deduce the characteristics of the elementary electromagnetic particles that constitute the fundamental level of objective reality from what we can indirectly detect and understand from the behaviour of atoms, and from the behaviour of the elementary particles that can be separated from them; *i.e.* electrons whose stabilization far from the nuclei determines the volume of space occupied by atoms, and from the behaviour of protons and neutrons that constitute their nuclei by occupying smaller volumes; as well as from the behaviour of the electromagnetic energy which is emitted or absorbed by these elementary particles during their transitions between the various stationary action equilibrium states in which atoms stabilize at the atomic level.

Finally, the means we have at our disposal to observe the behavior of atoms and their separable elements is precisely the electromagnetic energy which is emitted or absorbed during these stationary action equilibrium states variations, and whose “*infinitesimal granules*”, *i.e.* these localized electromagnetic photons coming from all objects in our surrounding, either directly from these objects or detected through our powerful microscopes and other sensing devices, that excite electrons from the atoms forming the photosensitive cells in our eyes, an excitation which is then progressively transmitted along our optic nerves to the brain that continuously updates the images of which we become aware from our environment and that we analyze to understand it [14].

These localized electromagnetic photons that can excite electrons sufficiently in the cells of our eyes for their arrival to be progressively signalled all along the optic nerve, can be of very variable intensities, and above a certain intensity level, succeed in separating the electrons from the atoms in our environment, and this is what allows us to study their separate behavior as well as that of the constituents of atomic nuclei, namely protons and neutrons, which can be completely separated from their electronic escorts and studied separately in the case of simple atoms such as hydrogen or helium atoms.

What was preventing us up to now from becoming as comfortable treating electromagnetic energy as being granular, that is quantized, at the subatomic level, as we are handling it as continuous electromagnetic waves at our macroscopic level, is that since about a hundred years, the quantized aspects of the subatomic level have been considered being the exclusive domain of Quantum Mechanics (QM), but that QM still has not been fully harmonized with Maxwell's electromagnetic equations, that successfully handle electromagnetic energy as a continuous wave at our macroscopic level; in other words, that treats it as a fluid, which is an incomplete harmonization that was clearly highlighted by Feyn-

man, who was the last researcher to attempt this reconciliation in the mid 20th century, as evidenced by this quote from his “*Lectures on Physics*” [15]:

“There are difficulties associated with the ideas of Maxwell’s theory which are not solved by and not directly associated with quantum mechanics... when electromagnetism is joined to quantum mechanics, the difficulties remain”.

As put in perspective in a recent article [16], all current theories mathematically treat macroscopic masses as if they had no internal granular structure, that is, as if they were made of a continuous substance uniformly spread within their whole volume, and even Quantum Mechanics currently treats the electron energy as if it was uniformly spread in the same manner within the volume defined by the Schrödinger equation. The reason for this is that the internal electromagnetic structure of the energy making up the mass of each elementary particles of which all macroscopic masses are made, such as the electron, as well as the internal electromagnetic structure of those making up the inner structures of the protons and neutrons, that constitute the nuclei of all atoms in the universe, have not yet been clearly established; and that the momentum energy as well as the energy causing the increase of the transverse magnetic field of accelerating particles have not yet been mathematically separated from the energy of which their rest masses are made.

Recently, however, new developments have made it possible to establish a coherent internal subatomic electromagnetic structure for localized electromagnetic photons and for all elementary electromagnetic particles in accordance with Maxwell’s equations, which finally makes it possible to find natural the perception that all atoms are made at the subatomic level of separate and localized elementary particles stabilized in various states of stationary action electromagnetic resonance states and that free moving electromagnetic energy is quantized at the subatomic level, even if we treat it as a continuous wave at our macroscopic level.

3. Two Recent Major Breakthroughs

Already in the 1930’s, Louis de Broglie proposed the hypothesis of a possible potentially quantized internal structure for localized electromagnetic photons at the subatomic level that would remain conform to Maxwell’s equations, but whose elaboration, by his own admission, seemed not to be possible in the restricted frame of the 4-dimensional geometry of Minkowski’s space-time [17]:

“...la non-individualité des particules, le principe d’exclusion et l’énergie d’échange sont trois mystères intimement reliés: ils se rattachent tous trois à l’impossibilité de représenter exactement les entités physiques élémentaires dans le cadre de l’espace continu à trois dimensions (ou plus généralement de l’espace-temps continu à quatre dimensions). Peut-être un jour, en nous évadant hors de ce cadre, parviendrons-nous à mieux pénétrer le sens, encore bien obscur aujourd’hui, de ces grands principes directeurs de la nouvelle physique” ([17], p. 273).

Translation:

“...the non-individuality of particles, the exclusion principle and exchange energy are three intimately related enigmas; all three are tied to the impossibility of exactly representing elementary physical entities within the frame of continuous three dimensional space (or more generally of continuous four dimensional space-time). Some day maybe, by escaping from this frame, will we better grasp the meaning, still quite cryptic today, of these major guiding principles of the new physics”.

Two recent developments, however, made it possible to elaborate this internal electromagnetic structure of the localized photon proposed by de Broglie in full conformity with the Maxwell equations, and to eventually observe that all stable massive and electrically charged elementary particles of which all atoms are made at the subatomic level can also be described in the same Maxwell compliant manner.

The new light shed by these recent developments on the nature of fundamental electromagnetic energy then made it possible to refocus according to this new perspective the bulk of the conclusions drawn in the past from all experimental data collected to date about the subatomic level. These refocused conclusions were then explained in about twenty separate articles, each of which analyses a specific aspect of the issue, most of which will be given in reference during this final synthesis.

4. The First Major Breakthrough

The first of these two breakthroughs was the elaboration of a more extensive geometry of space, based on the three-way orthogonal relationship that Maxwell related to the three fundamental aspects of electromagnetic energy of which light is made at the subatomic level, namely its electrical and magnetic aspects perceived as being perpendicular to each other and mutually inducing each other into a standing cyclic transverse oscillation mode of the energy that these fields measure with respect to the direction of motion in vacuum of this transversely oscillating electromagnetic energy in space, that is, a direction of motion of this energy which is perpendicular to the direction of the stationary transverse oscillation of the energy represented by the two fields (see **Figure 1**).

The trispatial geometry (see **Figure 3**) required to develop the LC equation derived from the de Broglie hypothesis [3] in accordance with Maxwell's interpretation (**Figure 1**) was formally presented at the event Congress-2000 in July 2000 at St Petersburg State University [18].

This expanded space geometry at the subatomic level is fully described in reference [4], but can be briefly summarized as follows. The method consists in geometrically expanding each of the 3 standard linear electromagnetic vectors i , j and k (**Figure 3(a)**), applicable to normal space, transforming them into 3 fully developed 3D vector spaces of their own (**Figure 3(b)**), each of these three spaces, now identified as spaces X , Y and Z (**Figure 3(c)**), each space remaining

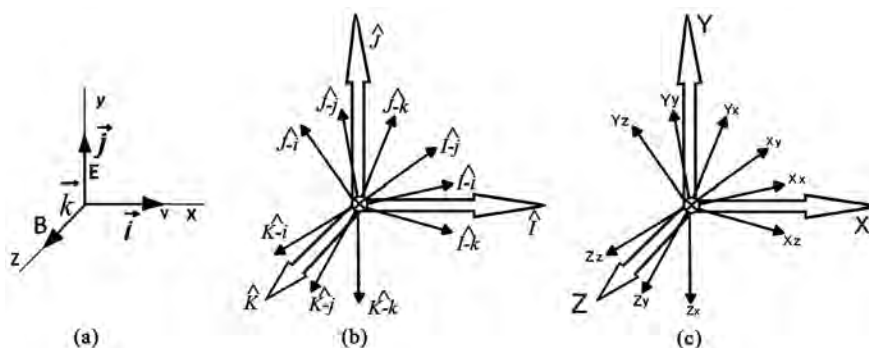


Figure 3. Major and minor vectors sets applicable to the trispatial geometry.

perpendicular to the other two and all three remaining connected via their common punctual origin.

This common centre can now be understood as serving as a passage point located at the centre of each localized electromagnetic quantum at the subatomic level, through which the “*energy substance*” of the particle would be free to circulate between the three spaces as if between communicating vessels, so as to allow the establishment of a stationary transverse oscillation of half the particle energy between its \mathbf{E} and \mathbf{B} aspects between the two YZ -spaces, as well as an equal sharing of the total energy of the particle between the transversely oscillating energy half-quantum of the \mathbf{E} and \mathbf{B} fields within the YZ -transverse-dual-space-complex, and the unidirectional energy half-quantum of the momentum of the particle residing in X -space.

To mentally visualize the motion of energy in this trispatial geometric complex of 9 mutually orthogonal dimensions, it suffices to imagine each of the 3 sets of minor vectors \mathbf{i} , \mathbf{j} and \mathbf{k} of **Figure 3(b)** as if they were the folded ribs of 3 metaphorical umbrellas. This allows any of them to be mentally opened at will one at a time up to full orthogonal expansion to observe and mathematically describe the behavior of energy in this fully deployed 3D space during each phase of its oscillating motion. **Figure 3(b)** and **Figure 3(c)** show the dimensions of the 3 spaces only half-deployed to allow a clear and unique identification of each of the 9 resulting internal orthogonal axes.

5. The Second Major Breakthrough

The second major development occurred a few years later, in 2003, when Paul Marmet published an important article describing a newly perceived relation between the progressive increase of the intensity of the transverse magnetic field of an accelerating electron and the simultaneous increase of its transversely measurable mass [19], that then allowed clearly distinguishing between the variable energy of the electron momentum that also increases during its acceleration, and the also variable energy of its transverse magnetic field, and also to clearly separate these two variable energy quantities from the invariant energy constituting the electron rest mass as described in an article published in 2007 in the same “*International IFNA-ANS Journal*” at Kazan State University [20].

This discovery then allowed observing that all charged elementary particles constituting atoms have the exact same internal electromagnetic LC structure in this expanded space geometry, each one being accompanied by an amount of carrying energy made of momentum energy and transverse magnetic field energy, which is structured in a manner identical to the internal electromagnetic structure described by the LC equation developed to account for localized double-particle photons as hypothesized by de Broglie [3] [21] [22] [23], which then allowed establishing their respective trispatial LC equations, as summarized in reference [4], as we will see further on.

Let us note here that this internal electromagnetic LC structure is also applicable to all of the electrically charged elementary electromagnetic particles constituting the complex unstable particles, be they electrically neutral or not, such as pions, kaons and other ephemeral complex particles resulting from destructive scattering between elementary particles [24].

We will study here however only the stable particles making up the scatterable structure of the set of atoms that can be found in the periodic table and of their nuclei, as well as positrons and free moving electromagnetic photons, because all of the unstable partons generated via destructive scattering play no role whatsoever in the establishment and stability of the universe, since they all almost instantly decay by releasing their excess energy in well known sequences of stages [25], until all that remains of them is one or other, or many of the very restricted set of stable electrically charged and massive elementary particles making up all atoms [24].

But attention must first be given to a typographical error in Equation (M-7) of Marmet's article that renders the seamlessness of his derivation difficult to perceive. For his unbroken sequence of reasoning to be made clear, his derivation down to Equation (M-7) from the Biot-Savart equation will be fully detailed here. The remainder of his derivation down to Equation (M-23) remains easy to follow directly in his article [19] and is also clearly explained and analyzed in another recently published article [4].

Although the second part of his article starting with Section 7 elaborates a personal hypothesis on a possible inner structure of the electron, which is of course subject to discussion, the first part of his article is in no way hypothetical, but rather elaborates a mathematically seamless derivation from the Biot-Savart equation, itself established directly from experimental data that can easily be re-obtained at will, that leads to the establishment of a new Equation (his equation M-23) that effectively seems to leave no doubt, quoting Marmet himself, that: "*the increase of the so-called relativistic mass [of an accelerating electron] is in fact nothing more than the mass of the magnetic field generated due to the electron velocity*" [19]:

$$\frac{\mu_0 (e^-)^2}{8\pi} \frac{1}{r_e} \frac{v^2}{c^2} = \frac{M_e}{2} \frac{v^2}{c^2} \quad (\text{M-23})$$

To avoid any confusion in the numbering of equations in the present article,

all equations quoted from Marmet's paper will be prefixed with "M-" followed by the actual number of this equation in the original paper [19], so readers can directly relocate them in his paper.

Equation (M-23) suggests numerous possibilities that never were considered before, the most important of which is that it highlights an inconsistency between the Special Relativity Theory (SR) and electromagnetism that could not be noticed otherwise, because the very idea that the energy that progressively increases the transverse magnetic field of an accelerating electron, as calculated with the equations of electromagnetism, could be the same energy measurable as its transverse mass progressively increasing with velocity, as calculable with the equations of relativistic mechanics, is absent from SR for a reason that will be highlighted later.

The first clue suggesting the possibility that a single quantum of energy might be responsible at the same time for the increase of the electron's transverse magnetic field and for the increase of its transversely measurable relativistic mass, is established by the well-known fact that the magnetic field, as measured around a wire conducting a stable electric current, which is of course made of electrons circulating all at the same velocity and in the same direction in the wire, is oriented perpendicularly, that is, transversely, with respect to the direction of motion of the electrons, which is what the Biot-Savart law accounts for, as put into perspective by Marmet at the beginning of his article [19].

An important point must already be highlighted regarding the habit acquired since Maxwell to think of the familiar three-way orthogonal relationship of electromagnetic energy as involving electric and magnetic "*fields*" perpendicular to each other, that would be at the same time perpendicular to the direction of motion of the energy.

It is a fact seldom mentioned in reference works that the idealized concept of the "*electric field*" was introduced by Gauss as an "*idealized geometrical and mathematical conceptual representation*" of the Coulomb interaction diminishing omnidirectionally towards zero at infinity according to the inverse square of the distance rule, from a maximum value located at the point in space where the single test charge remaining in the Coulomb equation would be located when the second charge is removed from the equation, as highlighted in a recent article [14]. This idealized concept was then also conceptualized geometrically and mathematically to represent in the form of a "*magnetic field*" the magnetic aspect of electromagnetic energy.

It will therefore be important for the remainder of this analysis to keep in mind Gauss's original intention that these "*fields*" should be considered only as "*idealized geometrical and mathematical tools*" intended only to "*represent*" the real energy which is deemed to physically exist, and that it is the electromagnetic energy itself that physically exists that would physically self-structure, so to speak, according to this dual perpendicular pattern resulting from its transverse electromagnetic oscillation, that is, an oscillation which is transversely oriented with respect to the unidirectional momentum energy that sustains its motion in

space.

It follows that the transverse energy itself that Marmet's derivation identifies as simultaneously accounting for the transverse magnetic field increase and the measurable transverse relativistic mass increase of the accelerating electron, can therefore only be oriented perpendicularly to the direction of motion of the electrons whose circulation generates the stable current measurable via the Biot-Savart equation.

This of course means that the energy that supports the increasing momentum of an accelerating electron, that can be calculated with relativistic mechanics equation " $\Delta K = \gamma m_0 v^2 / 2$ ", can in no way be the same as the energy that perpendicularly supports its increasing transverse magnetic field that can be calculated by means of the Biot-Savart equation, the latter now presumably corresponding to the energy of the transverse relativistic mass increment computable with the relativistic mechanics equation " $\Delta E = \Delta m c^2 = (\gamma m_0 c^2 - m_0 c^2)$ ", because it is physically and vectorially impossible for a single energy quantum to move in both of these two perpendicular directions simultaneously, and also because the total amount of only one of these two energy quantities is insufficient to single-handedly account for the simultaneous energy increase of both its longitudinal momentum and of its transverse magnetic field at any given velocity.

On the other hand, Maxwell's first equation, which is in fact Gauss's equation previously mentioned for the electric field, and that reconverts to the simple Coulomb equation when a second charge is introduced in the "idealized field" of the test charge, reveals that the total amount of energy induced in each accelerating charge amounts to twice the energy of the longitudinal momentum " $\Delta K = \gamma m_0 v^2 / 2$ ", or alternatively, to twice the energy of the transverse relativistic-mass/magnetic-field increment " $\Delta E = \Delta m_m c^2$ ". More to the point, this reveals that both amounts are always equal by structure and that this sum can only be made of their simultaneously induction, in which " ΔE " also accounts for the accelerating electron transverse magnetic field increment, both quantities thus making up the total amount of energy required to account for the simultaneous increase of the velocity and of the related transverse magnetic field, that is, " $\Delta E = \Delta K + \Delta m_m c^2 = \gamma m_0 v^2 / 2 + (\gamma m_0 c^2 - m_0 c^2)$ ", as demonstrated in reference [4].

We should therefore rather speak in reality of two energy "*half-quanta*" constituting a single quantum of induced energy. The fact that this total quantum of energy calculated with the Coulomb equation varies in an infinitesimally progressive manner uniquely as a function of inverse of the distance separating two charged particles, also demonstrates that this energy varies adiabatically, and this, uniquely as a function of the inverse of the distances separating all charged particles from each other on account of to the Coulomb interaction, whether they are moving or not.

An additional clue supporting the conclusion that these two energy half-quanta have to exist simultaneously, is that to even be able to calculate the $\Delta \mathbf{B}$ magnetic field increment related to any velocity of an accelerating electron with the gene-

ralized form of Marmet's Equation (M-7) established in reference [20], it is the wavelength of this double amount of energy given by the Coulomb equation that must be used to obtain this correct ΔB value of the transverse magnetic field increment of the moving electron, which will be demonstrated with Equation (9) further on.

6. Historical Context of the Development of the Theory of Special Relativity

But the very fact that these two energy half-quanta are always equal in quantity initially induced confusion in the community in the absence of this new information available only since Marmet's recent derivation. This confusion led to considering that a total amount corresponding to only one of these two half-quanta was induced during the electron relativistic acceleration process, which gave rise to a famous disagreement among the theoreticians of the beginning of the 20th century.

For example, Minkowski [26], Lorentz [27] and Einstein [28] related this half-quantum of energy strictly to momentum, a conclusion which is an integral part of the Theory of Special Relativity (SR), while Abraham [29], Poincaré [30] and Planck [31] related the half-quantum of measured motion energy strictly to an increase in the transversely measurable mass.

7. The Conclusion of Minkowski, Lorentz and Einstein

By consulting a famous article by Max Planck dating from 1906 [31], it can be noted that he refers to the energy constituting the mass of a moving electron " $E = \gamma m_0 c^2$ " by the terms "*lebendige Kraft*" (see his comment following Equation 8, page 140 of his text, identifying this energy by the term " L "), which is translated in the fundamental physics community by the terms "*kinetic force*" (or "*vibrating force*" or "*live force*" for a literal translation from German), which puts in perspective that at the beginning of the 20th century, the relation between the concept of "*force*", such as the force calculable with the Coulomb equation or with the fundamental mass acceleration equation " $F = ma$ ", that we conceptualize as having dimensions "*joules per meter*" [2], and the concept of "*energy induced by the Coulomb force*", which is obtained by multiplying the Coulomb force by the distance between two electric charges, and that we conceptualize as being in "*joules*" only [2], was not yet clearly established. The only reference to momentum in his text is "*Impulskoordinaten*" ("momentum coordinates"), which he does not associate with the energy that supports it in context of the ongoing debate at that time, and this at the very historical moment when this debate about the introduction of the SR Theory was raging.

By comparison, in the German fundamental physics community today, the momentum "*Impuls*" is immediately conceptualized as a quantity of kinetic energy "*kinetische Energie*" moving in a specific vectorial direction, as in the physical communities of other languages. Few today are fully aware that at the

beginning of the 20th century, the greatest advances in fundamental physics were made in Europe, and that the original articles were written mainly in German, but also in French and Italian, and that some of these founding articles have still not been formally translated to English, contrary to popular belief, and some very belatedly. For example, the text of a seminal presentation by Herman Minkowski from 1907, “*Das Relativitätsprinzip*”, was only very recently translated to English in 2012 by Fritz Lewertoff [26]. Practically all of Louis de Broglie’s writings, whose complete work has just been translated to Russian, have not yet been translated to English. It is therefore important to consult formal articles in their original language, to ensure that the translated versions are accurate, and more importantly to correctly put in perspective the lesser extent of the established knowledge pool at the time of their writing and on which they were grounded.

Analyzing Lorentz’s article of 1904 [27], that introduced the concept of relativity by incorporating the “ γ ” factor into the equations of classical mechanics, which is what prompted Planck to write his 1906 paper [31] previously quoted, it can be seen that the concept of the Coulomb force is clearly defined, but that the energy of the relativistic momentum of the electron is calculated in the manner that intuitively comes to all our minds initially; that is, by simply adding the γ factor to Newton’s initial non relativistic kinetic energy equation “ $K = m_0 v^2 / 2$ ”, but that he does not modify this equation to incorporate the half-quantum of transverse energy that supports the corresponding increment of its magnetic field, as described in reference [32], or alternatively, that he does not multiply the force obtained by means of the Coulomb equation by the distance separating the two charges to obtain the total amount of energy adiabatically induced in each charges by the Coulomb interaction at this distance, as described in reference [4].

We should therefore become fully aware that if two of the greatest discoverers of the time, Planck and Lorentz, had not become aware of the ontological relation now obvious to us between the Coulomb interaction and the induction of kinetic energy in charged particles, and of the relation between this electromagnetically induced energy and the kinetic energy causing massive bodies to move, from the classical/relativist mechanics perspective, macroscopic bodies whose masses can only be exclusively made of the sum of the masses of these electrically charged elementary particles, it necessarily means by extension that this relationship was not yet clearly established in the whole scientific community of the time, as unexpected as this may seem today.

It remains however astonishing that the great discoverers of that time were able to establish so precisely the equations of classical/relativistic mechanics without having benefited from the hindsight now provided us by a further century of experimentation, which now makes it possible to clearly perceive this relation between the so-called “*Coulomb force*”, obtained by multiplying the unit charge of the electric field equation established by Gauss “ $E = e / 4\pi\epsilon_0 d^2$ ” [6] by

a second charge “ e ”, which acts according to the rule of the inverse square of the distance between electric charges “ $1/d^2$ ”, that is “ $F = e \cdot E = e^2/4\pi\epsilon_0 d^2$ ”, and the amounts of *adiabatic kinetic energy* [33] that this force induces in these electric charges as a function of the simple inverse of the distance separating them “ $1/d$ ”, that is “ $E = d \cdot F = e^2/4\pi\epsilon_0 d$ ”, which are concepts that seemed difficult to clearly correlate through the fog of uncertainty that still pervaded the relations between these electromagnetic concepts that were then not in process of being methodically explored, and that still are not today (see following section), and the classical concept of “*mass*”, that belonged to the domain of classical mechanics, and that still was considered as unrelated to electromagnetism at that time.

This is what explains why the concept of “*force*” was not specifically incorporated to SR to justify the increase in energy of a moving or accelerating mass, and also why the very notion of “*force*” is simply absent from the theory of General Relativity (GR), in which it is replaced as the ontological cause of the existence of energy by an inertial motion of massive bodies caused by an assumed “*curvature*” of “*space-time*”, which prevented the Coulomb equation, which is based on the concept of a “*force*” associated with the acceleration of electrically charged particles, from being conceptually associated with the acceleration of the electron “*mass*” from this perspective, because no connection is made in this theory between the concept of “*classical mass*” and the fact that all macroscopic massive bodies can only be made of electrically charged massive elementary particles [16], as will be put into perspective later.

As strange as this may seem, more than one century after Kaufman’s defining experiments with electrons accelerating to relativistic velocities [34], no concept of an increase of the magnetic field of the accelerating electron mass exists in SRT, which makes it seem normal according to this theory that only the momentum energy half-quantum would be increasing with velocity, that is, a velocity apparently due to a theoretical “*inertial acceleration*”.

8. The Conclusion of Planck, Poincaré and Abraham

As mentioned previously, Abraham [29], Poincaré [30] and Planck [31] related the half-quantum of measured motion energy strictly to an increase in the transversely measurable mass, without relating it however in any way to the simultaneous increase of the related transverse magnetic field. From this perspective, the momentum of a moving mass does not have a physical existence, but is considered as an impulse propagating in an underlying ether that would propel the mass, which also makes it seem normal from this second perspective that only the energy half-quantum of the transversely measurable mass increases with velocity.

This disagreement between the position of Einstein, Minkowski and Lorentz on the one hand, and that of Poincaré, Abraham and Planck on the other hand is still the object of endless discussions in the community. In both cases, no relation is established with the double amount of energy revealed by the Coulomb

equation as being ontologically induced simultaneously by the Coulomb interaction in the accelerating electron; and neither of these solutions allows even suspecting that these two half-quanta could be increasing simultaneously.

Consequently, gaining a clear awareness of the mandatory simultaneousness of the existence of both of these two energy half-quanta perpendicularly oriented with respect to each other, in light of Marmet's discovery and in relation with the Coulomb equation, is therefore required for a complete harmonization of classical/relativistic mechanics and electromagnetism to be realized.

9. The Absolute Axiomatic Principles

Let us return for a moment to the previously mentioned "*fog of uncertainty*" that surrounded the concepts of the Coulomb force and the energy induced by this force as the theory of Special Relativity was being developed at the beginning of the 20th century.

Throughout history, before the extent of the momentary accumulation of knowledge about Nature made it possible to identify absolute constants in Nature on which theories could be grounded to explain the identifiable processes observable in objective reality, the method used to ground these theories consisted in establishing absolute axiomatic "*principles*" to be used as stable references to firmly ground rational explanations about the nature of energy, mass, electric charges, etc. These principles eventually became "*idealized dogmas*" that the scientific community adopted as being reliable references to ground the theories that were in process of being developed, such as the Principle of conservation of energy, the Pauli Exclusion Principle, the Principles of stationary action and of least action, etc.

Some of these Principles are "*positive*" idealized Principles, such as the Principle of conservation of energy, that bar all possible exceptions, but that do not actively discourage research as to possible limitations of their reach or of even the very validity of a principle with respect to its applicability to physical reality, that may have been less well understood when it was initially formulated.

Indeed, in the case of this last principle, for example, the current extent of knowledge allows now to better define its reach with respect to physical reality, because we can observe that the Principle of conservation of energy remains valid for a system as long as this system previously stabilized in some stationary action equilibrium state returns to this state after having been disturbed, but that if it is led to vary in such a way as to stabilize axially into a less energetic or in a more energetic stationary action state than the initial state, this change can only be adiabatic in nature [33].

This is precisely the case for the space probes that were taken away from Earth and launched on least action escape trajectories from the solar system, for example [35] [36] [37] [38], as we will see later. When such systems stabilize in such a new state of stationary action axial equilibrium, the Principle of energy conservation applies again, but with reference to this new state of stationary action axial equilibrium. Indeed, the masses of which these probes are made will never re-

turn to the state of stationary action axial equilibrium that they had before launch.

In reality, all stationary action states allowed in objective reality are part of a hierarchy of axially distributed stationary least action electromagnetic equilibrium states, ranging from the stationary states of the subatomic order of magnitude to those of the astronomic order of magnitude, whose detailed hierarchical correlation remains to be completely established, and the only way for an elementary particle or larger mass to move axially from one of these stationary equilibrium state to another is by means of a least action trajectory involving an adiabatic change in its carrier energy. This hierarchy of stationary states will be discussed further on, but let us return for now to the main theme of this section, which is the set of historically established absolute axiomatic principles.

Among the set of historically established “*positive*” axiomatic dogmas, however, is one, the *de facto* rejected concept of “*action-at-a-distance*”, also derogatively referred to as “*spooky-action-at-a-distance*”, which is universally and unjustifiably associated with the Coulomb’s so-called “*force*”, which is a “*negative*” and “*absolute*” dogma, in the sense that it actively discouraged any research in the community in trying to study and understand the nature of the Coulomb interaction, despite the fact that it directly underlies Maxwell’s first equation, that is, Gauss’s equation for the electric field as previously described, which is universally accepted as valid.

The misunderstanding that apparently led to the very idea of a so-called “*action-at-a-distance*” in reference to the Coulomb “*force*” seems to have been that this so-called “*force*” was associated to the concept of an “*attraction*”, as defined in Newton’s macroscopic gravitational theory, instead of having been associated to a “*process of energy induction, half of which provides unidirectional momentum*” in electrically charged particles at the subatomic level, and that an assumed “*attraction*” between charged particles was wrongly considered as being due to an “*attractive force*”, instead of being understood as a motion “*propelled by some unidirectional momentum energy*” of an electrically charged particle towards another electrically charged particle of opposite sign; and that an assumed “*repulsion*” wrongly interpreted as being due to a “*repulsive force*” between electrically charged particles of same sign, turns out to be in reality a motion of an electrically charged particle away from another electrically charged particle of same sign “*propelled by some unidirectional momentum energy*”, with no “*force*” whatsoever being involved in the process, as analyzed in reference [16].

The concept of Coulomb interaction having now been summarily formulated in a manner more in line with reality, and in order to distance ourselves from the concept of Newtonian “*force*”, which is useful at the macroscopic level, but is deceptive when dealing with massive and charged elementary particles at the subatomic level, the expressions “*Coulomb interaction*” will generally be used for the remainder of this article instead of the misleading expression “*Coulomb force*”.

A hundred years now after Lorentz, Planck, Einstein, de Broglie and Schrödinger, to name only a few of the extraordinarily dedicated scientists of the time who revolutionized fundamental physics at the beginning of the 20th century, it seems that we know enough now about the subatomic level to do away with such absolute axiomatic principles and dogmas, by either clearly identifying the physical limits of their applicability, as in the case of the Principle of conservation of energy, or by simply doing away with those that ultimately turn out to just having been misguided impediments to research due to insufficient initial information having been available as to the actual possible nature of the Coulomb interaction, for example, that we now know is the actual cause of the simultaneous adiabatic induction of both perpendicular energy half-quanta in all charged elementary particles in existence, that is, a Coulomb interaction whose nature still remains to be clearly understood.

10. Inappropriate Names Given to Some Processes and States

The very names given in the past to some stable observed characteristics and processes of elementary particles, before the electromagnetic nature of the energy of which their invariant rest masses is made was understood, also heavily contributed to the persistent confusion in the community as to the real nature of these characteristics and processes.

For example, the lower limit of integration of the energy of the rest mass of the electron obtained by means of the spherical integration mathematical means, was quite inappropriately named “*the electron classical radius*”, symbolized by “ r_e ”, which constantly tends to cause many researchers “*to think*” of this value as possibly representing the true physical radius of the electron mass, in the classical mechanics sense [20].

Another much more insidious misnomer is the term “*spin*” chosen to refer to the relative magnetic polarity of mutually interacting electrons and of their interaction with the electromagnetic subcomponents of nucleons, that induces the quite inaccurate beliefs that a transverse rotation of the electron mass has to be involved during these interaction states [39].

The use of these terms is so generalized however that changing them is likely to cause even more confusion, but the real nature of the states and processes being referred to should be clearly documented in formal reference repositories such as *NIST* [40] and the *CRC Handbook of Chemistry and Physics* [41], for example.

11. The Simultaneous Induction of Both Energy Half-Quanta

This new awareness of the simultaneous existence of these two energy half-quanta, mutually perpendicular to each other, that are permanently induced in all charged elementary particles, whether they are in motion or not, and whose amount progressively varies according to the inverse of the distances between

each charged particle and all others, now allows establishing at the subatomic level an internal electromagnetic structure of the energy quantum sustaining both the longitudinal momentum increase and the increase of the transverse magnetic field of any accelerating charged elementary particles, which is identical to that suggested by Louis de Broglie in the 1930's for localized electromagnetic photons [3], which is in complete agreement with Maxwell's equations, but which is not in contradiction with the manner in which free moving electromagnetic energy has mathematically been successfully dealt with at the macroscopic level from the viewpoint of Maxwell's continuous wave theory.

12. Description of Marmet's Derivation from Equation (M-1) Down to Equation (M-6)

In electromagnetism, the Biot-Savart equation is possibly the easiest equation to confirm experimentally because it only describes the transverse uniform and invariant cylindrical magnetic field generated by a stable continuous electric current flowing in a straight electric wire [8].

Grounding his reasoning on the fact experimentally observed during high energy particles accelerators experiments that the magnetic field of an accelerating electron increases despite the also observed fact that its unit charge remains constant irrespective of its velocity, Marmet succeeded, by theoretically reducing to one electron the current flowing in the wire, to derive Equation (M-23) from the Biot-Savart equation, which allows demonstrating that the transversely measurable relativistic mass increase of an accelerating electron, is directly related to its transverse magnetic field increase.

Finally, Equation (M-24) that directly emerges from Equation (M-23), directly establishes that exactly half of the energy making up the invariant rest mass of the electron is also representable as a magnetic field, presumably also transverse by analogy, and would also be in reality an invariant amount energy that would also be physically oriented transversely:

$$\frac{\mu_0 (e^-)^2}{8\pi} \frac{1}{r_e} = \frac{M_e}{2} \quad (\text{M-24})$$

This observed characteristic of the intrinsic magnetic field of the rest mass of the electron, among many others that Marmet's discovery allows at long last to correlate in a new mutually self-consistent perspective, will be analyzed further on, as well as the "*velocity-dependence*" aspect of the accelerating electron increasing transverse magnetic field, as well as the further developments that Equation (M-23) leads to. But let us first address the hurdle presented by Equation (M-7).

He began his derivation by introducing the following form of the Biot-Savart Equation (M-1), in which the cylindrical transverse magnetic field that appears about a current carrying rectilinear metallic wire when a stable electric current is circulating, is represented as being perpendicular to the current direction in the wire, as illustrated in **Figure 1** of his paper [19], that is, as being perpendicular

to the axis along which current “ I ” is graphically represented as flowing:

$$d\vec{B} = \frac{\mu_0 I}{4\pi} \frac{d\vec{s} \times d\vec{u}}{r^2} \quad (\text{M-1})$$

He then redefined current “ I ” by quantizing the electron charge to its invariant unit value ($e = 1.602176462\text{E-}19$ C), which allowed replacing the general variable charge symbol “ Q ” in the standard definition of “ I ” by the discrete number of electrons in one ampere:

$$I = \frac{dQ}{dt} = \frac{d(Ne^-)}{dt} \quad (\text{M-2})$$

Since the velocity of electrons in a conductor remains constant if current “ I ” remains constant, the time element “ dt ” can also be replaced by its traditional definition “ dx/v ”:

$$\text{since } v = \frac{dx}{dt}, \text{ then } dt = \frac{dx}{v} \quad (\text{M-3})$$

Replacing now “ dt ” of the definition of “ I ” as previously established with Equation (M-2) by its equivalent definition established with Equation (M-3), he obtained:

$$I = \frac{d(Ne)}{dt} = \frac{d(Ne^-)v}{dx} \quad (\text{M-4})$$

He then introduced the scalar version of the Biot-Savart equation:

$$dB = \frac{\mu_0 I}{4\pi r^2} \sin(\theta) dx \quad (\text{M-5})$$

Replacing “ I ” in Equation (M-5) by its new definition established with Equation (M-4) also eliminates the implied time factor from Biot-Savart equation, which can be done in context without affecting the value of the magnetic field considered since it remains constant by definition since the current remains constant:

$$dB = \frac{\mu_0 I}{4\pi r^2} \sin(\theta) dx = \frac{\mu_0}{4\pi r^2} \frac{d(Ne^-)v}{dx} \sin(\theta) dx = \frac{\mu_0 v}{4\pi r^2} \sin(\theta) d(Ne^-) \quad (\text{M-5a})$$

In summary, Marmet’s Equation (M-6) is now presented as follows, now involving a sum of quantized unit charges, represented by factor “ Ne^- ”, on top of being disconnected from the time factor, since the magnetic field intensity will remain stable as long as the current remains stable, irrespective of the time elapsed:

$$dB = \frac{\mu_0 v}{4\pi r^2} \sin(\theta) d(Ne^-) \quad (\text{M-6})$$

13. The Erroneous Equation (M-7) Published by Mistake

We now reach the equation that seems not to logically emerge from the seamless sequence that led to Equation (M-6) above, which is likely to have caused an undue loss of interest on the part of potentially interested researchers in reading

further, which may explain why this article has not attracted more attention up to now:

$$\text{Incorrect Equation (M-7): } dB_i = \frac{N\mu_0 e^- v}{4\pi r^2} d(Ne^-) \quad (\text{M-7})$$

It seems also that Paul Marmet did not become aware of this typographical error during the 2 years separating its publication in 2003 from his passing away in 2005, which would explain why he produced no *erratum* note to rectify this misprint, because it is absolutely certain that he derived the correct following form of Equation (M-7), that we will now correctly re-establish, since he used this correct form for the remainder of his derivation:

$$\text{Corrected Equation (M-7): } B_i = \frac{\mu_0 e^- v}{4\pi r^2} \quad (\text{M-7})$$

14. Re-Establishing the Correct Form of Equation (M-7)

As analyzed by Marmet in his explanatory text between Equations (M-6) and (M-7), two variables of Equation (M-6) will now be reduced to the constant value “1” by structure due to the number of electrons being brought down to a single one in Equation (M-7), in which case the charge distribution and magnetic field distribution become by structure isotropic and spherically centered on the location of this single electron, instead of being respectively conceptually linearly distributed for the charge and in transverse cylindrical distribution perpendicularly to the current direction for the magnetic field, as in the initial Biot-Savart equation. Here is then how the correct Equation (M-7) can be derived from Equation (M-6).

First, the “ N ” term in Equation (M-6) will become equal to “1” in Equation (M-7) since only one electron is being considered in the latter equation, so first the term “ $d(Ne^-)$ ” will become “ $d(e^-)$ ”, which is the first step in transiting from Equation (M-6) to the correct form of Equation (M-7):

$$dB_i = \frac{\mu_0 v}{4\pi r^2} \sin(\theta) d(e^-) \quad (\text{M-6a})$$

Since a single electron is being considered, it becomes impossible to conceptually determine a direction of continuous distribution of the electric charge, because no axis of distribution can now be defined. Consequently the “ $\sin(\theta)$ ” factor that was related to this now non-existent linear distribution also disappears from the equation. So we now have:

$$dB_i = \frac{\mu_0 v}{4\pi r^2} d(e^-) \quad (\text{M-6b})$$

Since charge “ e ” of the electron is invariant and thus becomes a numerical constant, calculating a derivative for Equation (M-6b) becomes meaningless. Consequently the two occurrences of the derivative operator “ d ” simplify out of Equation (M-6b), and we end up with the real equation that Marmet obviously meant to be published as Equation (M-7):

$$B_i = \frac{\mu_0 v}{4\pi r^2} e^- \quad (\text{M-6c})$$

then rearranged in the following form that he used as he proceeded with his derivation leading to Equation (M-23):

$$\text{Correct Equation (M-7): } B_i = \frac{\mu_0 e^- v}{4\pi r^2} \quad (\text{M-7})$$

This is how Marmet succeeded in modifying the Biot-Savart equation from representing the uniform macroscopic cylindrical static magnetic field generated by a stable electric current circulating in a rectilinear metallic wire, to representing the velocity related uniform subatomic theoretically spherical transverse magnetic field increment related to the velocity of a single electron, centered on its moving point-like location as it moves at constant velocity, represented by Equation (M-7).

According to the motion mechanics of electromagnetic energy in the expanded trispatial geometry that will be clarified later, this constant velocity of all electrons in the flow of electrons in a metallic wire is due to each electron being individually “propelled”, so to speak, by an amount of physically existing longitudinally oriented momentum energy ΔK , equal by structure to the transversely oriented energy making up the related transverse magnetic field increment ΔB , both amounts physically existing separately from the energy of which the invariant rest mass of the electron is made.

From this perspective, it turns out that the stable transverse and apparently stationary and uniform magnetic field $d\mathbf{B}$ of Biot-Savart Equation (M-1) measurable about the metallic wire simply is the sum of the individual moving transverse magnetic fields of the moving electrons, each electron dragging with it its local magnetic field. Since all electrons in the flow move in the same direction and in close proximity to each other, their individual magnetic fields are all *de facto* forced into mutual parallel magnetic spin alignment due to the inflexible triply orthogonal “*electric/magnetic/direction-of-motion-in-space*” relationship of electromagnetic energy, to which the energy of every elementary electromagnetic particle is subjected to; which explains why all of the individual magnetic fields of the electrons circulating in the wire are oriented in the same transverse direction about the wire, that results in the establishment of this cylindrical macroscopic transverse magnetic field measurable as being stable at any point along the length of a metallic wire in which a constant current is circulating. This is what the Biot-Savart equation is measuring. And this is why reducing the current to involve a single electron allows defining Equation (M-7) that can account for the velocity related subatomic magnetic field increment of a single electron.

It must be mentioned here that the same forced mutual parallel magnetic spin alignment of unpaired electrons in ferromagnetic materials is also what causes their individual magnetic fields to add up to become measurable at our macroscopic level as a single macroscopic magnetic field, as analyzed in references [39]

[42], and formally described in reference [41]. This confirms that the establishment of all macroscopically measurable magnetic fields, be they dynamic or static, can only be due to the same subatomic process, which is the forced parallel alignment of the magnetic spins of the energy of the elementary electromagnetic quanta involved.

We will see further on how Marmet's Equation (M-7) was generalized to calculate the magnetic field increment of any localized electromagnetic quantum, leading then to generalized forms allowing to calculate the velocity of any charged elementary massive electromagnetic particle by combining the intrinsic invariant magnetic field \mathbf{B} of its rest mass with the varying magnetic field $\Delta\mathbf{B}$ of this energy of motion induced in electrically charged massive particles by the Coulomb interaction.

The remainder of Marmet's derivation up to his determining conclusion represented by equivalence (M-26) is available in his paper [19], and is also analyzed in detail at the beginning of reference [4]:

$$\text{Relativistic Mass} \equiv \text{Magnetic Mass} \quad (\text{M-26})$$

15. The Implications of Marmet's Discovery

The first major consequence of the establishment of the Equation (M-23) is the establishment of electromagnetic equations that allow the calculation of the relativistic velocities of charged and massive elementary particles without any need to use the Lorentz γ factor.

16. Calculating Relativistic Velocities without the Lorentz γ Factor

Considering Equation (M-23) again, since “ c ” constitutes an *asymptotic velocity limit* that the electron cannot physically reach, then as “ v ” tends towards “ c ”, “ $M/2$ ” seems to tend towards an asymptotic transverse mass increment limit equal to “4.55469094E-31 kg”, corresponding to its transverse magnetic field increment, that apparently seems, at first glance, impossible to increase further, but we will see further on that this is not the case:

$$\frac{\mu_0 (e^-)^2}{8\pi} \frac{1}{r_e} \frac{v^2}{c^2} = \frac{M_e}{2} \frac{v^2}{c^2} \quad (\text{M-23})$$

At this stage of the analysis, Equation (M-23) can thus be formulated as follows to represent the electron transverse *relativistic-mass/magnetic-field* increment:

$$\Delta m_{(v \rightarrow c)} = \frac{\mu_0 e^2}{8\pi r_e} \frac{v^2}{c^2} = \frac{m_e}{2} \frac{v^2}{c^2} \quad (1)$$

On the other hand, when “ v ” tends towards zero in Equation (M-23), its transverse magnetic field increment also tends towards zero. And when this velocity approaches zero, the ratio “ v^2/c^2 ” reveals that the amount of energy of the

transverse increment of the magnetic field becomes negligible and that this ratio can then be removed from the equation, which still leaves part of the invariant rest mass an electron as being represented as a magnetic field, apparently finally revealing that exactly half of the energy making up the invariant rest mass of the electron would also be the source of its intrinsic invariant magnetic field, as represented by Equation (M-24), which is a conclusion that will be confirmed further on by the establishment of the Maxwell equation compliant LC Equation (30) that reveals the actual inner electromagnetic structure of the electron rest mass energy, that was previously established in the trispatial geometry in relation with de Broglie's hypothesis (**Figure 3**):

$$M_{e_magnetic(v \rightarrow 0)} = \frac{\mu_0 (e^-)^2}{8\pi} \frac{1}{r_e} \frac{v^2}{c^2} = \frac{\mu_0 (e^-)^2}{8\pi} \frac{1}{r_e} = \frac{M_e}{2} \quad (\text{M-24})$$

Equation (M-7), on the other hand, can be formulated as follows to represent the corresponding transverse magnetic field increment that represents the same amount of increasing energy measurable as the transverse mass increment represented by Equation (1) which adds to that of the invariant magnetic field of the electron's rest mass, calculable with Equation (M-24):

$$\Delta B_{(v \rightarrow c)} = \frac{\mu_0 e v}{4\pi r^2} \quad (2)$$

As a first step in confirming that Equations (1) and (2), both are representations of the same amount of transversely oriented energy in relation with the direction of motion of the accelerating electron, let us first resolve Equation (1) for a well known relativistic velocity, that is, velocity 2,187,647.561 m/s related to the Bohr ground orbit momentum energy in his theory about the hydrogen atom (2.179784832E-18 j), which also happens to be the real mean momentum energy given by the wave function of Quantum Mechanics for the electron ground state orbital of the hydrogen atom. This velocity will immediately confirm that Equation (1) provides the correct related relativistic mass increment:

$$\Delta m_m = \frac{\mu_0 e^2 v^2}{8\pi r_e c^2} = \frac{\mu_0 e^2 (2187647.561)^2}{8\pi r_e c^2} = 2.425337715\text{E}-35 \text{ kg} \quad (3)$$

By means of Equation (2), which is, let us remember, Marmet's Equation (M-7), we must now calculate the increase in the transverse magnetic field associated with this same relativistic velocity of the electron. For this purpose, we must define the value of the second variable in Equation (2), that is, the value of "r"; and it cannot outright be assumed that it will have the same value "r_e" of Equation (1), which is a constant known as the "*classical electron radius*", used in this equation in relation with the electron rest mass.

In the case of Equation (1), that is, Marmet's Equation (M-23) combining an electromagnetic definition of the electron mass with its classical/relativistic mechanics definition, a close examination shows that the relativistic-mass/magnetic-field increment can only synchronously increase with the velocity ratio "v²/c²", "c" being invariant and "v" ranging from zero to asymptotically close to "c", which,

as previously mentioned, seems to reveal that the theoretical maximum possible increment of transverse relativistic-mass/magnetic-field of a free moving electron seems not to really tend towards infinity as traditionally anticipated, but would rather tend to become asymptotically close to a value equal to half the invariant mass of the electron ($\Delta m_m = m_e/2 = 4.55469094E-31$ kg, corresponding to the induced transverse energy half-quantum of $4.09355207E-14$ j).

Let us remember at this point that the Marmet Equation (M-23) defines the relativistic-mass/magnetic-field increment as being dependent strictly on the value of the invariant half of the rest mass energy of the electron that defines its intrinsic invariant magnetic field. But a conversion to electromagnetic form of the classical Newton kinetic energy equation " $K = mv^2/2$ " completed by its correction to incorporate the transverse magnetic energy identified by Marmet and that was missing in Newton's equation [32], ultimately shows that as the transverse magnetic field increases, any further increase of this transverse relativistic-mass/magnetic field increment does not depend uniquely on half the energy of the electron rest mass, as non-relativistic Equation (M-23) suggests, but depends in reality on the total amount of momentarily accumulated transverse energy, that is, on the sum of the energy making up the mass of the intrinsic magnetic field of the electron " $m_e c^2/2$ " plus the energy of the momentarily accumulated transverse mass increment " $\Delta m_m c^2$ ".

This means that the transversely measurable relativistic mass of an accelerating electron " $m_{\text{relativistic}}$ " is always equal to " $m_0 + \Delta m_m$ ", which allowed establishing that this sum is always equal to the invariant rest mass of the electron multiplied by the well known gamma factor " γm_0 " that was established more than one century ago [32]. This is what allows calculating the whole range of relativistic velocities of the electron without using the gamma factor (known as the Lorentz factor).

For example, any relativistic velocity of an electron can be calculated with the following equation derived in reference [32], by setting " E " to " $8.18710414E-14$ j", that is, the energy of the invariant rest mass of the electron, and setting " K " to the sum of energy of the transverse relativistic-mass/magnetic-field increment " $\Delta m_m c^2$ " plus the related momentum energy " ΔK " that we now know is always equal by structure to " $\Delta m_m c^2$ ", that is, " $K = \Delta K + \Delta m_m c^2$ ":

$$v = c \frac{\sqrt{4E \cdot K + K^2}}{2E + K} \quad (4)$$

This equation can also be converted to a form making use of the wavelengths of the energies involved [32], allowing the very same calculation of the whole range of relativistic velocities of the electron strictly from the wavelengths of the energies involved:

$$v = c \frac{\sqrt{4\lambda \cdot \lambda_c + \lambda_c^2}}{2\lambda + \lambda_c} \quad (5)$$

From this equation, the gamma factor was directly derived as analyzed in ref-

erence [32], thus bringing the proof of the validity of Marmet's derivation that allowed the elaboration of these equations.

17. A Cause More Fundamental than Velocity of the Induction of Momentum and Transverse Magnetic Field Energy

Let us now return to the correlations that must be made between Equations (1) and (2). We observe in the electromagnetic definition of mass of Equation (1), that it is the "classical radius" of the electron " r_e " that connects this relation to the concept of mass. In the case of Equation (2), which emerges strictly from electromagnetism, it is also clear that the transverse magnetic field can only increase according to the same velocities ratio, because Marmet's demonstration clearly reveals that the energy half-quantum represented by mass increment " Δm_m " in Equation (1) is the same transversely oriented energy half-quantum which is also described by the transverse magnetic field increment $\Delta \mathbf{B}$; but the value that " r " must have in Equation (2) for the energy corresponding to the increase of $\Delta \mathbf{B}$ to coherently vary from zero to this asymptotic limit made up of the sum of the energy of the classical half-quantum of the electron's rest mass of "4.09355207E-14 j" plus the momentarily accumulated energy of $\Delta \mathbf{B}$, is not clearly established. To understand what this value should be, we must now understand the relation between " r_e " used in Equation (1) and the mass of the electron, or more precisely its relation with the energy constituting the invariant rest mass of the electron.

In a paper published in 2007 in the same Kazan State University International IFNA-ANS Journal [20], that describes a first wave of conclusions emerging from Marmet's discovery, it was conclusively established that " r_e " is in reality the lower limit of spherical integration of the energy making up the invariant rest mass of the electron ($E = m_e c^2 = 8.18710414E-14$ j), and that " r_e " turns out to be in reality the *transverse amplitude of electromagnetic oscillation* of the energy making up the measurable rest mass of the electron, which is obtained by multiplying the electron Compton wavelength by the fine structure constant " α " and dividing them by " 2π ", as determined in reference [21]:

$$r_e = \frac{\lambda_c \alpha}{2\pi} = 2.817940285E-15 \text{ m} \quad (6)$$

Consequently, and by similarity, the value of " r " that must be used in Equation (2) should thus also be that of the *transverse amplitude of electromagnetic oscillation* of the energy induced at the Bohr radius (4.359743805E-18 j), whose *longitudinal electromagnetic wavelength* would be ($\lambda = 4.556335256E-8$ m) if it was moving at velocity " c ", but that must already be multiplied by " α " to reach the value of the *longitudinal de Broglie wavelength* corresponding, for this energy, to the length of the Bohr orbit, whose radius is ($r_B = 5.291772083E-11$ m), keeping in mind that this radius remains valid in Quantum Mechanics since it is exactly equal to the mean axial resonance distance of the electron within the

volume defined by Schrödinger's wave equation for the electron captive in the hydrogen ground state orbital [4]:

$$r_B = \alpha r = \frac{\alpha \lambda}{2\pi} = \frac{\lambda_B}{2\pi} = 5.291772083E-11 \text{ m} \quad (7)$$

By similarity to the method used with Equation (6) to define the *transverse amplitude of electromagnetic oscillation* of the electron rest mass energy by multiplying the *longitudinal electromagnetic wavelength* " λ_C " of its energy by " α ", there is thus need to multiply also the *longitudinal de Broglie wavelength* " λ_B " defined in Equation (7) for the energy induced at the Bohr radius " r_B " again by " α " to finally reach the "*transverse*" value " αr_B " of the *transverse amplitude of the oscillation* of the electromagnetic energy induced at the Bohr radius ($\alpha r_B = 3.861592641E-13 \text{ m}$), which now makes it possible to establish the intensity of the transverse magnetic field increment ΔB which becomes measurable by being added for the velocity considered to the invariant transverse magnetic field of the rest mass of the electron. Let's now calculate the magnetic field corresponding to relativistic velocity "2,187,647.561 m/s" and to this value of " $r = \alpha r_B$ " with Equation (2):

$$\Delta B = \frac{\mu_0 e v}{4\pi(\alpha r_B)^2} = \frac{\mu_0 e (2187647.561)}{4\pi(\alpha \times 5.291772083E-11)^2} = 235047.0405 \text{ T} \quad (8)$$

It is interesting to note by the way that " r_e ", as calculated with Equation (6), is only distant from an additional multiplication by " α " from the value of " αr_B ", as established in reference [43], which suggests a possible axial resonances sequence establishing a sequence of stable stationary action electromagnetic states whose unit of axial progression seems to be the fine structure constant " α ", as put in perspective in the same reference.

To confirm the validity of the value obtained with Equation (8), which is also measurable as a transverse magnetic mass increment " Δm_m " with Equation (3), let's calculate it with Equation (9) which is the generalized version of Marmet's Equation (M-7) that was established in the 2007 article [20]. Unlike Equation (M-7), it can be observed that this generalized form does not require using the velocity of the particle to obtain the intensity of its transverse magnetic field increment.

Only the *longitudinal electromagnetic wavelength* of the total carrier energy of the electron is required, that is, the energy of its momentum plus the transverse energy representable either as a magnetic mass increment " Δm_m " or as a magnetic field increment ΔB . Since the total energy induced at the Bohr orbit is ($E = 4.359743805E-18 \text{ j}$), its *longitudinal electromagnetic wavelength* is thus ($\lambda = hc/E = 4.556335256E-8 \text{ m}$), and we obtain with this generalized equation the same value as with Equation (8):

$$\Delta B = \frac{\mu_0 \pi e c}{\alpha^3 \lambda^2} = \frac{\mu_0 \pi e c}{\alpha^3 (4.556335256E-8)^2} = 235051.7346 \text{ T} \quad (9)$$

We thus observe that without any need to imply any velocity, generalized Eq-

uation (9) provides in Tesla the very same transverse magnetic field increment energy density as the initial Marmet Equation (M-7) originally derived from the Biot-Savart equation, in which the intensity of the transverse magnetic field increment “*seems to depend*” on the velocity of the particle, since that in the Biot-Savart equation from which it was derived, the intensity of the increment of the magnetic field varies strictly according to the velocity of the electrons circulating in the wire.

The fundamental question that now comes to mind is the following, when considering Equation (9): “How come that it is possible, to calculate the correct intensity of the ‘supposedly’ velocity dependent variable transverse magnetic field increment of a moving electron, without this velocity being used to calculate it?”.

18. Momentum and Transverse Magnetic Field Energy Increase without Velocity Increase

This difference between Equation (M-7), that requires the use of a velocity to calculate the related intensity of the transverse magnetic field increment of the moving electron, and its generalized version used to solve Equation (9), that does not require this velocity, draws attention to a cause more fundamental than motion to explain the induction of energy in the electron even when no velocity is involved.

It is a long established fact in classical mechanics, from direct observation, that the kinetic energy traditionally named the “*energy momentum*” of a macroscopic mass in motion depends strictly on its velocity, and that this energy is considered to be the only motion related energy that exists in excess of the energy making up the rest mass of a massive body. The amount of energy of this momentum of an accelerating macroscopic mass is consequently defined in classical mechanics as increasing linearly, potentially without limit, only due to its velocity increase, itself also potentially without limit.

This definition of the increasing kinetic momentum of an accelerating macroscopic mass is also admitted in Special Relativity with this difference that the momentum energy is defined as increasing according to a non-linear curve that we know is correct, also theoretically without limit, as the velocity increases, but that this potentially infinite value would be reached before the velocity of light is reached, this velocity being defined as an unreachable asymptotic velocity limit deemed impossible to be reached by massive bodies. Confirmation of the accuracy of equation “ $K = m_0 c^2 (\gamma - 1)$ ” from Special Relativity was never obtained, however, by means of macroscopic masses in motion, since we do not have the technology required to accelerate macroscopic masses to relativistic velocities, but rather using the subatomic mass of the electron, with which the accuracy of this equation was confirmed by Kaufman’s first experiments [34].

As put in perspective at the beginning of this article, it must be understood that as the theory of Special Relativity was being developed, the fact that the invariant rest mass of the electron “ $m_0 = 9.10938188E-31$ kg” is also the seat of its

invariant unit electric charge “ $e = 1.602176462E-19$ C” was not yet understood as meaning that the Coulomb interaction, that induces the energy of the momentum and of the transverse magnetic field in all electrically charged elementary particles such as electrons strictly as a function of the inverse of the distance between them, and this, even if this distance does not vary, induces it *de facto* at the same time with respect to the rest mass of these charged and massive particles, since the charge and the mass of the electron are two characteristics of the same elementary particle.

Considering that the mass of all macroscopic bodies can only be the sum of the subatomic masses of the massive elementary particles of which it is made, how then can this be reconciled the fact that no increase in the magnetic field of any moving macroscopic masses seems to ever have been measured, since this increase is easily measurable for an accelerating electron, as abundantly demonstrated experimentally since Kaufman’s first experiments [34], which also provides experimental confirmation of the non-rectilinear growth of the momentum energy of an accelerating electron towards this theoretical infinite quantity that the asymptotic limit imposed by the speed limit of light suggests?

Indeed, such relativistic-mass/magnetic-field increments of macroscopic masses may well have been detected all the same for much lower velocities than those typical of electrons, but without having been recognized as such, due to the fact that the Special Relativity theory on which all analysis of relativistic effects are grounded does not recognize its existence, as previously put in perspective, and as we will now observe from experimental data.

19. The “Anomalous” Trajectories of the Pioneer 10 and 11 Space Probes

As previously mentioned, it must be realized here that it has never been possible to accelerate macroscopic masses to velocities comparable to those to which electrons are typically accelerated to at the subatomic level, that were sufficient to confirm the non linear increase of their momentum energy accounted for by SR, and that are also sufficient to confirm the simultaneous increase in transverse magnetic field energy which is not accounted for by SR.

The highest velocities reached by macroscopic projectiles launched into space have currently been reached by the Pioneer 10 and Pioneer 11 space probes, with respective approximate masses made available by NASA of 258 kg and 258.5 kg, as measured before liftoff. Their velocities varied greatly throughout their trajectories, with peaks of 132,000 km/h (36,667 m/s) for Pioneer 10, which is its peak velocity during its final acceleration by gravitational slingshot using Jupiter, and 175,000 km/h (48,611 m/s) for Pioneer 11, which is its peak velocity during its final acceleration by gravitational slingshot using Saturn.

We will analyze here more specifically the escape velocities of the two probes. The reader can make the calculations for the peak velocities mentioned above, that would reveal the increase in mass that can explain the so-called “anomalous” velocity peaks [38] observed during these acceleration phases of the two

probes, as well as during the similar phases of all other space probes subjected to gravitational slingshot acceleration, and that leave the entire astrophysical community perplexed and without explanation, because the SR theory that currently serves as the basis for any analysis of these trajectories is unable to account for them.

We will do calculations as an example with the solar system escape velocities of these two space probes, which have respectively reached escape velocities of 51,682 km/h (14,356 m/s) and 51,800 km/h (14,389 m/s), which are velocities 150 times lower than the theoretical velocity of 2,187,647.561 m/s of the electron in the theoretical Bohr's ground state orbit, for which the increment of its transverse magnetic field is just beginning to be experimentally measurable (see Equation (3)).

What is remarkable about the trajectories of these space probes, as well as about those of all other space probes launched throughout the solar system, is that an unexplained systematic anomaly has been noted. Without exception, they behave as if they were slightly more massive than their masses as measured before liftoff, showing a negative acceleration of about $8E-6$ m/s towards the Sun [36] [37] [38].

But as Rainer W. Kühne mentions in a note published in 1998, the extensive publicity given to these two cases leaves the general impression that this problem concerns only space probes launched by man [44], but it is well known in the astrophysics community that the trajectories of planets Uranus, Neptune and Pluto also show similar systematic anomalies, as well as many comets already studied in 1998, such as Halley, Encke, Giacobini-Zinner and Borelli, whose trajectories undergo a systematic deviation of unknown origin.

Given the understanding now provided by Marmet's discovery, even with the relatively low velocities of the Pioneer 10 and 11 space probes with respect to the typically relativistic velocities of the electron, it becomes easy to calculate this transverse energy increment of the relativistic-mass/magnetic-field that increases the transverse inertia of these two space probes, because we know now for certain by structure that the amount of transverse energy induced at the same time as their momentum is always equal to the latter. The characteristics of the two probes being almost identical, we will use the parameters of Pioneer 10 to analyze this situation.

So, with " $m = 258$ kg" and " $v = 14,356$ m/s", we first obtain the momentum energy of Pioneer 10 for this escape velocity:

$$\Delta K = mc^2 \left(\frac{c}{\sqrt{c^2 - v^2}} - 1 \right) = 2.658722735E10 \text{ j} \quad (10)$$

Given that the energy of " Δm_m " is equal by structure to ΔK , we then obtain for Pioneer 10 a transverse increment of relativistic-mass/magnetic-field of:

$$\Delta m_m = \frac{\Delta K}{c^2} = 2.958228E-7 \text{ kg} \quad (11)$$

Such a slight transverse inertia increase seems insufficient at first glance to ex-

plain on its own the systematic negative acceleration of about $8E-6$ m/s towards the Sun of these space probes launched on escape trajectories from the solar system, but the proposal becomes much more likely if we add to it the adiabatic increase of the rest mass of each probe due to the initial phase of their trajectory away from the incommensurably larger mass of the Earth, that is, an adiabatic rest mass increase that was easily observed during the famous Hafele and Keating experiment [45] when atomic clocks were raised just 10 km from the Earth's surface, but was misinterpreted as confirming a variation in the rate of time flow [35], here again only in light of the theory of General Relativity, that doesn't take into account the involvement of the Coulomb interaction, nor the fact that all rest masses are exclusively made of electrically charged particles. This adiabatic increase in rest masses will be put in correct electromagnetic perspective further on.

20. Maximum Intensity of the Transverse Magnetic Field Increment

Coming back now to the comparison between generalized Equation (9) and Equation (8), which is actually Marmet's Equation (M-7), we observe that Equation (9) provides the same magnetic field energy density in Tesla as the initial Marmet Equation (M-7), but requires only one variable, that is, the "*longitudinal electromagnetic wavelength*" of the energy quantum involved, without any need to relate this energy with the electron velocity.

This is what makes this magnetic field equation general and appropriate for calculating the intrinsic magnetic field of any elementary electromagnetic particle, whether it is moving or not. For example, the invariant intrinsic magnetic B_e field of the electron, that accounts for half of its invariant rest mass energy, can be calculated as follows, using the electron Compton wavelength, also involving the fine structure constant that establishes the amplitude of this energy's transverse electromagnetic oscillation:

$$B_e = \frac{\mu_0 \pi e c}{\alpha^3 \lambda_C^2} = \frac{\mu_0 \pi e c}{\alpha^3 (2.426310215E-12)^2} = 8.289000221E13 \text{ T} \quad (12)$$

Of course, this figure remains mostly meaningless without a solid confirmation that it really represents a physically existing "quantity", that is, a confirmation that could be obtained by showing that relativistic velocity $v = 2,187,647.561$ m/s, related to the magnetic field energy density calculated with Equation (9), for example, can really be calculated by providing only the electromagnetic wavelength of the related energy as the only variable in an equation otherwise involving only fundamental physical constants.

Such a confirmation can indeed be provided by means of the following equation, well known in high energy accelerator circles, that allows calculating the straight line relativistic velocity of an electron being accelerated by external equal intensities electric and magnetic fields:

$$v = \frac{E}{B} \quad (13)$$

The proper value for the required composite \mathbf{B} field is established in a simple manner by simply adding Equations (9) and (12), as analyzed in reference [20], here calculated with the longitudinal wavelength of the energy induced at the Bohr ground state radius ($\lambda = 4.556335256\text{E}-8$ m), to account for the required $\Delta\mathbf{B}$ field increment, and the electron longitudinal Compton wavelength ($\lambda_C = 2.426310215\text{E}-12$ m) to account for the invariant internal \mathbf{B}_e field of the rest mass of the electron:

$$\mathbf{B} = \mathbf{B}_e + \Delta\mathbf{B} = \frac{\mu_0\pi e c}{\alpha^3\lambda_C^2} + \frac{\mu_0\pi e c}{\alpha^3\lambda^2} = \frac{\mu_0\pi e c}{\alpha^3} \frac{(\lambda^2 + \lambda_C^2)}{\lambda^2\lambda_C^2} = 8.289000246\text{E}13 \text{ T} \quad (14)$$

Resolving Equation (13) also requires of course the establishment of the definition of the composite \mathbf{E} field that must be set in equilibrium with this composite \mathbf{B} field. The related general \mathbf{E} field equation was also established in reference [20], thanks to a reformulation of the Coulomb equation established in the same article, a reformulation that was analyzed in depth in reference [4] and that allows calculating the transverse energy that generates and maintains the corresponding magnetic field in elementary electromagnetic particles, whatever state of least action motion or of electromagnetic equilibrium stationary action they may be in into atomic structures:

$$E = \int_{a_0}^{\infty} \frac{1}{4\pi\epsilon_0} \frac{e^2}{(\alpha\lambda/2\pi)^2} \cdot dr = 0 - \frac{1}{4\pi\epsilon_0} \frac{e^2 2\pi}{\alpha\lambda} = \frac{e^2}{2\epsilon_0\alpha\lambda} \quad (15)$$

This particular form of the Coulomb equation indeed allows calculating the energy of any electromagnetic quantum uniquely from its wavelength, without any need to use the Planck constant:

$$E = hf = \frac{e^2}{2\epsilon_0\alpha\lambda} \quad (16)$$

This form of the Coulomb equation also allowed unifying all classical force equations in reference [46] by showing that the “ $F = ma$ ” fundamental acceleration equation can be derived from all of them, which actually proves that the Coulomb interaction is the common denominator of all classical force equations.

The general \mathbf{E} field equation corresponding to the general \mathbf{B} field Equation (9) was thus established in reference [20] as follows, here resolved using the longitudinal wavelength of the energy induced at the Bohr ground state ($\lambda = 4.556335256\text{E}-8$ m), to harmonize with the $\Delta\mathbf{B}$ field value obtained with Equation (9):

$$\Delta\mathbf{E} = \frac{\pi e}{\epsilon_0\alpha^3\lambda^2} = 7.046673727\text{E}13 \text{ N/C} \quad (17)$$

Consequently, the invariant \mathbf{E}_e field related to the other half of the energy making up the invariant rest mass of the electron can be established with the electron longitudinal Compton wavelength as follows:

$$\mathbf{E}_e = \frac{\pi e}{\epsilon_0 \alpha^3 \lambda_c^2} = 6.029331754 \text{E}10 \text{ N/C} \quad (18)$$

But, contrary to the composite magnetic \mathbf{B} field that must be used to calculate the relativistic velocity of the electron with Equation (13), and which is obtained from the simple addition of the electron's intrinsic invariant \mathbf{B}_e field and of the $\Delta\mathbf{B}$ field of its velocity related magnetic field increment, the corresponding composite \mathbf{E} field involving the \mathbf{E}_e field and the $\Delta\mathbf{E}$ field of Equations (17) and (18), cannot be obtained in this simple manner, due to the fact that the electric dipole that induces the accompanying $\Delta\mathbf{B}$ field is oriented perpendicularly with respect to the monopolar \mathbf{E}_e field of the electron rest mass within electrostatic Y -space, as clarified in reference [21]. As established in reference [20], this composite \mathbf{E} field, also involving here both the wavelength of the Bohr ground state energy ($\lambda = 4.556335256 \text{E}-8 \text{ m}$) and the electron Compton wavelength ($\lambda_c = 2.426310215 \text{E}-12 \text{ m}$), will have the following value:

$$\mathbf{E} = \frac{\pi e}{\epsilon_0 \alpha^3} \frac{(\lambda^2 + \lambda_c^2) \sqrt{\lambda_c (4\lambda + \lambda_c)}}{\lambda^2 \lambda_c^2 (2\lambda + \lambda_c)} = 1.813341121 \text{E}20 \text{ N/C} \quad (19)$$

By means of Equation (13) the well known and exact relativistic velocity of an electron whose magnetic field is increased by an amount of $\Delta\mathbf{B}$ will then be obtained as follows if it is not impeded by the local electromagnetic equilibrium state:

$$v = \frac{\mathbf{E}}{\mathbf{B}} = \frac{1.813341121 \text{E}20}{8.289000246 \text{E}13} = 2187647.566 \text{ m/s} \quad (20)$$

Calculating with Equation (9) for the $\Delta\mathbf{B}$ field and with Equation (17) for the $\Delta\mathbf{E}$ field with any longitudinal wavelength of the carrying energy will mathematically show that by combining them with the \mathbf{B}_e and \mathbf{E}_e fields that account for the energy of the invariant rest mass of the electron obtained with Equations (12) and (18) to ultimately resolve Equation (20), that the whole range of all relativistic velocities up to the asymptotic limit of the speed of light, in the case of any elementary massive particle such as the electron, can be obtained, and this, for a very mechanical reason which is clearly explained in reference [32].

21. Separation of the Electron Carrying Energy from the Energy of Its Rest Mass

As analyzed in reference [20], the most significant progress resulting from Marmet's derivation was the new possibility of clearly separating the invariant energy constituting the electron's rest mass from the variable adiabatic energy supporting its motion and its transverse relativistic-mass/magnetic-field increment. After analysis, this variable adiabatic carrying energy of the electron turned out to have the same internal electromagnetic structure that Louis de Broglie proposed for the double-particle electromagnetic photon in the 1930's [3] [17] [43], as mathematically described with Equation (21), and graphically symbolized with **Figure 4**, in accordance with Maxwell's interpretation, according

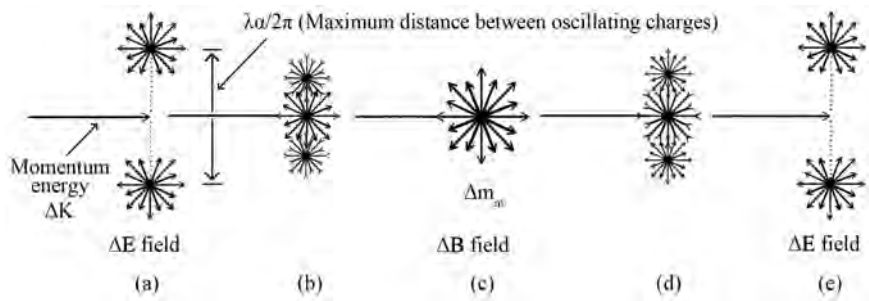


Figure 4. Representation of the transverse oscillation cycle of the electromagnetic half-quantum of the electron carrier-photon and of its unidirectional momentum energy half-quantum that propels this first half-quantum on top of also propelling the complete quantum of the electron invariant rest mass energy (the latter not illustrated).

to which the electromagnetic component of the energy of a localized photon has to be oriented transversely with respect to its momentum energy, and is captive in a standing oscillation motion causing it to cyclically transit between a state corresponding to its electric field and a state corresponding to its magnetic field.

This is what justified coining the term “*carrier-photon*” to name the carrying energy of the electron or that of any other elementary charged particle in articles describing the various consequences of integrating Marmet’s discovery into electromagnetic theory on the one hand, and into classical/relativistic mechanics on the other, with the consequence that their equations can now be derived from each other [4].

The LC equation for the de Broglie double particle photon thus established in the only manner possible in the trispatial geometry proposed at the event Congress-2000 [18], and as formally published in reference [3] in complete accordance with Maxwell’s equations, already made it possible to calculate from an electromagnetic photon’s wavelength, the maximum intrinsic magnetic field energy of a photon structured according to Maxwell’s initial interpretation that both fields induce each other, as established in reference [43]:

$$E = \frac{hc}{2\lambda} + \left[\frac{e^2}{2C_\lambda} \cos^2(\omega t) + \frac{L_\lambda i_\lambda^2}{2} \sin^2(\omega t) \right] \tag{21}$$

where

$$E_{E(\max)} = \frac{e^2}{2C_\lambda} \quad \text{and} \quad E_{B(\max)} = \frac{L_\lambda i_\lambda^2}{2} \tag{22}$$

and

$$C_\lambda = 2\varepsilon_0\alpha\lambda, \quad L_\lambda = \frac{\mu_0\alpha\lambda}{8\pi^2}, \quad i_\lambda = \frac{2\pi ec}{\alpha\lambda} \tag{23}$$

Marmet’s derivation, on its part, made it possible to establish in reference [20] the generalized electric and magnetic field equations previously mentioned, that directly match the representations of their energy in the form of capacitance and inductance as illustrated by Equations (22):

$$\mathbf{E} = \frac{\pi e}{\varepsilon_0 \alpha^3 \lambda^2}, \quad \mathbf{B} = \frac{\mu_0 \pi e c}{\alpha^3 \lambda^2} \quad (24)$$

and to also establish *the theoretical stationary isotropic volume* corresponding to the maximum energy density of each of these two mutually inducing fields:

$$V = \alpha^5 \frac{\lambda^3}{2\pi^2} \quad (25)$$

which made it possible to redefine in reference [3] the LC equation initially developed in reference [20] in a form making use of the more familiar \mathbf{E} and \mathbf{B} fields definitions, which confirmed that the localized electromagnetic photon as de Broglie conceived it and the electron carrying energy actually have the same internal electromagnetic structure, *i.e.* one half oriented longitudinally, supporting its momentum, and the other half oriented transversely, defining its \mathbf{E} and \mathbf{B} fields inducing each other, this transversely oriented energy half being propelled in space by the unidirectional energy of its momentum:

$$E = \left(\frac{hc}{2\lambda} \right) + \left[2 \left(\frac{\varepsilon_0 \mathbf{E}^2}{4} \right) \cos^2(\omega t) + \left(\frac{\mathbf{B}^2}{2\mu_0} \right) \sin^2(\omega t) \right] V \quad (26)$$

22. Conversion of Electromagnetic Energy into Charged and Massive Elementary Particles

We have the experimental proof since Carl David Anderson's experiments in 1933 [12] that any electromagnetic photon of energy 1.022 MeV or more, generated as a by-product of cosmic radiation, will destabilize when grazing a massive atomic nucleus, and will convert into a pair of massive elementary particles, which are one electron and one positron, whose equal rest masses of 0.511 MeV/c² are each made of 0.511 MeV of the destabilizing photon energy. Any energy in excess of this specific amount of 1.022 MeV that the photon had before conversion is then expressed as longitudinal momentum energy and related transverse electromagnetic energy equally shared between both elementary massive particles, which causes them to move away from each other with a velocity corresponding to this excess momentum energy [21].

The following equation describes how the energy of the incident photon is distributed between the two charged and massive particles generated, by associating the Coulomb equation with the rest mass equation of classical/relativistic mechanics [4]. It should be noted in passing that the opposite charges of the electron and the positron are meaningless in classical/relativist mechanics, and that considered according to only their mass characteristic, they are identical, which makes it possible to build the equation in the following way:

$$E_{\left(\frac{1}{\lambda_1} \geq \frac{1}{2\lambda_C}\right)} = \frac{e^2}{2\varepsilon_0 \alpha \lambda_1} = 2(\Delta K + \Delta m_m c^2 + m_0 c^2) \quad (27)$$

where

$$(\Delta K + \Delta m_m c^2) = \frac{e^2}{2\varepsilon_0 \alpha \lambda_2} \quad \text{in which} \quad \frac{1}{\lambda_2} = \frac{1}{2} \left(\frac{1}{\lambda_1} - \frac{1}{2\lambda_C} \right) \quad (28)$$

In Equation (27), “ m_0 ” represents the identical individual rest masses of the electron and positron, and “ λ_1 ” is the electromagnetic wavelength of the incident photon being destabilized, while in Equation (28), “ λ_2 ” is the wavelength of the residual energy in excess of the energy of 1.022 MeV that just converted into the invariant rest masses of the two particles, after separation of this residual energy in equal parts between the two now separate particles.

More interesting yet, an experiment carried out in 1997 at the Stanford Linear Accelerator (SLAC), *i.e.* experiment #e144, confirmed that by converging two sufficiently concentrated electromagnetic photon beams towards a single point in space, one beam involving electromagnetic photons exceeding the 1.022 MeV threshold, massive electron/positron pairs were generated without any massive atomic nuclei being close by [13]. This last experiment opens up an entirely new perspective on the possible origin of the universe, as analyzed in reference [47].

The interest of the trispatial geometry developed from the expansion in the form of 3 perpendicular vector spaces emerging from the three-way orthogonal relationship of the vector product of the fundamental \mathbf{E} and \mathbf{B} vectors of electromagnetism (Figure 3), is that the more complete vector harnessing now applicable to Equation (26) in the following way, as analyzed in reference [3], allowed establishing for the first time in reference [21] a clear mechanics of conversion of the energy of an electromagnetic photon of 1.022 MeV or more, which is only partially oriented perpendicularly to the energy of its momentum, into the invariant energy completely oriented transversely constituting the internal structure of the individual rest masses “ m_0 ” of the electron and positron represented in Equation (27), *i.e.* the following equation:

$$E\vec{i} = \left(\frac{hc}{2\lambda}\right)_x \vec{i} + \left[2\left(\frac{\varepsilon_0 \mathbf{E}^2}{4}\right)_y (\vec{J}\vec{j}, \vec{J}\vec{j}) \cos^2(\omega t) + \left(\frac{\mathbf{B}^2}{2\mu_0}\right)_z \vec{K} \sin^2(\omega t)\right] \mathbf{V} \quad (29)$$

converting into the following two equations to represent the internal electromagnetic structure of the rest masses of the electron and positron:

$$m_{e_0} \vec{\mathbf{0}} = \frac{V_m}{c^2} \left\{ \left[\frac{\varepsilon_0 \mathbf{E}^2}{2} \right]_y \vec{J}\vec{i} + \left[2\left(\frac{\varepsilon_0 \mathbf{V}^2}{4}\right)_x (\vec{J}\vec{j}, \vec{J}\vec{j}) \cos^2(\omega t) + \left(\frac{\mathbf{B}^2}{2\mu_0}\right)_z \vec{K} \sin^2(\omega t) \right] \right\} \quad (30)$$

and

$$m_{p_0} \vec{\mathbf{0}} = \frac{V_m}{c^2} \left\{ \left[\frac{\varepsilon_0 \mathbf{E}^2}{2} \right]_y \vec{J}\vec{i} + \left[2\left(\frac{\varepsilon_0 \mathbf{V}^2}{4}\right)_x (\vec{J}\vec{j}, \vec{J}\vec{j}) \cos^2(\omega t) + \left(\frac{\mathbf{B}^2}{2\mu_0}\right)_z \vec{K} \sin^2(\omega t) \right] \right\} \quad (31)$$

in which ($V_m = 1.497393267\text{E}-47 \text{ m}^3$) is the *maximum theoretical stationary isotropic volume* that the energy of the electron’s intrinsic magnetic field reaches after having evacuated X -space during the mutual energy induction cycle that causes it to oscillate between constituting in alternance this magnetic field \mathbf{B} and the neutrinoic field “ \mathbf{V} ”, which is an oscillation that replaces, in the structure of massive elementary particles [21], the oscillation between the fields \mathbf{B} and \mathbf{E}

characteristic of electromagnetic photons [3] and of massive elementary particles carrier-photons [21] [22]:

$$V_m = \frac{\alpha^5 \lambda_c^3}{2\pi^2} = 1.497393267E - 47 \text{ m}^3 \quad \text{and} \quad \mathbf{v} = \frac{\pi(e')}{\varepsilon_0 \alpha^3 \lambda_c^2} \quad (32)$$

The neutrinic field “ \mathcal{V} ”, that the trispatial geometry allows identifying for the first time, is introduced in reference [21] and is completely analyzed in reference [23], which also analyses the emission mechanics of neutrinos in the trispatial geometry. The *theoretical stationary isotropic volume* of energy of any elementary quantum was defined in reference [20].

During the decoupling process of an electromagnetic photon of 1.022 MeV or more, the energy in excess of the exact amount of 1.022 MeV that converts into the now invariant energy constituting the separated masses of an electron and a positron, retains the LC structure of the incident double particle photon, but mechanically separates into equal parts between the two massive particles now separated as shown in Equations (27) and (28) and becomes their *carrier-photons*, propelling them in opposite directions in space at the velocity corresponding to the energy of their momentum, calculable with Equation (20), or with one of the following electromagnetic equations, developed in reference [32]:

$$v = c \frac{\sqrt{\lambda_c (4\lambda + \lambda_c)}}{(2\lambda + \lambda_c)} \quad \text{or} \quad v = c \frac{\sqrt{4EK + K^2}}{2E + K} \quad (33)$$

A particular point of interest about the latter two equations is that if the Compton wavelength of the electron (“ λ_c ” in the first equation) or the energy of the rest mass of the electron (“ E ” in the second equation) are reduced to zero, only the energy of its carrier-photon remains in the equation, and its velocity can then only be the velocity of light, thus confirming the identity of its structure with that of de Broglie’s double-particle photon [3] [32].

It is very easy to verify the validity of LC Equations (30) and (31) of the electron and positron, because all of their terms are very well known invariant physical constants. For example, by multiplying the maximum energy of the magnetic field in Equation (30) by the *theoretical stationary isotropic volume* of this amount of energy defined in reference [20], we effectively obtain half the energy of the invariant rest mass of the electron, which corresponds to its intrinsic magnetic field:

$$\frac{B^2}{2\mu_0} V_m = \left(\frac{\mu_0 \pi e c}{\alpha^3 \lambda_c^2} \right)^2 \frac{1}{2\mu_0} \frac{\alpha^5 \lambda_c^3}{2\pi^2} = 4.093552068E - 14 \text{ j} \quad (34)$$

23. Construction of Stable Complex Particles

It has been confirmed long ago that all atoms are made of only three distinct types of stable subcomponents, electrons, protons and neutrons. All three are typically regrouped under the general term “*elementary particles*” in the community, that is, a term currently “general” that induces a certain amount of confusion because of these three, only the electron has been found to truly be a

charged and massive elementary particle, that is, not made of smaller subcomponents, but is demonstrably made exclusively of the electromagnetic energy that was the “substance” of the electromagnetic photon from which it emerged, as just put in perspective, and as analyzed in detail in reference [21].

The other two subcomponents of all atoms, the proton and the neutron, were found not to be charged and massive elementary particles of the same sense as the electron, but rather *systems of such elementary particles* in a state of stable stationary action electromagnetic equilibrium, just as the solar system is not a celestial body, but a system of celestial bodies stabilized in a state of stationary action equilibrium. Historically, the first suspicions that protons and neutrons were not really elementary particles were aroused by the difference in their behavior compared to that of electrons and positrons during the first non-destructive collision experiments between these particles in the first particle accelerators (**Figure 5**).

On their side, electrons and positrons always behave during mutual collision experiments as if they had at best a “*point-like*” presence in space, meaning that in their cases, unlike protons and neutrons, no seemingly unbreachable limit is detectable by collision, no matter how close two electrons or two positrons come to each other’s centers during truly frontal collisions, which is a type of backward rebound seldom observed given that such frontal collisions between electrons or positrons are similar to bringing the highly sharpened tips of sewing needles into frontal collision (**Figure 6**).

It is this “*quasi-punctual*” or “*point-like*” behavior of truly elementary particles during mutual interaction or collisions experiments such as the electron, positron and electromagnetic photons that clearly differentiates them at the subatomic level from complex particles such as the proton and neutron.

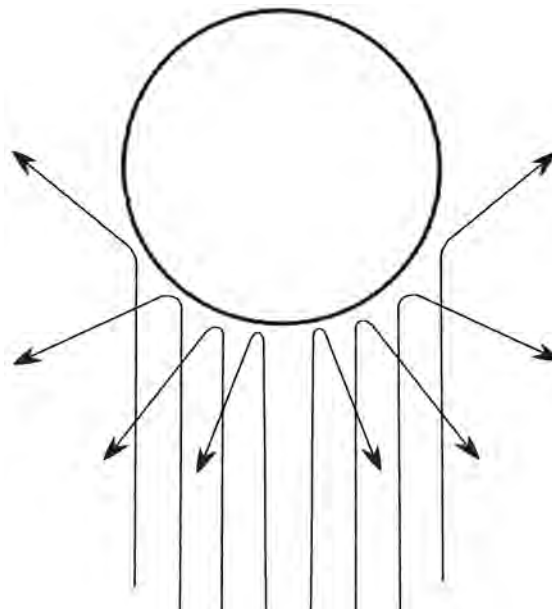


Figure 5. Perfectly elastic scattering between incident electrons and target proton.

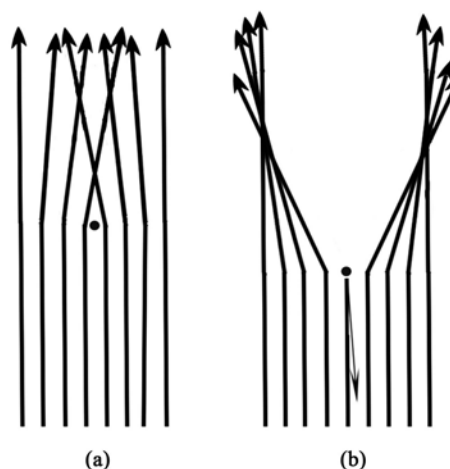


Figure 6. Non-destructive interaction between incident electrons and target positron a), and interaction and direct scattering between incident electrons and target electron b), demonstrating their point-like behavior.

What happened in the case of interactions between truly elementary charged particles was typically that incident electrons were deflected convergently as they crossed the position of positrons moving in the opposite direction, or when incident positrons crossed the path of electrons moving in opposite direction (**Figure 6(a)**); or that incident electrons were deflected divergently after crossing the positions of other electrons moving in the opposite directions or when incident positrons crossed the position of other positrons moving in the opposite direction (**Figure 6(b)**). Given the quasi-punctual behavior of the particles involved, only occasionally was one of the incident particles in an ideal situation to directly collide head-on in order to bounce back directly (**Figure 6(b)**).

While electron and positron beams launched so as to interact head-on with each other generated virtually no reverse rebounds (**Figure 6**), protons and neutrons caused the incident particles (electron or positron beams) to rebound in all directions (**Figure 5**), due to a state of permanent magnetic repulsion between the inner charged subcomponents of protons and the incoming electrons, as analyzed and described in reference [4], which revealed that they occupy a measurable volume in space, contrary to electrons and positrons, that is perfectly elastic rebound patterns identical to those that can be observed at our macroscopic level between two magnets repelling each other [39].

The study of these rebound patterns in the 1940s and 1950s led to the conclusion that the radius of this volume was of the order of $1.2E-15$ m for proton and neutron [48], a volume that seemed to reveal that they could be made up of smaller particles whose interactions would determine this volume, just like the volume defined by planetary orbits determine the potential volume that the solar system can occupy in space, that is, theoretically at the time, truly elementary electromagnetic particles with *quasi-punctual* behavior of the same nature as the electron and the positron.

The first particle accelerator powerful enough to overcome the resistance of

this proton volume to penetration by sufficiently energetic electrons or positrons, the Stanford Linear Accelerator (SLAC), came into service in 1966. From 1966 to 1968, a series of high energy non-destructive scattering experiments carried out by M. Breidenbach *et al.* [10] of electrons against protons effectively revealed the presence of three quasi-punctual behaving electrically charged sub-components (**Figure 7**), whose deflection spread patterns of the incoming electrons' trajectories and subsequent analysis allowed associating an electric charge equal to $1/3$ of that of an electron to one subcomponent and a charge equal to $2/3$ that of the positron to the other two subcomponents (uud). Neutrons on the other hand revealed a structure made up of one $2/3$ positive charge subcomponent and two $1/3$ negative charge subcomponents (udd).

Moreover, incoming electrons backscattered in a highly inelastic manner and subsequent experiments also involving positrons revealed that the $2/3$ positively charged subcomponents were only slightly more massive than electrons and that the $1/3$ negatively charged subcomponent was only slightly more massive than the positively charged subcomponents [22] [25].

Given that these presumably invariant rest masses were eventually confirmed as being only slightly higher than those of electrons and positrons [41], combined with the fact that these sub-components of nucleons demonstrate exactly the same quasi-punctual behavior that characterizes electrons and positrons, and the also confirmed fact that electrons and positrons are the only massive and electrically charged elementary particles that can be generated from free electromagnetic energy in a well understood and exhaustively confirmed manner [12] [13], it seemed possible that these sub-components of nucleons could actually be positrons and electrons whose masses and charges would be altered in this way by the stresses imposed by those ultimate stationary action electromagnetic equilibrium states in which electrons and positrons could become captive of, if the latter truly are the only building material that nature has at its disposal to build nucleons.

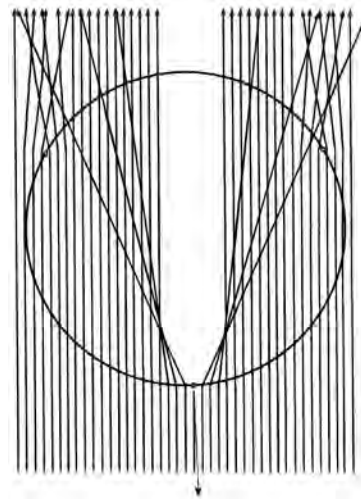


Figure 7. Detection of the proton inner structure via non-destructive scattering.

This conclusion immediately explains why none of these nucleon sub-components could ever be ejected from a nucleon while still retaining its fractional charge, because if they really originally were electrons and positrons, then of course, they will naturally adiabatically recover their normal mass and charge characteristics as soon as they escape the electromagnetic stresses they are subjected to while being part of the stabilized stationary action nucleon structures [24].

The trispatial geometry indeed made it possible to calculate precise mean rest masses for these elementary positive and negative subcomponents of protons and neutrons corresponding to a sequence of stable axial resonance states that can be related to a sequence of integers, which locates these masses within the experimentally estimated possible mass ranges in both cases (see **Table 1**), that is, a sequence of three related masses that can be obtained from one of the possible equations that allows this calculation, such as the following equation established in reference [22], and analyzed in a more general perspective in reference [24], that is, a resonance sequence for the masses of stable elementary particles similar to the resonance sequence of the electronic orbitals of the hydrogen atom that Louis de Broglie was the first to notice at the beginning of the 20th century [4] [49]:

$$m_{i[d,u,e]} = \frac{k}{a_0} \left(\frac{3e}{n\alpha c} \right)^2 \quad (n = 1, 2, 3) \quad (35)$$

where “ e ” is the unit charge, “ α ” is the fine structure constant, “ c ” is the speed of light, “ a_0 ” is the Bohr radius, *i.e.* the mean axial distance between the fundamental electronic orbital of the hydrogen atom and the proton, and “ k ” is the Coulomb constant:

$$k = \frac{1}{4\pi\epsilon_0} = 8.987551788E9 \quad (36)$$

Effectively, the masses obtained from Equation (35) fall right into the ranges experimentally established within which their true rest mass has to lie, that is, between 1 and 5 MeV/ c^2 for the positive subcomponent, and between 3 and

Table 1. Sequence of masses in axial resonance state of elementary particles obtained using Equation (35).

	Rest mass	Energy	Charge	Reference
Free moving electron or positron	9.10938188E-31 kg	0.511 MeV	$\pm 1 =$ 1.602176462E-19 C	[21]
Electromagnetically stressed positron 1 in the neutron 2 in the proton	2.049610923E-30 kg	1.1497473 MeV	$+2/3 =$ 1.068117641E-19 C	[22]
Electromagnetically stressed electron 2 in the neutron 1 in the proton	8.198443693E-30 kg	4.59899 MeV	$-1/3 =$ 5.340588207E-20 C	[22]

10 MeV/c² for the negative subcomponent [41]. These precise rest masses were established with respect to the distances separating the electromagnetically stressed electrons and positrons from the coplanar axis about which each stabilized triad is in *rotation/resonance* within electrostatic *Y*-space (Figure 3) as analyzed in reference [22].

The expression “*rotation/resonance*” is used here to clearly put in perspective that the same amount of energy is adiabatically induced by the Coulomb interaction in the rest masses of the electromagnetically stressed electrons and positrons, whether they are actually rotating on circular orbits about the coplanar axis and/or translation about the normal axis, or simply are in a state of “*stationary axial resonance*” at these distances from these two *rotation/translation/resonance* mutually perpendicular axes.

Let us note, by the way, that at the time of the Breidenbach experiments [10], a mathematical theory developed separately by Murray Gell-Mann and George Zweig was considered confirmed by the Breidenbach experiments, which resulted in these electromagnetically stressed positrons and electrons captive of the nucleons’ internal structures being named “*up quark*” and “*down quark*” respectively at a time when the conclusion had not yet been drawn that these nucleons’ subcomponents could be simple positrons and electrons whose mass and charge characteristics were altered by the intensity of the electromagnetic interactions at such short distances within these structures.

Since the Gell-Mann and Zweig theory also predicted the existence other virtual particles also named “*quarks*”, but that never were detected by non-destructive collisions within nucleons, unlike the two that were named “*up*” and “*down*”, the outcome was an enormous and persistent confusion in the community fuelled by multiple references to the Gell-Mann and Zweig theory, and the almost total absence of references to the experimental data gathered and analyzed by Breidenbach *et al.*, which left the impression during the following decades that even the sub-components actually detected by Breidenbach *et al.* were only theoretical and that their physical existence had never been confirmed.

The most edifying demonstration of this confusion is that in a major work on quantum field theory (QFT) published in 1993, that is, 25 years later, by a renowned physicist in the community, we find the following mention in section 1.2 of his book [50], that shows that he had never heard about the Breidenbach *et al.* experiments that were carried 25 years before, otherwise it seems obvious that he would have taken them into account:

“Ironically, one problem of the quark model was that it was too successful. The theory was able to make qualitative (and often quantitative) predictions far beyond the range of its applicability. Yet the fractionally charged quarks themselves were never discovered in any scattering experiment”.

However, in order to maintain continuity with the literature that was historically produced naming the electromagnetically constrained positrons and electrons as “*up quarks*” and “*down quarks*”, including the other articles of this series, we will keep the symbols “*u*” (for “*up*”) and “*d*” (for “*down*”), that histori-

cally symbolized them when referring to the fractionally charged scatterable subcomponents of nucleons detected by Breidenbach, *i.e.* “uud” for the proton and “udd” for the neutron.

$$m_U = \frac{E_U}{c^2} = \frac{V_m}{c^2} \left\{ S_U \left[\frac{\epsilon_0 \mathbf{E}^2}{2} \right]_Y + (2 - S_U) \left[2 \left(\frac{\epsilon_0 \mathbf{V}^2}{4} \right)_X \cos^2(\omega t) + \left(\frac{B^2}{2\mu_0} \right)_Z \sin^2(\omega t) \right] \right\} \quad (37)$$

$$m_D = \frac{E_D}{c^2} = \frac{V_m}{c^2} \left\{ S_D \left[\frac{\epsilon_0 \mathbf{E}^2}{2} \right]_Y + (2 - S_D) \left[2 \left(\frac{\epsilon_0 \mathbf{V}^2}{4} \right)_X \cos^2(\omega t) + \left(\frac{B^2}{2\mu_0} \right)_Z \sin^2(\omega t) \right] \right\} \quad (38)$$

The trispatial LC equations for the electromagnetically stressed positrons (initially named “*up quarks*”) and electromagnetically stressed electrons (initially named “*down quarks*”) constituting the non-destructively scatterable nucleon structure are slightly different from Equations (30) and (31) that describe free moving electrons and positrons that are not being subjected to these electromagnetic stresses, because the transverse drift of the energy that defines the intensity of their fractional charges towards a more intense magnetic state, which is imposed on them by the very short gyroradius of their stationary action states [51], does not allow an equal density of their electrical and magnetic states, unlike the default equal electric vs magnetic density state of the electromagnetic energy of electrons and positrons moving on straight line trajectories.

The expressions “ S_U ” and “ S_D ” are the *magnetic drift constants* of the energy of the stabilized rest masses of the electromagnetically stressed positrons and electrons, respectively equal to “2/3” and “1/3” and which are analyzed and explained in references [22] and [4].

It is important to be aware that the sum of the stabilized rest masses of electromagnetically stressed electrons and positrons (Table 1) making up the scatterable structure of the proton (uud) constitutes only about 2% of its total measured mass, and that this sum for the neutron (udd) constitutes only about 2.4% of its total measured mass. The difference can only be due, of course, to the energy of their respective carrier-photons [22], whose intensity depends directly on the inverse of the distance between charged elementary particles and the translation axis of normal X -space (Figure 3) with respect to which each triad is in *translation/resonance*, an axis that is perpendicular to the coplanar *rotation/resonance* axis with respect to which the rest masses and fractional charges of the electromagnetically stressed electrons and positrons are determined.

As in the case of the expression “*rotation/resonance*” previously mentioned in relation with the Y -space coplanar axis, the expression “*translation/resonance*” is used here to clearly put in perspective that the same amount of energy is adiabatically induced by the Coulomb interaction in each electromagnetically stressed electron and positron carrier-photon, whether they are in actual translation in

circular orbit around the normal X -space axis or simply are in a state of stationary axial resonance with respect to this mean distance from this translation/resonance axis, that is, a resonance motion oriented perpendicularly with respect to such a circular orbit.

24. The Conceptual “Translation/Resonance” Transposition

The same “*translation/resonance*” relationship also applies to the electron’s rest orbital in the hydrogen atom for the same reason. In fact, it was Louis de Broglie who first understood in 1923 that the electron could only be in a state of axial resonance when stabilized at a mean distance of the proton in the hydrogen atom corresponding to the Bohr radius, even if it could also be theoretically perceived as being in translation on a closed orbit around the proton.

This conclusion of major importance was published in a note in which he proposed this first preliminary interpretation of the conditions that could explain the stability of the electron within atomic structures [4], since it was in harmony with the stability condition determined by Bohr and Sommerfeld for a trajectory traveled by a mass at constant velocity [49]. Here is a quote of his major conclusion:

“L’onde de fréquence ν et de vitesse c/β doit être en résonance sur la longueur de la trajectoire. Ceci conduit à la condition”:

Translation

“The wave of frequency ν and velocity c/β must be in resonance over the length of the trajectory. This leads to the condition”:

$$\frac{m_0 \beta^2 c^2}{\sqrt{1 - \beta^2}} T_r = nh \quad (\text{“}n\text{” being an integer)} \quad (39)$$

It is this conclusion that gave Schrödinger the idea of representing the resonance volume visited by the electron in the rest orbital of the hydrogen atom by a wave function [7], as put in perspective at reference [4]. When de Broglie made his discovery, however, it was not yet clear that the very substance of the electron was truly electromagnetic in nature [21], and also that of its carrier-photon, that he intuitively identified as a “*pilot wave*” meant to propel the electron, but whose electromagnetic nature could not be identified at the time [4].

As mentioned earlier, it was not until the early 1930s that it was experimentally confirmed that the very substance of the invariant mass of the electron was nothing more than the “*electromagnetic energy substance*” of an electromagnetic photon of minimum energy 1.022 MeV decoupling into a pair of massive particles of equal masses, namely an electron and a positron [12]. Before this event, no one had had the opportunity to associate electromagnetic energy with the very substance of the mass of elementary particles, so none of the theories developed before this observation could take into account this new discovery in their elaboration, which of course includes Einstein’s two theories of Special Relativity and General Relativity, as well as Quantum Mechanics in its traditional form.

De Broglie related the energy of the electron momentum at the Bohr orbit with Planck's constant and classical mechanics, but like the entire scientific community at that time, he did not relate it with the Coulomb interaction as represented with Equation (16) emerging from Maxwell's first equation and therefore he did not have at his disposal the conclusion that the half-quantum energy of the electron's momentum that would theoretically support the electron's motion longitudinally on its theoretical orbit around the proton is the same that also supports its axial resonance motion oriented perpendicularly to this orbit, as well as the associated half-quantum of its electromagnetic energy oriented transversely to this momentum energy, and that the unidirectional energy of its momentum can only be structurally oriented towards the proton.

In fact, the structural axial orientation of the momentum energy of the electron towards the proton does not exclude the possibility that the electron may move transversely on a closed orbit about the proton, in addition to oscillating simultaneously in axial resonance mode as de Broglie concluded, but at such a short distance between the electron and the proton and at such an intense level of induced energy, it can be expected that the axial resonance mode clearly dominates.

It is a fact that the Planck constant associates the emission of electromagnetic energy strictly with the time factor. But this association of the induction of energy with the time factor is due to the fact that this constant was established by the analysis of the energy frequencies emitted during the de-excitation of electrons, that had previously been momentarily excited towards metastable orbitals further away from atomic nuclei, when they return to their rest orbitals of stationary action, which all are resonance states directly related to the frequency of the mean energy induced at the electron's rest orbital in the hydrogen atom, taken as fundamental, as analyzed and described in reference [24], and that the energy of Planck's quantum of action corresponds to the energy of a single cycle of this ultimate reference frequency, as subsequently determined by de Broglie:

$$h = m_0 v_B \lambda_B = 6.62606876 \times 10^{-34} \text{ j}\cdot\text{s} \quad (40)$$

where " m_0 " is the rest mass of the electron, " v_B " is the conventional reference classical velocity of the Bohr orbit (2,187,691.253 m/s) and " λ_B " is the length of the Bohr orbit (3.32491846E-10 m), whose radius is the fundamental constant ($a_0 = r_0 = 5.291772083 \times 10^{-11}$ m), that is, the mean distance from the fundamental resonance orbital of the hydrogen atom to its nucleus, which defines the energy induced at this distance from the proton, or " $E_B = 4.359743808 \times 10^{-18}$ j" (27.21138346 eV) as easily calculated with the Coulomb equation [24]. Its frequency is therefore " $f_B = 6.579683921 \times 10^{15}$ Hz".

A simple calculation shows that at velocity " v_B ", the duration of a single cycle of this frequency corresponds exactly to the length of the Bohr orbit " λ_B ", which is why multiplying the length of this absolute reference orbit by the Planck constant makes it possible to obtain the energy induced at the Bohr orbit as precisely as with the Coulomb equation.

This is also why the energy corresponding to this reference frequency seems to correspond to the number of orbits that must be run in one second to supposedly “accumulate” all of the energy induced at the Bohr orbit, which has long created the perception that this induced energy “seems” to be distributed over all these cycles and that it takes one second for all the energy of the quantum to be accumulated:

$$E_B = h \cdot f_B = \frac{e^2}{4\pi\epsilon_0 r_B} = 4.359743808\text{E-}18 \text{ j} \quad (41)$$

in which “ r_B ” is the Bohr radius, *i.e.* “5.291772083E-11 m” (see Equation (7)).

Just as Marmet’s Equation (M-7) can be generalized to use *the longitudinal electromagnetic wavelength* of any amount of electromagnetic energy, the same generalization was also made for the Coulomb equation in reference [20], as analyzed and described in detail at reference [4]:

$$E = h\nu = \frac{e^2}{2\epsilon_0\alpha\lambda} \quad (42)$$

where “ α ” is the fine structure constant (7.297352533E-3). The longitudinal wavelength of an amount of electromagnetic energy is also obtained using the following well-known equation, so the longitudinal electromagnetic wavelength of the energy “ E_B ” obtained with Equation (41) is:

$$\lambda = \frac{hc}{E_B} = 4.556335252\text{E-}8 \text{ m} \quad (43)$$

which allows re-obtaining the same amount of energy with generalized Equation (42) already obtained with standard Equation (41):

$$E = h\nu_B = \frac{e^2}{2\epsilon_0\alpha\lambda} = 4.359743808\text{E-}18 \text{ j} \quad (44)$$

It is in fact the relationship established with Equation (42) between the standard equation used to calculate electromagnetic photons energy and the generalized Coulomb equation that makes it possible to carry out the conceptual “*translation/resonance*” transposition required to be able to alternate between the analysis of the stable quantized energy states corresponding to all electronic and nucleonic stationary action orbitals in atoms, that relates Planck’s constant with the number of theoretical cycles that the electron must theoretically run on the Bohr orbit; and that also allows the analysis of the infinitesimally progressive adiabatic induction of energy, which is a constantly active function of the inverse of the distance separating the charged elementary particles constituting all atoms, and which is induced “perpendicularly” by structure to any orbital motion, whether theoretical or effective.

This transposition in no way diminishes the usefulness of the Planck constant for calculations involving the study of the stable and metastable stationary action states of the various orbitals and the quantized emission of Bremsstrahlung photons, when de-exciting electrons move from a metastable orbital to a stable resonance orbital, whose emission mechanics we will analyze later, but it makes

it possible to add to the body of mathematical tools the constants required to adequately deal with the infinitely progressive variations in the amount of energy adiabatically induced in electrons' carrier-photons by the Coulomb interaction during the axial resonance motion sequences into which they are captive when stabilized in the various stationary action orbitals in atoms, as analyzed in reference [4], as well as when they are in free least action motion, *i.e.* in process of moving towards these stabilized axial stationary action states, as analyzed at reference [33].

25. Electromagnetic Energy Adiabatic Induction Constants

25.1. The Electromagnetic Intensity Constant

As analyzed and described in reference [20], since the speed of light is constant in vacuum, it can therefore be stated that the amount of energy of which an electromagnetic photon is made is inversely proportional to the distance it must travel in vacuum for one cycle of its wavelength to be completed, which can be represented by " $E = 1/\lambda$ ". This means that by isolating product " $E\lambda$ " on the left side of this relation, the value obtained will be constant.

A quick analysis of Equation (44) reveals that this constant can alternatively be defined from the familiar set of electromagnetic constants that also defines the generalized Coulomb equation and the *longitudinal electromagnetic wavelength* of any amount of electromagnetic energy (λ):

$$H = E\lambda = \frac{e^2}{2\varepsilon_0\alpha} = 1.98644544\text{E}-25 \text{ j}\cdot\text{m} \quad (45)$$

That is, the quantum of action in joules-meter (j·m), which is the counterpart dissociated from the time factor of the Planck quantum of action defined in joules-seconds (j·s), and that was named "*the electromagnetic intensity constant*" in reference [20]. Dividing now constant " H " by the speed of light " c ", we observe that the Planck constant is obtained, which reveals that " $H = hc$ " directly links Planck's constant to electromagnetism, whereas it is historically considered a measured constant not derived from electromagnetic equations:

$$h = \frac{H}{c} = 6.62606876\text{E}-34 \text{ j}\cdot\text{s} \quad (46)$$

The unexpected result of this relation is that the Planck time based quantum of action can now be obtained from the same set of electromagnetic constants that defines constant " H ", by combining Equations (45) and (46), which makes available to the community this newly established definition of the Planck constant, established strictly from known fundamental constants and derived from experimentally confirmed equations, which is currently absent from both the "*CRC Handbook of Chemistry & Physics*" [41] and from the list of constants of the "*National Institute of Standards and Technology*" (NIST) [40]:

$$h = \frac{e^2}{2\varepsilon_0\alpha c} = 6.62606876\text{E}-34 \text{ j}\cdot\text{s} \quad (47)$$

25.2. The Electrostatic Energy Induction Constant

Metaphorically speaking, Planck's constant allows an "horizontal" (that is, "translational") exploration of the stable orbital states of the hydrogen atom, so to speak, but the Coulomb Equation (41), which provides the same energy, was used to define *an electrostatic energy induction constant* that allows a "vertical" (that is, "axial") exploration of the hydrogen atom and of its nucleus.

The required *electrostatic energy induction constant*, which was named " K " in reference [22] and could be considered as an "*induction quantum*", was established in two different ways. The first method emerged from the analysis of the decoupling mechanics of a photon of energy 1.022 MeV into an electron-positron pair in the trispatial geometry, as established in reference [21], and the second method simply consists in multiplying Equation (41) by " r_B " squared:

$$K = E_B \cdot r_B^2 = \frac{e^2 \cdot r_B}{4\pi\epsilon_0} = 1.220852596\text{E}-38 \text{ j} \cdot \text{m}^2 \quad (48)$$

It is with this constant that it became possible to enter the hydrogen nucleus "vertically", or "axially" so to speak, by varying distance " r " between two charged particles in equation " $E = K/r^2$ ", and thus establish the exact amounts of adiabatic energy induced in each of the internal components of the proton and neutron (see **Table 1**), thus allowing to finally establish coherent trispatial LC equations for the electromagnetically stressed electrons and positrons (see Equations (37) and (38) previously mentioned) and their carrier photons that determine their effective masses and volumes, as analyzed at reference [22].

26. Gravitation

In fact, such a "vertical" exploration, so to speak, of atomic and nuclear structures induces an acute awareness of the adiabatic nature of the energy induced in all of the charged particles making up their structures [24] [33], that is, an adiabatic energy that can only vary in an infinitesimally gradual manner with any variation in the distances separating them; an energy that moreover does not depend in any way on the velocity of particles, but that manifests its existence under the form of this velocity each time that local electromagnetic circumstances allow and that remains fully induced even if this velocity cannot be expressed due to local electromagnetic equilibrium states.

As analyzed in references [4] and [16], when this velocity cannot be expressed, the momentum energy of each charged particle remains induced all the same and can then only exert a "*pressure*" in the vectorial direction imposed on it by the local electromagnetic equilibrium.

In atomic structures, this vectorial direction can only be towards the center of each atom due to the very nature of the Coulomb interaction. In accumulations of atoms making up larger masses, the tendency seems to be that this "*pressure*" tends to apply towards the centre of mass of these masses, which becomes obvious with masses such as that of the Earth, for example, on the surface of which all objects seem to be "*attracted*" to its centre of mass. But this supposed "*attrac-*

tion” can only be the “pressure” exerted by the total sum of the individual momentum energies of each charged particle constituting each object being applied against the surface of Earth, because their vectorial direction of application can only be by structure towards the Earth’s centre of mass [4] [16].

In summary, the “weight” of an object as measured at the Earth’s surface can only be a measure of this “pressure” exerted by the sum of the individual momentum energies vectorially oriented towards its centre of mass, belonging to the whole set of separate charged particles that constitute the measurable mass of this object. If this object is elevated above the ground and then left free to move, the velocity allowed by this sum of momentum energies can again be expressed until its motion becomes hindered again as the object meets again the surface of the Earth, at which point it will again exert a pressure equivalent to the amount of momentum energy induced by Coulomb interaction at this distance between each charged particle of this object and each charged particle of the Earth’s mass [33].

At the astronomical level, the celestial bodies of the solar system seem to be captive of stable stationary action resonance states at mean distances from the Sun similar to that which de Broglie assumed to apply to the electron in the hydrogen atom [49], *i.e.* a state of axial resonance limited by very precise minimum and maximum stable distances from the central star, that is, their perihelion and aphelion. These two boundary distances combined with the mean radius of the elliptical orbit of each celestial body constitute three stable references that allow clearly defining the volumes of space visited over time by each celestial body about the central star.

On the other hand, unlike the case of the hydrogen atom, as analyzed in reference [4], for which the intensity of the momentum energy level induced in the electron at the mean distance from Bohr radius distance clearly favors a localized high frequency axial oscillation motion, rather than a translational motion along the theoretical Bohr ground orbit, the level of adiabatic energy induced in each charged particle of the Earth’s mass at the average distance from the Earth’s orbit being insufficient to generate such a high frequency axial oscillation, given the inertia of the macroscopic mass of which each charged particles is captive, rather favors the stabilization of celestial bodies in the observed states of stationary action orbital motion.

The volume of space visited over time by each celestial body about a central star can evolve into fairly complex shapes for celestial bodies that have satellites, which induces beats frequencies that modify the otherwise regular volumes visited by bodies that do not have a satellite. In fact, all bodies stabilized in such axial resonance systems mutually influence each other’s trajectories and the shape of the resonance volumes they visit. It is this type of interaction, combined with the occultation process of the central star as these bodies pass between this star and our position in space that allowed the identification of the many planets orbiting nearby stars that have recently been discovered.

A similar electromagnetic dynamics defined by Quantum Mechanics (QM) is

also applicable at the subatomic level to the elementary particles making up every atom of which all macroscopic masses are made, including our own bodies. In their cases, however, high-frequency axial stabilization, rather than orbital motion, is clearly favored due to the intensity of the adiabatic energy induced in each charged elementary particle at such short distances between the particles compared to their inertia.

An analysis initiated in references [35] and [52], completed in reference [16], of the sequence in decreasing order of intensities of the various stationary action states of electromagnetic equilibrium in which elementary particles can stabilize, shows that all possible cases of force application traditionally distributed among 4 fundamental forces: 1) *Strong interaction*, 2) *Weak interaction*, 3) *Electromagnetic force*, and finally 4) *Gravitational force*, can only be four quantized levels of Coulomb interaction intensity corresponding to the various energy levels of these stationary action equilibrium states.

Just like it seemed sensible to keep the terms “*up*” and “*down*” to designate positrons and electrons electromagnetically constrained within nucleon structures to maintain consistency with the bulk of previously published literature, it also seems sensible for the same reason to keep the easy to relate to concept of “*attraction*” to identify individual occurrences of Coulomb interaction between any pair of oppositely signed electrically charged particles. So, to facilitate the establishment of a mental image of the various orders of magnitude of electrostatic interaction application between any pair of such particles, the term “*attractor*” was defined in reference [35], embodying the idea that an “*individual-inverse-square-of-distance-attractor*” would be in action between each pair of these elementary particles in the universe. So, for simplicity’s sake, any occurrence of the mentally easy to visualized concept of an electrostatic attraction between a pair of oppositely signed charged particles in the universe is referred to as an “*attractor*” in **Table 2**.

It now becomes possible to separate the Coulomb interaction gradient into four ranges of intensities, the boundaries of which correspond to the various ranges of stationary action resonance intensities that can be identified in nature (**Table 2**). As put into perspective in reference [35], the most intense level is determined by the resonance states characterizing the interacting electromagnetically constrained electrons and positrons forming the internal scatterable structure of nucleons, corresponding to the traditional “*strong interaction*”. The second level applies to the stabilization states of nucleons within atomic nuclei, corresponding to the traditional “*weak interaction*”. The third level applies to electronic resonance states within atoms and molecules, as well as between atoms and molecules in direct contact with each other in any accumulation of matter, corresponding to the traditional “*electromagnetic force*”. And finally, a fourth and final level of intensity applies to any atom, molecule and larger mass in a state of least action free fall, and those captive in stationary action orbits at the astronomical level, and corresponds to the traditional “*gravitational force*”.

Table 2. Coulomb interaction quantized intensity ranges (see Reference [35]).

Table of electrostatic attractors		
Name	Range	Related Traditional force
Primary Attractor	Between electromagnetically stressed electrons and positrons inside a proton or neutron	Strong
Secondary Attractor	Between electromagnetically stressed electrons and positrons belonging to different protons and neutrons in a nucleus	Weak
Tertiary Attractor	Between an orbiting electron and each electromagnetically stressed positron of an atomic nucleus and between each electron and each electromagnetically stressed positrons of other nuclei in all close by atoms	Electromagnetic
Temporary Local Attractor	Between half-photons inside a photon	Electromagnetic
Temporary Far Attractor	Between any half-photon and every other heterostatic particle in the universe	Electromagnetic
Quaternary Attractor	Between each charged particle in an atom and each heterostatic particle in relative free fall in the universe	Gravity

These various levels of adiabatic carrier energy induction intensity by the Coulomb interaction, one of the major components of which is their transverse electromagnetic energy increment, corresponding to a variable increment of permanently induced adiabatic mass, provided for each charged particle in existence, can then be directly related with the 4 forces of the Standard Model as put into perspective in reference [35]; four forces that ultimately turn out to be simple alternative representations of the various levels of intensity of application of a single “force”, namely the underlying adiabatic energy induction Coulomb interaction, as analyzed at reference [16].

27. Nucleon Expansion/Compression as a Function of the Gravitational Gradient Intensity

The fact that the momentum half-quantum of adiabatic energy which is permanently induced by the Coulomb interaction in each electron is oriented axially towards the center of each atom taken separately, and that this energy can only be expressed as a pressure oriented towards the center of the atom when it cannot be expressed as a velocity, as analyzed and described in reference [4], also has the consequence that when atoms accumulate to form larger masses, the vectorial resultant of all interactions between electrons and nuclei accumulated in close proximity will tend to orient the direction of application of these momentum half-quanta towards the centre of such masses, resulting in an addition of their individual pressures towards the centre of these masses.

When these accumulations of atoms become sufficient to form macroscopic masses, the resulting increase in pressure by addition as the depth increases in these bodies can only result in a forced contraction of the outer electronic orbitals of their atoms towards each their nuclei, as put into perspective in reference [35] and analyzed in depth in reference [33].

It is well verified that heat increases with depth in the Earth's mass [53]. However, it is also very well understood that heat in macroscopic masses is nothing more than an increase in the energy of the electrons of atoms, an increase which, when exceeding certain levels specific to each atom, forces the electrons of the outer layers of these atoms to jump to a metastable orbital further away from each nucleus involved. Since these levels are extremely unstable, these electrons return almost instantaneously to their stable stationary action orbital by then emitting a Bremsstrahlung photon that evacuates the energy (*i.e.* heat) accumulated as an electromagnetic photon, whose emission mechanics will be analyzed in the next section.

In the case of such heat increase with depth in planetary masses such as that of the Earth, it is well established that this increase is adiabatic in nature [53], and can only coincide with an adiabatic increase in energy by compression of the electronic orbitals towards their central atomic nuclei, because it is the resulting greater proximity between electrons and nuclei that causes the Coulomb interaction to induce this increased energy as a function of the inverse of the distance separating the electrons from the nuclei.

However, given that the atoms are in direct contact with each other in these masses and that this pressure is constant, this excess adiabatic energy cannot be evacuated by the emission of electromagnetic photons and simply increases with depth in the mass as the captive electrons of the outer electronic layers of the atoms approach the nuclei more and more as the depth increases, until an estimated temperature of about 5100 degrees Kelvin is reached at the centre of the Earth [53], as analyzed in reference [33].

Consequently, at the centre of proto-stellar masses in formation, following a sufficient accumulation of interstellar hydrogen, this compression of the electron orbitals makes the hydrogen atoms electrons eventually reaches the distance to the proton that coincides with the induction of a carrier-energy in each electron reaching the critical decoupling threshold of 1.022 MeV for those at the very center of the proto-stellar mass, at which point decoupling into electron-positron pairs is forced by the immediate proximity of the high-frequency resonating charges of the proton, resulting in the formation of neutrons with enormous bremsstrahlung energy emission that trigger and will subsequently maintain the nuclear fusion chain reaction in stars as analyzed in reference [35].

A side effect of the contraction of electronic orbitals towards nuclei in macroscopic masses such as planetary masses is that these atomic nuclei approach each other more and more as the depth increases in the mass, which reduces the distances between these nuclei, intensifying the Coulomb interaction between the nuclei of these atoms.

The result is an increase in the outward “pull” involving the Coulomb interaction on all the charges of each nucleon of the various nuclei, which forces an increase in the *translation/resonance* distances of each triad relative to their central axis of *translation/resonance* in *X*-space, decreasing the amount of variable adiabatic energy induced in their carrier-photons, thus decreasing the effective mass of all nucleons at this depth of the macroscopic masses, as analyzed in references [22] [35]. The overall effect is that atomic nuclei become less and less massive as depth increases in macroscopic masses.

On the other hand, when small masses are taken away above the Earth’s surface, the opposite effect can only occur by structure, because the energy of the electromagnetically constrained electrons’ and positrons’ carrier-photons of the nuclei of the atoms making up such small masses can only increase as a result of the increase in distances between them and all of the elementary charged particles making up the Earth’s mass, which results in a contraction of the *translation/resonance* distances within each triad of the small mass with respect to the normal x-axis as a result of the weakening of the Coulomb interaction between the charges of these small masses and those of the Earth.

This contraction of the nucleonic orbitals within the nucleons of atomic nuclei making up such small masses moving away from the Earth, can only result in a proportional contraction of the electronic layers of these atoms, the measurable consequence of which is the increase in adiabatic energy induced at these shorter distances between the captive electrons and the nuclei, and therefore, in an increase in the electromagnetic frequency of the Bremsstrahlung photons emitted by electrons momentarily excited moving to a metastable orbital further away from the nucleus, as they de-excite almost instantaneously when returning to their stationary action orbitals.

It is this mass increase of atomic nuclei with increasing altitude above the Earth’s surface that really explains the increase in the frequency of Bremsstrahlung photons used in an atomic clock during the Hafele and Keating experiment [45] mentioned previously to measure time flow, supposedly demonstrating an alleged acceleration in the rate of “time” flow with altitude, then considered as “evidence” of the validity of SR [35]; which is a conclusion that was drawn before the adiabatic nature of the momentum energy and of the transverse magnetic field energy permanently induced in each charged elementary particle was put in perspective.

In reality, such atomic clocks, whose accuracy depends on the frequency of Bremsstrahlung photons emitted by electrons being de-energized, remain accurate as long as they are not moved from where they were calibrated. Any axial displacement in the gravitational gradient or change in its state of motion, such as when used in an orbiting satellite for example, requires recalibration that takes into account the local electromagnetic equilibrium.

Finally, the systematic “anomalies” observed about the trajectories of all space probes, extensively publicized in the case of the Pioneer 10 and 11 space probes about their escape trajectories from the solar system, that all behave systemati-

cally in deep space as if they were slightly more massive than measured on the ground before launch, also find a logical explanation in the previously analyzed fact that the rest masses of nucleons and macroscopic masses can only vary as a function of any axial displacement in the gravitational gradient.

There is then no doubt that the “anomalies” of the elliptical trajectories of Uranus, Neptune and Pluto, as well as those of comets Halley, Encke, Giacobini-Zinner, Borelli and others, that undergo systematic deviations of unknown origin as mentioned by R.W. Kühne [44], and in fact, all of the elliptical trajectories of the planets of the solar system, would benefit from being reconsidered with regard to this variability of their rest masses as a function of their axial oscillation in the Sun’s gravitational gradient, and the variation of their transverse magnetic field as a function of their variable velocity on their elliptical trajectories.

28. The Bremsstrahlung Photon Emission Mechanics

Now that the main conclusions that were drawn in the past about elementary particles, originating from already accumulated trustable experimental data, have been put in perspective in light of Maxwell’s initial interpretation, the de Broglie hypothesis and Marmet’s derivation within the broader framework of the trispatial geometry, let us now look at the Bremsstrahlung photon emission mechanics that this geometry allows establishing, that is, an emission mechanics that de Broglie and Schrödinger were looking forward to establishing in the 1920s, but that elicited little interest in the community at the time, for lack of a potential avenue of resolution to be explored at this time [4].

For this purpose, we will analyze the specific case of an electron in process of being captured by a proton to form a hydrogen atom, whose final stable least action equilibrium state, more precisely describable as state of “stationary” action, was analyzed in reference [4]. Before proceeding to the description of the actual emission mechanics, let us put some numerical figures in perspective with regard to the inertia of the various amounts of energy involved.

Immediately prior to its capture and stabilization at mean rest orbital distance from the proton ($a_0 = 5.291772083E-11$ m), the electron will have reached the relativistic velocity of 2,187,647.561 m/s, driven by the precise amount of “ ΔK ” momentum energy that its carrier-photon will have accumulated at this distance as it accelerated towards the proton [33]:

$$E_K = \Delta K = m_0 c^2 (\gamma - 1) = 2.179784832E-18 \text{ j} \quad (49)$$

This velocity generates the “forward inertia” of the amount of momentum energy (13.6 eV) that will cause its own evacuation as an electromagnetic Bremsstrahlung photon as the forward motion of the electron is suddenly brought to a dead stop as a first step in the establishment of its stable axial stationary action orbital state. In addition to the forward inertia provided by this momentum energy, the total inertia of the incoming electron will also involve the inertia of the total amount of energy making up its carrier-photon transverse

half-quantum and that of its invariant rest mass ($E = m_0c^2 = 8.18710414E-14$ j), both of which will not be evacuated during the stabilization process:

$$E_e = \Delta K + \Delta m_m c^2 + m_0 c^2 = 8.187540114E-14 \text{ j} \quad (50)$$

On the other hand, the “*stationary inertia*” of the proton towards which the electron is accelerating depends on a much larger amount of energy:

$$E_p = m_p c^2 = 1.503277307E-10 \text{ j} \quad (51)$$

So the well known ratio of the inertias of both interacting components will of course be:

$$\frac{E_e}{E_p} = \frac{1}{1836.054891} \quad (52)$$

We can observe that the forward inertia of the incoming electron is 4 orders of magnitude less than the stationary inertia of the proton, whose magnetic fields are its component that will stop the motion of the electron, by interacting in counter-pressure with respect to those of the incoming electron due to repulsive mutual parallel magnetic spin alignment imposed by structure, as clearly put in perspective in reference [4]. But the factual disproportion between the forward inertia of the electron momentum energy and the stationary inertia of the proton is immensely larger:

$$\frac{E_K}{E_p} = \frac{1}{68694481.49} \quad (53)$$

This ratio reveals that whereas the forward inertia of the incoming electron will be countered by the stationary inertia close to 2000 times its own inertia, the forward inertia of the momentum energy of the incoming electron, that will be evacuated from the electron-proton system during the stoppage process, will be countered by a stationary inertia close to 69 million times its own forward inertia as the electron is coming in at a sizable fraction of the speed of light. This ratio puts in very clear perspective how instantaneously the forward motion of this momentum energy towards the proton will find itself countered during the stopping process.

However, contrary to the momentum energy of a moving object hitting a wall at our macroscopic level, for example, that we know experimentally will be communicated to the wall as the object hits it, we also know experimentally that the momentum energy of the incoming electron is not communicated to the proton, but will be ejected right out of the electron-proton system as a detectable and measurable outgoing electromagnetic photon of energy “ $2.179784832E-18$ j”, wavelength “ $9.113034513E-8$ m” and frequency “ $3.289710552E15$ Hz”, moving at the speed of light.

The issue of how the separation and ejection of this bremsstrahlung photon mechanically proceeds has been pending ever since Louis de Broglie and Erwin Schrödinger began studying this process in the 1920's [4], but it was not really possible to resolve it before the expanded Maxwell compliant trispatial geometry

previously described was elaborated and presented in 2000 at the event Congress-2000 [18].

This new space geometry now allows understanding that although the electron and its carrier-photon are suddenly stopped in their forward motion towards the proton while being abruptly captured at mean ground state orbital distance from the proton in a hydrogen atom, the forward motion of its “ ΔK ” momentum energy component calculated with Equation (49) is not stopped in its forward motion “*within*” the internal trispatial structure of the electron carrier-photon (Figure 3(a) and Figure 3(b)), whose three separate spaces of its trispatial inner configuration act as communicating vessels [3], a forward inertia of moving electromagnetic photons that was confirmed by the Einstein’s photoelectric proof.

The key to understanding why the motion of the “ ΔK ” momentum energy half-quantum of the electron carrier-photon is not stopped inside the carrier-photon as the latter is itself stopped in its forward motion, relates to step (c) of its trispatial electromagnetic cycle, as represented with Figure 4, which is the step, during its transverse oscillating cycle, during which all of its transverse energy reaches its maximum volume within magnetostatic Z -space (Figure 3).

The manner in which the forward moving momentum energy “ ΔK ” of the electron being captured by the proton first crosses over to Z -space, as its own forward inertia forces it across the central point-like junction area interconnecting the three spaces through which the particle’s energy freely transits within its own trispatial complex; and is then ejected backwards as a magnetic pulse during the electric phase of the carrier-photon’s transverse oscillation cycle (Figure 4(e)), as the two separated charges behave in Y -space, during the electron stopping process, as a fixed-length dipole antenna [54], can be summarized in a four steps sequence illustrated with Figure 8.

Figure 8(a) represents the electron accompanied by its carrier-photon internally reaching step 4-c (Figure 4(c)) of its transverse oscillating cycle, as both of their magnetic fields begin colliding with the relatively huge magnetic field of the proton, as they repel each other by momentarily all being in parallel magnetic spin alignment, as analyzed in reference [4].

Figure 8(b) represents the second step of the ejection process, and illustrates the actual stopping sequence, as the complete complement of the “ $\Delta K = 2.179784832E-18$ J” momentum energy has just been forced into Z -space by its own forward inertia, which actually momentarily doubles the amount of energy

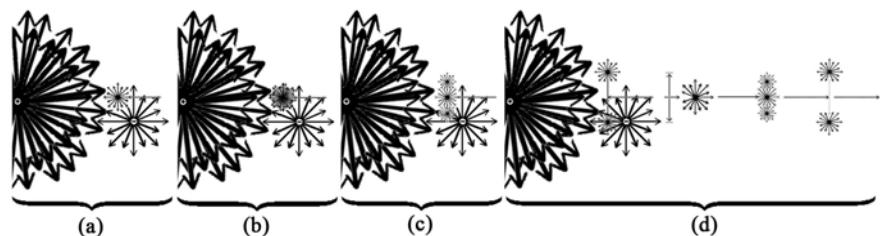


Figure 8. Representation of a Bremsstrahlung emission mechanics.

making up the magnetic field of the incoming carrier-photon, a doubling which is graphically represented by an increased visual density of the carrier-photon magnetic sphere:

$$2 \cdot \Delta B = \frac{\mu_0 \pi e c}{\alpha^3 \lambda^2} = 470103.4692 \text{ T} \quad (54)$$

where “ $\lambda = 4.556335256\text{E}-8 \text{ m}$ ”, which is the wavelength of the electron carrier-photon at the very beginning of the stopping process caused by the mutual magnetic repulsion of their magnetic fields.

As it stands, this momentary doubling of the electron carrier-photon magnetic field as the electron begins to be captured in the hydrogen atom ground state should be detectable as a recordable magnetic intensity peak coinciding with the Bremsstrahlung photon emission, which would directly confirm the present photon emission mechanics.

Something else might already have drawn the reader’s attention in **Figure 8(b)**. Although the momentum energy initially belonging to X -space, and represented by the left-pointing arrow leading to the carrier-photon magnetic sphere in **Figure 8(a)**, was just mentioned as having been forced into Z -space by its own forward inertia to add up with the already residing magnetic energy as calculated with Equation (54), an identical arrow still is present in **Figure 8(b)**. This requires an additional explanation, because this is no misrepresentation, because given that both the electron and the proton are electrically charged in opposition, the Coulomb interaction does not allow by structure that no momentum energy be induced in the electron carrier-photon at this distance from the proton, as put in perspective in reference [33].

Moreover, reference [42] clearly puts in perspective that a clear distinction must be made between an “*uncompensated mechanically induced rotation or translation motion*” and a “*permanently compensated electrostatically or gravitationally induced rotation or translation*”. Such uncompensated motion characterizes the state of a satellite launched into a metastable inertial orbit about the earth for example, or any object artificially rotated at our macroscopic level by means of a single initial impulse. The orbit of such an artificial satellite always degrades causing the satellite to crash, and the rotation of such an artificially rotated object always stops, unlike the natural permanently compensated orbit of the Earth for example, and its natural permanently compensated rotation. Considering the clear correlation previously established between translational, rotational motions and the states of stationary action resonance, the capture and stabilization of an electron in the stationary action resonance orbital of a hydrogen atom clearly belongs to the “*permanently compensated*” category, as put into perspective in reference [33].

Since the amount of “ ΔK ” momentum energy induced by the Coulomb interaction at this distance from the proton can in no way be different from 13.6 eV, it can be concluded that as the initial amount of forward moving “ ΔK ” momentum energy is evacuated from X -space, a replacement 13.6 eV amount of “ ΔK ”

momentum kinetic energy has to synchronously be adiabatically induced by the permanently acting Coulomb interaction, an energy whose vectorial direction of application will now be expressed as a “*stationary pressure*” exerted towards the proton, increasing, so to speak, the permanent counter-pressure established between the parallel-aligned magnetic fields involved [4]. This means that momentarily, the carrier-photon will involve 40.8 eV, including now the momentary double intensity magnetic field, until the 13.6 eV temporarily transferred to *Z*-space is subsequently evacuated as a separate out-going electromagnetic photon.

Figure 8(c) represents the setting up of the metaphorical dipole antenna that will emit the excess 13.6 eV energy as an electromagnetic photon. As the carrier-photon magnetic field reached maximum “*presence*” in *Z*-space as represented in **Figure 8(b)**, the related dipole electric field was down to zero “*presence*” in *Y*-space, which corresponds to the two rods of a fixed length dipole antenna being neutral when no alternating current is provided to the antenna [54].

As the magnetic energy represented in **Figure 8(c)** starts moving back into electrostatic *Y*-space, the energy builds up in *Y*-space as two opposite charges moving in opposite directions on the *Y-y'*/*Y-z* plane [3] [24], causing the two opposite charges to eventually peak at their maximum allowed value, which cannot exceed the maximum transverse *E*-field energy authorized mean value of “ $2.179784832\text{E}-18$ J (13.6 eV)” at this distance between the positively charged proton and the negatively charged electron, which combined with the newly induced equal authorized momentum energy value which is now “*stationarily pressuring*” the electron against the magnetic field of the proton, and is adiabatically maintained by the Coulomb interaction at this mean distance.

It is this maximum *E*-field energy limit enforced by the Coulomb interaction that causes the sudden maximizing of the distance between both charges in *Y*-space causing it to act similarly the two fixed length dipole antenna rods, which allows the extra energy that was forced into *Z*-space, initially coming from *X*-space, to now moves on into *Y*-space and overload the now fixed maximized length of the *Y*-space dipole, causing it to emit the excess 13.6 eV energy as a magnetic pulse in magnetostatic *Z*-space, in the same manner as electromagnetic energy pulses are emitted from a very normal dipole antenna at our macroscopic level, which is represented with **Figure 8(d)**.

The question comes up here as to why does the electron not simply fly away from the proton since it is universally known to do so when precisely this amount of “ $\Delta K = 2.179784832\text{E}-18$ j” energy that it now already possesses is provided to it from an incoming electromagnetic photon, which is the case that will be addressed in the next and last section of this paper. The answer is really simple in this specific case, and is provided by simply becoming aware that the whole practically instantaneous sequence represented by **Figure 8** occurs while the “*forward inertia*” of the total amount of energy making up the electron invariant rest mass and its carrier-photon is applying its maximum pressure against the magnetic field of the proton, momentarily defeating any possibility for the

electron to be ejected at this precise moment, and also defeating any possibility for the distance between the electron and the proton to vary during this so brief stopping sequence process.

Right after having been chased into Z -space by the Y -space electric dipole, the first thing that will happen to the freed energy will be the transfer from Z -space to X -space of half its energy to build the momentum energy half-quantum that will then start propelling it at the speed of light away from the proton, in the first step of the re-establishment of its natural trispatial electromagnetic equilibrium. Once both energy half-quanta have reached their default equal longitudinal and transverse energy levels as could be determined according to de Broglie's hypothesis and from Marmet's derivation, the energy of its transverse magnetic B -field will naturally start transversely oscillating by crossing over to Y -space to induce the corresponding E -field, thus initiating the stable transverse electromagnetic oscillation of the new Bremsstrahlung photon, now moving freely at the speed of light, as represented with **Figure 8(d)** [3].

Note that although the complete process took a noticeable amount of time to describe, the actual sequence of events causing the electron to come to a momentary dead stop as it is being captured by a proton, has to be practically instantaneous, due to the velocity of the incoming electron, combined with the fact that the whole sequence definitely has to be completed during the fleeting half-cycle of the carrier-photon transverse electromagnetic oscillation, beginning with its parallel magnetic spin alignment (**Figure 4(c)**) with respect to the spin orientation of the magnetic field of the proton and ending with the maximum E -field charges separation (**Figure 4(e)**) as represented at the beginning of **Figure 8(d)**; the whole sequence occurring, as previously mentioned, while the inertia of the total amount of energy making up the electron invariant rest mass and the momentarily invariant mass of its carrier-photon are applying maximum pressure against the magnetic field of the proton [4].

29. The Electromagnetic Photon Absorption Mechanics

As soon as the bremsstrahlung photon has been emitted, the “*forward inertia*” of the electron invariant mass/electromagnetic-fields and of its carrier-photon variable mass/electromagnetic-fields half-quantum, due to their incoming velocity, will be replaced by their default “*stationary inertia*”, to which must be added the “*adiabatically variable forward pressure*” provided by the newly induced ΔK carrier-photon momentum energy half-quantum, which is permanently oriented towards the proton, that jointly interact in counter-pressure with respect to the “*oscillating*”, but nevertheless “*stationary inertia*” of the much larger mass/electromagnetic-fields of the proton, which interaction establishes and maintains the electron on its axial least action resonance trajectory within the stationary action volume of space that Schrödinger meant to describe with the wave equation [7], as described in reference [4].

Now that only the permanent “*forward pressure*” of the recently and adiabatic-

ically induced “ ΔK ” momentum is preventing the electron from escaping, and that the “*momentary pressure*” that was initially exerted towards the proton due to the “*forward inertia*” of the electromagnetic fields of the electron and carrier-photon, which initially prevented the electron carrier-photon transverse E field energy from exceeding its incoming initial value of “ $2.179784832E-18$ j”, is no more in action, but which is what caused the bremsstrahlung photon to be emitted, as described in the previous section; any energy coming from outside the electron-proton system will be captured by the Y -space electric dipole of the carrier-photon, presumably still acting as a dipole antenna, but whose length can now vary, and will be equally distributed between both carrier-photon half-quanta, to the extent that the electron’s magnetic gyroradius in the hydrogen atom will allow [51].

The resulting increase in the axial resonance volume that the electron will visit as a result, will cause the electron to eventually jump to an authorized metastable orbital further from the proton before returning almost immediately to the rest orbital, emitting in the process a Bremsstrahlung photon that will evacuate the corresponding excess energy, or to escape completely from the proton if the energy supplied from outside the electron-proton system reaches the escape level of “ $\Delta K = 2.179784832E-18$ j”, either by progressive accumulation or by collision with an incident photon of energy $2.179784832E-18$ j.

All possible cases of energy emission and absorption must of course be explained and documented in the context of trispatial geometry, but since this document is intended only to put in perspective the underlying electromagnetic context that allows a general description of the mechanics of electromagnetic photon emission and absorption by electrons in the trispatial geometry, as a complement to the establishment of the electron stabilization mechanics in the hydrogen atom previously described in reference [4], their development is beyond the scope of the present paper.

30. Conclusions

This analysis highlights the point that it is no more difficult to conceive that electromagnetic energy can consist of localized photons at the subatomic level than it is to conceive that water consists of localized molecules at the submicroscopic level, even if at our macroscopic level we treat electromagnetic energy as if it was made of continuous wave impulses and water as if it was a fluid without internal structure.

The main conclusion of this paper, however, is that when Maxwell’s initial interpretation is correlated with the de Broglie hypothesis about the double-particle photon and Marmet derivation in context of the trispatial geometry, electromagnetism can finally be completely harmonized with Quantum Mechanics, as analyzed in reference [4]; a harmonization that now allows a first mechanical explanation to the processes of electromagnetic photon emission and absorption by electrons, as previously described.

It must also be clearly put in perspective that Maxwell’s initial interpretation is

a conclusion firmly grounded on the study and analysis of experimental data collected earlier during easily reproducible experiments that were performed by many experimentalists, as well as on the conclusions and equations that they drew from this data. The electromagnetic equations generally referred to as “*Maxwell equations*” are in fact a set of mutually complementary equations that have been established mainly by Coulomb, Gauss, Ampère and Faraday and whose mutual coherence was established by Maxwell. Lorentz, Biot, Savart and a few others then completed the current set of mutually complementary electromagnetic equations from the analysis of more data obtained from other experiments equally easy to reproduce.

Intrigued at not finding any evidence of an experiment confirming the point-like magnetic behavior of spherical magnetic fields whose two poles coincide geometrically, which must be the *de facto* magnetic structure of electrons, given their systematic point-like behavior during all scattering experiments, this author designed and carried out in 1998 an easily reproducible experiment with magnets magnetized accordingly, whose data and subsequent analysis were published in 2013, for the experiment to become available in the education community [39]. One year later, S. Kotler *et al.* published an article describing an experiment performed with electrons that directly confirmed the prediction of the 1998 experiment [55].

The education community now has at its disposal a complete set of demonstration experiments easily reproducible during hands-on laboratory teaching sessions, ranging from the first Coulomb electric experiment to the 1998 magnetic experiment to help teaching and confirming every aspect of electromagnetic energy behavior.

Conflicts of Interest

The author declares no conflicts of interest regarding the publication of this paper.

References

- [1] Rousseau, P. (1959) *La Lumière*. Collection “Que sais-je?”, Presses Universitaires de France.
- [2] Michaud, A. (2013) *International Journal of Engineering Research and Development*, **7**, 32-39. <http://ijerd.com/paper/vol7-issue4/G0704032039.pdf>
- [3] Michaud, A. (2016) *Journal of Physical Mathematics*, **7**, 153. <https://www.gsjournal.net/Science-Journals/Research%20Papers-Mechanics%20/%20Electrodynamics/Download/5789>
- [4] Michaud, A. (2018) *Journal of Modern Physics*, **9**, 1052-1110. https://file.scirp.org/pdf/JMP_2018042716061246.pdf
<https://doi.org/10.4236/jmp.2018.95067>
- [5] Cornille, P. (2003) *Advanced Electromagnetism and Vacuum Physics*. World Scientific Publishing, Singapore. <https://doi.org/10.1142/5272>
- [6] Sears, F., Zemansky, M. and Young, H. (1984) *University Physics*. 6th Edition, Ad-

dison Wesley, Boston.

- [7] Eisberg, R. and Resnick, R. (1985) *Quantum Physics of Atoms, Molecules, Solids, Nuclei, and Particles*. 2nd Edition, John Wiley & Sons, New York.
- [8] Griffiths, D.J. (1999) *Introduction to Electrodynamics*. Prentice Hall, Upper Saddle River.
- [9] Jackson, J.D. (1999) *Classical Electrodynamics*. John Wiley & Sons, Hoboken.
- [10] Breidenbach, M., *et al.* (1969) *Physical Review Letters*, **23**, 935-939.
<https://journals.aps.org/prl/abstract/10.1103/PhysRevLett.23.935>
<https://doi.org/10.1103/PhysRevLett.23.935>
- [11] Ohanian, H.C. and Ruffini, R. (1994) *Gravitation and Spacetime*. 2nd Edition, W. W. Norton & Company, New York, 194.
- [12] Anderson, C.D. (1933) *Physical Review*, **43**, 491.
<https://journals.aps.org/pr/pdf/10.1103/PhysRev.43.491>
<https://doi.org/10.1103/PhysRev.43.491>
- [13] McDonald, K., *et al.* (1997) *Physical Review Letters*, **79**, 1626.
<http://www.slac.stanford.edu/exp/e144>
<https://journals.aps.org/prl/abstract/10.1103/PhysRevLett.79.1626>
- [14] Michaud, A. (2019) *Creative Education*, **10**, 353-406.
http://www.scirp.org/pdf/CE_2019022016190620.pdf
<https://doi.org/10.4236/ce.2019.102028>
- [15] Feynman, R.P., Leighton, R.B. and Sands, M. (1964) *The Feynman Lectures on Physics*. Addison-Wesley, Boston, Vol. II, 28.
- [16] Michaud, A. (2017) *Journal of Astrophysics & Aerospace Technology*, **5**, 152.
<https://www.gsjournal.net/Science-Journals/Research%20Papers-Unification%20Theories/Download/6879>
- [17] De Broglie, L. (1993) *La physique nouvelle et les quanta*, Flammarion, France 1937. 2nd Edition.
- [18] Michaud, A. (2000) On an Expanded Maxwellian Geometry of Space. *Proceeding of Congress 2000, Fundamental Problems of Natural Sciences and Engineering*, St Petersburg, Vol. 1, 291-310.
- [19] Marmet, P. (2003) *International IFNA-ANS Journal*, **9**, 64-76.
<http://www.newtonphysics.on.ca/magnetic/index.html>
- [20] Michaud, A. (2007) *International IFNA-ANS Journal*, **13**, 123-140.
<https://www.gsjournal.net/Science-Journals/Research%20Papers-Relativity%20Theory/Download/2257>
- [21] Michaud, A. (2013) *International Journal of Engineering Research and Development*, **6**, 36-49. <http://ijerd.com/paper/vol6-issue10/F06103649.pdf>
- [22] Michaud, A. (2013) *International Journal of Engineering Research and Development*, **7**, 29-53. <http://www.ijerd.com/paper/vol7-issue9/E0709029053.pdf>
- [23] Michaud, A. (2013) *International Journal of Engineering Research and Development*, **7**, 1-8. <http://www.ijerd.com/paper/vol7-issue7/A07070108.pdf>
- [24] Michaud, A. (2017) *Journal of Physical Mathematics*, **8**, 217.
<https://www.gsjournal.net/Science-Journals/Research%20Papers-Unification%20Theories/Download/6877>
- [25] Bartels, J., Haidt, D. and Zichichi, A. (2000) *The European Physical Journal C—Particles and Fields*. Springer, Berlin.
- [26] Petkov, V. (2012) *Space and Time—Minkowski’s Papers on Relativity*. Translated

- by Fritz Lewertoff and Vesselin Petkov, Minkowski Institute Press, Montreal.
<https://www.amazon.com/Space-Time-Minkowskis-papers-relativity/dp/0987987143>
- [27] Lorentz, H.A. (1904) Electromagnetic Phenomena in a System Moving with Any Velocity Smaller than That of Light. *KNAW, Proceedings*, Vol. 6, Amsterdam, 809-831. https://en.wikisource.org/wiki/Electromagnetic_phenomena
- [28] Einstein, A. (1934) *Comment je vois le monde*, Flammarion, France, 1958.
- [29] Abraham, M. (1902) Dynamik des Elektrons, *Nachrichten von der Gesellschaft der Wissenschaften zu Göttingen, Mathematisch-Physikalische Klasse*, 1902, S.20. http://gdz.sub.uni-goettingen.de/dms/load/img/?PPN=PPN252457811_1902&DMDID=DMDLOG_0009
- [30] Poincaré, H. (1902) *La science et l'hypothèse*, France, Flammarion 1902, 1995 Edition.
- [31] Planck, M. (1906) Das Prinzip der Relativität und die Grundgleichungen der Mechanik. In: *Verhandlungen Deutsche Physikalische Gesellschaft*, No. 8, Vorgetragen in der Sitzung vom 23. März 1906, Friedrich Vieweg und Sohn, 136-141. <https://archive.org/details/verhandlungende00goog/page/n179>
- [32] Michaud, A. (2013) *International Journal of Engineering Research and Development*, **6**, 1-10. <http://www.gsjournal.net/Science-Journals/Essays/View/3197>
- [33] Michaud, A. (2016) *Journal of Physical Mathematics*, **7**, 177. <https://www.gsjournal.net/Science-Journals/Research%20Papers-Mechanics%20/%20Electrodynamics/Download/6056>
- [34] Kaufmann, W. (1903) Über die “Elektromagnetische Masse” der Elektronen, *Kgl. Gesellschaft der Wissenschaften Nachrichten, Mathem.-Phys. Klasse*, 91-103. http://gdz.sub.uni-goettingen.de/dms/load/img/?PPN=PPN252457811_1903&DMDID=DMDLOG_0025
- [35] Michaud, A. (2013) *International Journal of Engineering Research and Development*, **8**, 10-33. <http://ijerd.com/paper/vol8-issue1/B08011033.pdf>
- [36] Anderson, J.D., Laing, A., Lau, E.L., Liu, A.S., Nieto, M.M., *et al.* (1998) Indications from Pioneer 10/11, Galileo, and Ulysses Data, of an Apparent Anomalous, Weak, Long-Range Acceleration. <http://arxiv.org/pdf/gr-qc/9808081v2.pdf>
<https://doi.org/10.2172/353450>
- [37] Nieto, M.M., Goldman, T., Anderson, J.D., Lau, E.L. and Perez-Mercader, J. (1994) Theoretical Motivation for Gravitation Experiments on Ultra Low Energy Antiprotons and Antihydrogen. <http://arxiv.org/pdf/hep-ph/9412234.pdf>
- [38] Anderson, J.D., Campbell, J.K. and Nieto, M.M. (2006) The Energy Transfer Process in Planetary Flybys. <http://arxiv.org/pdf/astro-ph/0608087.pdf>
- [39] Michaud, A. (2013) *International Journal of Engineering Research and Development*, **7**, 50-66. <http://www.ijerd.com/paper/vol7-issue5/H0705050066.pdf>
- [40] National Institute of Standards and Technology (NIST). https://www.physics.nist.gov/cgi-bin/cuu/Value?h|search_for=universal_in
- [41] Lide, D.R. (2003) *CRC Handbook of Chemistry and Physics*. 84th Edition, CRC Press, New York.
- [42] Michaud, A. (2013) *International Journal of Engineering Research and Development*, **6**, 7-11. <http://ijerd.com/paper/vol6-issue12/B06120711.pdf>
- [43] Michaud, A. (2013) *International Journal of Engineering Research and Development*, **6**, 31-45. <http://ijerd.com/paper/vol6-issue8/G06083145.pdf>
- [44] Kühne, R.W. (1998) Remark on “Indication, from Pioneer 10/11, Galileo, and Ulysses Data, of an Apparent Anomalous, Weak, Long-Range Acceleration”.

- <https://arxiv.org/pdf/gr-qc/9809075.pdf>
- [45] Hafele, J.C. and Keating, R.E. (1972) *Science, New Series*, **177**, 166-168.
http://www.personal.psu.edu/rq9/HOW/Atomic_Clocks_Experiment.pdf
<https://doi.org/10.1126/science.177.4044.166>
- [46] Michaud, A. (2013) *International Journal of Engineering Research and Development*, **6**, 27-34. <http://www.ijerd.com/paper/vol6-issue6/F06062734.pdf>
- [47] Michaud, A. (2016) *American Journal of Modern Physics, Special Issue: Insufficiency of Big Bang Cosmology*, **5**, 44-52.
<http://article.sciencepublishinggroup.com/pdf/10.11648.jajmp.s.2016050401.17.pdf>
- [48] Resnick, R. and Halliday, D. (1967) *Physics*. John Wiley & Sons, New York.
- [49] De Broglie, L. (1923) *Comptes Rendus des Séances de l'Académie des Sciences*, **177**, 507-510.
http://www.academie-sciences.fr/pdf/dossiers/Broglie/Broglie_pdf/CR1923_p507.pdf
- [50] Kaku, M. (1993) *Quantum Field Theory*. Oxford University Press, New York.
- [51] Michaud, A. (2013) *International Journal of Engineering Research and Development*, **7**, 21-25. <http://ijerd.com/paper/vol7-issue3/E0703021025.pdf>
- [52] Michaud, A. (2013) *International Journal of Engineering Research and Development*, **7**, 1-9. <http://www.ijerd.com/paper/vol7-issue11/A07110109.pdf>
- [53] Lowrie, W. (2007) *Fundamentals of Geophysics*. Second Edition, Cambridge University Press, Cambridge. <https://doi.org/10.1017/CBO9780511807107>
- [54] Auger, A. and Ouellet, C. (1998) *Vibrations, ondes, optique et physique moderne*. 2th Édition. Le Griffon d'argile.
<http://collegialuniversitaire.groupemodulo.com/2252-vibrations-ondes-optique-et-physique-moderne-2e-edition-produit.html>
- [55] Kotler, S., Akerman, N., Navon, N., Glickman, Y. and Ozeri, R. (2014) *Nature Magazine*, **510**, 376-380.
http://www.nature.com/articles/nature13403.epdf?referrer_access_token=yoC6RXrPyxwvQviChYrG0tRgN0jAjWel9jnR3ZoTv0PdPJ4geER1fKVR1YXH8GThqECstdb6e48mZm0qQo2OMX_XYURkzBSUZCrXm8VipvnG8FofxB39P4lc-1UIKEO1

Expression of Some Special Functions through q -Exponentials of the Nonadditive Statistical Mechanics

Leonardo S. Lima

Department of Physics, Federal Education Center for Technological Education of Minas Gerais, Belo Horizonte, Brazil

Email: lslima@cefetmg.br

How to cite this paper: Lima, L.S. (2020) Expression of Some Special Functions through q -Exponentials of the Nonadditive Statistical Mechanics. *Journal of Modern Physics*, 11, 81-90.

<https://doi.org/10.4236/jmp.2020.111004>

Received: November 28, 2019

Accepted: January 7, 2020

Published: January 10, 2020

Copyright © 2020 by author(s) and Scientific Research Publishing Inc.

This work is licensed under the Creative Commons Attribution International License (CC BY 4.0).

<http://creativecommons.org/licenses/by/4.0/>



Open Access

Abstract

Generalized q -exponentials functions are employed to make a generalization of complete and incomplete gamma functions. We obtain a generalization of this class of special functions which are very important in the fields of probability, statistics, statistical physics as well as combinatorics and we derive some of its properties. One gets that the generalized gamma function obtained whether approaches of the standard gamma function for a specific q values such as $q = q_0 \approx 0.9$ value suffering a large variation with the variation of q .

Keywords

q -Exponential Function, Special Function, Gamma Function

1. Introduction

The generalization of elementary functions such as exponential function in q -exponential has been proposed since long time ago [1]. However, more recently, another type of q -exponential has been introduced in the environment of the nonadditive statistical mechanics [2], where the theory has been proposed as a generalization of the standard Boltzmann-Gibbs statistical mechanics for the class of system that is non-ergodic. Many other q -representations were proposed such as the q -algebra [3], the q -Fourier transform [2] [4], the q -Dirac's delta function [5] [6], the q -Gaussian [5] [7] [8] and so on. Moreover, combinations of complex q -exponentials were used to make a new representation of the classical nonlinear oscillator [9], where a combination of complex q -exponentials have been of interest also for recent q -generalized Schrödinger and Dirac equations and other field equations [7]. In the non-additive statistical mechanics the

entropy is described by the so called Tsallis entropy [2], previously introduced by Havrdat-Charvát [10] and later on by Daróczy [11], parameterized by an exponent q . The distribution that maximizes the Tsallis entropy under the constraint of the fixed energy generalizes the Boltzmann distribution through a generalized q -exponential function. Furthermore, in the nonadditive statistical mechanics, when the limit of the parameter of non-extensiveness q is $q \rightarrow 1$, one recovers the standard exponential (and thus, the Gaussian or Boltzmann distribution). Many other classical equations (e.g. the Schrödinger equation) were generalized, replacing the classical exponential with the q -exponential. One example of non-ergodic systems that have been studied is system with long range interactions [12] [13] [14].

In addition, there is another definition of q -exponential given in combinatorial mathematics, where q -exponential is a q -analog of the standard exponential function namely, the eigenfunction of a q -derivative. There are many q -derivatives, for example, the classical q -derivative, the Askey-Wilson operator and so on [15]. Therefore, unlike the classical exponentials, q -exponentials are not unique. Moreover, it has been constructed rational expansions to e^x by Németh and Newman in Ref. [16].

A special function very important is the gamma function $\Gamma(z)$, $z \in \mathbb{C}$, $\Re\{z\} > 0$. This is an extension for the complex plane of the factorial function $n!$, for $n \in \mathbb{N}$, with its argument shifted down by 1, to real and complex numbers. Thus, the gamma function is defined for all complex numbers except for non positive integers. It raises as component in various probability distributions, and as such it is applicable in the fields of probability, statistics and statistical physics, as well as in combinatorics [17] [18] [19] [20] [21]. For instance, the well known Stirling formula depends on the factorial function as [22]

$$\sqrt{2\pi n} \left(\frac{n}{e}\right)^n \leq n! \leq \sqrt{2\pi n} \left(\frac{n}{e}\right)^n e^{(1/12n)}. \quad (1)$$

Furthermore, this function if relate with the Shannon's entropy that gives an approach to the information measure

$$\lim_{n \rightarrow \infty} \frac{1}{n} \ln \left[\frac{n!}{(p_1 n)! (p_2 n)! \cdots (p_k n)!} \right] = - \sum_{i=1}^k p_i \ln p_i. \quad (2)$$

The gamma function is extended by analytic continuation to all complex numbers except the non-positive integers (where the function has simple poles), yielding a meromorphic function which we call the gamma function. It has no zeroes and hence, the reciprocal gamma function $1/\Gamma(z)$ is a holomorphic function. In fact, gamma function corresponds to Mellin transform [23] of the negative exponential function: $\Gamma(z) = \{ \mathcal{M} e^{-x} \}(z)$.

The generalized gamma function can be applied to nonlinear systems (NL) class obeyed by the nonlinear equations. This has become an important subject in the mathematical physics in recent years due to their ability to explain several complex behaviors in the nature [24] [25]. Many areas of physics such as plasma

physics and non-equilibrium have benefited from the study of NL equations [7]. However, it is well known that, in general, nonlinear problems are impossible to solve analytically. The essential difference is that linear systems can be broken down into parts while the nonlinear not. When the parts of a system interfere, either cooperate or compete. The interactions are nonlinear and hence, the principle of superposition fails [26]. Within the realm of physics, the nonlinearity is vital for many areas, for instance, for the superconductivity and Josephson junctions arrays [26].

In this work, we propose the representation of some special functions such as the gamma function in terms of q -exponentials functions of nonadditive statistical mechanics. The plan of this paper is the following. In Section 2, we represent the generalized gamma function expressed in terms of q -exponential functions. In Section 3, we use another representation for the q -exponential in the literature to represent the generalized gamma function. In the last section, Section 4, we present our conclusions and final remarks.

2. Generalized Gamma Function

The generalized gamma function, defined using the q -exponential distribution, is defined by the integral

$$\Gamma_q(z+1) = \int_0^\infty x^z e_q^x dx, \quad (3)$$

where $q \in (0, 1]$ and $z \in \mathbb{C}$ and $\Re\{z\} > 0$. In the limit $q \rightarrow 1$, we have $\Gamma_q(z) = \Gamma_1(z) = \Gamma(z)$ and $\Gamma(n) = (n-1)!$ for $n \in \mathbb{N}$ and $\Gamma(z+1) = z\Gamma(z)$ for $z \in \mathbb{C}$.

Since $e_q^{x-1} \ll x^{z-1}$, when x is positive and $x \in (0, 1]$, we can write

$$\left| \int_0^1 e_q^x x^{z-1} dx \right| < \left| \int_\epsilon^1 x^{z-1} dx \right| = \frac{1}{z} - \frac{\epsilon^z}{z} \quad (4)$$

and, for $x > 0$ the integral is limited for $1/x$.

By making x fixed and ϵ decreasing the value of integral increases monotonically, *i.e.*

$$\int_0^1 e_q^x x^{z-1} dx = \lim_{\epsilon \rightarrow 0} \int_\epsilon^1 e_q^x x^{z-1} dx \quad (5)$$

$$\exists \forall x > 0.$$

e_q^{ix} presents the properties $[e_q^{ix}]^* = [e_q^{-ix}]$. The q -exponential function is a deformation of the standard exponential function using the real parameter q [27] [28]

$$e_q^x = \begin{cases} [1 + (q-1)x]^{1/(q-1)}, & -\infty < x \leq 0, \\ [1 + (1-q)x]^{1/(1-q)}, & 0 \leq x < \infty. \end{cases} \quad (6)$$

The inverse of the q -exponential function is the q -logarithm function, $\ln_q(x)$, defined as

$$\ln_q(x) = \begin{cases} \frac{x^{q-1} - 1}{q-1}, & 0 < x \leq 1, \\ \frac{x^{1-q} - 1}{1-q}, & 1 \leq x < \infty. \end{cases} \tag{7}$$

The formulae in Equation (6) hold true only for $q \in (0, 1]$. In this interval x and q are mathematically independent. The complete definitions can be given in two equivalent ways: one either changes the full expression of the q -deformed functions appropriately and uses the interval $q \in (0, 1]$ only as in the equation above or one can consider a unique expression and change the deformation parameter interval as [28]

$$e_q^x = [1 + (1-q)x]^{1/(q-1)} \begin{cases} -\infty < x \leq 0, & q \in [1, 2), \\ 0 \leq x < \infty, & q \in (0, 1]. \end{cases}$$

$$\ln_q(x) = \frac{x^{1-q} - 1}{1-q} \begin{cases} 0 < x \leq 1, & q \in [1, 2), \\ 1 \leq x < \infty, & q \in (0, 1]. \end{cases} \tag{8}$$

The parameter q represents the degree of non-additivity. Thus, solving the integral, Equation (3) and using the definition of q -exponential, we obtain the generalized gamma function given as

$$\Gamma_q(p+1) = \frac{p(p-1)(p-2)(p-3)\cdots \times [p-(p-1)]}{(2-q)(3-2q)(4-3q)(5-4q)\cdots \times [p+2-(p+1)q]} \int_0^\infty (e_q^{-x})^{(p+2)(1-q)+q} dx, \tag{9}$$

where $\Gamma(p+1) = p!$ for $p \in \mathbb{N}$ and $\Gamma(z+1) = z\Gamma(z)$, $z \in \mathbb{C}$. Therefore, using the standard factorial function, we have the recurrence relation obeyed for the generalized gamma function given by

$$\Gamma_q(z+1) = \frac{z\Gamma(z)}{\prod_{j=1}^p [j+2-(j+1)q]}, \tag{10}$$

Consequently, we can obtain the expression for the q -factorial, $[p]_q!$ as

$$[p]_q! = \frac{p!}{\prod_{j=1}^p [j+2-(j+1)q]} \tag{11}$$

where $p \in \mathbb{N}$.

We also obtain the generalized incomplete gamma functions

$$\Gamma_q(a, x) = \int_x^\infty z^{a-1} e_q^z dz. \tag{12}$$

$$\gamma_q(a, x) = \int_0^x z^{a-1} e_q^z dz, \tag{13}$$

with $\Re(a) > 0$, where

$$\Gamma_q(a, x) + \gamma_q(a, x) = \Gamma_q(a). \tag{14}$$

In addition, we have the following generalized functions that if relate with the

incomplete generalized gamma function

$$\operatorname{erfc}_q(x) = \frac{1}{\sqrt{\pi}} \gamma_q(1/2, x^2) \quad (15)$$

that is the generalized complementary error function, besides

$$E_{qn}(x) = \int_1^\infty \frac{e_q^{-xt}}{t^n} dt, \quad (16)$$

where we define the generalized exponential integral function

$$E_{q1}(x) = -E_q i(-x) \quad \text{as}$$

$$E_{q1}(x) = \int_{-\infty}^x \frac{e_q^t}{t} dt. \quad (17)$$

In **Figure 1** we plot the generalized gamma function $\Gamma_q(z)$ for q value $q = 0.9$ and for standard gamma function $\Gamma(z)$ (that corresponds to $q = 1$ case). The graphic of $\Gamma_q(z)$ changes a lot with q value as showed in **Figure 2**. This is due to the fact the q -exponential function to represent a family of functions (one for each value of q within interval $(0,1)$ where the case $q = 1$ (the standard exponential function, e^x) corresponds to only one function of these class of q -exponential functions. We get that for the particular case $q = 0.9$, the q -gamma function exhibits a behavior nearest to standard exponential than q -exponentials defined for other q values.

By using the definition of q -exponential, we obtain the generalized incomplete q -gamma function given as

$$\Gamma_q(a, x) = \frac{x^{a-1}}{2-q} (e_q^{-x})^{2-q} + \frac{a-1}{2-q} \Gamma_q(a-1, x) \quad (18)$$

and

$$\gamma_q(a, x) = \frac{x^{a-1}}{q-2} (e_q^{-x})^{2-q} + \frac{a-1}{2-q} \gamma_q(a-1, x). \quad (19)$$

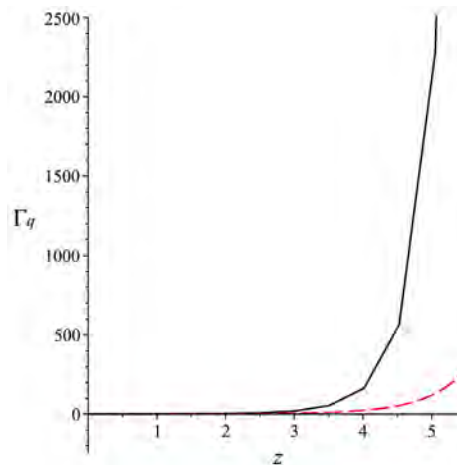


Figure 1. Plot of the generalized gamma function $\Gamma_q(z)$ for q value $q = 0.9$ and for standard gamma function $\Gamma(z)$ (that corresponds to $q = 1$ case).

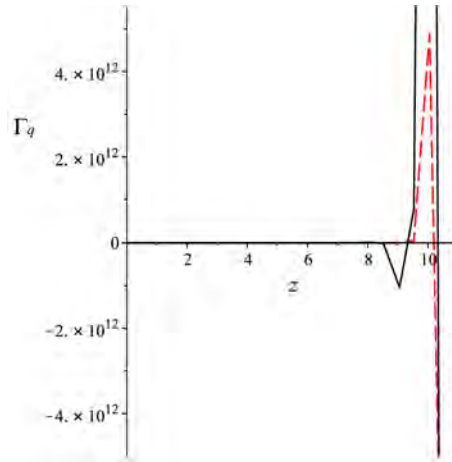


Figure 2. Plot of the generalized gamma function $\Gamma_q(z)$ for q values $q = 0.91$ (red-dashed-line) and $q = 0.89$ (black-solid-line). The standard gamma function $\Gamma(z)$ case corresponds to $q = 1$ case.

In addition, we also obtain the generalized exponential integral function as

$$E_{q1}(x) = \frac{1}{2-q} \left(e_q^x \right)^{\frac{2-q}{1-q}}. \tag{20}$$

Finally, we have the generalized logarithm integral function $li_q(x) = E_q i(\ln_q(x))$, given by

$$li_{q1}(x) = \int_0^x \frac{dt}{\ln_q(t)}. \tag{21}$$

Consequently, we obtain $li_q(x)$ given as

$$li_{q1}(x) = \int_0^x \frac{dt}{\ln_q(t)} = (1-q) \int_0^x \frac{dt}{t^{1-q} - 1} = - \int_0^x dt \sum_{n=0}^{\infty} (t^{1-q})^n = - \sum_{n=0}^{\infty} \frac{x^{n(1-q)+1}}{n(1-q)+1}, \tag{22}$$

where $|x| < 1$.

3. Another Representation

Another type of q -exponential is defined using the following series expansion [1]

$$e_q^{-x} = \sum_{n=0}^{\infty} \frac{(-x)^n}{[n]_q!} = \sum_{n=0}^{\infty} \frac{(-x)^n (1-q)^n}{(q; q)_n}, \tag{23}$$

where $[n]_q!$ is the q -factorial [29]

$$\begin{aligned} [n]_q! &= [1]_q [2]_q \cdots [n-1]_q [n]_q \\ &= \frac{1-q}{1-q} \frac{1-q^2}{1-q} \cdots \frac{1-q^{n-1}}{1-q} \frac{1-q^n}{1-q} \\ &= 1 \cdot (1+q) \cdots (1+q+\cdots+q^{n-2}) (1+q+\cdots+q^{n-1}) \\ &= \frac{(q; q)_n}{1-q^n}, \end{aligned} \tag{24}$$

where we use the q -bracket given by

$$[n]_q = \frac{1-q^n}{1-q} \tag{25}$$

In addition, we have the q -Pochhammer symbol given as [30] [31]

$$(q; q)_n = (1-q^n)(1-q^{n-1}) \cdots (1-q) \tag{26}$$

The graphic of $y = e_q^{-x}$, given by Equation (23), for q value of $q = 0.9$ is given in **Figure 3**. The black-solid-line corresponds to series in Equation (23) until $n = 10$. The red-dashed-line correspond to sum until $n = 100$. So, for $n > 100$, the behavior of graphic does not change a lot (for $n \rightarrow \infty$).

The generalized gamma function given by the integral

$$\Gamma_q(z+1) = \int_0^\infty x^z e_q^{-x} dx, \tag{27}$$

In **Figure 4**, we plot the generalized gamma function $\Gamma_q(z)$ for $z \in \mathbb{N}$ and q value as $q = 0.9$. The behavior of the graphic changes with q as in the before case. However, we have here, $q \in \mathbb{R}$ and $z \in \mathbb{N}$ and $\Re\{z\} > 0$. Remembering that here, this q -exponential is not that defined in the nonadditive statistical mechanics. Therefore, we obtain the integral Equation (27) as (**Figure 4**)

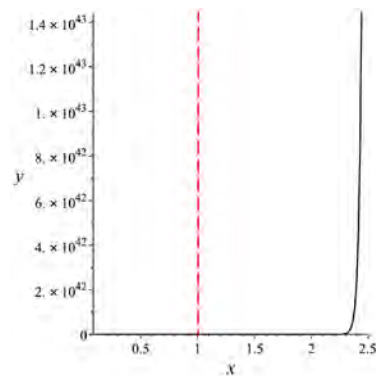


Figure 3. Plot of $y = e_q^{-x}$, given by Equation (23), for q value of $q = 0.9$. The black-solid-line corresponds to series in Equation (23) until $n = 10$. The red-dashed-line correspond to sum until $n = 100$.

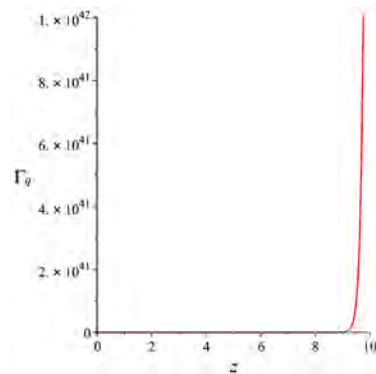


Figure 4. Graphic of generalized gamma function $\Gamma_q(z)$ for integer z , and $q = 0.9$. The sum in series given by Equation (23) is for $n = 100$. The Γ_q axis has been rescaled as $\Gamma_q \rightarrow \Gamma_q / 7.773783455 \times 10^{40005}$.

$$\Gamma_q(z+1) = \int_0^\infty x^z e_q^{-x} dx = \sum_{n=0}^\infty \frac{(-1)^n}{[n]_q!} \int_0^\infty \frac{dx}{x^{n+z}}, \tag{28}$$

where the integration contour C in the integral above is represented in **Figure 5**; and $z < -n - 1$. The integral above can be solved using the residue technique as

$$\oint_C \frac{dz}{z^{n+\xi}} = \int_\epsilon^\infty \frac{dx}{x^{n+\xi}} + \int_\infty^\epsilon \frac{dx}{x^{n+\xi}} + \int_{C'} \frac{dz}{z^{n+\xi}}, \tag{29}$$

where $z = \epsilon e^{i\theta}$, $dz = i\epsilon e^{i\theta} d\theta$, where we have taken the limit $\epsilon \rightarrow 0$ and thus, from the above integral

$$\left[e^{2\pi i(n+\xi)} - 1 \right] \int_0^\infty \frac{dx}{x^{n+\xi}} = \frac{2\pi i}{(n+\xi+1)!} \frac{d^{n+\xi+1}}{dz^{n+\xi+1}} \left[(z-z_0)^{n+\xi} \frac{1}{z^{n+\xi}} \right] \Big|_{z_0=0} = 0 \tag{30}$$

which cancels for $\forall z | z < -n - 1$. For other z values the integral of the generalized gamma function diverges. However, for the incomplete gamma function

$$\gamma_q(z+1, x) = \int_0^x t^z e_q^{-t} dt = \sum_{n=0}^\infty \frac{(-1)^n}{[n]_q!} \int_0^x t^{n+z} dt = \sum_{n=0}^\infty \frac{(-1)^n}{[n]_q!} \frac{x^{n+z+1}}{n+z+1}, \tag{31}$$

The integral of the incomplete generalized gamma function converges $\forall n, z$ values. Because of the complicated behavior of the derivative of the q -exponential function, the generalized gamma function here does not obey the property $\Gamma(z+1) = z\Gamma(z)$ obeyed by the standard gamma function.

For the generalized exponential integral function, we obtain

$$E_q i(x) = \int_x^b \frac{e_q^{-t}}{t} dt = \sum_{n=0}^\infty \frac{(-1)^{n-1}}{[n]_q!} \int_x^b t^{n-1} dt,$$

where $b \in \mathbb{R}$. However for $b \rightarrow \infty$ the integral above diverges. The same behavior we have for the generalized integrals Equation (16).

4. Final Remarks

In summary, we have proposed a generalization of the complete and uncomplete gamma functions using q -exponential functions. This subject can be of interest

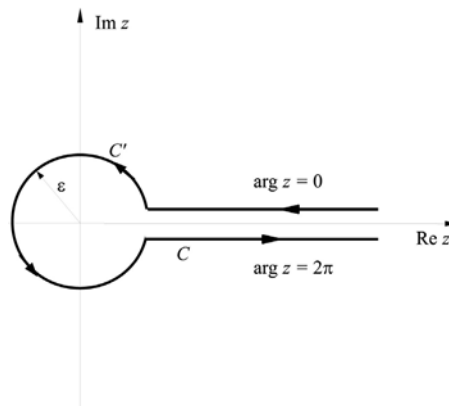


Figure 5. Contour for the calculation of the integral in the Equation (29).

in many branches of physics due to the many phenomena associated with the nonlinearity. Recently, a connection between generalized functions of the non-additive statistical mechanics framework and nonlinear equations has been investigated. In literature, were proposed other deformations of the Γ -function in terms of deformed factorials [32], where the q -factorial is

$x! \otimes_q = e^{\sum_{i=1}^x \ln_q(i)} = \Gamma_q(x+1)$. These definitions are different from the proposed here.

Acknowledgements

This work was partially supported by CNPq (National Council for Scientific and Technological Development).

Conflicts of Interest

The author declares no conflicts of interest regarding the publication of this paper.

References

- [1] Exton, H. (1983) *Q-Hypergeometric Functions and Applications*. Halstead Press, New York.
- [2] Tsallis, C. (1988) *Journal of Statistical Physics*, **52**, 479-487.
<https://doi.org/10.1007/BF01016429>
- [3] Tsallis, C. (2009) *Introduction to Nonextensive Statistical Mechanics*. Springer, Santa Fé, New Mexico.
- [4] Jauregui, M. and Tsallis, C. (2011) *Physics Letters A*, **375**, 2085-2088.
<https://doi.org/10.1016/j.physleta.2011.04.014>
- [5] Tsallis, C. (2012) *International Journal of Bifurcation and Chaos*, **22**, Article ID: 1230030. <https://doi.org/10.1142/S0218127412300303>
- [6] Jauregui, M. and Tsallis, C. (2010) *Journal of Mathematical Physics*, **51**, Article ID: 063304. <https://doi.org/10.1063/1.3431981>
- [7] Nobre, F.D., Rego-Monteiro, M.A. and Tsallis, C. (2012) *Europhysics Letters*, **97**, Article ID: 41001. <https://doi.org/10.1209/0295-5075/97/41001>
- [8] Nobre, F.D., Rego-Monteiro, M.A. and Tsallis, C. (2011) *Physical Review Letters*, **106**, Article ID: 140601. <https://doi.org/10.1103/PhysRevLett.106.140601>
- [9] Lima, L.S. (2017) *The European Physical Journal B*, **90**, 180.
<https://doi.org/10.1140/epjb/e2017-80255-8>
- [10] Havrda, J. and Charvát, F. (1967) *Kybernetika*, **3**, 30-35.
- [11] Daróczy, Z. (1970) *Information and Computation*, **16**, 36-51.
[https://doi.org/10.1016/S0019-9958\(70\)80040-7](https://doi.org/10.1016/S0019-9958(70)80040-7)
- [12] Cirto, L.J.L., Lima, L.S. and Nobre, F.D. (2015) *Journal of Statistical Mechanics*, **4**, P04012. <https://doi.org/10.1088/1742-5468/2015/04/P04012>
- [13] Cirto, L.J.L., Assis, V.R.V. and Tsallis, C. (2014) *Pysica A*, **393**, 286-296.
<https://doi.org/10.1016/j.physa.2013.09.002>
- [14] Nobre, F.D. and Tsallis, C. (2003) *Physical Review E*, **68**, Article ID: 036115.
<https://doi.org/10.1103/PhysRevE.68.036115>
- [15] Gasper, G. and Rahman, M. (2004) *Basic Hypergeometric Series*. Cambridge Uni-

- versity Press, Cambridge. <https://doi.org/10.1017/CBO9780511526251>
- [16] Komarov, M.A. (2018) (2019) *Journal of Approximation Theory*, **240**, 126-128. <https://doi.org/10.1016/j.jat.2018.10.001>
- [17] Dar, S.A. and Paris, R.B. (2019) *Journal of Computational and Applied Mathematics*, **348**, 237. <https://doi.org/10.1016/j.cam.2018.08.045>
- [18] Wang, X. (2016) *Integral Transforms and Special Functions*, **27**, 347. <https://doi.org/10.1080/10652469.2015.1128432>
- [19] Abd-Elhameed, W.M. (2015) *Integral Transforms and Special Functions*, **26**, 586-599. <https://doi.org/10.1080/10652469.2015.1029924>
- [20] Brychkov, Y.A. and Saad, N. (2014) *Integral Transforms and Special Functions*, **25**, 111-123. <https://doi.org/10.1080/10652469.2013.822207>
- [21] Bibby, B.M. and Vth, M. (2011) *Statistics and Probability Letters*, **81**, 884. <https://doi.org/10.1016/j.spl.2010.12.019>
- [22] Dutka, J. (1991) *Archive for History of Exact Sciences*, **43**, 225-249. <https://doi.org/10.1007/BF00389433>
- [23] Whittaker, E.T. and Watson, G.N. (1996) *A Course of Modern Analysis*. Cambridge University Press, Cambridge. <https://doi.org/10.1017/CBO9780511608759>
- [24] Habib, G. and Kerschen, G. (2016) *Physica D*, **332**, 1-8. <https://doi.org/10.1016/j.physd.2016.06.001>
- [25] Fernández-García, S., Krupa, M. and Clément, F. (2016) *Physica D*, **332**, 9-22. <https://doi.org/10.1016/j.physd.2016.06.002>
- [26] Strogatz, S.H. (1994) *Nonlinear Dynamics and Chaos*. Cambridge University Press, Cambridge.
- [27] Umarov, S., Tsallis, C. and Steinberg, S. (2008) *Milan Journal of Mathematics*, **76**, 307-328. <https://doi.org/10.1007/s00032-008-0087-y>
- [28] Oikonomou, T. and Gagci, G.B. (2010) *Physics Letters A*, **374**, 2225-2229. <https://doi.org/10.1016/j.physleta.2010.03.038>
- [29] McIntosh, R.J. (1999) *The Ramanujan Journal*, **3**, 205. <https://doi.org/10.1023/A:1006949508631>
- [30] Guidottia, P. and Shaob, Y. (2017) *Nonlinear Analysis*, **150**, 114. <https://doi.org/10.1016/j.na.2016.11.003>
- [31] Schmidt, M.D. (2017) Combinatorial Identities for Generalized Stirling Numbers Expanding ℓ -Factorial Functions and the ℓ -Harmonic Numbers.
- [32] Oikonomou, Th. (2007) *Physica A*, **386**, 119-134. <https://doi.org/10.1016/j.physa.2007.08.025>

Effect of Reactor Neutrinos on Beta-Decay

Boris V. Vasiliev

Dubna, Russia

Email: bv.vasiliev@yandex.com

How to cite this paper: Vasiliev, B.V. (2020) Effect of Reactor Neutrinos on Beta-Decay. *Journal of Modern Physics*, 11, 91-96.

<https://doi.org/10.4236/jmp.2020.111005>

Received: November 23, 2019

Accepted: January 7, 2020

Published: January 10, 2020

Copyright © 2020 by author(s) and Scientific Research Publishing Inc. This work is licensed under the Creative Commons Attribution International License (CC BY 4.0).

<http://creativecommons.org/licenses/by/4.0/>



Open Access

Abstract

The pulsed nuclear reactor was used to measure the effect of neutrinos on the beta-decay of $^{90}\text{Sr}/^{90}\text{Y}$ nuclei. This measurement shows that some increase in the decay rate occurs in a few tens of milliseconds after reactor flashes.

Keywords

Neutrino, Pulse Nuclear Reactor, Short-Lived Isotope, Beta-Decay

“Something that doesn’t really interact with anything is changing something that can’t be changed.”

E. Fischbach, J. H. Jenkins [1]

1. Introduction

1.1. Beta-Decay

The state of radioactive nuclei is energetically unstable. At decay, they pass from a certain excited state to a state with lower energy.

The question arises: what is the reason that at the some moment there is a decay of a particular nucleus? And in general, is such a deterministic approach to this problem legitimate?

The assumption that the cause of the decay of radioactive nuclei may be their interaction with the neutrino flux was repeatedly expressed earlier [1] [2] [3].

It can be assumed that in order to cause a radioactive decay occurring with the energy releasing, a quasi-elastic collision of neutrino with a nucleus is enough.

The electromagnetic model of neutron [4] allows to calculate all its main parameters—mass, spin, magnetic moment, decay energy. Only the time of its life defies calculation.

According to this model, proton and electron forming the neutron are bound by electromagnetic forces. These forces do not carry any mechanism of degrada-

tion of the bound state. There is no internal cause that could cause the loss of stability of neutron and its decay.

Therefore, we can assume that β -decay is a forced phenomenon that occurs under the external influence of the neutrino flux.

This assumption can be verified if the correlation between the neutron lifetime or the rate of the nuclei β -decay and the intensity of the neutrino flux incident on them can be studied.

1.2. The Neutron Time of Life

Careful measurements of the neutron lifetime were carried out repeatedly. The results of these measurements, carried out at different reactors, differ markedly.

According to measurements made in the past century at relatively small reactors, the average neutron lifetime is 885.7 ± 0.8 s [5].

In 2005, these measurements were repeated on the powerful research reactor in Grenoble.

These measurements showed that the neutron lifetime is equal to $878.5 \pm 0.7 \pm 0.3$ sec [5].

It can be assumed that the discrepancy is caused by a more powerful neutrino flux of the Grenoble reactor.

1.3. The Effect of Solar Neutrinos on β -Decay

Extremely interesting results were published by E. Fischbach, J. H. Jenkins *et al.* [1].

According to experiments conducted earlier at different times and in different countries of the world, the nuclear decay rate under terrestrial conditions is variable. It depends on the Earth-Sun distance.

Summarizing these measurement data, authors [1] expressed a hypothesis about the possible influence of the solar neutrino flux on the nuclear decay rate.

Accordingly to measurement data [6], the sunny neutrino flux is

$$\Phi_{\odot} \approx 6 \times 10^{10} \nu / \text{cm}^2 \cdot \text{s}. \quad (1)$$

Proceeding from the Fischbach-Jenkins assumption, then the rate of measured in our laboratories beta-decay should change throughout the year due to the movement of the Earth in the elliptical orbit around the Sun. Since the difference between the distances to the Sun at perihelion and aphelion is about 3.5%, then the corresponding solid angle of the earth laboratory changes by approximately 7% at the same time. If the β -decay of nuclei would be caused only by the solar neutrino flux, then we can expect that the rate of β -decay in the terrestrial laboratory must be modulated to a depth of 7% with a period equal to year.

It is remarkable that the experiments basically confirmed the Fischbach-Jenkins theory. The decay rate of a number of nuclei really turned out to be sinusoidally modulated with a period equal to year.

The only difference was that the modulation depth was about 10 times smaller.

This can be explained if we assume that the solar neutrino flux is only 1/10 of the total neutrino flux, which affects the decay of nuclei in our laboratories, and the total neutrino flux from all cosmic sources

$$\Phi_{\text{cosmic}} \approx 10^{12} \nu/\text{cm}^2 \cdot \text{s}. \quad (2)$$

2. Measurement of the Effect of Reactor Neutrinos on β -Decay

2.1. The Flux of Reactor Neutrinos

Neutrinos emitted by nuclear reactors usually have fluxes that are much smaller than cosmic neutrinos, but the energy of reactor neutrinos is higher [7].

In our experiment, the pulse reactor IBR-2 (Dubna) was used as the neutrino source. Its average power was equal to

$$W_{\text{IBR-2}} \approx 1.6 \text{ MW} \approx 10^{19} \text{ MeV/sec}. \quad (3)$$

Short explosions of its activity follow one after the other every

$$\tau_r = 0.2 \text{ s}. \quad (4)$$

The duration of the flash was equal to

$$\tau_f \approx 300 \text{ mks}. \quad (5)$$

As fission of one nucleus into nuclear fuel releases energy [7] [8]

$$E_f \approx 200 \text{ MeV} \quad (6)$$

the reactor produces

$$N_f \approx 5 \times 10^{16} \text{ fission/s} \quad (7)$$

acts of fission per second.

The mechanism leads to the generation of neutrinos in the fission reaction, due to the fact that β -active nuclei born as fragments of the fuel fission.

However, basically these fragments in our case can be considered as long-lived because their half-life is longer than the period between our reactor flashes τ_r . Neutrinos emitted during the decay of these β -active nuclei are not "tied" to a specific reactor flash.

They created in our experiment a small increase in the background.

There are few short-lived isotopes that have a half-life of $T_{1/2} < \tau_r$ [9]. These are, for example, the nuclei ^{12}B ($T_{1/2} \approx 20 \text{ ms}$).

If we assume that one act of plutonium fission produces one short-lived isotope, emitting one neutrino during its decay, then the flux of these neutrinos Φ_{react} in the experimental hall of the reactor at a distance of about 20 meters from its core will be only a small part of the flux of cosmic neutrinos (Equation (2)):

$$\frac{\Phi_{\text{react}}}{\Phi_{\text{cosm}}} \approx 1.5 \times 10^{-3}. \quad (8)$$

However, the effect of this flux can be registered, since the impact of the pulse reactor can be accumulated if the addition of the measurement data is carried

out synchronously with the reactor flashes.

The discriminator that sets the threshold for recording photomultiplier pulses played an important role in the setup we used (Figure 1). The nuclei of strontium-90 at beta-decay starts a chain of transformations:



The energy distribution of beta electrons in this chain is shown in Figure 2.

The presence of a significant difference in the energy of beta-electrons formed during the decay of ^{90}Sr and ^{90}Y atoms gives rise to the assumption that the effect of reactor neutrinos on these decays may also be different.

In order to register this difference, the influence of reactor neutrinos on beta-decay was measured at different levels of beta-electron pulse energy discrimination (Figure 3). The exponential component of the complete set of measured data was obtained by computer calculation.

It should be noted that curve 5 in Figure 3 when constructed on a large scale is also an exponent with a small pre-exponential multiplier.

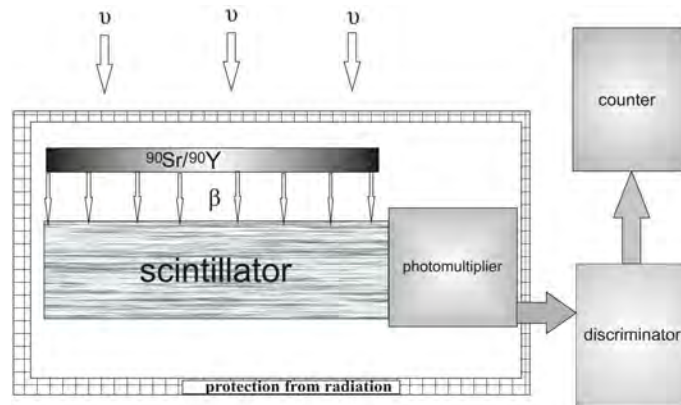


Figure 1. The scheme of measuring equipment.

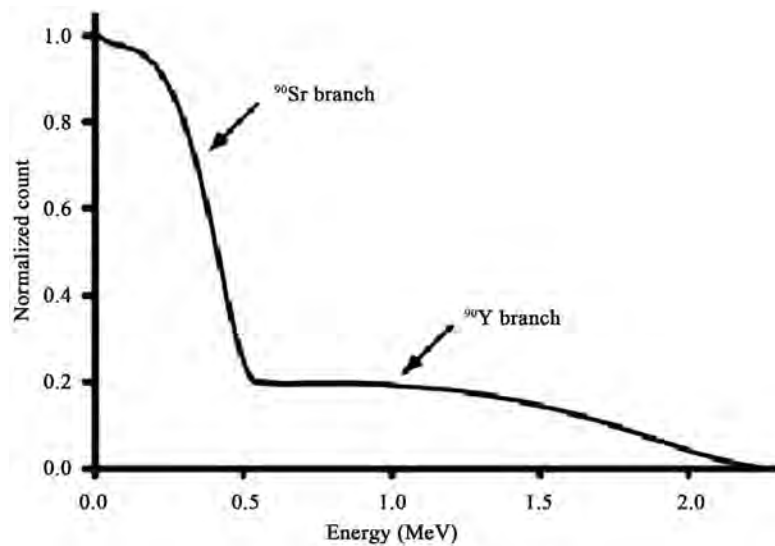


Figure 2. The energy distribution of beta-electrons generated by $^{90}\text{Sr}/^{90}\text{Y}$ nuclei.

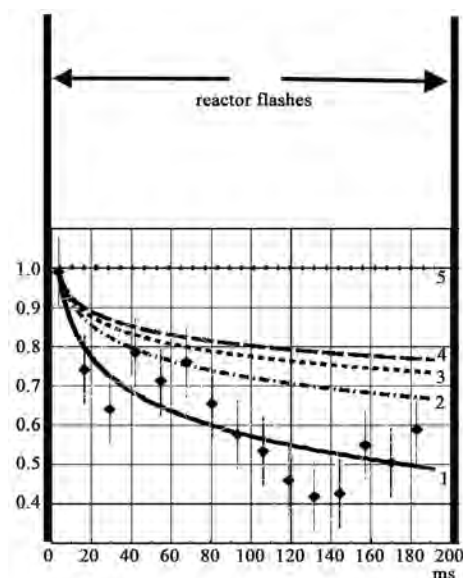


Figure 3. The result of the accumulation of registered data for beta-electrons emitted by the $^{90}\text{Sr}/^{90}\text{Y}$ -source in the time interval between reactor flashes. Accumulation was carried out in various cases from 1 day to almost 6 days. The curves in this figure are exponential components extracted by computer from a complete set of measured data. The full sets of these data were obtained at different levels of discrimination D . The curve 1: $D = 0.2 - 0.3$ MeV, curves 2, 3 and 4: $D = 0.4 - 0.5$ MeV, the curve 5: $D = 1.5 - 2$ MeV.

2.2. Experimental Equipment and Measurement Results

In our experiment, the search was made for a correlation between the rate of β -decay of $^{90}\text{Sr}/^{90}\text{Y}$ isotopes and activity pulses of nuclear reactor.

For this, the β -electrons emitted by $^{90}\text{Sr}/^{90}\text{Y}$ nuclei were recorded by a scintillator equipped with a photomultiplier (Figure 1). Electronics made it possible to amplify and discriminate photomultiplier pulses before registering them.

The radiation-sensitive part of the apparatus was protected from direct penetration of neutrons and γ -quanta from reactor with the help of a small box made of lead bricks and borated polyethylene.

The measuring system was located at a distance of about 20 meters from the core of a pulsed reactor.

Preliminary measurements showed that in the absence of the β -source, the measuring system, when the reactor is operating, gives false positives no more than once every few minutes.

Additional measurements have shown that this phenomenon is absent when the reactor is switched off and the beta-source creates a statistically uniform count in all channels.

The measurement results are shown in Figure 3.

From these data it can be seen that, at the reactor flash, there is indeed some visible increase of beta-decays intensity.

3. Conclusions

Thus, the results of measurements show that the flux of reactor neutrinos does

indeed have some quite noticeable effect on the phenomenon of beta-decay.

At that, the value of the ratio of flows is close to

$$\frac{\Phi_{react}}{\Phi_{cosm}} \approx 3 \times 10^{-4}. \quad (10)$$

This confirms the point of view on this problem that the phenomenon of beta-decay is a consequence of the neutrino flux action.

The discovered phenomenon of the impact of reactor neutrinos on beta-decay suggests that the modern approach to the problem of beta-decay should be revised. Many scientists dealing with this problem have argued that the theory of beta-decay in its present state is unsatisfactory [10]. Naturally, the fact that the beta-decay is a consequence of the impact of neutrino flux on nuclei requires the creation of a new theory of this phenomenon.

The author is sincerely grateful to Valery V. Zhuravlev for careful measurements at the reactor IBR-2 and to Evgeny P. Shabalin for discussing the problem of short-lived isotopes.

Conflicts of Interest

The author declares no conflicts of interest regarding the publication of this paper.

References

- [1] Jenkins J.H., *et al.* (2009) *Astroparticle Physics*, **32**, 42-46
- [2] Falkenberg, E.D. (2001) *Apeiron*, **8**, 32-45.
<https://pdfs.semanticscholar.org/3a21/346203f836847e60016770d931b324a46be9.pdf>
- [3] Vasiliev, B.V. (2017) *Journal of Modern Physics*, **8**, 338-348.
<http://www.scirp.org/Journal/PaperInformation.aspx?PaperID=74443>
<https://doi.org/10.4236/jmp.2017.83023>
- [4] Vasiliev, B.V. (2015) *Journal of Modern Physics*, **6**, 648-659.
<http://www.scirp.org/Journal/PaperInformation.aspx?PaperID=55921>
<https://doi.org/10.4236/jmp.2015.65071>
- [5] Serebrov, A.P. (2005) *Physics-Uspekhi*, **48**, 867-885.
<http://ufn.ru/ru/articles/2005/9/a/>
<https://doi.org/10.1070/PU2005v048n09ABEH003536>
- [6] SNO Collaboration, Ahmed, S.N., Anthony, A.E., Beier, E.W., *et al.* (2004) arXiv:nuclxex 0309004.
- [7] Hayes, A.C. and Vogel, P. (2016) arXiv:1605.02047v1.
<https://arxiv.org/pdf/1605.02047.pdf>
- [8] Krane, K.S. (1988) *Introductory Nuclear Physics*. John Wiley and Sons, Hoboken.
- [9] Kikoine, I.K. (1978) *Physical Tables*. Atomizdat, Moscow. (In Russian)
- [10] Frauenfelder, H. and Henly, E. (1974) *Subatomic Physics*. Prentice-Hall, Englewood Cliffs, NJ, USA.

Erratum to “Hypothesis of Primary Particles and the Creation of the Big Bang and Other Universes” [Journal of Modern Physics Volume 10 (2019) 1532-1547]

Slobodan Spremo

Mathematical Grammar School, Belgrade, Serbia

Email: slobodan.spremo@gmail.com

Received: October 14, 2019

Accepted: November 17, 2019

Published: November 20, 2019

Copyright © 2020 by author(s) and
Scientific Research Publishing Inc.

This work is licensed under the Creative
Commons Attribution International

License (CC BY 4.0).

<http://creativecommons.org/licenses/by/4.0/>



Open Access

The original online version of this article (Slobodan, S. (2019) Hypothesis of Primary Particles and the Creation of the Big Bang and Other Universes. *Journal of Modern Physics*, 10, 1532-1547. <https://doi.org/10.4236/jmp.2019.1013102>) unfortunately contains two mistakes.

1) Equation (13) contains an error, so it has to be replaced by this equation.

$$x' = C^2 \left(x' + ct' - ct' - \frac{c^2}{u^2} x' \right)$$

2) The Sections 6 and 7 should not be read because the way of calculation in them is not in accordance to the third postulate. These sections do not affect the results stated in the article.

Reciprocity as an Ever-Present Dual Property of Everything

Hans Hermann Otto

Department of Materials Science and Crystallography, Clausthal University of Technology, Clausthal-Zellerfeld, Germany

Email: hhermann.otto@web.de

How to cite this paper: Otto, H.H. (2020) Reciprocity as an Ever-Present Dual Property of Everything. *Journal of Modern Physics*, 11, 98-121.
<https://doi.org/10.4236/jmp.2020.111007>

Received: October 29, 2019

Accepted: January 11, 2020

Published: January 14, 2020

Copyright © 2020 by author(s) and Scientific Research Publishing Inc. This work is licensed under the Creative Commons Attribution International License (CC BY 4.0).

<http://creativecommons.org/licenses/by/4.0/>



Open Access

Abstract

Reciprocity may be understood as relation of action and reaction in the sense of *Hegel's* philosophical definition. Quoting *Kant*, freedom and ethical necessities are reciprocally limited. In this contribution, a more mathematical than philosophical reflection about reciprocity as an ever-present dual property of everything was given. As a crystallographer, the author is familiar with the action of *Fourier* transforms and the relation between a crystal lattice and its reciprocal lattice, already pointing to the duality between particles and waves. A generalization of the reciprocity term was stimulated by results of the famous *Information Relativity (IR)* theory of *Suleiman* with its proven physical manifestation of matter-wave duality, compared to the set-theoretical *E-Infinity* theory developed by *El Naschie*, where the zero set represents the pre-quantum particle, and the pre-quantum wave is assigned to the empty set boundary surrounding the pre-particle. Expectedly, the most irrational number $\varphi = (\sqrt{5} - 1)/2$ of the golden mean is involved in these thoughts, because this number is intimately connected with its inverse. An important role plays further *Hardy's* maximum quantum entanglement probability as the fifth power of φ and its connection to the dark matter. Remembering, the eleven dimensions in *Witten's M-theory* may be decomposed into the *Lucas* number $L_5 = 11 = \varphi^{-5} - \varphi^5$. Reciprocity is indeed omnipresent in our world as piloting waves that accompany all observable earthen and cosmic matter. As a side effect of the *IR* theory some fundamental constants such as the gyromagnetic factor of the electron, *Sommerfeld's* fine-structure constant as well as the charge of the electron must be marginally changed caused by altered relativistic corrections. Consequences also arise for our vision about the evolution of life and consciousness.

Keywords

Reciprocity, Reciprocal Lattice, *Fourier* Transform, *Archimedes'* Constant,

Matter-Wave Duality, Pilot Wave, Golden Mean, *E-Infinity* Theory, Information Relativity Theory, Gyromagnetic Factor, Fine-Structure Constant, Quantum Entanglement, Dark Matter and Cosmos, Superconductivity

1. Introduction

Recently, the author reported on a reciprocity relation between the mass constituents of the universe and *Hardy's* maximum quantum entanglement probability of two quantum particles [1] [2] [3] [4]. *Hardy's* maximum probability was before connected with the dark energy question, using a fractal *Cantorian* set theory developed by *El Naschie* (*E-infinity* theory) [5] and further elaborated by *Marek-Crnjac* [6]. However, in the last years a step was made in direction of a unification of physical theories with the *Information Relativity* theory of *Suleiman* [7] [8]. Whereas great philosophers understood reciprocity as relation between action and reaction (*Hegel* [9]) or as connection between freedom and ethical necessities (*Kant* [10]), in this contribution a more mathematical as well as physical view on reciprocity was given. Because the term reciprocity has something in common with the concepts of duality and complementarity, their different meaning was shortly addressed in **Appendix I**.

The following chapter deals with the *Fourier* transform and the reciprocal lattice of crystallography that describes results of diffraction on crystals as a special kind of particle-wave duality. The reciprocity relation between boundary and enclosed area of a circle is shortly treated, followed by the reciprocity property of the golden ratio in a separate chapter. Then the fractal *Cantorian* set theory of *El Naschie* [5] and *Marek-Crnjac* was appreciated [6]. The final chapter illuminates consequences of the famous scale-free *Information Relativity* theory of *Suleiman* with its proven particle-wave duality, which explains for instance the double-slit experiment [11] and suggests dark energy as piloting waves of moving matter, touching up the old *De-Broglie-Bohm* theory [12] [13] [14]. The work was supplemented by thoughts of the author about further consequences of the *IR* theory. It seems that the secrets of the electron, spin, tremor and the anomalous gyromagnetic factor (g_e) as well as electron pairing in superconductors [15] [16], can simply be explained or corrected with this new theoretical approach to demystifying the physics even more. The inferred *Sommerfeld* fine-structure constant α may be altered as well as the experimental g_e value, concerning the relativistic shift correction. Related to it, the charge of the electron has to be changed, too. In addition, a corrected version of the *Niehaus EZBW* (extended *Zitterbewegung*) may serve as a probabilistic model for the electron [17]. Consequences also arise for our vision about the evolution of life and consciousness. The conjecture is that all things are interwoven with the reciprocal, where connection with the golden ratio indicates some system stability.

The particle-wave duality is also essential in the quantum information theory,

where the unit of information is given by the quantum bit (qubit) coined by Schumacher [18], which exhibits the aspects of particle localization (counting) and wave interference to represent a signal with high fidelity [19]. Such two-state quantum system can be represented by the superposition principle:

$$SU(2) \cong H_1 \ni Q = z_1 |Yes\rangle + z_2 |No\rangle$$

where z_1 and z_2 are complex numbers, and $z_1^2 + z_2^2 = 1$ [19]. However, the quantum information aspect cannot be a main topic of this limited contribution.

2. Fourier Transform and Reciprocal Space

The diffraction of X-rays of sufficient wavelength on crystals leads to a characteristic diffraction pattern, where the electron density $\rho(\mathbf{r})$ of a crystal structure is transformed to a reciprocal lattice, weighted with intensities $I(\mathbf{h}) \propto |F(\mathbf{h})|^2$, where $F(\mathbf{h})$ represents structure amplitudes (*Fourier* coefficients) according to the transform

$$F(\mathbf{h}) = \int_V \rho(\mathbf{r}) e^{2\pi i \mathbf{h} \cdot \mathbf{r}} dV. \quad (1)$$

The vectors $\mathbf{r} = x\mathbf{a} + y\mathbf{b} + z\mathbf{c}$ and $\mathbf{h} = h\mathbf{a}^* + k\mathbf{b}^* + l\mathbf{c}^*$ are position vectors of the crystal lattice respectively the reciprocal lattice of a diffraction pattern. The lattice parameters $\mathbf{a}, \mathbf{b}, \mathbf{c}$ respectively $\mathbf{a}^*, \mathbf{b}^*, \mathbf{c}^*$ are the repeat units along the lattice axes. The reader may follow a reciprocal lattice exercise in more detail, given as a lecture in [20].

The inverse *Fourier* transform, using the structure amplitudes as coefficients, delivers the electron density $\rho(\mathbf{r})$ of the crystal

$$\rho(\mathbf{r}) = \int_{V^*} F(\mathbf{h}) e^{-2\pi i \mathbf{h} \cdot \mathbf{r}} dV^*, \quad (2)$$

where V^* is the reciprocal volume.

In this way, a crystal structure can be completely solved by means of a diffraction experiment.

However, because only intensities $I(\mathbf{h})$ are measured, phases of the structure amplitudes are lost and must be recovered by elaborated crystallographic methods.

Applying a transform such as the *Fourier* transform one goes from the object space to the image space or reciprocal space. If the original variable would be the time, then the transformed reciprocal variable would be a frequency, exemplified by the *Laplace* transform of electrical decay processes. Going from the object space to the reciprocal space one may heretically ask, what could be the *Fourier* transform of the entire cosmos, delivering an inverse universe or whatever else?

3. Relationship between Boundary and Enclosed Area of a Circle

Quoting the references [21] [22], the area enclosed by a circle of radius 1 yields

$$A = \pi = 4 \int_0^1 \sqrt{1-x^2} dx, \quad (3)$$

where π is *Archimedes'* constant, the well-known circle constant. One obtains the circumference C by using the reciprocal of the integrand

$$C = 2\pi = 4 \int_0^1 \frac{1}{\sqrt{1-x^2}} dx. \quad (4)$$

This connection between the boundary and the enclosed area is of fundamental importance. It may be thought of as a geometrical analog to the more general matter-wave duality that is being treated below. Besides, *Archimedes'* constant π and the golden ratio φ as the fractal numerical dominators of our existence show an intimate numerical connection, and we may ask, in which manner nature makes use of this [3] [23]. An elegant continued fraction representation of π was given by *Lange* [24].

4. *Mushkolaj's* Reciprocal Transition Temperatures

In 2014 *Mushkolaj* [25] has presented a theory of critical temperatures for phase transitions such as superconductivity, using an elastic atomic collisions model as well as an elastic spring model. He found two inverse T_c functions of the form

$$T_c(\text{collision}) \propto (\sqrt{M_1 \cdot M_2} \cdot \Delta x^2)^{-1}, \quad T_c(\text{spring}) \propto \sqrt{M_1 \cdot M_2} \cdot \Delta x^2 \quad (5a, b)$$

where M_1 , M_2 are the colliding or by a spring connected masses, and Δx is the distance between atoms respectively the spring stretch length in *Hooke's* region.

If we associate the atomic collision model with particles and the spring model with waves, we are faced with a reciprocity relation between the two excitation variants and again with the duality between particles and waves in a special form.

5. The Golden Mean Beauty and Its Intrinsic Reciprocity Property

The golden mean or golden ratio φ is an omnipresent number in nature, found in the architecture of living creatures as well as human buildings, music, finance, medicine, philosophy, and of course in physics and mathematics [26] [27]. It is the most irrational number known and a number-theoretical chameleon with a self-similarity property. On the other hand, its infinite continued fraction representation is the simplest of all and is represented by [28]

$$\varphi = \frac{\sqrt{5}-1}{2} = \frac{1}{1 + \frac{1}{1 + \frac{1}{1 + \dots}}} \quad (6)$$

It impressively underlines the fractal character of this number. Most obviously, the golden mean mediates stability of a system, because only "particles" as the center of gravity of vibrations with most irrational winding survive. Important relations involving φ are summarized below. However, to prevent confusion, in textbooks of mathematics the reciprocal value for φ is frequently used.

$$\varphi = \frac{\sqrt{5}-1}{2} = 0.618033988\dots, \quad \varphi^{-1} = 1 + \varphi = \frac{\sqrt{5}+1}{2} = 1.618033988\dots \quad (7a, 7b)$$

$$\varphi^2 = 1 - \varphi = 0.381966011\dots, \quad \varphi^{-2} = 2 + \varphi = 2.618033988\dots \quad (8a, 8b)$$

$$(\varphi^2 + 1)^{-1} = (\varphi^{-2} + 1)/5 \quad (9a)$$

$$\text{or equivalently } (\varphi^{-2} + 1)^{-1} = (\varphi^2 + 1)/5 \quad (9b)$$

$$\varphi^5 = \frac{1-\varphi}{1+\varphi} \varphi^2 = 0.090169943\dots \quad (10)$$

$$\frac{\varphi^5}{2} + \frac{5}{2} \varphi^2 = 1 \quad (11)$$

$$\varphi^3 + 2\varphi^2 = 1 \quad (12)$$

Hardy's maximum quantum entanglement probability of two quantum particles [1] [2] exactly equals the fifth power of φ (Figure 1). This asymmetric probability distribution function with p_τ as entanglement variable, running from not entangled states to completely entangled ones, is given by

$$P = p_\tau^2 \frac{1-p_\tau}{1+p_\tau} \quad (13)$$

This function, displayed in Figure 1, turns out to be a central topic of the *Information Relativity* theory of Suleiman [7] [8] by mapping the transformation of his relative energy density (see Chapter 9 and compare the red curves in Figure 3 and Figure 4).

The probability function according to Equation (13) can be recast to an adapted distribution by means of a varied Fisher transformation (Figure 2) [29]

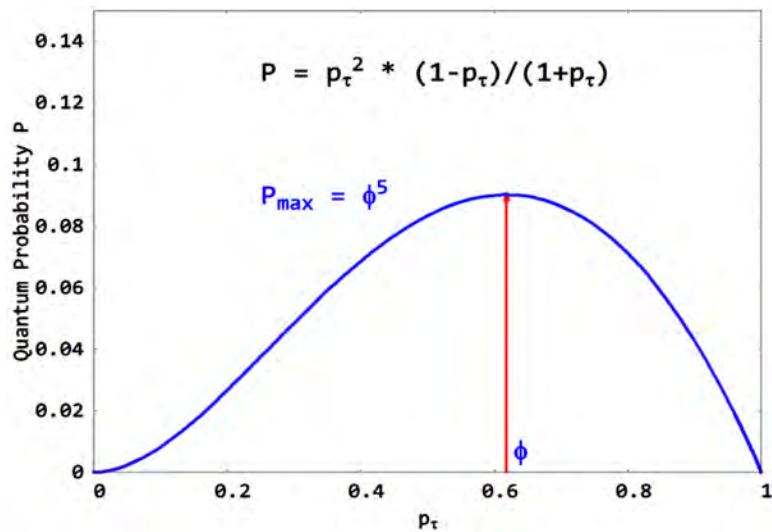


Figure 1. Hardy's quantum probability P for two particles [1], where p_τ can be thought of as entanglement variable, running from not entangled states to completely entangled ones. Compare it with the equivalent red curve in Figure 3 [3] [7].

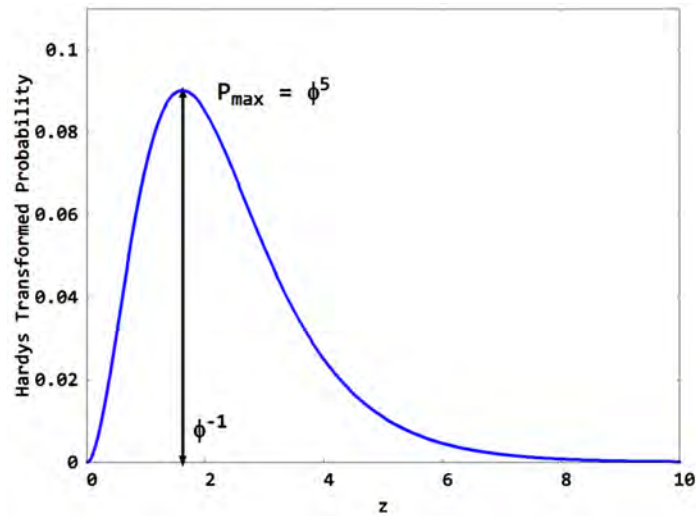


Figure 2. Fisher transform of Hardy's probability function, representing an asymmetrical distribution with its maximum now at $z = \varphi^{-1}$ (see Equation (15) and **Figure 3**).

$$z = \frac{\sqrt{5}}{2} \ln \left(\frac{1+p_\tau}{1-p_\tau} \right) = \sqrt{5} \cdot \operatorname{artanh}(p_\tau) \tag{14}$$

where the pre-factor was chosen as $a = \frac{\sqrt{5}}{2} = \varphi + \frac{1}{2}$. Then one gets for $f(z)$

$$f(z) = \left(\frac{\exp\left(\frac{z}{a}\right) - 1}{\exp\left(\frac{z}{a}\right) + 1} \right)^2 \exp\left(\frac{z}{a}\right)^{-1} \tag{15}$$

A comparison is made between the curves displayed in **Figure 1** and **Figure 2** with the result of the *IR* theory in **Figure 3**, but in logarithmic representation.

Moreover, in a subsequent contribution a geometric analog to Hardy's probability function will be presented with significance, besides geometry, to crystallography, electrostatic, botany, coding theory and other disciplines.

Infinite continued fraction representations of φ^5 and its inverse yield

$$\varphi^5 = \frac{1}{11 + \frac{1}{11 + \frac{1}{11 + \dots}}} \tag{16}$$

$$\varphi^{-5} = 11 + \varphi^5 = 11 + \frac{1}{11 + \frac{1}{11 + \frac{1}{11 + \dots}}} \tag{17}$$

We notice that $L_5 = 11$ is a *Lucas* number. It results from the definition

$$L_n = \varphi^{-n} + (-\varphi)^n \tag{18}$$

The L_n number series was named after the *French* mathematician *François Édouard Anatole Lucas* (1842-1891).

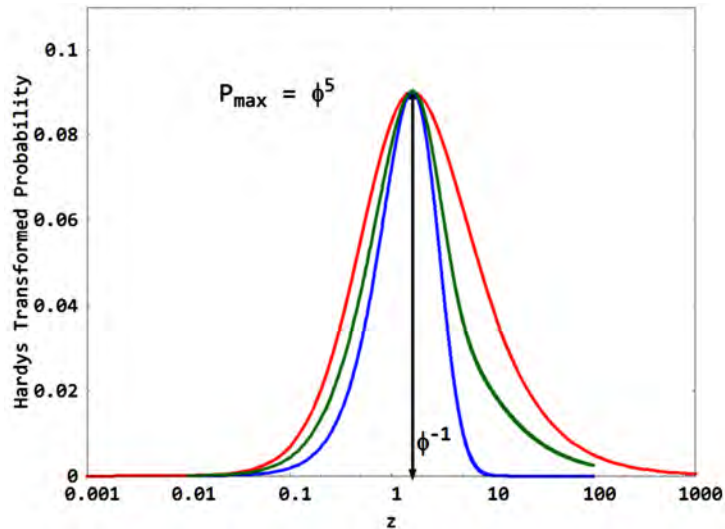


Figure 3. Fisher transform [29] of Hardy’s probability function (blue curve) [1], compared with the more convincing, but nevertheless slightly asymmetric redshift representation of the energy density according to the information relativity theory (red curve) [8] (see also Figure 4). The green curve is a further adaption in direction of the red curve.

Many researchers have found the golden ratio to be important by trying to uncover secrets of the universe and its mass respectively energy distribution [3]-[8]. In the next Chapters this significance will be demonstrated.

If one deals with exponential functions, the author has learnt from *Sherbon* [25] that the *Lambert W*-function can serve as an analog to the golden ratio for exponential functions. Again, it is shown a sort of reciprocity, if one writes the relation as follows

$$\exp(W(z)) = W(z)/z \tag{19}$$

Especially is

$$\Omega = W(1) = \exp(-W(1)) = 0.5671432904\dots \tag{20}$$

$$W(2) = \frac{1}{2} \exp(-W(2)) \tag{21}$$

and

$$W\left(\frac{1}{2}\right) = 2 \cdot \exp\left(-W\left(-\frac{1}{2}\right)\right) \tag{22}$$

The quoted publication of *Sherbon* [25] is highly interesting for all researchers, who want to learn more about of the fundamental nature of *Sommerfeld’s* fine-structure constant.

6. Golden Ratio, Archimedes’ Constant and Sommerfeld’s Fine-Structure Constant

Often you wonder why our world is what it is. Fundamental numbers such as the golden ration ϕ , the circle constant π as well as *Sommerfeld’s* fine-structure constant α and their obvious similarities play an important role. Some approxima-

tions should illustrate it. So one can connect the number π with the reciprocal of the *Sommerfeld* constant $\alpha^{-1} \approx 137$ [23] [27] or with *Hardy's* quantum probability φ^5 [23].

$$\pi \approx 3 + \frac{16}{137 - 24} = 3.1415929\dots \quad (23)$$

$$\frac{\pi - 3}{\pi} = 0.04507\dots \approx \frac{\varphi^5}{2} = 0.04508\dots \quad (24)$$

$$\frac{3}{\pi} = 0.9549296\dots \approx \frac{5}{2}\varphi^2 = 0.954915\dots \quad (25)$$

$$\alpha^{-1} = 137 + \frac{2}{5}\varphi^5 = 137.0360\dots \quad (26)$$

These approximations, believed to be accidental by others, may find now and then application in the following discussions.

7. Golden Mean and Madelung Constant for a Rocksalt-Type 2D-Lattice

In a previous publication the author drew attention to the numerical similarity between the golden mean and the *Madelung* constant [30] for a two-dimensional rocksalt-type lattice [4].

The *Madelung* constant α_{2D} was iteratively determined with very high precision by *Triebel* [31] giving

$$\alpha_{2D-\text{NaCl}} = 1.615542626711299\dots \quad (27)$$

The α_{2D} value is very close to the quotient of two *Fibonacci* numbers, $21/13 = 1.615385, \dots$ and can be adapted to φ^{-1} by only slight distortion of the square net along the two dimensions or by involving the third one to allow a quite flat curvature [4].

The difference to the inverse of the golden mean φ^{-1} is only marginal and gives

$$\varphi^{-1} - \alpha_{2D-\text{NaCl}} = 0.002491362\dots \quad (28)$$

This almost numerical equality was applied to *Villata's* lattice universe [32] consisting of matter and antimatter with gravitational charges of opposite sign at positions of a 2D rocksalt-type lattice. Then the ratio of repulsive contribution to the attractive one gives

$$1 + \alpha_{2D} \approx 1 + \varphi^{-1} = \varphi^{-2} \quad (29)$$

This relation leads the author to a proposal for the golden mean based calculation of the mass constituents of the universe [4] independent from other approaches and with only marginal differences to such results [5] [6].

A certain reciprocity property may be suggested for a two dimensional rock-salt-type matter-antimatter lattice independent of whether it is a real possibility. The question is whether a conditionally flat lattice universe with a *Madelung* constant of φ^{-1} would guarantee sufficient stability to exist over long periods of time.

8. Golden Mean as Dimension of Empty Set and Zero Set

El Naschie's E-infinity (ϵ^∞) theory [33], not commonly known or accepted by physicists, originates from a fractal *Cantorian* set theory [34] as a number-theoretical route of physics for explaining the dualism between particles and waves that can help solving cosmological mysteries such as dark matter and dark energy [35]. The quantum particle P_Q is symbolized by the bi-dimension of the zero set, while the guiding wave W_Q surrounding the quantum particle is given by the bi-dimension of the empty set according to

$$\dim(X) = (n, d_c^{(n)}) \tag{30}$$

where n is the *Urysohn-Menger* topological dimension [36] [37] and

$$d_c^{(n)} = (\varphi^{-1})^{n-1} \tag{31}$$

represents the *Hausdorff* dimension [38], where φ is the golden mean as defined before.

$$\text{It results for } P_Q \dim(P_Q) = (0, \varphi) \tag{32}$$

$$\text{respectively for } W_Q \dim(W_Q) = (-1, \varphi^2) \tag{33}$$

By using these dimensions a probabilistic quantum entanglement calculation [6] [33] with velocity restriction $v \rightarrow c$ delivers effective quantum gravity formulas for the cosmological mass (energy) constituents of baryonic matter e_M , dark matter e_{DM} , entire dark constituents e_{ED} and pure dark energy e_{PD} as follows

$$e_M = \frac{1}{2} \frac{1-\varphi}{1+\varphi} \varphi^2 = \frac{\varphi^5}{2} = 0.04508497 \tag{34}$$

$$e_{ED} = 1 - e_M = \frac{5}{2} \varphi^2 = 0.9549150 \tag{35}$$

$$e_{DM} = \frac{3}{2} \varphi^4 = 0.218847 \tag{36}$$

$$e_{PD} = 2\varphi - \frac{1}{2} = 0.736068 \tag{37}$$

$$e_M + e_{DM} + e_{PD} = 1 \tag{38}$$

Recasting the matter amounts into a suitable form,

$$e_M = \frac{1}{10} 5\varphi^5, \quad e_{DM} = \frac{1}{10} (5\varphi^5)^{-1} = 0.2218 \tag{39}$$

a reciprocity relation was confirmed between e_M and e_{DM} giving a persuasive equation for the pure dark energy [3]

$$e_{PD} = 1 - \frac{1}{10} (5\varphi^5 + (5\varphi^5)^{-1}) = 0.7331 (73.31\%) \tag{40}$$

Such quantum entanglement based coincidence means that the constituents of the cosmos should not be considered independent of each other, which was confirmed by the *IR* theory.

Importantly, if one compares the results given here with the following ones of the information relativity (*IR*) theory, then *El Naschie's* set theoretical approach is restricted to $v \rightarrow c$, whereas the more general *IR* theory delivers results for the recession velocity $\beta = \frac{v}{c}$ in the hole range $0 \leq \beta \leq 1$ (c is the speed of light).

9. Information Relativity Theory of Suleiman and Golden Mean

Many formal explanations or physical constructs that bothered long time the world of physics are overcome by the new exciting *Information Relativity* theory, developed by Suleiman [7] [8]. It is not the intention of the author to keep the reader away from studying this theory in detail for himself. Therefore, only a sparse introduction was given. *Suleiman* found an overlooked flaw in *Newton's* physics and corrected physical processes for time displacements between observer and moving bodies. Transformations for time duration, length, mass density as well as energy density were applied to a whole bunch of physical phenomena, which could be explained now in simple and beautiful clarity. For instance, *Suleiman* derived for the matter energy density e_M of a moving body with velocity v and rest density ρ_o

$$e_M = \frac{1}{2} \rho v^2 = \frac{1}{2} \rho_o c^2 \frac{1-\beta}{1+\beta} \beta^2 = e_o \frac{1-\beta}{1+\beta} \beta^2, \quad (41)$$

where $\beta = \frac{v}{c}$ is the recession velocity respectively $e_o = \frac{1}{2} \rho_o c^2$.

The matter energy density reached its maximum at a recession velocity of $\beta = \varphi$. Replacement of this special value in Equation (41) gives

$$(e_M)_{\max} = e_o \frac{1-\varphi}{1+\varphi} \varphi^2 = e_o \varphi^5 = e_o \cdot 0.09016994 \dots \quad (42)$$

Remembering, φ^5 represents *Hardy's* quantum probability at the maximum. This result was commented by the author in a publication before mentioned [3].

Suleiman aptly characterized the behavior at the critical point $\beta_{cr} = \varphi$ as phase criticality at cosmic scale [8]. The dark matter density transforms as

$$\frac{e_{DM}}{e_o} = \frac{2\beta^3}{1+\beta} \quad (43)$$

The relations are depicted in **Figure 4**. If one calculates the energy density amounts (ratios) of matter and dark matter contributions at this point, one gets again a golden mean representation like *Russian* dolls nesting

$$\varphi^3 + 2\varphi^2 = 0.236067976 \dots + 0.763932023 \dots = 1 \quad (44)$$

The difference gives $2\varphi^2 - \varphi^3 \approx (\sqrt{2} - 1) \frac{4}{\pi}$.

The case, where according to the *Information Relativity* theory of *Suleiman* [7] [8] just at the recession velocity of $\beta = 1/3$ the matter and the dark matter density will be the same, delivers for the density amount the reciprocal of another *Lucas* number, namely $L_6 = 18$ (see Chapter 5 and **Figure 4**)

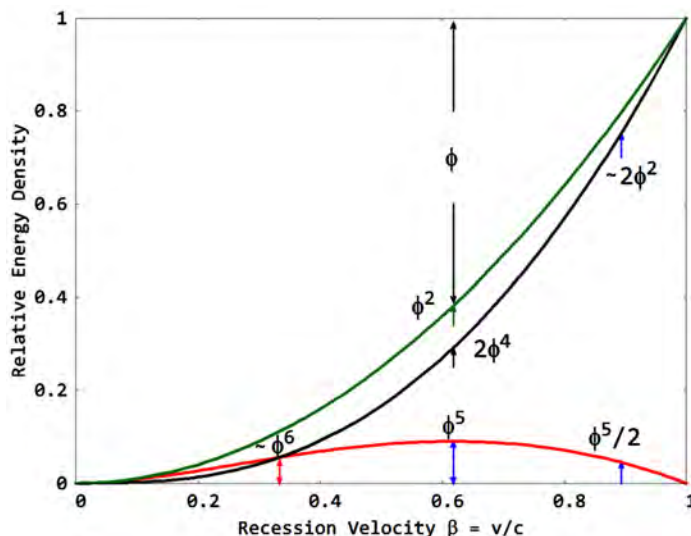


Figure 4. Golden mean dominance in the evolvement of the energy density with the recession velocity according to the information relativity theory of *Suleiman* [7] [8]. Φ^5 represents *Hardy's* maximum quantum probability. Red curve: matter energy density, black curve: dark matter energy density, green curve: energy density sum.

$$e_M = e_{DM} = L_6^{-1} = \frac{1}{18} = 0.055555\dots = (\varphi^6 + \varphi^{-6})^{-1} \approx 0.055728089\dots = \varphi^6 \quad (45)$$

Furthermore, if the recession velocity at $\beta_{eq} = 1/3$ is mirrored at $\beta_{cr} = \varphi$, it resulted $\beta_{mir} = 0.9027$. In its vicinity at $\beta = 0.89297$ the matter energy density would be exactly $\varphi^5/2 = 0.04508497\dots$ respectively the dual dark component $0.7523\dots \approx 0.763932\dots = 2\varphi^2$ (**Figure 1**).

It approximately indicated a situation that is elaborated for $v \rightarrow c$ by means of the fractal set theory summarized before in Chapter 8.

In **Figure 5** the energy densities were illustrated via the redshift, which reads as $z = \beta/(1 - \beta)$. It is suggested to fit the only slightly asymmetric red curve with the aid of a *Cauchy* function of exotic non-integer order on the basis of the golden mean introduced by the present author some time ago [39].

Suleiman's IR theory validates once more the importance of the golden mean in solving physical phenomena. Reciprocity is given by the proposed duality between particle and wave.

As was demonstrated by *Suleiman* (**Figure 6**), an increase of the redshift z caused the matter density of the travelling corpuscular particle successively to diminish, while energy is transformed into the wave-like dark component and vice versa [8]. This supports elegantly the concerns of the work here presented.

10. Mystery of the Electron and Golden Mean

The electron, considered as center of compacted information, still keeps its secrets, but not for long. Whereas the hydrogen atom problem was just solved by *Suleiman* [8] without any assumption of quantization of the electron's orbits and using IR transformation of length as

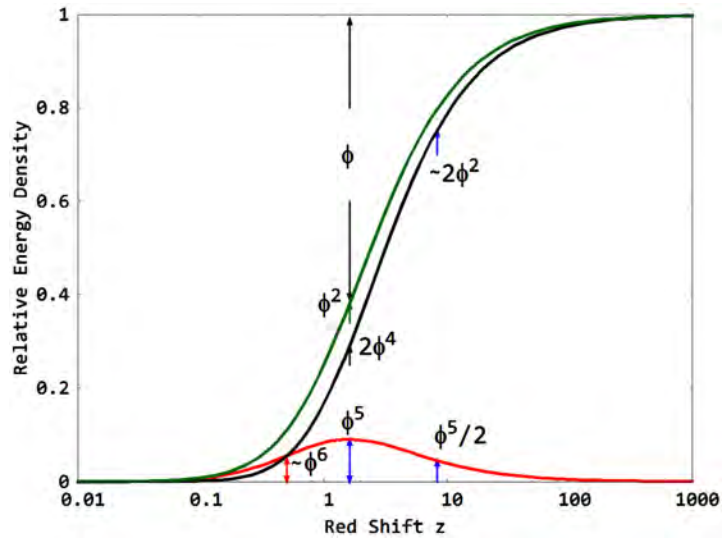


Figure 5. Energy densities related to the red shift $z = \beta/(1 - \beta)$ (logarithmic scale) according to *Suleiman* [8]. Colored curves have the same meaning as in *Figure 1*. Now the coincidence point is at $z = 1/2$.

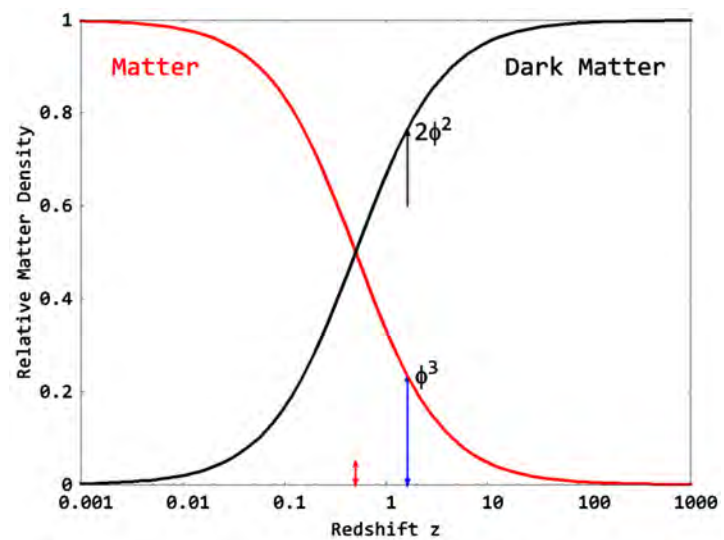


Figure 6. *Suleiman's* famous reciprocal (complementary) duality between matter density and dark matter one. Logarithmic scale, red arrow at $z = 1/2$, blue arrow at $z = \varphi^{-1} = 1.61803398\dots$ (see also Equation (39)). Applied matter density transformations in terms of the redshift [8]: $\frac{\rho_M}{\rho_0} = \frac{1}{2z+1}, \frac{\rho_{DM}}{\rho_0} = \frac{2z}{2z+1}$.

$$\frac{l}{l_0} = \frac{1+\beta}{1-\beta} \tag{46}$$

other constructs like the electron spin [25] or the measured anomalous gyromagnetic factor of the electron may be solved fractal-deterministic, supported by application of *IR* transformations. Also the fractal nature of electron pairing in superconductors should be reassessed this way.

The g_e factor of the electron, conceived as a classical charged particle, is de-

terminated by the relation

$$\vec{\mu} = g_e \mu_B \frac{\vec{S}}{\hbar}, \quad \mu_B = \frac{e}{2m} \quad (47)$$

where $\vec{\mu}$ is the observable magnetic moment, μ_B is the *Bohr* magneton, and \vec{S} is the spin of the electron, e respectively m are charge respectively mass of the electron, and \hbar is the reduced *Planck* constant.

However, the spin as half-integer quantum number of the electron was introduced without any physical justification [40]. Very recently, a first attempt has been undertaken by *He et al.* [41] to connect the golden mean with the ad hoc spin-1/2 construct. Such golden mean approach may be the result of dark halo movement around the stretched electron in the sense of the *Information Relativity* theory.

Remembering that the “anomalous part” of the gyromagnetic factor Δg_e was recently given by a simple and solely golden mean representation with sufficient accuracy [42]

$$\Delta g_e = \ln \left(1 + \frac{\phi^6}{24} \right) = 0.002319312 \dots \quad (48)$$

while a series expansion yields a value more accurate up to the tenth decimal place

$$g_e = 2 + \frac{\phi^6}{24} - \frac{1}{2} \left(\frac{\phi^6}{24} \right)^2 - \frac{1}{4} \left(\frac{\phi^6}{24} \right)^3 = 2.002319304 \dots \quad (49)$$

This result may be compared to the high accuracy of the best known experimental value for g_e determined as one-electron cyclotron transition for an electron trapped in an electrostatic quadrupol potential (*Penning* trap) [43]

$$g_e = 2.00231930436182(52) \quad (50)$$

In a subsequently presented seminal idea of *He et al.* [41] the spin quantum number s in the spin momentum term $\frac{\vec{S}}{\hbar} = \sqrt{s(1+s)}$ was replaced by a quantized golden mean $\tilde{\phi}$ giving

$$\frac{g_e}{2} = \sqrt{\tilde{\phi}(1+\tilde{\phi})} \quad (51)$$

with the value $\tilde{\phi} = 0.6190713336307(34)$ as *He-Chengtian* average [44] [45] to adapt the full accuracy of $g_e/2$. One can calculate $\tilde{\phi}$ by a very simple formula, which resembles the representation for ϕ (Equation 7(a)) and delivers exactly the given value

$$\tilde{\phi} = \frac{1}{2} \left(\sqrt{5 + (g_e + 2)(g_e - 2)} - 1 \right) = \frac{1}{2} \left(\sqrt{1 + g_e^2} - 1 \right) \quad (52)$$

and for the *IR* corrected value of $g_e = 2.0023190900$ (see Chapter 11)

$$\tilde{\phi} = 0.619071237 \dots \quad (53)$$

Using this formula, the gyromagnetic factor resulted simply as function of a/π

[46]

$$g_e \approx 2\sqrt{1 + \frac{v_K}{2\pi c}} = 2\sqrt{1 + \frac{\alpha}{\pi}} = 2.00232147 \tag{54}$$

$$\text{giving } \tilde{\varphi} = 0.619072302\dots \tag{55}$$

where v_K is the *Klizing* speed and c the speed of light.

The latest released values of *Sommerfeld's* fine-structure constant α [47] respectively its reciprocal value is quoted according to *NIST* [48] being

$$\alpha = 0.0072973525693(11) \tag{56}$$

$$\alpha^{-1} = 137.035999084(21) \tag{57}$$

An approximation using the α/π series expansion yielded

$$g_e \approx 2\sqrt{1 + \frac{\alpha}{\pi} - \frac{1}{2}\left(\frac{\alpha}{\pi}\right)^2} = 2.002318778\dots \tag{58}$$

$$\text{or } g_e \approx 2\sqrt{1 + \ln\left(1 + \frac{\alpha}{\pi}\right)} = 2.002318782\dots \tag{59}$$

$$\begin{aligned} \tilde{\varphi} &= \frac{1}{2} \left(\sqrt{5 + 4 \cdot \ln\left(1 + \frac{\alpha}{\pi}\right)} - 1 \right) \\ \text{and further} \tag{60} \\ &= \frac{1}{2} \left(\sqrt{5 + \ln\left(1 + \frac{\alpha}{\pi}\right)^4} - 1 \right) = 0.619071099\dots \end{aligned}$$

The deviation between this a bit underdetermined $\tilde{\varphi}$ value and the newly relativistic corrected one is in the seventh decimal place as well as the corresponding g -factors. It is hoped that precisely re-determined experimental factors may lessen these deviations further.

One may ask, what the infinitely continued fraction representation of $\tilde{\varphi}$ would result in. We can write similar to the golden mean [28]

$$\tilde{\varphi} = \frac{\sqrt{5 + \delta} - 1}{2} = \frac{1}{1 - \delta_1 + \frac{1}{1 - \delta_1 + \frac{1}{1 - \delta_1 + \dots}}} \tag{61}$$

The calculation with $\delta_1 = 0.00374774 \approx \frac{1}{266.\bar{6}} \approx \frac{\delta}{\varphi} \approx \frac{\varphi^5}{4!}$ yielded

$\tilde{\varphi} = 0.619071096$. Indeed, the number $266.\bar{6}$ is very interesting. Division of this number by integers frequently delivers numbers with repeating decimals, exemplified by $266.\bar{6}/24 = 11.\bar{1}$. If one associates this number with rounds, then one would need 27 ones to complete 20-times the full 360 degrees extent.

With an assumed involvement of the fifth power of the golden mean in the continued fraction representation one may speak of a nested golden mean representation. This result supports once more the fractal-deterministic approach chosen for the physics of the electron beyond the ad hoc half-spin assumption, characterizing the electron as complexly nested resonating entity. An alternating approach for the gyromagnetic factor is given in **Appendix II**.

11. Alteration of Fundamental Constants

The calculation of the electron’s gyromagnetic factor is the prime example for application of the *QED*. However, a cascade of *Feynman* diagram calculation must be done to determine the pre-factors of systematic perturbative expansions in powers of α/π [46] [49]. It is not so long ago that *Gabrielse et al.* asked “whether it is likely that other adjustments of the *QED* theory will shift the α that is determined from the electron g ?” and answered “we hope not” [50]. Nevertheless, the *QED* theory should be corrected for *IR* transformations to iron out some flaws, and the author suggests a considerable simplification of *QED* calculations as a renewed successful tool, altering the inferred α constant, and related to it, the charge of the electron. Also importantly, the experimental value of g must be corrected, too. The applied relativistic shift of the cyclotron frequency $\omega_c = \frac{eB}{\gamma m}$ (ω_c = cyclotron frequency, B = magnetic field strength in Tesla) was performed using the familiar relativistic factor γ . However, γ should be replaced by the mass transformation according to the *IR* theory [8]

$$\frac{m}{m_0} = \frac{1 - \beta}{1 + \beta} \tag{62}$$

For the classical case the corrected frequency ω_c is

$$\omega_c = \omega_0 \left(1 - \frac{E_n}{mc^2} \right) \tag{63}$$

where the energy E_n of the n th quantum state of a harmonic cyclotron oscillator is given as

$$E_n = \left(n + \frac{1}{2} \right) \hbar \omega_c \tag{64}$$

The classical relativistic shift δ in the cyclotron frequency per energy quantum was approximated by the level spacing of the harmonic oscillator giving [51]

$$\delta = -\hbar \omega_c^2 / (mc^2) \tag{65}$$

For the *IR* theory one yields a much greater and positive shift because the cyclotron frequency yields now

$$\omega_c \approx \omega_0 \cdot \left(1 + 2 \cdot \sqrt{\frac{2E_n}{mc^2}} \right) \tag{66}$$

The relativistic shift δ is approximated by

$$\delta \approx \frac{d\omega_c}{dn} = 2\omega_0 \sqrt{\frac{2}{mc^2}} \cdot \frac{d\sqrt{E_n}}{dn} = \omega_0 \sqrt{\frac{2}{mc^2 E_n}} \cdot \hbar \omega_c = 2 \cdot \omega_0 \sqrt{\frac{2E_n}{mc^2}} \tag{67}$$

The gyromagnetic factor as $g/2$ can be determined from the observed eigenfrequencies [51]

$$\frac{g_e}{2} = 1 + \frac{\bar{\omega}_a - \bar{\omega}_m}{\bar{\omega}_c - \bar{\omega}_m} \tag{68}$$

where the $\bar{\omega}$ values are marginally modified with respect to the free-space values, ω_a is the anomalous frequency, and the spin frequency is $\omega_s = \omega_c + \omega_a$,

$\frac{\bar{\omega}_c^2}{2\bar{\omega}_c} = \bar{\omega}_m$ is the magnetron frequency, using the dip frequency ω_z in Hz [51].

For the experimentally chosen cyclotron frequency of $\nu_c = 149.2$ GHz, the classical relativistic shift is calculated to be $\delta = -2\pi \cdot 182.1$ Hz compared to the *IR* corrected one giving $\delta = +2\pi \cdot 14.78$ Mhz. One can estimate that g_e becomes noticeably smaller by a factor of approximately 1.0001, meaning a correction of g_e from the seventh decimal point downwards to about $g_e \approx 2.00231909$?

Now the scientific community is waiting for a most precise redetermination of the g -factor as well as the related *Sommerfeld* constant by experts [49] [51]. The aforementioned *Zitterbewegung* approach of *Niehaus* [17] should be revised by that author himself. The comment of the present author may have fulfilled its true purpose, if research on this topic proceeds well with application of the *IR* theory [52].

12. Fractal Superconductivity

Nature presents much more relationships to keep in mind, where the golden mean is involved, and superconductivity is no exception. However, we must reassess the theory considering the dark matter surrounding the moving electrons, which dive into the dark after marriage, or in other words, become superconducting under special conditions. Before a golden ratio in the spin dynamics of the quasi-one-dimensional *Ising* ferromagnet CoNb_2O_8 was experimentally verified next a phase critical point by *Coldea et al.* [53], the present author suggested linking the optimum hole doping σ_0 of high- T_c superconductors with the golden mean in the form of *Hardy's* maximum quantum probability of two particles [15]

$$\sigma_0 \approx \frac{8}{\pi} \varphi^5 = 0.2293 \quad (69)$$

Obviously, this optimum is again near a quantum critical point in the phase diagram. In addition, the relation of the *Fermi* speed to the *Klitzing* speed comes out as

$$\frac{v_F}{v_K} \approx \frac{2}{\pi} \varphi^5 = 0.0571 \quad (70)$$

Both relations document the fractal nature of the electronic response in superconductors. It was suggested recently that the same is true for conventional superconductors [16]. Also *Prester* had reported before about evidence of a fractal dissipative regime in high- T_c superconductors [54].

Interestingly, some time ago the present author connected the optimum transition temperature T_{co} of high- T_c superconductors with a *Fibonacci* number f_i , proportional to a domain width, by the relation $T_{co} = 12,000/f_i$ [15]. One yields the integer number 45, again as a product of solely *Fibonacci* numbers, when dividing this number by the number $266.\bar{6}$ (see Chapter 10).

Quantum entanglement of two moving electrons may be influenced by local interaction of their interwoven dark matter surroundings, quoting the cogwheel

picture of *Suleiman* [8]. What happens, if two stretched electrons locally interact to become superconducting? May such particle stretching in the end lead to a double-helically wounded wavy entity, which escapes in the dark? Nature is known to copy itself again and again. So the double-helix approach is not only beautiful, if we quote *Gauthier's* proposed entangled double-helix superluminal photon model [55]. Therefore, a model calculation for superconducting electron strands is suggested based on this idea, addressing the problem of left and right (mirrored) strands as well as objections against an apparent superluminal velocity. The double helix strand in nature is a special fabric of duality.

13. Evolution of Life

Nature repeatedly applied its building plans, based on the hierarchical golden number system, from largest to smallest dimensions, from the cosmos to the smallest living cell. Inasmuch the golden ratio is involved, reciprocity is considered as a vital element of life. Recently, thoughts to the link between cosmology and biology are impressively formulated [56]. Self-similarity as an element of chaos is intimately connected with self-organization of life producing compacted information and consciousness. However, visions about life such as *England's* provocative approach of dissipation-driven adaption [57] or *Pitkänen's* formulation [58] suffer from not considering duality of particle and wave or reciprocity of matter and dark matter [8] and should be adapted to the new physics.

The evolution of life may take place similar to the statistical bootstrap model of colliding heavy particles, so the *Hagedorn* temperature T_H comes into play. I quote the formulation of *Rafelski and Ericson* [59] to explain this: "When a drop of particles and resonances is compressed to the 'natural volume', it becomes another more massive resonance. This process then repeats, creating heavier resonances, which in return consist of resonances, and so on".

This nesting looks like a *Menger* sponge [56] [60]. The process could explain the evolution of life with T_H around ambient temperatures.

With respect to the entire energy density of φ^2 at the phase critical point $\beta = \varphi$ one may suggest formulating the *Hagedorn* temperature T_H proportional to the squared golden mean φ , where α' is formally the tension of a string.

$$T_{Hag} \approx \varphi^2 \cdot \frac{1}{\alpha'} \quad (71)$$

It remains to interpret the not liked string tension by a more appropriate thermodynamic quantity at ambient equilibrium conditions.

14. Conclusion

The duality between a compacted entity and its surrounding in general as well as the duality between a moving particle or body and the accompanying wave or reciprocity between matter and dark matter is the very spice of life. This was proven by the beautiful information relativity theory of *Suleiman*. Reciprocity is impressively formulated by the words of *Wolfgang Pauli*: "God made the bulk;

surfaces were invented by the devil” (quoted from [56]). As a consequence of the *IR* theory some natural constants such as the gyromagnetic factor of the electron, *Sommerfeld's* fine-structure constant as well as the charge of the electron are proposed to be marginally altered. The interpretation of superconductivity is influenced by the *IR* approach, too. Also the evolution of life may find a new basis. If we have fully understand the new *IR* physics with its particle-wave reciprocal dualism and intrinsic harmony, then we can shape our environment more effectively to achieve a balance between plants, animals and human beings, which enables a long-term life for all of us on earth. In this sense the golden mean should provide more beauty than chaos.

Acknowledgements

The author appreciated the critical reading of the manuscript by *Prof. Ramzi Suleiman*, University of Haifa, and the Triangle Research and Development Center (TCRD), who enriched the scientific community with his famous information relativity theory. The author is also grateful for the constructive criticism of a very creative reviewer.

Conflicts of Interest

The author declares no conflicts of interest regarding the publication of this paper.

References

- [1] Hardy, L. (1993) *Physical Review Letters*, **71**, 1665-1668.
<https://doi.org/10.1103/PhysRevLett.71.1665>
- [2] Mermin, N.D. (1994) *American Journal of Physics*, **62**, 880-887.
<https://doi.org/10.1119/1.17733>
- [3] Otto, H.H. (2018) *World Journal of Condensed Matter Physics*, **8**, 30-35.
<https://doi.org/10.4236/wjcmp.2018.82003>
- [4] Otto, H.H. (2018) *Journal of Modern Physics*, **9**, 1-13.
<https://doi.org/10.4236/jmp.2018.91001>
- [5] El Naschie, M.S. (2013) *Journal of Quantum Information Science*, **3**, 57-77.
<https://doi.org/10.4236/jqis.2013.32011>
- [6] Marek-Crnjac, L. (2013) *Cantorian Space-Time Theory*. Lambert Academic Publishing, Saarbrücken, 1-50.
- [7] Suleiman, R. (2018) *World Journal of Condensed Matter Physics*, **8**, 130-155.
<https://doi.org/10.4236/wjcmp.2018.83009>
- [8] Suleiman, R. (2019) *Relativizing Newton*. Nova Scientific Publisher, New York, 1-207.
- [9] Inwood, M.J. (1995) *A Hegel Dictionary*. Blackwell Reference, Oxford, U.K.
- [10] Caygill, H.A. (1992) *A Kant Dictionary*. Blackwell Reference, Oxford, U.K.
- [11] Suleiman, R. (2016) A Relativistic Model of Matter-Wave Duality Explains the Result of the Double-Slit Experiment. *5th International Conference on New Frontiers in Physics*, Zurich, 6-14 July 2016, 1-14.

- [12] De Broglie, L. (1923) *Nature*, **112**, 540. <https://doi.org/10.1038/112540a0>
- [13] Bohm, D. (1952) *Physical Review*, **85**, 166-179. <https://doi.org/10.1103/PhysRev.85.166>
- [14] Bohm, D. (1952) *Physical Review*, **85**, 180-193. <https://doi.org/10.1103/PhysRev.85.180>
- [15] Otto, H.H. (2016) *World Journal of Condensed Matter Physics*, **6**, 244-260. <https://doi.org/10.4236/wjcmp.2016.63023>
- [16] Otto, H.H. (2019) *World Journal of Condensed Matter Physics*, **9**, 22-36. <https://doi.org/10.4236/wjcmp.2019.91002>
- [17] Niehaus, A. (2017) *Journal of Modern Physics*, **8**, 511-521. <https://doi.org/10.4236/jmp.2017.84033>
- [18] Schumacher, B. (1995) *Physical Review A*, **51**, 2738-2747. <https://doi.org/10.1103/PhysRevA.51.2738>
- [19] Ionescu, L. (2008) On the Arrow of Time. arXiv: 4180v2, 1-22.
- [20] Otto, H.H. (1980) The Reciprocal Lattice: An Exercise. Lecture Given at the Universities of Regensburg, TU Berlin and TU Clausthal.
- [21] Assmus, E.F. (1985) *The American Mathematical Monthly*, **92**, 213-214. <https://doi.org/10.1080/00029890.1985.11971581>
- [22] Finch, S.R. (2003) Mathematical Constants. In: *Encyclopedia of Mathematics and Its Applications*, Vol. 94, Cambridge University Press, New York.
- [23] Otto, H.H. (2017) *Nonlinear Science Letters A*, **8**, 410-412.
- [24] Lange, L.J. (1999) *The American Mathematical Monthly*, **106**, 456-458. <https://doi.org/10.1080/00029890.1999.12005070>
- [25] Mushkolaj, S. (2014) *Journal of Modern Physics*, **5**, 1124-1138. <https://doi.org/10.4236/jmp.2014.512115>
- [26] Olson, S. (2006) *The Golden Section: Nature's Greatest Secret*. Bloomsbury, New York, 64 p.
- [27] Sherbon, M.A. (2014) *International Journal of Physical Research*, **2**, 1-9. <https://doi.org/10.14419/ijpr.v2i1.1817>
- [28] Otto, H.H. (2017) Continued Fraction Representations of Universal Numbers and Approximations. Researchgate, 1-4.
- [29] Fisher, R.A. (1915) *Biometrika*, **10**, 507-521. <https://doi.org/10.2307/2331838>
- [30] Madelung, E. (1918) *Physikalische Zeitschrift*, **19**, 524-533.
- [31] Triebel, R. (2011) Iterative Bestimmung der Madelung-Konstante für zweidimensionale Kristallstrukturen. Physikalische Projektarbeit, TU Graz.
- [32] Valleta, M. (2013) *Astrophysics and Space Science*, **345**, 1-9. <https://doi.org/10.1007/s10509-013-1388-3>
- [33] El Naschie, M.S. (2004) *Chaos, Solitons & Fractals*, **19**, 209-236. [https://doi.org/10.1016/S0960-0779\(03\)00278-9](https://doi.org/10.1016/S0960-0779(03)00278-9)
- [34] Cantor, G. (1932) *Gesammelte Abhandlungen mathematischen und philosophischen Inhalts*. Springer, Berlin. <https://doi.org/10.1007/978-3-662-00274-2>
- [35] El Naschie, M.S. (2017) *International Journal of High Energy Physics*, **4**, 65-74. <https://doi.org/10.11648/j.ijhep.20170406.11>
- [36] Urysohn, P. (1922) *Comptes Rendus*, **175**, 440-442.
- [37] Menger, K. (1928) *Dimensionstheorie*. Springer-Verlag, Leipzig und Berlin.
- [38] Hausdorff, F. (1918) *Mathematische Annalen*, **79**, 157-179.

- <https://doi.org/10.1007/BF01457179>
- [39] Otto, H.H. (2018) An Exercise: Cauchy Functions Compared to the Gaussian for Diffraction Line Profile Fitting. Researchgate.
- [40] Uhlenbeck, G.E. and Goudsmit, S. (1926) *Nature*, **117**, 264-265.
<https://doi.org/10.1038/117264a0>
- [41] He, J.H., Tian, D. and Otto, H.H. (2018) *Results in Physics*, **11**, 362-362.
<https://doi.org/10.1016/j.rinp.2018.09.027>
- [42] Otto, H.H. (2017) *Nonlinear Science Letters A*, **8**, 413-415.
- [43] Odom, B., Hanneke, D., D'Urso, B. and Gabrielse, G. (2006) *Physical Review Letters*, **97**, Article ID: 030801. <https://doi.org/10.1103/PhysRevLett.97.030801>
- [44] He, J.H. (2004) *Applied Mathematical Computing*, **151**, 887-891.
[https://doi.org/10.1016/S0096-3003\(03\)00531-9](https://doi.org/10.1016/S0096-3003(03)00531-9)
- [45] Lin, L., Yu, D.N., He, C.H. and Liu, Y. (2018) *Thermal Science*, **22**, 1849-1852.
<https://doi.org/10.2298/TSCI1804849L>
- [46] Schwinger, J. (1948) *Physical Review*, **73**, 416-417.
<https://doi.org/10.1103/PhysRev.73.416>
- [47] Sommerfeld, A. (1919) *Atombau und Spektrallinien*. Friedrich Vieweg & Sohn, Braunschweig.
- [48] The NIST Reference of Constants, Units and Uncertainty. NIST, Gaithersburg, MD.
- [49] Gabrielse, G., Hanneke, D., Kinoshita, T., Nio, M. and Odom, B. (2006) *Physical Review Letters*, **97**, Article ID: 030802.
<https://doi.org/10.1103/PhysRevLett.97.030802>
- [50] Gabrielse, G., Hanneke, D., Kinoshita, T., Nio, M. and Odom, B. (2007) *Physical Review Letters*, **99**, Article ID: 039902.
<https://doi.org/10.1103/PhysRevLett.99.039902>
- [51] Odom, B. (2004) Fully Quantum Measurement of the Electron Magnetic Momentum. Harvard University, Cambridge, MA.
- [52] Otto, H.H. (2018) Does Nature Journal Once again Oversleep the New Era of Physics. Researchgate.
- [53] Coldea, R., Tennant, D.A., Wheeler, E.M., Wawrzynska, E., Prabhakaram, D., Telling, M., Habicht, K., Smeibidl, P. and Kiefer, K. (2010) *Science*, **327**, 177-180.
<https://doi.org/10.1126/science.1180085>
- [54] Prester, M. (1999) *Physical Review B*, **60**, 3100-3103.
<https://doi.org/10.1103/PhysRevB.60.3100>
- [55] Gauthier, R. (2013) Transluminal Energy Quantum Models of the Photon and the Electron. In: *The Physics of Reality: Space, Time, Matter, Cosmos*, World Scientific, Hackensack, NJ, 445-452. https://doi.org/10.1142/9789814504782_0045
- [56] El Naschie, M.S., Olsen, S., Helal, M.A., Marec-Crnjac, L. and Nada, S. (2018) *International Journal of Innovation in Science and Mathematics*, **6**, 11-13.
- [57] England, J.L. (2013) *Journal of Chemical Physics*, **139**, Article ID: 121923.
<https://doi.org/10.1063/1.4818538>
- [58] Pitkänen, M. (2015) Jeremy England's Vision about Life and Evolution: Comparison with TGD Approach. Researchgate.net, 1-9.
- [59] Rafelski, J. and Ericson, T. (2019) The Tale of the Hagedorn Temperature. In: Rafelski, J., Ed., *Melting Hadrons, Boiling Quarks-From Hagedorn Temperature to Ultra-Relativistic Heavy-Ion Collisions at CERN*, Springer, Cham, 41-48.
https://doi.org/10.1007/978-3-319-17545-4_6

- [60] Menger, K. (1928) Dimensionstheorie. B. G. Teubner Publisher, Stuttgart.
<https://doi.org/10.1007/978-3-663-16056-4>
- [61] Bohr, N. (1934) Atomic Theory and the Description of Nature. Cambridge University Press, Cambridge, UK.
- [62] Bedau, H. and Oppenheim, P. (1961) *Synthese*, **13**, 201-232.
<https://doi.org/10.1007/BF00489884>

Appendix I

About the Meaning of the Terms Reciprocity, Duality and Complementarity

These terms, omnipresent in many disciplines of science (physics, mathematics, philosophy, music, economy, etc.) can certainly have different meanings, even if they have something in common.

In mathematics, a reciprocal of a number is its multiplicative inverse, but an inverse is not necessarily a reciprocal. Reciprocity in the amounts of matter and dark matter is formulated according to Equation (39) of the main text. Important for mathematics and physics, a reciprocal vector system can be created by *Fourier* transformation. However, reciprocity in physics may have a more general meaning when describing a mutual dependence or influence.

Duality in mathematics can be demonstrated on platonic solids, also familiar for a crystallographer. The convex hull of the center points of each face of a starting polyhedron results in a dual polyhedron such that, for instance, the cube and the octahedron form a dual pair, but the tetrahedron is self-dual. In physics, the most prominent example for duality is that between matter and piloting wave in the sense of the *De Brogly-Bohm* approach [12]. According to the *IR* theory of *Suleiman* [8] the relation between matter density and the dark matter surrounding may be quantified as “reciprocal duality”, where an amount of matter is transformed into an equal amount of dark matter depending of the recession velocity respectively redshift of a moving body (Figure 6).

Finally, the concept of complementarity in quantum physics has been formulated and coined by *Bohr* in his *Como* lecture of 1927, describing the familiar case of reciprocal uncertainty between position and momentum of an electron as conjugate variables [61]. It means that it is hardly possible to know simultaneously with an arbitrary accuracy the outcomes of these variables. Another example of conjugate variables is the magnetic field strength in comparison to the electric one. An elaborated logical analysis of complementarity has been given by *Bedau* and *Oppenheimer* [62]. In his late years *Bohr* was interested in philosophical aspects of complementarity as given in the *Yin* and *Yang* conjugate principle of the ancient *Tao*, and on his gravestone the *Taoist* symbol is engraved.

In mathematics, a number and the complement to a number add up to a whole of some amount. If one performs the reciprocal of these numbers and re-normalize the resulting values, then complement and primal number change their values [4]. In this way one may speak also of reciprocity when dealing with matter density and the dual dark matter density according to Figure 6.

Appendix II

Another approach for the gyromagnetic factor used the fifth power of $\tilde{\varphi}$ with the value $\tilde{\varphi}^5 = 0.09092922100312$. An approximation is the inverse *Lucas* number $L_5 = 11$ as combination of two inversely related irrational numbers (see Equations (13) to (15))

$$(\varphi^{-5} - \varphi^5)^{-1} = (11)^{-1} = 0.0909090\dots \tag{72}$$

However, physically more convenient is the expression

$$\frac{2\pi \cdot v_K}{c} = 0.0917012\dots$$

where v_K is the *Klizing* speed and c the speed of light. This term keeps no dimension, as required. If we are working with a speed, according to the *IR* theory the information offset has to be corrected. The speed transforms as

$$\frac{v}{v_0} = 1 + \beta \tag{73}$$

combining the length transformation $\frac{l}{l_0} = \frac{1 + \beta}{1 - \beta}$ with the time transformation

$\frac{t}{t_0} = \frac{1}{1 - \beta}$, where $\beta = v/c$ is the recession speed [8]. Surprisingly, an additional

$\left(\frac{t}{t_0}\right)^{-1} = 1 - \beta$ term is needed to give more accuracy and the following simple formula

$$\sqrt[5]{\frac{2\pi v_K}{c} \left(1 + \frac{2\pi v_K}{c}\right) \left(1 - \frac{2\pi v_K}{c}\right)} = \sqrt[5]{\frac{2\pi v_K}{c} \left(1 - \left(\frac{2\pi v_K}{c}\right)^2\right)} = 0.61907254 \tag{74}$$

leading to $\frac{g_e}{2} = 1.00116100597109$ or $g_e = 2.00232201$ (75)

Remarkably, this value is almost identical to the result of [37], because

$$2 + \frac{\varphi^6}{24} = 2.002322003 \tag{76}$$

Only now we are allowed to associate the term $\frac{2\pi v_K}{c}$ with *Sommerfeld's* fine-structure constant α [41] applying

$$\frac{2\pi v_K}{c} = 4\pi\alpha \tag{77}$$

where α is a measure of the strength of interaction of an electron and a photon in the quantum electrodynamics theory (*QED*). The charge of the electron in *QED* (*Lorentz-Heaviside*) units has the numerical value of $e = -\sqrt{4\pi\alpha}$.

The accurate experimental value for the gyromagnetic constant could be attained from Equation (74) using an adapted fine-structure constant of

$$\alpha' = 0.007297279955669 \tag{78}$$

$$\text{respectively } \alpha'^{-1} = 137.037362698897742 \tag{79}$$

$$\text{where } \alpha' - \alpha = 6.43 \times 10^{-7} \tag{80}$$

Tackling the problem of the not fully adapted accuracy in comparison to the experimental value, one can multiply the term under the fifth root of Equation (74) by a factor of 0.9999902180 or alternatively reduce the *Klizing* speed by a

factor of 0.99999004931863 respectively the charge of the electron by a factor of 0.99999502464694. This adjustment may result partly from a correction of g as well as α with respect to the IR theory, besides needed radiative corrections.

An Introduction to Information Sets with an Application to Iris Based Authentication

Madasu Hanmandlu¹, Mamta Bansal², Shantaram Vasikarla³

¹CSE Department, MVSR Engineering College, Hyderabad, India

²Hella India Automotive Pvt. Ltd., Pune, India

³CSE Department, California State University, Los Angeles, CA, USA

Email: mhmandlu@ee.iitd.ernet.in

How to cite this paper: Hanmandlu, M., Bansal, M. and Vasikarla, S. (2020) An Introduction to Information Sets with an Application to Iris Based Authentication. *Journal of Modern Physics*, 11, 122-144. <https://doi.org/10.4236/jmp.2020.111008>

Received: December 23, 2019

Accepted: January 14, 2020

Published: January 17, 2020

Copyright © 2020 by author(s) and Scientific Research Publishing Inc. This work is licensed under the Creative Commons Attribution International License (CC BY 4.0).

<http://creativecommons.org/licenses/by/4.0/>



Open Access

Abstract

This paper presents the *information set* which originates from a fuzzy set on applying the Hanman-Anirban entropy function to represent the uncertainty. Each element of the information set is called the information value which is a product of the information source value and its membership function value. The Hanman filter that modifies the information set is derived by using a filtering function. Adaptive Hanman-Anirban entropy is formulated and its properties are given. It paves the way for higher form of information sets called Hanman transforms that evaluate the information source based on the information obtained on it. Based on the information set six features, Effective Gaussian Information source value (EGI), Total Effective Gaussian Information (TEGI), Energy Feature (EF), Sigmoid Feature (SF), Hanman transform (HT) and Hanman Filter (HF) features are derived. The performance of the new features is evaluated on CASIA-IRIS-V3-Lamp database using both Inner Product Classifier (IPC) and Support Vector Machine (SVM). To tackle the problem of partially occluded eyes, majority voting method is applied on the iris strips and this enables better performance than that obtained when only a single iris strip is used.

Keywords

Information Sets, Energy Feature (EF), Sigmoid Feature (SF), Hanman Transform (HT), Hanman Filter (HF), Hanman-Anirbanentropy Function

1. Introduction

Representing the uncertainty in the fuzzy sets conceptualized by the pioneering work of Zadeh [1] is the main theme of this work. The fuzziness of a fuzzy set is called the uncertainty by another exponent of fuzzy sets, Yager [2] who has in-

roduced the concept of specificity as an important measure of uncertainty in a fuzzy set or possibility distributions. As we are aware any crisp set is deemed to have zero fuzziness, finding the difference between the uncertainty and the specificity [3] of a fuzzy subset containing one and only one element is one way of measuring the uncertainty. Representing the uncertainty in the fuzzy sets by the entropy functions is another way.

Most of the entropy functions were defined in the probabilistic domain as an entropy measure gives the degree of uncertainty associated with a probability distribution. The Shannon entropy function [4] defined in the probabilistic domain has the logarithmic gain function which creates problems with zero probability; so it is replaced with the exponential gain in Pal and Pal entropy function [5]. The Hanman-Anirban entropy function [6] contains polynomial exponential gain with free parameters which enable it to become a membership function.

Motivation

The motivation for this work stems from two reasons. 1) To expand the scope of information sets in [6] by defining an adaptive exponential gain function that empowers a membership function to act as an agent, and 2) To develop higher form of information sets such as Hanman Transform that helps evaluate the information source values by way of higher level uncertainty representation and Hanman filter that helps modify the information.

In our previous work [7] we have introduced the information set and also developed some features and inner product classifier (IPC) for the authentication based on ear. In the present work we embark on extending the information sets to represent higher forms of uncertainty in addition to formulating a new classifier. The original information set features were derived from the non-normalized Hanman-Anirban entropy, which is not suitable for representing higher forms of uncertainty because of its constant parameters; hence this entropy needs to be made adaptive by assuming its parameters as variables. The power of the resulting adaptive entropy is immense as it can tackle both time varying and spatially varying situations. Our main consideration is here to see the applicability and suitability of information set based features for the distinct and unique iris textures.

The paper is organized as follows: Section 2 introduces the information set and describes the extraction of features based on this set in Section 3. Segmentation of iris and use of the information set based features for iris authentication are discussed in Section 4. Inner Product classifier (IPC) is described along with the formulation of Hanman Transform classifier in Section 5. The results of application of IPC on the Iris database using the proposed features are given in Section 6 followed by the conclusions in Section 7.

2. An Introduction to Information Sets

Assume a fuzzy set formed from a set of gray levels $\{I_{ij}\}$ termed as the information source values and the corresponding membership function values $\{\mu_{ij}\}$. Each pair (I_{ij}, μ_{ij}) in the fuzzy set becomes a product in the informa-

tion set on representing the uncertainty in the information source values using the Hanman-Anirban entropy function proved later.

Probability vs. Possibility. We consider here two types of uncertainty: probabilistic uncertainty which results from the probability distribution of the information source values (gray levels) and possibilistic uncertainty which results from their possibility distribution. The uncertainty in the probability distribution is defined by the Shannon entropy function [4] as

$$H^{Sh} = -\sum \sum p_{ij} \log p_{ij} \tag{1}$$

where $\sum \sum p_{ij} = 1$. Pal and Pal [5] have used the exponential gain function in place of the logarithmic gain function to define

$$H^{PP} = \sum \sum p_{ij} e^{1-p_{ij}} \tag{2}$$

These two entropy functions give a measure of the probabilistic uncertainty. If we replace p_{ij} by the normalized I_{ij} in the range [0,1] the logarithmic gain function $\log I_{ij}$ from (1) and the exponential gain function $e^{1-I_{ij}}$ from (2) can't model the possibility distribution of I_{ij} due to lack of parameters in them. Unlike probability distribution the possibilistic distribution requires a membership function which in turn needs parameters to model the distribution. As Hanman-Anirban entropy function being information theoretic entropy function contains parameters in its exponential gain function, which we can use to convert the gain function into a membership function. The non-normalized form of this function is defined as.

$$H = \sum \sum p_{ij} e^{-(ap_{ij}^3 + bp_{ij}^2 + cp_{ij} + d)} \tag{3}$$

Just as (1) and (2), (3) is also probability based but it can represent the possibility distribution of I_{ij} after substituting it to replace p_{ij} in (3) and then choosing the parameters in the exponential gain function as statistical. The well known membership functions to represent possibility distribution are exponential and Gaussian membership functions, given by

$$\mu_{ij}^e = e^{-\left\{ \frac{|I_{ij} - I_{ref}|}{f_{h(ref)}^2} \right\}} \tag{4}$$

$$\mu_{ij}^g = e^{-\left[\frac{|I_{ij} - I_{ref}|}{\sqrt{2} f_{h(ref)}} \right]^2} \tag{5}$$

where μ_{ij}^e is the exponential membership function, μ_{ij}^g is the Gaussian membership functions and I_{ref} is taken as I_{max} . The fuzzifier $f_{h(ref)}^2$ [8] that gives the spread of the information source values with respect to the reference is defined as

$$f_{h(ref)}^2 = \frac{\sum_{i=1}^W \sum_{j=1}^W (I_{ref} - I_{ij})^4}{\sum_{i=1}^W \sum_{j=1}^W (I_{ref} - I_{ij})^2} \tag{6}$$

This gives more spread than possible with variance. We will now consider a triangular membership function given by

$$\mu_{ij}^{rr} = \frac{|I_{avg} - I_{ij}|}{I_{max}} \tag{7}$$

Note that $I_{ref} = I_{max}$ is the maximum of I_{ij} in a window or sub image. Assuming $(aI_{ij}^3 + bI_{ij}^2 + cI_{ij} + d) > 0$ and setting the parameters as, $a = 0$, $b = 0$, $c = \frac{1}{f_{h(ref)}^2}$, $d = -\frac{I_{ref}}{f_{h(ref)}^2}$, Equation (3) takes the form with gain function becoming exponential:

$$H_e = \sum \sum I_{ij} \mu_{ij}^e \tag{8}$$

Similarly with another choice of parameters, $a = 0$, $b = \frac{1}{2f_{h(ref)}^2}$, $c = -\frac{2I_{ref}}{2f_{h(ref)}^2}$, $d = \frac{I_{ref}^2}{2f_{h(ref)}^2}$, Equation (3) takes another form with gain function becoming Gaussian:

$$H_g = \sum \sum I_{ij} \mu_{ij}^g \tag{9}$$

It may be noted that in the derivation of (8) and (9) the parameters are chosen to be statistical computed from the statistics of the sub images in windows and we are avoiding the normalization of the information, H in all equations but the normalization is inevitable during feature generation because of practicality. For the generality of membership function we ignore the superscripts e and g in Equations (8) and (9) respectively and represent the information set as

$$\mathcal{H}(I) = \{I_{ij} \mu_{ij}\} = \{H_{ij}(I)\} = \int_I \frac{H_{ij}}{I_{ij}}; I \in [0,1] \tag{10}$$

We can also derive the entropy function using the triangular membership function. Assuming $a = 0$, $b = 0$, $c = \frac{1}{I_{max}}$, $d = -\frac{I_{avg}}{I_{max}}$; we have,
 $H_{rr} = \sum \sum I_{ij} e^{-\mu_{ij}^{rr}} = \sum \sum I_{ij} \bar{\mu}_{ij}^{rr}$ since $e^{-\mu_{ij}^{rr}} = 1 - \mu_{ij}^{rr} = \bar{\mu}_{ij}^{rr}$. The information set denoted by $\mathcal{H}_{rr}(I) = \{I_{ij} \bar{\mu}_{ij}\}$ contains the complement of membership function. In the context of information sets, the role of the membership is enlarged by terming it as an agent, which can be its complement, square or intuitive. The agent can take care of both spatially and time varying information source values.

Definition of Information Set: A set of information source values can be converted into an Information set by representing the uncertainty in their distribution. The basic information set consists of a set of information values with each value being the product of information source value (property/attribute) and its membership value (agent in the general case). It is denoted by

$$\mathcal{H}(I) = \{I_{ij} \mu_{ij}\} \tag{11}$$

Note that the membership function not only represents the distribution of information source values but also acts as an agent that helps generate different information sets such as $\{I_{ij} \mu_{ij}^2\}$, $\{I_{ij}^2 \mu_{ij}\}$, $\{I_{ij} \mu_{ij}^{1/2}\}$.

Derivation of Information Sets by the Mamta-Hanman Entropy Function:

The 2D non-normalized form of this entropy function [9] is given by

$$H^{MH} = \sum_{i=1}^n \sum_{j=1}^n p_{ij}^\gamma e^{-(cp_{ij}^\alpha + d)^\beta} \tag{12}$$

This entropy function allows us to change not only the exponential gain function but also the information source values thereby facilitating the generation of different types of information sets very easily. It is easy to derive (9) by fixing $p_{ij} = I_{ij}$, $c = \frac{1}{f_{h(ref)}^2}$, $d = \frac{I_{ref}}{f_{h(ref)}^2}$, $\gamma = 1$, $\alpha = 1$ and $\beta = 2$. The exponential

gain function in (11) becomes $\mu_{ij}^\beta = e^{-\left\{\frac{I_{ij}-I_{ref}}{f_{h(ref)}^2}\right\}^\beta}$ leading to $H = \sum \sum I_{ij}^\gamma \mu_{ij}^\beta$ and the corresponding information set is $\mathcal{H}(I) = \{I_{ij}^\gamma \mu_{ij}^\beta\}$. This form allows to derive different information sets $\{I_{ij}^\gamma \mu_{ij}^2\}$ and $\{I_{ij}^\gamma \mu_{ij}^{1/2}\}$ with $\beta = 2$ and $\beta = \frac{1}{2}$ respectively by converting the exponential gain function, $e^{-(ap_{ij}^\alpha + b)^\beta}$ into a membership function μ_{ij} .

2.1. Hanman Transforms

These transforms are higher form of information sets. Note that information sets are the result of determining the uncertainty in the information source values whereas the transforms will be shown to be the result of determining the uncertainty in the information source values by the information gathered on them. The formulation of transforms is only possible if the parameters in the Hanman-Anirban entropy function are varying though they are assumed to be constant [6]. We now present the adaptive entropy function and its properties.

2.2. The Adaptive Hanman-Anirban Entropy Function

The non-normalized Hanman-Entropy function with the varying parameters is called the adaptive entropy function which is relevant to spatially varying and time varying information source values. To this end, we modify this entropy function by taking two parameters a and b as zeros and other two parameters c and d as variables. The resulting adaptive entropy function is therefore:

$$H^T(I) = \sum_{i=1}^n \sum_{j=1}^n I_{ij} e^{-(c_{ij}I_{ij} + d_{ij})} \tag{13}$$

$0 \leq I_{ij} \leq 1$. We will now prove that (13) satisfies the properties of an entropy function when c_{ij} and d_{ij} are varying.

The Proof of Properties:

1) The exponential gain function also called the information gain $I(p_{ij}) = e^{-(c_{ij}p_{ij} + d_{ij})}$ is the continuous function (here $I(p_{ij})$ should not be confused with I_{ij} which stands for the information source) for all $p_{ij} \in [0,1]$ and $c_{ij}, d_{ij} \in [0,1]$, so $p_{ij} e^{-(c_{ij}p_{ij} + d_{ij})}$ is a continuous function being the product of two continuous functions and hence H being the sum of continuous functions is also a continuous function.

- 2) $I(p_{ij})$ is bounded. Since $e^{-(c_{ij}p_{ij}+d_{ij})} < 1$ which means that $p_{ij}e^{-(c_{ij}p_{ij}+d_{ij})} < 1$. As $p_{ij}e^{-(c_{ij}p_{ij}+d_{ij})}$ is bounded for each I , H is also bounded.
- 3) With increase in p_{ij} , $I(p_{ij})$ decreases since $c_{ij} > 0$.
- 4) When $p_{ij} = \frac{1}{n}$, then H is an increasing function of n .

$$H = \sum_{i=1}^n \sum_{j=1}^n p_{ij} e^{-(c_{ij}p_{ij}+d_{ij})} = \sum_{i=1}^n \sum_{j=1}^n \frac{1}{n} e^{-\left(\frac{c_{ij}}{n}+d_{ij}\right)} = e^{-\left(\frac{c_{ij}}{n}+d_{ij}\right)} \tag{14}$$

$$\frac{\partial H}{\partial n} = \frac{c_{ij}}{n^2} e^{-\left(\frac{c_{ij}}{n}+d_{ij}\right)} > 0 \tag{15}$$

so H is an increasing function of n .

- 5) $H = \sum_{i=1}^n \sum_{j=1}^n p_{ij} e^{-(c_{ij}p_{ij}+d_{ij})}$ is a concave function where $p_{ij} \in [0,1]$ and $\sum_{i=1}^n \sum_{j=1}^n p_{ij} = 1$.

The function is concave if the Hessian matrix is negative definite.

$$\frac{\partial H}{\partial p_{ij}} = e^{-(c_{ij}p_{ij}+d_{ij})} - c_{ij}p_{ij}e^{-(c_{ij}p_{ij}+d_{ij})} \tag{16}$$

$$\frac{\partial^2 H}{\partial p_{ij}^2} = -2c_{ij}e^{-(c_{ij}p_{ij}+d_{ij})} + c_{ij}^2p_{ij}e^{-(c_{ij}p_{ij}+d_{ij})} = c_{ij}e^{-(c_{ij}p_{ij}+d_{ij})} (c_{ij}p_{ij} - 2) \tag{17}$$

as c_{ij} and p_{ij} are in the range $[0, 1]$.

$$p_{ij} = \frac{1}{n}, \frac{\partial^2 H}{\partial p_{ij}^2} = c_{ij} \left(\frac{c_{ij}}{n} - 2 \right) < 0 \tag{18}$$

The Hessian matrix $H_F = \frac{\partial^2 H}{\partial p_{ij}^2}$ is the second order partial derivative of square matrix having the following form:

$$H_F = \begin{bmatrix} \beta_1 & 0 & 0 & \dots & 0 \\ 0 & \beta_2 & 0 & \dots & 0 \\ 0 & 0 & \beta_3 & \dots & 0 \\ \vdots & \vdots & \vdots & \ddots & \vdots \\ 0 & 0 & 0 & \dots & \beta_n \end{bmatrix} \tag{19}$$

where $\beta_i = c_{ij} (c_{ij}p_{ij} - 2) < 0$; hence all the Eigen values of this Hessian matrix are negative. Thus Hessian is negative definite. So the entropy H is concave.

- 6) Entropy H is maximum when all p_{ij} 's are equal. In other words,

$$p_{ij} = \frac{1}{n}, \forall i, j$$

$$p_{ij} = \frac{1}{n} \tag{20}$$

In that case, $\beta_i = c_{ij} \left(\frac{c_{ij}}{n} - 2 \right) < 0, \forall i$.

- 7) The entropy is minimum if and only if all p_{ij} 's are equal to 0's and single $p_{ij} = 1$.

Significance of Adaptive Hanman-Anirban Entropy Function: We have already seen the role of the information gain as an agent when the parameters are constant. We will now examine its usefulness in the context of varying parameters, i.e. $I(p_{ij}) = e^{-(c_{ij}p_{ij}+d_{ij})}$. Taking the derivative of $I(p_{ij})$ w.r.t. “ c_{ij} ” we get, $\frac{\partial G(p_{ij})}{\partial c_{ij}} = -p_{ij}e^{-(c_{ij}p_{ij}+d_{ij})}$. This means that the absolute derivative of the infor-

mation gain with respect to the parameter, i.e. $\left| \frac{\partial I(p_{ij})}{\partial c_{ij}} \right|$ gives the information

value. When the information gain is changing as a result of change in the parameter responsible for modifying the information source value, i.e. p_{ij} in this case, it produces the information set $\left\{ p_{ij}e^{-(c_{ij}p_{ij}+d_{ij})} \right\}$ after adjusting the sign as the information value must be positive. The higher form of the information set results if the parameter is also an agent by itself. We will now derive the transforms based on this concept.

2.3. The Adaptive Hanman-Anirban Entropy Function as the Transform

Fixing $d = 0$, $c_{ij} = \mu_{ij}/I_{\max}$ in (13) the entropy function takes the new incarnation called Hanman transform which transforms the spatial domain information source values into the information domain as:

$$H_T(I) = \sum \sum I_{ij} e^{-(\mu_{ij}I_{ij}/I_{\max})} \tag{21}$$

In this, the exponential gain is made as a function of information value $\mu_{ij}I_{ij}$ which is already shown to be a measure of the uncertainty. The new gain function termed as an agent is a function of the information value.

Note that the information source value weighted by this new agent in Hanman transform (21) gives a better representation of the uncertainty. The division of μ_{ij} by the maximum gray level in a window, I_{\max} is necessitated from the fact that this ratio serves as a better statistic than mere μ_{ij} in (21). Note that if information source values are normalized already, no division is needed.

Proof: The zero order transform can be obtained if we take $c_{ij} = 0$, $d_{ij} = \mu_{ij}$ in (13) leading to $H_T(\mu) = \sum \sum I_{ij} e^{-\mu_{ij}} = \sum \sum I_{ij} (1 - \mu_{ij})$. Similarly we can have $H_T(p) = \sum \sum I_{ij} e^{-p_{ij}} = \sum \sum I_{ij} (1 - p_{ij})$. Note that the deviations of possibility distribution and probability distribution from unity are causing the uncertainty in the information source values. Here agents are $e^{-\mu_{ij}}$ and $e^{-p_{ij}}$. In the case of Laplace transform the agent is e^{-st} where $s = 1/t$. If we choose $d_{ij} = i\mu_{ij}t$; then the agent in Fourier transform is $e^{-(i\mu_{ij}t)}$ which is complex. On the other hand $H_T(p) = \sum \sum p_{ij} e^{-p_{ij}} = \sum \sum p_{ij} (1 - p_{ij})$ is not a transform as it is a function of p_{ij} only. The first order transforms are: $\sum \sum I_{ij} e^{-I_{ij}\mu_{ij}}$ and $\sum \sum I_{ij} e^{-I_{ij}p_{ij}}$ where $I_{ij}\mu_{ij}$ and $I_{ij}p_{ij}$ represent possibilistic and probabilistic information values respectively. In view of this discussion the definition of transform now follows.

Definition of Transform: The gain function in the adaptive entropy function can be a function of the probabilistic information (distribution) or possibilistic information (distribution) and it weights the information source values giving rise to the first order (zero order) transform.

The Relevance of Transforms to the Real Life Scenario: The information source values received by our senses are perceived by the mind as the information values; hence these are natural variables just as the fuzzy variables. That is, using the information values perceived by the agent on the information source values, the entropy improves its uncertainty representation.

The Relation between Information Sets and Hanman Transforms: The information sets are derived directly from the Hanman-Anirban entropy function and those derived from the adaptive Hanman-Anirban entropy function are higher form of information sets. The latter are useful for the representation of time varying and spatially varying information source values.

The Heterogeneous Transforms:

If the agent $e^{-(\mu_{ij}I_{ij}/I_{\max})}$ is from another information source I_{ij} along with its membership function μ_{ij} and the reference parameter I_{\max} then (21) becomes what is called Heterogeneous Transform.

$$\bar{H}_T(I) = \sum \sum I_{ij} e^{-(\mu_{ij}I_{ij}/I_{\max})} \quad (22)$$

In this the agent from a different information source evaluates the information source of interest.

Algorithm for Hanman Transform Features

- 1) Compute the membership function value for each gray level in a window of size $W \times W$. In our experimental study we have used μ_{ij}^e using Equation (4) for computing the membership value.
- 2) Obtain the normalized information value by dividing the information value with the maximum gray level in the window.
- 3) Multiply the normalized information value from Step 2 with the corresponding gray level in Equation (21).
- 4) Repeat Steps 2 and 3 in a window and sum all the products to get a feature value.
- 5) Form a feature vector by repeating Steps 1 - 4 on all windows of an iris strip.

2.4. Hanman Filter

Invariably the information sets derived from the fuzzy sets may not possess desirable characteristics. By modifying the information sets by certain functions or operators it is possible to get better features. The modification of the information is required to meet certain objectives like better classification or a new interpretation.

Let us see how to modify the information $H_{ij} = I_{ij}\mu_{ij}$ at a pixel in a window. This is done by taking the membership function as a function of parameter s . The modified H_{ij} is defined as

$$H_{ij}(s) = I_{ij} \mu_{ij}(s) \tag{23}$$

The dependency of the membership function in (22) on s is incorporated as

$$\mu_{ij}(s) = e^{-\left| \frac{I_{ij} - I_{avg}}{s f_{h(ref)}^2} \right|} \text{ for } s \in \{0.4, 0.6, 0.8, 1\} \tag{24}$$

In type-1 fuzzy sets, the fuzzier is constant as in (24) but the type-2 fuzzy sets result from varying $f_{h(ref)}^2$. Here the membership function depends on scale. We will modify $\{H_{ij}(s)\}$ by using an agent to provide a new content through the Hanman-Anirban entropy function with the substitution: $p_{ij}(s) = H_{ij}(s)$, $c = 0$, $d_{ij} = -\log(\cos 2\pi F_{ij}(s, u))$ leading to

$$H_F(I) = \sum_{i=1}^n \sum_{j=1}^n H_{ij}(s) \cos 2\pi F_{ij}(s, u) \tag{25}$$

where the parametric frequency of the cosine function is defined as

$$F_{ij}(s, u) = \frac{F_{max}}{2^{u/2}} \left[\frac{I_{ij} - I_{avg}}{2^s} \right]; \quad u \in [1, 2, 3], \quad s \in [0.4, 0.6, 0.8, 1] \text{ with } F_{max} = 0.1.$$

We can write the r.h.s. of Equation (25) as

$H_{ij}(s) \cos 2\pi F_{ij}(s, u) = I_{ij} \mu_{ij}(s) \cos 2\pi F_{ij}(s, u)$, which is a product of the information value and the cosine function. This filter is different from Gabor filter which is the convolution of image and the product of the Gaussian and cosine functions. We have no such restriction for $\mu_{ij}(s)$ in (25). By using F_{ij} we can create several information images having varied frequency components. These images are aggregated to get a composite image. Next windows of varying size are used to partition this image and the values within a window are averaged to get a feature value.

Definition of 1st Order Filter: If $\mu_{ij}(s)$ is a function of I_{ij} as in (24) then (25) is termed as the first order Hanman filter.

Definition of Zero-Order Filter: If $\mu_{ij}(s)$ is not a function of I_{ij} but only a constant then (25) is termed as the zero-order Hanman filter. Let us choose $d = \frac{i^2 + j^2}{s f_{h(ref)}^2}$ in the exponential gain function by keeping $a = b = c = 0$ then it

converts the zero-order Hanman-filter similar to Gabor type as given by

$$\mu_{ij}(s) = e^{-\left(\frac{i^2 + j^2}{s f_{h(ref)}^2} \right)} \tag{26}$$

We can fix “ s ” in (25) to any value. In the general case s is fixed to the window size, i.e. $s = w$. Then we have

$$\mu_{ij}(s) = e^{-\left(\frac{i^2 + j^2}{w^2 f_{h(ref)}^2} \right)} \tag{27}$$

An algorithm for the extraction of Hanman filter features is as follows: 1) Generate 12 information sets using a window of size $W \times W$ for $W = 7$ from an image for 3 values of u and four values of s , 2) Form the composite information set by aggregating all 12 sets, 3) Consider the average value in a window as the feature, 4) Repeat Steps 1 - 3 on all windows in an iris image to produce a feature vector,

and 5) Generate different feature vectors corresponding to different values of W .

The Utility of Hanman Filter. Its utility is vested with the choice of a suitable type of functions that can modify the information. Consider an example of charcoal the elements of which may be represented as $\{I_i \mu_i\}$ whereas the elements of the burning charcoal may be represented as the product of information value and temperature of charcoal, i.e. $\{I_i \mu_i f(T^A)\}$.

The Difference between the Hanman Transform and the Hanman Filter. The function of Hanman transform is to evaluate the information source values by the gain function using the information already obtained on it while the function of Hanman filter is to modify the information using a suitable function. They lead to higher forms of the information sets because the gain functions used are functions of information values.

Hanman Filter Features

An Example. Let us consider window of size 5×5 from Iris strip. The original gray levels are represented by I_{ij}^0 , the normalized gray levels by p_{ij} , probability distribution by p_{ij} and membership function values (Gaussian) μ_{ij} . Features of the First order HF are extracted using Equation (25) and those of the Zero order HF are extracted using Equation (26).

Two typical feature values for three values of frequency change (u) and two values of scale change (s) are shown in **Table 1**. A comparison of recognition rates due to different feature types is shown in **Table 2** in which the basic Information values yield (3rd column) the highest recognition rate and the next highest recognition rate is by a kind of Hanman transform (5th column) that evaluates the information source values based on the membership function values instead of information values as in Hanman transform (7th column).

2.5. Divergence

If two memberships in the role of agents evaluate the same information source value, we get the divergent information. Let I_{ij} be the set of information source values and let μ_{ij}^1 and μ_{ij}^2 be the two membership functions that look at I_{ij} differently. Then the divergent information is expressed as

Table 1. Typical feature values of Hanman filter.

Image	Normalized image	$\mu = 1, s = 0.4$	$\mu = 1, s = 0.6$	$\mu = 2, s = 0.6$	$\mu = 3, s = 0.6$
		feature values	Feature values	Feature values	Feature values
65	0.25	1.51	1.64	1.672	1.687
69	0.27	1.53	1.65	1.679	1.69

Table 2. Comparison of different features based on the results of authentication.

Features	$p_i e^{-p_i}$	$\mu_{ij} e^{-\mu_{ij}}$	$\mu_{ij} I_{ij}$	$g_i e^{-p_i}$	$I_{ij} e^{-\mu_{ij}}$	$g_i e^{-g_i p_i}$	$I_{ij} e^{-\mu_{ij} I_{ij}}$
Recognition Rates in %	72.30	96.9	98.73	91.0	98.1	94.5	96.8564

$$H_D = \sum \sum I_{ij} (\mu_{ij}^1 - \mu_{ij}^2) \tag{28}$$

The divergent evaluation simply follows from Hanman Transform as given by

$$H_{DE} = \sum \sum I_{ij} e^{-I_{ij}(\mu_{ij}^1 - \mu_{ij}^2)} \tag{29}$$

We can use this measure in quantifying the quality of evaluation of any information source.

2.6. Random Information

By changing the membership function values randomly one can distort the distribution pattern present in the information values. If r is the random number the basic information can be turned into random by using:

$$H_R = \sum \sum r I_{ij} \mu_{ij} \tag{30}$$

The corresponding random evaluation is expressed as,

$$H_{RE} = \sum \sum I_{ij} e^{-r I_{ij} \mu_{ij}} \tag{31}$$

Assuming $r I_{ij} \mu_{ij} = I_{ij} \bar{\mu}_{ij}$ as the complementary information I_{RE} can be termed as the twisted information. This leads to the twisted evaluation expressed as,

$$H_{TE} = \sum \sum I_{ij} e^{-I_{ij} \bar{\mu}_{ij}} \tag{32}$$

3. Derivation of Information Set Based Features

3.1. Effective Information Source Value

This feature directly emerges from the definition of the basic information set. The Effective Information source value from the k^{th} window is computed from:

$$\bar{I}_k = \frac{\sum_i \sum_j \mu_{ij} I_{ij}}{\sum_i \sum_j \mu_{ij}} \tag{33}$$

Replacing μ_{ij} with the Gaussian membership function μ_{ij}^g in (33) leads to what we term as Effective Gaussian Information (EGI):

$$\bar{I}_g(k) = \frac{\sum_i \sum_j \mu_{ij}^g I_{ij}}{\sum_i \sum_j \mu_{ij}^g} \tag{34}$$

3.2. Total Effective Gaussian Information (TEGI)

Just as the above, this feature also comes directly from the basic information. TEGI is defined as the product of Effective Gaussian Information $\bar{I}_g(k)$ and the Effective Gaussian membership function value $\bar{\mu}^g(k)$, given by

$$\bar{I}_T(k) = \bar{I}_g(k) \cdot \bar{\mu}^g(k) \tag{35}$$

where $\bar{\mu}^g(k)$ is computed using:

$$\bar{\mu}^g(k) = \frac{\sum_i \sum_j \mu_{ij}^g I_{ij}}{\sum_i \sum_j I_{ij}}$$

We can also consider μ_{ij}^e instead of μ_{ij}^g or any arbitrary function but we have adopted only μ_{ij}^g in our study.

3.3. Energy Features (EF)

From (12) we can write the gain function as $\left\{ e^{-\left(\frac{I_{ij}-I_{avg}}{I_{max}}\right)} \right\}^2 = \left\{ e^{-\mu_{ij}^{tr}} \right\}^2 = \left(\bar{\mu}_{ij}^{tr} \right)^2$.

Here we have converted the gain function into the triangular function. Hence the energy feature from k^{th} window taking $\gamma = 1$ is written as:

$$E_k = \frac{1}{m \times n} \sum_{i=1}^m \sum_{j=1}^n I_{ij} \cdot \left(\bar{\mu}_{ij}^{tr} \right)^2 \quad (36)$$

It may be noted that the choice of an appropriate membership function is an important issue that is evaded here by going in for an experimentally proven function.

3.4. Sigmoid Features (SF)

Unlike the energy features, these features are the result of considering the information values $\left\{ \mu_{ij}^{tr} I_{ij} \right\}$ in the form of the sigmoid function, SF expressed as

$$S_k = \frac{1}{m \times n} \sum_{i=1}^m \sum_{j=1}^n \frac{I_{avg}}{1 + e^{-\mu_{ij}^{tr} I_{ij}}} \quad (37)$$

where I_{avg} is the average gray level in the k^{th} window.

To extract features an iris strip is divided into windows of size 7×7 and the gray levels are normalized. The number of features is equal to the number of non overlapping windows fitted into an iris strip. The classification of features is performed using the Inner Product Classifier (IPC) in [7].

4. Formulation of Inner Product Classifier (IPC)

This classifier makes use of the error vectors between the training feature vectors of a user and a single test feature vector. As our objective is to get the error vector of the least disorder we generate all possible t-normed error vectors by applying t-norms on any two error vectors of a user at a time. As each normed error vector involves two training feature vectors; these are averaged to get the aggregated training feature vector. The inner product of each t-normed error vector and the corresponding aggregated training feature vector must be the least to represent a user. The infimum of all the least inner products of all users gives the identity of a user. This is the concept behind the design of IPC.

Before presenting an algorithm, let us denote the number of users by N_t , the number of training samples per user by N_i and the number of feature values N_r . The features are normalized by using:

$$H_f = \frac{H_f - \min(H_f)}{\max(H_f) - \min(H_f)} \quad (38)$$

where H_f denotes the Information set based feature such as Effective Gaus-

sian Information $\bar{I}_g(k)$ (EGI), Total Effective Gaussian Information $\bar{I}_T(k)$ (TEGI), Energy feature E_k (EF), Sigmoid feature S_k (SF), Hanman Transform H_T (HT) feature and Hanman Filter H_F (HF) feature. Note that H_f stands for any one of the feature type $\{\bar{I}_g(k), \bar{I}_T(k), E_k, S_k, H_T, H_F\}$.

Algorithm for IPC

1) Compute the error vector $e_{il}(j)$ pertaining to a user (l) between the feature vectors H_V denoted as the feature vectors, $H_{tr}^l(i, j)$ of the training samples of each user and as the feature vector $H_{te}^l(k, j)$ of the unknown test sample, given by

$$e_{il}(j) = |H_{tr}^l(i, j) - H_{te}^l(k, j)| \tag{39}$$

where $i = 1, 2, \dots, N_i$; $j = 1, 2, \dots, N_r$; $l = 1, 2, \dots, N_l$ where i stands for i^{th} sample of i^{th} user and N_i is the number of samples of a user and N_r is the number of feature values.

2) Compute the normed error vectors from all possible pairs (i, k) of error vectors $(e_{il}(j), e_{kl}(j))$ belonging to the l^{th} user using the Frank t-norm as follows:

$$C_{ik}(j, l) = t_F(e_{il}(j), e_{kl}(j)) \tag{40}$$

where t_F is the Frank t -norm given by:

$$t_F = \log_{\psi} \left[1 + \frac{(\psi^{e_{il}(j)} - 1)(\psi^{e_{kl}(j)} - 1)}{\psi - 1} \right] \text{ for } \psi = 2$$

As $i, k = 1, \dots, N_i$, the number of pairs (i, k) generated from (35) is $N_c = \sum_{i=2}^{N_i} (N_i - i + 1)$. Let $q = 1, \dots, N_c$ be the index for the number of pairs.

3) Find the average feature value of i^{th} and k^{th} training samples from

$$f_q(j, l) = f_{ik}(j, l) = \frac{H_{tr}^l(i, j) + H_{te}^l(k, j)}{2} \tag{41}$$

The above normed error vectors $C_q(j, l)$ act as support vectors and the average feature vectors $f_q(j, l)$ act as weights. The necessary and sufficient condition is that the inner product of $C_q(j, l)$ and $f_q(j, l)$ must be the least for the training sample to be matched with the test sample.

4) Evaluate the inner product from

$$E_q(l) = \sum_{j=1}^{N_r} C_q(j, l) f_q(j, l); i \neq k \tag{42}$$

The $h(l) = \min\{E_q(l)\}$ overall q is the error measure of associated with the l^{th} user. While matching, which ever user yields the minimum of all $\min\{h(l)\}$ over all l provides the identity of the test user that owns the training sample.

Extensions of IPC

Assuming that the exponential membership function of $C_q(j, l)$ is $\mu_q(j, l) = e^{-C_q(j, l)}$ and the corresponding information value is $C_q(j, l)\mu_q(j, l)$. Then replacing $f_q(j, l)$ with the exponential of this information value in (42) gives the Hanman Transform classifier, expressed as,

$$E_{qT}(l) = \sum_{j=1}^{Nu} C_q(j, l) e^{-C_q(j, l) \mu_q(j, l)}; i \neq k \quad (43)$$

Another extension is to have the weighted Hanman Transform classifier obtained by combining (42) and (43) as

$$E_{qwT}(l) = \sum_{j=1}^{Nu} f_q(j, l) C_q(j, l) e^{-C_q(j, l) \mu_q(j, l)}; i \neq k \quad (44)$$

5. Application to Iris Based Authentication

The above information-set based features are now implemented on iris textures to demonstrate their effectiveness in the authentication of users. Many approaches are in vogue in the literature for the iris recognition but they fail to yield good recognition rates on the partially occluded irises. As the texture is a region concept the proposed approach proceeds with the granularization of an image by varying the window size on the iris strip so as to get an appropriate texture representation. Moreover the proposed information set based approach is capable of modifying the information on the texture to facilitate easy classification. No new approach is attempted on segmentation of iris, so we have used the existing methods for segmentation. In this case study our emphasis is mainly on the texture representation and classification using the information set based features.

5.1. A Brief Review of Iris as a Biometric

Iris has been a topic of interest for person authentication ever since the pioneering works of Daugman [10] and Wildes [11]. In iris recognition, the onus is on selecting the most suitable features that enable accurate classification. As iris is endowed with a specific texture, it can be used for investigating new texture representations and classifiers.

Gabor filter has played a significant role in characterizing the iris texture by way of iris codes generated using the phase information; hence it is one of the best tools to characterize and classify textures [12]. The advantage of using Gabor filter is its ability to quantify the spatio-temporal component of texture. It may be noted that better recognition of irises can only stem out of better understanding of textures. Even after nearly 20 years of the inception of iris technology, efforts are still on finding better features and classifiers [13] [14].

5.2. Literature Survey

The original works of Daugman [10] and Wildes [11] are the harbinger for the iris based personal authentication. Daugman [10] [15] uses Gabor wavelet phase information whereas Wildes uses the Laplacian of the Gaussian filter at multiple scales as features. Some important contributions on iris recognition are now discussed.

Segmentation of iris texture region plays a pivotal role in the iris recognition. Different approaches like morphological operations [16], thresholding using histogram curve analysis [17] are used for segmentation. Camus and Wildes [18]

have presented a method that doesn't rely on the edge detection by Hough transform for segmentation. The method of Du *et al.* [19] determines the accuracy of iris recognition for a partial iris image. There are a host of problems such as non-circular shape of iris and pupil and off axis images, which have prompted special consideration [20] [21]. It has been proved that better iris segmentation will help in improving the overall performance of iris recognition [22]. Many new methods on iris segmentation can be found in [23].

Gabor filter features are the most sought after so far as the texture is concerned [24]. Other feature extraction methods like Hilbert transform [25], Wavelet based filters [26] are also extensively used in the literature. About the classification algorithms, mention may be made of the correlation of phase information from windows [27], Support Vector Machine (SVM) [28] apart from simple Euclidean distance classifiers.

Practical implementation of iris based biometrics requires faster and more efficient data storage and a possible solution to this problem is suggested using FPGA [29]. Spoofing of iris from iris codes is a sure bet and to circumvent this, counterfeiting measures are developed in [30]. Factors affecting the quality of iris images captured using visible wavelength are investigated in [31]. Concerns regarding degradation of quality due to compression techniques are dispelled in [32]. The quality of iris images and its effect on the recognition rates are analysed with respect to the visible area of the iris texture region [33]. An attempt is made to enable iris recognition using directional wavelets [34]. New methodology on biometric recognition using periocular region (facial region close to the eye) rather than the texture features from the visible iris in Near Infrared (NIR) lighting conditions are discussed in [35] whereas iris recognition using the score level fusion techniques on video frames is presented in [36].

5.3. Segmentation of Iris and Generation of Strips

Segmentation forms a very important part of iris recognition as is evident from its effect on the performance improvement [22]. Though segmentation is not the main concern of this paper we will discuss the segmentation methodology briefly. The iris segmentation is done using the Hough transform based approach [37]. In this, Canny edge detector [38] is applied to get the segmented regions followed by the Hough transform that detects the boundaries of circular regions in the segmented regions. For strip generation polar to rectangular conversion is employed without recourse to the interpolation. A sample image from the database and the corresponding iris are depicted in **Figure 1**. The iris strips are affected by the occlusion of eyes due to eyelids and eyelashes as evident from **Figure 1(b)**. To rectify this problem the iris strip is juxtaposed with itself and the middle portion of the resulting strip is bereft of occlusion as in **Figure 2(b)**. These middle rectangular strips are enhanced and normalized before feature extraction.

The database, CASIA-Iris-V3-Lamp [39] collected using a hand-held iris sensor has eye images of 411 people with at least 10 images per user. The intra class



Figure 1. Sample image of iris and the rectangular strip that is generated from it.

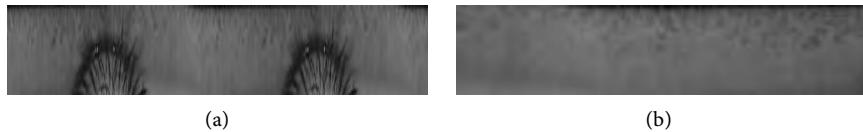


Figure 2. Generation of iris strip devoid of occlusions and eyelids.

variation was introduced in the database by turning the lamps on or off during the acquisition. The experiments were carried out on 4100 left eye images of 411 people with the training to test sample ratio of 9:1 using k -fold validation. This database also contains some samples having rotation, translation, occlusion and illumination effects as shown in **Figure 3**.

6. Results and Discussion

The extracted features from each iris strip are EGI, TEGI, SF, EF, HF and HT. The dimensions of all test strips are normalized before matching with the training strips.

6.1. The Features Used for Comparison

The performance of the above feature types is evaluated and compared with that of the conventional Gabor filter using SVM in [40]. After numerous trials the parameters of Gabor filter are set as follows: The standard deviations: $\sigma_x = 3$ and $\sigma_y = 3$, Phase offset: 0, Aspect ratio: 1, Orientations: $\theta = \pi/4, 2\pi/4, 3\pi/4$ and π and Wavelengths: $\lambda = 1, 2, 3$.

6.2. Performance Evaluation of the Proposed Features

As shown in **Table 3**, IPC and Linear SVM (SVML) show comparable results with the proposed features and Gabor features but Polynomial SVM (SVMP) gives good results only with HT and HF. The accuracies are the mean values of the recognition rates under the k -fold validation. IPC gives the best recognition rate of 98.1% with EF while SVML gives the best recognition rate of 99.2% with SF. The recognition rates with Gabor filter are 90.3% and 97.3% using IPC and SVML respectively. As Gabor features are very large numbering more than 10,000, all classifiers are slower by 10 times.

To tackle the problem of partially occluded eyes, we will apply the majority voting on the iris strips which enables better performance than that of the individual iris strips.

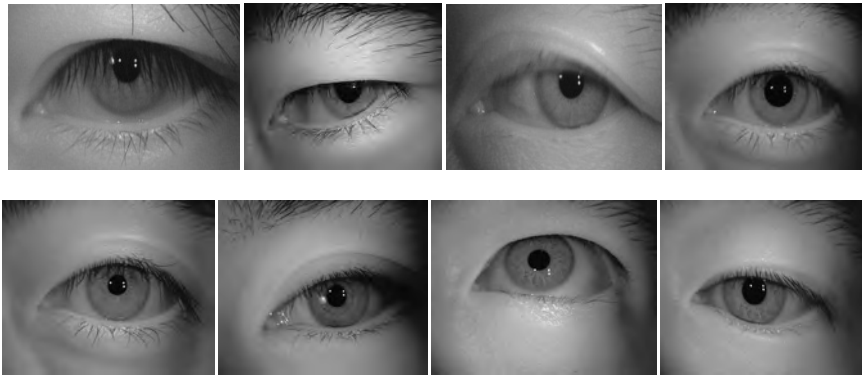


Figure 3. Example iris images in CASIA-Iris-Lamp.

Table 3. Features and their mean recognition rates with different classifiers after k fold validation.

Features	Classifiers	IPC	SVML	SVMP
	EGI		97.3	99
TEGI		97.3	98.6	89.8
SF		97.8	99.2	89.8
EF		98.1	98.9	89.3
HT		97.6	98.2	98
Zero-order HF (Case 1)		97.1	98.76	98.3
Zero-order HF (Case 2)		97.2	98.71	98.3
Zero-order HF (Case3)		97	98.73	98.5
First-order HF		97	98.71	98.6
Gabor		90.3	97.3	97

6.3. Majority Voting

As noted in [41] certain regions of an iris strip like the middle region possess the discriminative texture. It may be noted that significant texture regions are present in iris at different radial distances away from the papillary boundary. This might be attributed to the fact that for some persons, the iris textures are spread over the region between the papillary boundary and the limbic boundary [41] while the majority of people have iris texture features lying closer to the papillary boundary. The aggregation of results from iris strips of different sizes enhances the overall recognition rate. In a few cases, correct classification is obtained with the small sized iris strips; hence the need for considering features from iris strips of different sizes.

Based on the above observation, the iris region between the papillary boundary and limbic boundary is divided into three sizes along with full size. The number of features depends upon the window size chosen to partition an iris. In our study, the window size is taken as 7. The feature vectors corresponding to iris strips of 1/4, 1/2, 3/4 and full size are 78, 156, 234 and 273 respectively. The

original iris strip size is 48×270 . The accuracy achieved with IPC on a particular strip size is given in the 3rd column of **Table 4**. The maximum recognition rate is obtained on 3/4 size strip by all feature types. The features extracted closer to the papillary boundary have less accuracy of detection than those closer to the middle of the iris region.

At the matching stage, each region of the test iris strip is matched with the corresponding regions of all the training strips considering only one type out of the six types of features using IPC. With a view to improve the results of IPC on individual strips, majority voting method is applied on the results of four iris strips obtained using features of one type at a time. It gives the identity of the concerned user which ever training iris strip gets the maximum votes (validation) from four strips of different sizes (similar to four classifiers) [42].

Table 4. Majority voting results for different features with IPC.

Features	Fraction of size	Accuracy of the individual strips (%)	Accuracy after the fusion (%)	The overall accuracy (%)
EGI	Full	97.3	99	100
	3/4	98.5		
	1/2	97.5		
	1/4	93.6		
TEGI	Full	97.8	99.3	
	3/4	98.8		
	1/2	98.0		
	1/4	94.0		
SF	Full	98.3	99.3	
	3/4	99.3		
	1/2	99.3		
	1/4	93.6		
EF	Full	98.5	99.8	
	3/4	99.3		
	1/2	99.3		
	1/4	93.3		
HT	Full	99.7	99.8	
	3/4	99.3		
	1/2	97.8		
	1/4	72.0		
HF	Full	98.3	99.5	
	3/4	99.3		
	1/2	98.8		
	1/4	91.8		

As mentioned above, when the decisions from the individual feature types on strips of different sizes are combined using the majority voting method, the final decision is as shown in the last but one column of **Table 4**. Further enhancement in the recognition rates is obtained when the results from all iris strips are combined using the classification accuracies due to individual feature types as weights similar to ranks [43] using IPC. Then the combined recognition rate from all the feature types on all four strips attains 100% as shown in the last column of **Table 4**. By applying the majority voting on the matching results of four iris strips of different sizes the effect of occlusions can be minimized to a great extent.

This type of segmental approach for iris recognition is proposed in [44]. Instead of accept option that we have used in the majority voting method, the reject option can also be used to detect the possibility of erroneous classification in case we are unable to reach a consensus by the accept option.

6.4. A Comparison with the Existing Methods

We have also compared the performance of our features as in **Table 4** in which the results correspond to 3/4th size of iris with that of the existing features such as PCA, ICA [45], Local binary patterns (LBP) [46], Gabor [24] and Log Gabor [47] on the same database using k -fold validation in **Table 5**. The highest performance (99.35%) is obtained with HF, EF, SF and HT using IPC whereas the highest performance of 96.2% is obtained with ICA using SVMML.

6.5. Verification Evaluation

At the verification level, IPC is compared with Euclidean distance classifier (EC) on the proposed features. The performance of IPC and EC is shown in terms of two separate ROCs on six features denoted by EF, HF, SF, EGI, TEGI, and HT also judged by the recognition rates.

The Euclidean distance based ROC plot in **Figure 4(b)** shows the maximum GAR of 93.3% at FAR of 0.1% with HF features. A maximum GAR of 99% at FAR of 0.1% is achieved with HT by IPC in ROC of **Figure 4(a)**. The performance of IPC is better than that of EC as shown in **Figure 4(a)** and **Figure 4(b)**.

At the verification level the proposed features are also compared with Gabor filter as it is extensively used for iris. As shown in **Figure 4(a)** the proposed features perform better than Gabor filter.

Table 5. Comparison of the existing features using SVMML.

Features	Accuracy in %
PCA	94.1
ICA	96.2
LBP	55.12
Gabor	94.1
Log Gabor	94.08

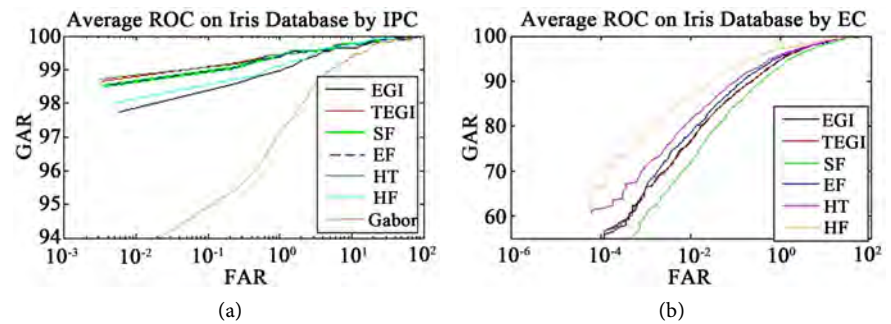


Figure 4. ROC of average authentication by k -fold validation using different features with (a) IPC; (b) EC.

7. Conclusions

This paper moots the important concept of transform to represent higher form of uncertainty. This transform derived from the adaptive Hanman-Anirban entropy function is called the Hanman transform (HT). The transforms have an immense potential as they cater to both spatially varying and time varying situations. As the information need not be in the desirable form, this paper shows how to modify the information sets using a filter function resulting in Hanman Filter (HF) of zero-order and the first order. In addition to these two types of features, we have formulated four feature types that include: Effective Gaussian Information source value (EGI), Total Effective Gaussian Information (TEGI), Energy feature (EF) and Sigmoid Feature (SF). These features are extracted from the rectangular iris strip by partitioning it into windows of different sizes. The performance of IPC is similar to that of SVM, but consistent on all feature types. IPC gives the best results on EF whereas SVM gives the best results on SF. Out of all feature types EF and HT have an edge over other features. Thus the new features and IPC are shown to be effective on the iris database.

The results of authentication using iris strips of four sizes show that 3/4 size strips yield the best results on all feature types using IPC. An application of majority voting on the authentication results obtained with a single feature type on all four strips provides 99.8% accuracy whereas the second level majority voting with six feature types on all four strips achieves the 100% accuracy.

This paper makes several contributions that include: 1) proof of properties of the adaptive Hanman-Anirban entropy, 2) extension of information sets to Hanman filter and Hanman transforms, 3) derivation of information set based features, viz., EGI, TEGI, EF and SF and validation of these features on iris based authentication, and 4) formulation of Hanman Transform classifier.

One ramification of this work is that we can generate a plethora of features from information sets for tackling different kinds of problems though we have chosen iris to vindicate the effectiveness of our features.

Acknowledgements

This research work was funded by Department of Science and Technology (DST),

Government of India. We acknowledge the database CASIA-IrisV3 from the Chinese Academy of Sciences, Institute of Automation.

Conflicts of Interest

The authors declare no conflicts of interest regarding the publication of this paper.

References

- [1] Zadeh, L.A. (1965) *Information and Control*, **8**, 338-353. [https://doi.org/10.1016/S0019-9958\(65\)90241-X](https://doi.org/10.1016/S0019-9958(65)90241-X)
- [2] Yager, R.R. (2008) *Fuzzy Sets and Systems*, **159**, 2193-2210. <https://doi.org/10.1016/j.fss.2007.12.026>
- [3] Yager, R.R. (1992) *Fuzzy Sets and Systems*, **50**, 279-292. [https://doi.org/10.1016/0165-0114\(92\)90226-T](https://doi.org/10.1016/0165-0114(92)90226-T)
- [4] Shannon, C.E. (1948) *Bell System Technical Journal*, **27**, 379-423. <https://doi.org/10.1002/j.1538-7305.1948.tb01338.x>
- [5] Pal, N.R. and Pal, S.K. (1992) *Information Sciences*, **66**, 113-117. [https://doi.org/10.1016/0020-0255\(92\)90090-U](https://doi.org/10.1016/0020-0255(92)90090-U)
- [6] Hanmandlu, M. and Das, A. (2011) *Defence Science Journal*, **61**, 415-430. <https://doi.org/10.14429/dsj.61.1177>
- [7] Mamta and Hanmandlu, M. (2013) *Expert Systems with Applications*, **40**, 6478-6490. <https://doi.org/10.1016/j.eswa.2013.05.020>
- [8] Hanmandlu, M., Jha, D. and Sharma, R. (2003) *Pattern Recognition Letters*, **24**, 81-87. [https://doi.org/10.1016/S0167-8655\(02\)00191-5](https://doi.org/10.1016/S0167-8655(02)00191-5)
- [9] Mamta and Hanmandlu, M. (2014) *Expert Systems with Applications*, **36**, 269-286. <https://doi.org/10.1016/j.engappai.2014.06.028>
- [10] Daugman, J. (1993) *IEEE Transactions on Pattern Analysis and Machine Intelligence*, **15**, 1148-1161. <https://doi.org/10.1109/34.244676>
- [11] Wildes, R.P. (1997) *Proceedings of the IEEE*, **85**, 1348-1363. <https://doi.org/10.1109/5.628669>
- [12] Daugman, J. (1998) *IEEE Transactions on Acoustics Speech and Signal Processing*, **36**, 1169-1179. <https://doi.org/10.1109/29.1644>
- [13] He, Z., Tan, T., Sun, Z. and Qiu, X. (2009) *IEEE Transactions on Pattern Analysis and Machine Intelligence*, **31**, 1670-1684. <https://doi.org/10.1109/TPAMI.2008.183>
- [14] Bowyer, K.W., Hollingsworth, K. and Flynn, P.J. (2008) *Computer Vision and Image Understanding*, **110**, 281-307. <https://doi.org/10.1016/j.cviu.2007.08.005>
- [15] Daugman, J. (1998) *Journal of the Optical Society of America A*, **2**, 1160-1170. <https://doi.org/10.1364/JOSAA.2.001160>
- [16] Bonney, B., Ive, R., Etter, D. and Du, Y. (2004) Iris Pattern Extraction Using Bit Planes and Standard Deviations. *38th Asilomar Conference on Signals, Systems, and Computers*, Vol. 1, 582-586.
- [17] Lili, P. and Mei, X. (2005) The Algorithm of Iris Image Processing. *4th IEEE Workshop on Automatic Identification Advanced Technologies*, Vol. 1, 134-138.
- [18] Camus, T.A. and Wildes, R.P. (2002) Reliable and Fast Eye Finding in Close-Up Images. *16th International Conference on Pattern Recognition*, Quebec, Vol. 1, 389-394.

- [19] Du, Y., Bonney, B., Ives, R., Etter, D. and Schultz, R. (2005) Analysis of Partial Iris Recognition Using a 1-D Approach. *International Conference on Acoustics, Speech, Signal Processing*, Philadelphia, Vol. 2, 961-964.
- [20] Pillai, J.K., Patel, V.M., Chellappa, R. and Ratha, N.K. (2011) *IEEE Transactions on Pattern Analysis and Machine Intelligence*, **33**, 1877-1893. <https://doi.org/10.1109/TPAMI.2011.34>
- [21] Abhyankar, A., Hornak, L. and Schuckers, S. (2005) Off-Angle Iris Recognition Using Bi-Orthogonal Wavelet Network System. *4th IEEE Workshop Automatic Identification Advanced Technologies*, Buffalo, 16-18 October 2005, 239-244.
- [22] Vatsa, M., Singh, R. and Noore, A. (2008) *IEEE Transactions on Systems, Man, and Cybernetic B*, **38**, 1021-1035. <https://doi.org/10.1109/TSMCB.2008.922059>
- [23] Daugman, J. (2007) *IEEE Transactions on Systems, Man, and Cybernetic B*, **37**, 1167-1175. <https://doi.org/10.1109/TSMCB.2007.903540>
- [24] Ma, L., Wang, Y. and Tan, T. (2002) Iris Recognition Based on Multichannel Gabor Filtering. *Proceedings of the 5th Asian Conference on Computer Vision*, Vol. 1, 279-283.
- [25] Tisse, C., Martin, L., Torres, L. and Robert, M. (2002) Person Identification Technique Using Human Iris Recognition. *15th International Conference on Vision Interface*, Calgary, 27-29 May 2002, 294-299.
- [26] Huang, H. and Hu, G. (2005) Iris Recognition Based on Adjustable Scale Wavelet Transform. *27th Annual International Conference of the IEEE Engineering in Medicine and Biology Society*, Shanghai, 1-4 September 2005, 7533-7536.
- [27] Miyazawa, K., Ito, K., Aoki, T., Kobayashi, K. and Nakajima, H. (2005) An Efficient Iris Recognition Algorithm Using Phase-Based Image Matching. *International Conference on Image Processing*, Genoa, Vol. 2, 49-52. <https://doi.org/10.1109/ICIP.2005.1529988>
- [28] Roy, K. and Bhattacharya, P. (2006) Iris Recognition with Support Vector Machines. *Lecture Notes in Computer Science* Vol. 3832, *International Conference on Biometrics*, Hong Kong, 5-7 January 2006, 486-492. https://doi.org/10.1007/11608288_65
- [29] Rakvic, R.N., Ullis, B.J., Broussard, R.P., Ives, R.W. and Steiner, N. (2009) *IEEE Transactions on Information Forensics and Security*, **4**, 812-823. <https://doi.org/10.1109/TIFS.2009.2032012>
- [30] Venugopalan, S. and Savvides, M. (2011) *IEEE Transactions on Information Forensics and Security*, **6**, 385-396. <https://doi.org/10.1109/TIFS.2011.2108288>
- [31] Proença, H. (2011) *IEEE Transactions on Information Forensics and Security*, **6**, 82-95. <https://doi.org/10.1109/TIFS.2010.2086446>
- [32] Daugman, J. and Downing, C. (2008) *IEEE Transactions on Information Forensics and Security*, **3**, 52-62. <https://doi.org/10.1109/TIFS.2007.916009>
- [33] Belcher, C. and Du, Y. (2008) *IEEE Transactions on Information Forensics and Security*, **3**, 572-578. <https://doi.org/10.1109/TIFS.2008.924606>
- [34] Velisavljevic, V. (2009) *IEEE Transactions on Information Forensics and Security*, **4**, 410-418. <https://doi.org/10.1109/TIFS.2009.2024025>
- [35] Park, U., Jillela, R.R., Ross, A. and Jain, A.K. (2011) *IEEE Transactions on Information Forensics and Security*, **6**, 96-106. <https://doi.org/10.1109/TIFS.2010.2096810>
- [36] Hollingsworth, K., Peters, T., Bowyer, K.W. and Flynn, P.J. (2009) *IEEE Transactions on Information Forensics and Security*, **4**, 837-849. <https://doi.org/10.1109/TIFS.2009.2033759>

- [37] Masek, L. and Kovesi, P. (2003) MATLAB Source Code for a Biometric Identification System Based on Iris Patterns. The University of Western Australia, Crawley.
- [38] Canny, J.F. (1986) *IEEE Transactions on Pattern Analysis and Machine Intelligence*, **8**, 679-697. <https://doi.org/10.1109/TPAMI.1986.4767851>
- [39] CASIA-IrisV3-Lamp.
- [40] Burges, C.J.C. (1998) *Data Mining and Knowledge Discovery*, **2**, 121-167. <https://doi.org/10.1023/A:1009715923555>
- [41] Hollingsworth, P.K., Bowyer, K.W. and Flynn, P.J. (2009) *IEEE Transactions on Pattern Analysis and Machine Intelligence*, **31**, 964-973. <https://doi.org/10.1109/TPAMI.2008.185>
- [42] Narasimhamurthy, A. (2005) *IEEE Transactions on Pattern Analysis and Machine Intelligence*, **27**, 1988-1995. <https://doi.org/10.1109/TPAMI.2005.249>
- [43] Monwar, M.M. and Gavrilova, M.L. (2009) *IEEE Transaction on system Man and Cybernetics B*, **39**, 867-878. <https://doi.org/10.1109/TSMCB.2008.2009071>
- [44] Sayeed, F., Hanmandlu, M., Ansari, A.Q. and Vasikarla, S. (2011) Iris Recognition Using Segmental Euclidean Distances. *8th International Conference on Information Technology: New Generations*, Las Vegas, 11-13 April 2011, 520-525. <https://doi.org/10.1109/ITNG.2011.96>
- [45] Wang, Y. and Han, J.-Q. (2005) Iris Recognition Using Independent Component Analysis. *Proceedings of the 4th International Conference on Machine Learning and Cybernetics*, Guangzhou, 18-21 August 2005, 18-21.
- [46] Sun, Z., Tan, T. and Qiu, X. (2006) Graph Matching Iris Image Blocks with Local Binary Pattern. *International Conference on Biometrics*, Hong Kong, 5-7 January 2006, 366-372. https://doi.org/10.1007/11608288_49
- [47] Seif, A., Zewail, R., Saeb, M. and Hamdy, N. (2003) Iris Identification Based on Log-Gabor Filtering. *IEEE 46th Midwest Symposium on Circuits and Systems*, Vol. 1, 333-336.

Relativistic Paradox of a Uniformly Charged Sphere Moving with Constant Velocity

Vladimir Alexander Leus

Department of Electrical Engineering and Electronics, University of Liverpool, Liverpool, UK

Email: v.leus@liverpool.ac.uk

How to cite this paper: Leus, V.A. (2020) Relativistic Paradox of a Uniformly Charged Sphere Moving with Constant Velocity. *Journal of Modern Physics*, 11, 145-155. <https://doi.org/10.4236/jmp.2020.111009>

Received: November 11, 2019

Accepted: January 14, 2020

Published: January 17, 2020

Copyright © 2020 by author(s) and Scientific Research Publishing Inc. This work is licensed under the Creative Commons Attribution International License (CC BY 4.0). <http://creativecommons.org/licenses/by/4.0/>



Open Access

Abstract

A magneto-electric field appearing in a laboratory due to moving charges has unusual properties. In particular, such a field of kinematical origin does not obey the wave equation with a non-relativistic velocity instead of light speed; so, its movement resembles that of a rigid body. In this paper the field of a uniformly charged sphere moving at constant velocity is considered. Relativistic axiom, implicitly used in the derivation of formulas describing a kinematic deformation for the proper spherical field from the point of view of a fixed observer, is revealed. A discrepancy was found between the generally accepted idea of the configuration of a deformed field and its real geometry. It is shown that the correct interpretation of known formulas leads to a logical contradiction, which cannot be eliminated within the framework of the theory of relativity. A scheme of a decisive experiment is proposed.

Keywords

Charged Sphere, Uniform Motion, Deformed Field, Implicit Axiom, Relativistic Paradox

1. Introduction

The Coulomb field of a stationary point charge, which has the simplest spherical symmetry with a strength decreasing inversely proportional to the square of the distance from the source, undergoes a very exotic deformation, if a charge (or an observer) is forced to enter a state of uniform rectilinear motion. It was first pointed out by Oliver Heaviside [1].

The chronological continuity between the relativistic concept of electromagnetism and Maxwell's theory is well known. It was clearly manifested in the study of the motion of a point charge, whose field, from the point of view of a stationary observer in the laboratory, loses its Coulomb configuration. In this

case, the vector field of electric strength \mathbf{E} satisfies the wave equation

$$\nabla^2 \mathbf{E} - \frac{1}{c^2} \frac{\partial^2 \mathbf{E}}{\partial t^2} = \mathbf{0}.$$

As a parameter, it includes the speed of light c . The accompanying magneto-kinematic field of vectors \mathbf{H} is subject to the same equation

$$\nabla^2 \mathbf{H} - \frac{1}{c^2} \frac{\partial^2 \mathbf{H}}{\partial t^2} = \mathbf{0}.$$

Consequently, the displacement of a field in the laboratory space with a velocity \mathbf{v} has a non-wave nature; rather, it is akin to the motion of a rigid body for the non-relativistic case [2] and for the relativistic one [3] as well.

The following demonstrates the fact that in deriving formulas describing the kinematic deformation of a field for a stationary observer, a special relativistic axiom is implicitly applied. At the same time, a discrepancy between the generally accepted idea of the configuration of a deformed field with respect to its real geometry is revealed. The field of a uniformly charged sphere moving at a constant speed is considered. It is shown that the correct interpretation of known formulae leads to a logical contradiction, which cannot be eliminated within the framework of the theory of relativity. A scheme of the experiment is proposed which is to confirm or refute the generally accepted formula for a deformed electrostatic field of a charge moving at a constant velocity.

2. Relativistic Derivation of the Expression for the Field of a Moving Charge, Based on a Hidden Axiom

Recall how the expressions for the fields of a moving point charge are derived. Using the four-dimensional formalism of the special theory of relativity (STR), the authors of the book “Field Theory” [4] come to expressions of the scalar and vector potentials, derived by Lienard and Wiechert long before the birth of the STR. Using then Maxwell’s electromagnetic theory, in the end, a general formula is obtained for the electric and magnetic field vectors of a single point charge making a given motion along a path $\mathbf{r} = \mathbf{r}_0(t)$ (Figure 1).

“According to the formulas for retarded potentials, the field at the point of observation $P(x, y, z)$ at time t is determined by the state of motion of the charge at the earlier time t' , for which the time of propagation of the light signal from the point $\mathbf{r}_e(t')$, where the charge was located, to the field point P just

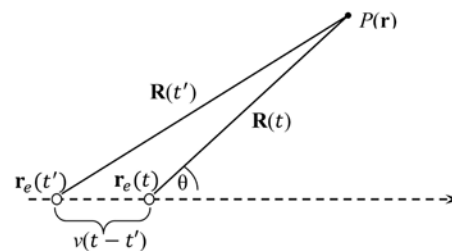


Figure 1. A point charge moving along a given path.

coincides with the difference $t-t'$. Let $\mathbf{R}(t) = \mathbf{r} - \mathbf{r}_e(t)$ be the radius vector from the charge e to the point P , like $\mathbf{r}_e(t)$ it is a given function of the time. Then the time t' is determined by the equation

$$\frac{t' + R(t')}{c} = t. \quad (*)$$

For each value of t this equation has just one root t' ([4], p. 212). This is how §63 “Lienard-Wiechert potentials” begins in the book by Landau and Lifshitz.

“Passing now again to three-dimensional notation, we obtain the following expressions for the field potentials of an arbitrarily moving point charge.

$$\varphi = \frac{e}{\left(R - \frac{\mathbf{v} \cdot \mathbf{R}}{c}\right)}, \quad \mathbf{A} = \frac{e\mathbf{v}}{c \left(R - \frac{\mathbf{v} \cdot \mathbf{R}}{c}\right)}, \quad (**)$$

where \mathbf{R} is the radius vector, taken from the point where the charge is located to the point of observation P , and all the quantities on the right sides of the equations must be evaluated at the time t' determined from the previous equation. The potentials of the field, in the form (**), are called the Lienard-Wiechert potentials” ([4], p. 213).

Let us turn to the case of uniform and rectilinear motion of a point charge along the trajectory $\mathbf{r} = \mathbf{r}_0(t)$ with a constant velocity \mathbf{v} . We introduce the notation \mathbf{R}' and \mathbf{R} for the vectors $\mathbf{R}(t')$ and $\mathbf{R}(t)$, respectively (Figure 1). Maxwell formulas are applied to obtain the strengths of the electric and magnetic fields:

$$\mathbf{E} = -\frac{1}{c} \frac{\partial \mathbf{A}}{\partial t} - \text{grad} \varphi, \quad \mathbf{H} = \text{rot} \mathbf{A}, \quad (1)$$

which yields the expressions

$$\mathbf{E} = e \frac{1 - v^2/c^2}{\left(R' - \frac{\mathbf{R}' \cdot \mathbf{v}}{c}\right)^3} \left(\mathbf{R}' - \frac{\mathbf{v}}{c} R'\right); \quad \mathbf{H} = \frac{1}{R'} [\mathbf{R}' \mathbf{E}]. \quad (2)$$

Here, the symbol $[\dots]$ denotes vector product.

“Indeed, at constant speed, the difference

$$\mathbf{R}' - \frac{\mathbf{v}}{c} R' = \mathbf{R}' - \mathbf{v}(t-t') \quad (***)$$

there is a vector \mathbf{R} from charge to observation point at the very moment of observation. It is also easy to verify by checking directly that

$$\mathbf{R}' - \frac{\mathbf{v}}{c} R' = \sqrt{R^2 - \frac{1}{c^2} [\mathbf{v} \mathbf{R}]^2} = R \sqrt{1 - \frac{v^2}{c^2} \sin^2 \theta_t}, \quad (***)$$

where θ_t is the angle between \mathbf{R} and \mathbf{v} ” ([4], p. 215).

Now you can substitute the right side of the Formula (***) in the numerator, and the right side of the Formula (***) in the denominator of the first term in the expression (2):

$$\mathbf{E}(\theta) = e \frac{(1 - v^2/c^2) \mathbf{R}}{R^3 (1 - (v^2/c^2) \sin^2 \theta)^{3/2}}.$$

We have arrived at a formula that describes the distribution in space of the electric intensity in a field of a point charge, which moves relative to the observer along a straight line at a constant speed. The authors of the book [4] use the CGSE system of units, while the entry in the international system of units (SI) is

$$\mathbf{E} = \frac{q(1 - v^2/c^2)}{4\pi\epsilon_0 r^3 (1 - (v^2/c^2) \sin^2 \theta)^{3/2}} \mathbf{r}, \quad (3)$$

where the designation of the individual charge of an electron is replaced by the universal letter q .

As you can see, in the SRT there is complete continuity in what is concerning the terminology of retarded potentials. This way of reasoning leaves behind the scene an arbitrary assumption of an incessant outflow of a field from its source, the charge. In fact, since the potential propagates from the field source at the speed of light “ c ” regardless of the kind of movement the charge performs, this outflow also takes place when the charge moves with a constant velocity \mathbf{v} . And since the speed of light does not depend on \mathbf{v} , the outflow of potential from the charge remains unchanged when the speed \mathbf{v} tends to zero. Therefore, we have to agree that an unceasing extrovert flow from a charged source exists in any electrostatic field. This statement should be explicitly introduced into the axiomatic basis, when the SRT is transferred to the realm of electromagnetism.

3. Relativistic Paradox

The expression (3) can be obtained within the framework of a pure STR, without resorting to the Lienard-Wiechert potentials. Section 20 of the textbook [5], called “Moving charge field”, Part II, entitled “Theory of Relativity”, deals with the Coulomb field of a point charge deformed to a configuration (3) for an observer moving at a constant velocity $-\mathbf{v}$ along with respect to charge. Of course, with the same success, we can speak of the charge moving at a velocity \mathbf{v} relative to the observer. “In the reference frame K , moving along with the charge, there is no magnetic field, and the electric field potential is expressed by the formula $\varphi' = e/r'$.” ([5], p. 254). The following conclusion is based on the relativistic formula for the transformation of the scalar potential:

$$\varphi = \frac{\varphi' + \frac{v}{c} A'_x}{\sqrt{1 - \frac{v^2}{c^2}}}.$$

On page 256 we read: “*The scalar potential φ has a constant value on the surface of the ellipsoid*”

$$(x-vt)^2 + \left(1 - \frac{v^2}{c^2}\right)(y^2 + z^2) = \text{const}.$$

This ellipsoid is obtained from the sphere by compressing it in the direction of the x -axis into $1:\sqrt{1-\frac{v^2}{c^2}}$ times⁹. We apply the formalism used there to the field of the conducting sphere of unit radius, over which the charge q is uniformly distributed.

This sphere has a centre at the origin (x', y', z') of a primed IRF' (Inertial Reference Frame), moving in a straight line with a constant speed $\mathbf{v} = (v, 0, 0)$ relative to the non-primed (laboratory) IRF with coordinate axes $(0x, 0y, 0z)$ parallel to corresponding axes of the primed coordinate system. For the origin of time, the moment is taken when the origins of spatial coordinate systems coincide; therefore, the position of the centre of the sphere in the non-primed IRF is the point with coordinates $x = vt, y = 0, z = 0$. The scalar potential outside the sphere in its own IRF' coincides with the Coulomb potential (in this section, formulas are written in the Gaussian system of units)

$$\varphi' = \frac{q}{r'}.$$

On the sphere itself and inside it, it has a constant value $\varphi'_0 = q/1$. According to the Lorentz transformations for electromagnetic fields, the scalar potential in a non-primed system is

$$\varphi = \gamma\varphi' = \gamma\frac{q}{r'}, \quad (4)$$

since the vector potential here is zero. The Lorentz transformations for coordinates give the expression of the primed radius-vector from the point of view of the non-primed IRF in the form $r' = \sqrt{\gamma^2(x-vt)^2 + y^2 + z^2}$. Substitute this expression in (4):

$$\varphi = \gamma \frac{q}{\sqrt{\gamma^2(x-vt)^2 + y^2 + z^2}} = \frac{q}{\sqrt{(x-vt)^2 + \frac{1}{\gamma^2}(y^2 + z^2)}}.$$

Hence, the surface of level $\varphi = a = \text{const}$ is described by the equation

$$(x-vt)^2 + \frac{1}{\gamma^2}(y^2 + z^2) = \frac{q^2}{a^2}. \quad (5)$$

Here it is logical to investigate the question on the deformation of the charge carrier—the conducting sphere of a unit radius—upon transition to a non-primed IRF. From the point of view of the non-primed IRF, the carrier of the moving charge loses its spherical shape. Consider the section of the sphere by the plane $z = 0$ (**Figure 2**). Let at the moment t' of the own time in the primed IRF' the x' -coordinates at the ends of the chord, parallel to the x -axis, be measured. We have two events (x'_1, y', t') and (x'_2, y', t') , where y' is the ordinate of the chord. We translate them by the transformations of Lorentz into a non-primed IRF:

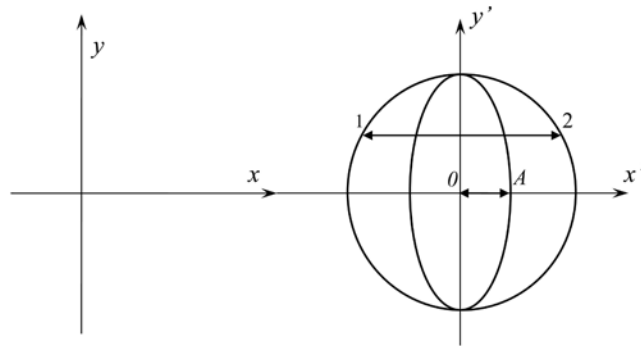


Figure 2. Deformation of the surface of a charged sphere.

$$x_1 = \gamma(x'_1 + vt'), \quad y_1 = y', \quad t_1 = \gamma\left(t' + \frac{v}{c^2}x'_1\right);$$

$$x_2 = \gamma(x'_2 + vt'), \quad y_2 = y', \quad t_2 = \gamma\left(t' + \frac{v}{c^2}x'_2\right).$$

For the time interval $t_2 - t_1 = \gamma\left(\frac{v}{c^2}x'_2 - \frac{v}{c^2}x'_1\right) = \gamma\frac{v}{c^2}(x'_2 - x'_1)$ the second end of the chord managed to drive off at a speed v to a distance $\gamma\frac{v^2}{c^2}(x'_2 - x'_1)$, which should be subtracted from the abscissa difference $x_2 - x_1$ to get chord length in non-primed IRF:

$$l = (x_2 - x_1) - \gamma\frac{v^2}{c^2}(x'_2 - x'_1)$$

$$= \gamma(x'_2 - x'_1) - \gamma\frac{v^2}{c^2}(x'_2 - x'_1)$$

$$= \gamma\left(1 - \frac{v^2}{c^2}\right)(x'_2 - x'_1) = \frac{l'}{\gamma}$$

By virtue of the arbitrariness in the choice of the chord and in the choice of the section by the plane passing through the abscissa axis, we conclude that the entire sphere undergoes longitudinal compression by γ times and turns into an ellipsoid of rotation. The half-axis OA turns out to be γ times shorter than the radius of the sphere, that is, its length is $1/\gamma$. Just the same deformation is mentioned in the cited above excerpt from the textbook [5] with respect to the equipotential surface (a surface of the potential equivalency).

On the unit sphere itself, the potential is $\varphi'_0 = q/1$, and this spherical surface of level $a = q/1$ becomes, according to [5], an ellipsoid with the equation

$$(x - vt)^2 + \frac{1}{\gamma^2}(y^2 + z^2) = 1 \tag{6}$$

in terms of the non-primed IRF. If you believe the textbook's statement [5] that “*This ellipsoid is obtained from a sphere by compressing it along the x-axis by $1:\sqrt{1-\frac{v^2}{c^2}}: \textit{times}$* ”, then there is nothing better to desire. Indeed, the quantity

1: $\sqrt{1 - \frac{v^2}{c^2}} = \textit{times}$ and, as we found out, namely by γ times that the sphere—a

carrier of charge is compressed. Thus, the potential of a charged sphere promises to be an invariant of Lorentz transformations. But, alas, it appears to be too good to be true. The ideal is “only a dream” for us, and the desired harmony does not withstand the “checking up with algebra”!

To put it mildly, strange misunderstandings are associated with the field configuration of a uniformly moving charge. For example, on the behaviour of vectors E we read in ([4], p. 126): “*It can be said visually about the electric field of a moving charge as though it is ‘compressed’ in the direction of motion*”. In fact, the deformation also contains transverse dilatation, and the lines of the constant module $E = \textit{const}$ have a rather complicated guitar-like shape (see [6]).

As for the picture of the equipotential surfaces, we are faced with *fata morgana*, which for decades has been unconditionally accepted by all readers for an objective reality (“When there is no real life, they live in mirages. Still, better than nothing.” A.P. Chekhov). The fact is that the notorious equation in the quotation from ([5], p. 256) pertains to the ellipsoid, which is obtained from the sphere when it is **stretched** in directions **orthogonal** to the x -axis by γ times. The elimination of the traditional ghost has fatal consequences for the relativistic interpretation of the field of a uniformly moving charge. When transforming to IRF, the equipotential surface of the charged sphere is converted not into a sphere compressed to an ellipsoid, but into an ellipsoid stretched across the velocity. Whereas into the ellipsoid—the charge carrier—the sphere of radius $r' = 1$ is converted so that this ellipsoid proves to be situated in the internal cavity of the equipotential ellipsoid.

In **Figure 3** the section by the plane $z = 0$ is present where two ellipsoids are shown. One is being a result of the longitudinal compression of the “unit” sphere by a factor of γ , and another is being a result of the transverse dilatation of this sphere by a factor of γ . The first of them is a charge carrier such as it exists in the IRF where it is described by the equation

$$\gamma^2 (x - vt)^2 + y^2 + z^2 = 1.$$

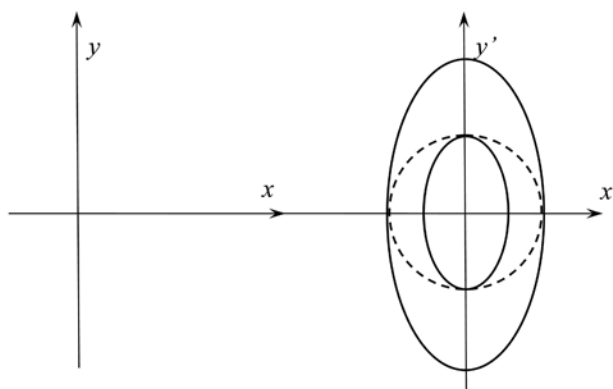


Figure 3. Separation of equipotential surface from charged ellipsoid.

The second is the equipotential surface $\varphi_0 = q/l$ of the electrostatic field, objectively existing in the same IRF, with Equation (6). The second ellipsoid encloses the first, and between them is a layer of variable thickness. In the longitudinal direction, the layer thickness is $(\gamma-1)/\gamma$, and in the transverse direction, the thickness is $(\gamma-1)$, so that with increasing speed \mathbf{v} , the longitudinal thickness approaches unity, while the transverse one increases without limit.

What lies within this layer? In accordance with the relativistic tradition, an ellipsoidal charge carrier retains a spherical potential, and in the layer under consideration everywhere we have

$$\mathbf{E} = -\frac{1}{c} \frac{\partial \mathbf{A}}{\partial t} - \text{grad} \varphi = \mathbf{0},$$

because the scalar potential $\varphi = q/l = \text{const}$ in a finite region, on the boundary of which it is constant, and the vector potential $\mathbf{A} = \varphi \mathbf{v}$, as a result, is also constant in this region and the partial derivative with respect to time is zero. It turns out that the charged ellipsoidal shell is paradoxically immersed in a volume free of the electrostatic field, and only from the outer boundary of this volume does the space, penetrated by the field (3) with equipotential surfaces of type (5), is starting.

The Ostrogradsky-Gauss theorem does not work in the resulting bizarre electrostatic field. This becomes apparent when the test closed surface surrounding the charge carrier is selected entirely inside the neutral layer. The flux of vector \mathbf{E} through this surface is zero, while the integral charge inside is non-zero.

We will try to get away from this electric monster by allowing the scalar potential φ_1 of the ellipsoidal charge carrier to be different from φ_0 : $\varphi_1 < q/l$ or $\varphi_1 > q/l$. In this case, we are faced with another paradox. Suppose there are two identical and equally charged conductive spheres uniformly moving in the laboratory IRF to meet one another. Own IRF' of the first sphere moves with velocity \mathbf{v} and own IRF'' of the second sphere moves with velocity $(-\mathbf{v})$, relative to the non-primed IRF. At the zero moment of time ($t = t' = t'' = 0$), when the origins of all three IRFs coincide, the charge carriers touch each other by the top and bottom limit points respectively. From the point of view of the laboratory IRF, both ellipsoids have the same values of scalar potentials $\varphi_1 = \varphi_2 \neq q/l$ and the voltage between them is zero. But in the IRF' the picture is devoid of such symmetry, because the first sphere has the potential $\varphi'_1 = q/l$, whereas the second sphere, compressed into an ellipsoid, has the potential $\varphi'_2 \neq q/l$. Between them there is a voltage $U = \varphi'_2 - \varphi'_1 \neq 0$, causing a discharge. An electrical discharge occurs also in IRF'', but only with oppositely directed current. The pulsed current arising from the discharge becomes a source of electromagnetic wave, and its objective existence does not depend on the inertial reference frame. Consequently, the EM-wave should also appear in the laboratory IRF, where there is no current at all, that is, radiation arises from literally nothing! A sceptic who doubts the "promptness" of conduction electrons can be calmed by a metal tape longitudinally stretched in IRF, which will sufficiently prolong the contact time of charged spheres (ellipsoids).

4. The Possibility of Experimental Verification

So, contrary to the generally accepted opinion of the complete compatibility of the SRT with Maxwellian electrodynamics, the field of a uniformly moving charge throws to physicists in general, and to experimenters especially, a serious challenge. Indeed, since the time of Heaviside's guess, that is, for more than 130 years, the "relativistic" configuration of such a field has not been confirmed by experience. In [6], the idea of a decisive experiment was proposed, promising to establish whether the prevailing view really corresponds to the natural state of affairs.

Suppose there is a high-ampere electron beam supported in a rectilinear vacuum tube with a length of $2s$ (x -axis in **Figure 4**). At the point $(0, h)$, the beam element dx generates an electric field with intensity $d\mathbf{E}'$, and a beam element symmetric to it generates a field with intensity $d\mathbf{E}''$. The sum $d\mathbf{E}' + d\mathbf{E}'' = d\mathbf{E}$ is directed along the y axis and has an absolute value

$$dE = \frac{2\sigma dx}{4\pi\epsilon_0} \frac{(1-\beta^2)\sin\theta}{(x^2+h^2)(1-\beta^2\sin^2\theta)^{\frac{3}{2}}} = \frac{\sigma(1-\beta^2)dx}{2\pi\epsilon_0 [x^2+(1-\beta^2)h^2]^{\frac{3}{2}}}$$

according to Formula (3). Here the letter σ denotes the linear charge density, $\sin\theta = h/\sqrt{x^2+h^2}$, and $\beta = v/c$. The total electrical intensity is obtained by integrating over the length of the beam:

$$E = \int_0^s dE = \frac{\sigma(1-\beta^2)}{2\pi\epsilon_0} \int_0^s \frac{dx}{[x^2+(1-\beta^2)h^2]^{\frac{3}{2}}} = \frac{\sigma}{2\pi\epsilon_0} \cdot \frac{s}{h[s^2+(1-\beta^2)h^2]^{\frac{1}{2}}}.$$

Expressing the charge density through the electron velocity in the beam and the current strength in it $I = \sigma v$, we get

$$E(h, s, \beta, I) = \frac{Is}{2\pi\epsilon_0 v h \sqrt{s^2+(1-\beta^2)h^2}} = \frac{Is}{2\pi\epsilon_0 \beta c h \sqrt{s^2+(1-\beta^2)h^2}}. \quad (7)$$

If the electric field of a moving point charge remains Coulomb at any speed, then the dependence of E on β will be different:

$$E_0(\beta) = \frac{Is}{2\pi\epsilon_0 \beta c h \sqrt{s^2+h^2}}. \quad (8)$$

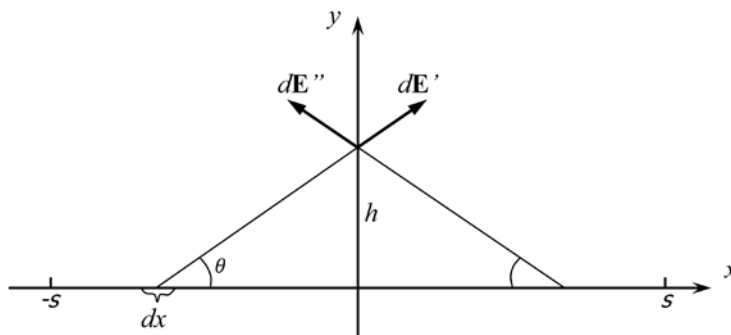


Figure 4. Experiment in a rectilinear vacuum tube.

The well-known experiment on the detection of the electric field around a superconducting ring with current [7] is extremely difficult to perform, since it is necessary to detect the effect of the second order of smallness with respect to the ratio $v/c = \beta$. The difference between the electro-kinematic field created by the moving conduction electrons and the electrostatic field of the stationary ions of the conductor crystal lattice leads to it. The letter v refers here to the drift velocity of conduction electrons, which no snail would envy. Moreover, as was shown later, the result of the experiment cannot be interpreted unambiguously: “*the experiment performed by Edwards et al. is not a test of Maxwell’s equations in the most general case, but a test of these equations in the particular case of the superconducting state*” [8].

The experimental scheme proposed here is completely free from the main obstacle facing the authors of the work [7]. At a current of one ampere at a distance of half a meter from the middle of the beam one meter in length, the electric intensities calculated by Formulas (7) and (8), respectively, are equal to 287 V/m and 281 V/m with $\beta = 0.3$. When $\beta = 0.99$, the values of 119 V/m and 85 V/m are obtained. The point is now small: prepare the equipment and take measurements. The equipment required for the experiment is rather modest, especially in comparison with the giant modern particle accelerators. The electron, accelerated to just an energy of 10 Mev, has a speed close to $0.99c$, so the outcome would be worth investment.

5. Conclusion

In the paper [9], an example of an irreconcilable contradiction between the special theory of relativity on the one hand and the general theory of relativity on the other, arising in a mechanical system of a cyclic type, is sorted out. The subject of the present work is a strange situation emerged in the doctrine of electromagnetism based on the relativistic approach. First, it is the presence of an implicit axiom about the constant expiration of the potential with the speed of light in an electrostatic field from its source—a point charge. For an accelerated charge, the role of carriers can be assigned to the emitted photons. However, in the case of a charge moving without acceleration, it remains an unsolved mystery: what kind of “superfine matter” constantly transports the potential in an electrostatic field? Secondly, the type of deformation of the Coulomb field of a point charge is observed in uniform motion with a constant velocity $v = const$. The correct interpretation of the geometry arising in this way leads to the unavoidable inconsistency in the picture of the equipotential surfaces in the electrostatic field of the charged sphere. Third, it is the nature of the movement of static fields when moving their carriers. These psychological invisibilities, surprisingly escaping the attention of physicists for a whole century, caused a distorted view of physical reality, in which there is no room for electro-magneto-kinematics. The absence to this day of experimental confirmation of the deformed configuration of the field of a point charge, moving with a constant velocity v , presents a serious challenge for experimenters.

Acknowledgements

The author sincerely thanks Mr Michael Kyle for his valuable help while preparing this paper.

Conflicts of Interest

The author declares no conflicts of interest regarding the publication of this paper.

References

- [1] Heaviside, O. (1888) *The Electrician*, **22**, 147-148.
- [2] Leus, V.A. (2013) *Progress in Electromagnetics Research M*, **32**, 27-41.
<https://doi.org/10.2528/PIERM13043008>
- [3] Leus, V.A. and Taylor, S. (2018) *International Journal of Applied Mathematics and Theoretical Physics*, **4**, 91-97.
- [4] Landau, L.D. and Lifshitz, E.M. (1967) *Teorija Polja [Field Theory]*. 5th Edition, Nauka, Moscow. (In Russian)
- [5] Levich, V.G. (1962) *Kurs teoreticheskoj fiziki [Course of Theoretical Physics]*. Vol. 1, Fizmatgiz, Moscow. (In Russian)
- [6] Leus, V.A. (2018) *Science and Engineering Investigations*, **7**, 30-36.
<http://www.ijsei.com/papers/ijsei-77918-03.pdf>
- [7] Edwards, W.F., Kenyon, C.S. and Lemon, D.K. (1976) *Physical Review D*, **14**, 922-938. <https://doi.org/10.1103/PhysRevD.14.922>
- [8] Bonnet, G. (1981) *Physics Letters*, **82A**, 465-467.
[https://doi.org/10.1016/0375-9601\(81\)90282-6](https://doi.org/10.1016/0375-9601(81)90282-6)
- [9] Leus, V.A. (2018) *Journal of Modern Physics*, **9**, 1043-1051.
<https://doi.org/10.4236/jmp.2018.95066>



Call for Papers

Journal of Modern Physics

ISSN: 2153-1196 (Print) ISSN: 2153-120X (Online)
<https://www.scirp.org/journal/jmp>

Journal of Modern Physics (JMP) is an international journal dedicated to the latest advancement of modern physics. The goal of this journal is to provide a platform for scientists and academicians all over the world to promote, share, and discuss various new issues and developments in different areas of modern physics.

Editor-in-Chief

Prof. Yang-Hui He

City University, UK

Subject Coverage

Journal of Modern Physics publishes original papers including but not limited to the following fields:

Biophysics and Medical Physics
Complex Systems Physics
Computational Physics
Condensed Matter Physics
Cosmology and Early Universe
Earth and Planetary Sciences
General Relativity
High Energy Astrophysics
High Energy/Accelerator Physics
Instrumentation and Measurement
Interdisciplinary Physics
Materials Sciences and Technology
Mathematical Physics
Mechanical Response of Solids and Structures

New Materials: Micro and Nano-Mechanics and Homogeneization
Non-Equilibrium Thermodynamics and Statistical Mechanics
Nuclear Science and Engineering
Optics
Physics of Nanostructures
Plasma Physics
Quantum Mechanical Developments
Quantum Theory
Relativistic Astrophysics
String Theory
Superconducting Physics
Theoretical High Energy Physics
Thermology

We are also interested in: 1) Short Reports—2-5 page papers where an author can either present an idea with theoretical background but has not yet completed the research needed for a complete paper or preliminary data; 2) Book Reviews—Comments and critiques.

Notes for Intending Authors

Submitted papers should not have been previously published nor be currently under consideration for publication elsewhere. Paper submission will be handled electronically through the website. All papers are refereed through a peer review process. For more details about the submissions, please access the website.

Website and E-Mail

<https://www.scirp.org/journal/jmp>

E-mail: jmp@scirp.org

What is SCIRP?

Scientific Research Publishing (SCIRP) is one of the largest Open Access journal publishers. It is currently publishing more than 200 open access, online, peer-reviewed journals covering a wide range of academic disciplines. SCIRP serves the worldwide academic communities and contributes to the progress and application of science with its publication.

What is Open Access?

All original research papers published by SCIRP are made freely and permanently accessible online immediately upon publication. To be able to provide open access journals, SCIRP defrays operation costs from authors and subscription charges only for its printed version. Open access publishing allows an immediate, worldwide, barrier-free, open access to the full text of research papers, which is in the best interests of the scientific community.

- High visibility for maximum global exposure with open access publishing model
- Rigorous peer review of research papers
- Prompt faster publication with less cost
- Guaranteed targeted, multidisciplinary audience



**Scientific
Research
Publishing**

Website: <https://www.scirp.org>

Subscription: sub@scirp.org

Advertisement: service@scirp.org